Bond Behavior of FRP-to-Concrete under Cyclic Fatigue Loading of RC Structures Strengthened with EB-FRP Composites

by

Abbas FATHI

MANUSCRIPT-BASED THESIS PRESENTED TO ÉCOLE DE TECHNOLOGIE SUPÉRIEURE IN PARTIAL FULFILLMENT FOR THE DEGREE OF DOCTOR OF PHILOSOPHY
Ph.D.

MONTREAL, JULY 04, 2023

ÉCOLE DE TECHNOLOGIE SUPÉRIEURE
UNIVERSITÉ DU QUÉBEC

BOARD OF EXAMINERS

THIS THESIS HAS BEEN EVALUATED

BY THE FOLLOWING BOARD OF EXAMINERS

Mr. Georges El-Saikaly, Thesis Supervisor
Department of Construction Engineering at École de Technologie Supérieure

Mr. Omar Chaallal, Thesis Co-supervisor
Department of Construction Engineering at École de Technologie Supérieure

Mr. Anh Dung Ngô, President of the Board of Examiners
Department of Mechanical Engineering at École de Technologie Supérieure

Mr. Lotfi Guizani, Member of the jury
Department of Construction Engineering at École de Technologie Supérieure

Mr. Amir Mofidi, External Evaluator
Yousef Haj-Ahmad Department of Engineering, Faculty of Mathematics and Science, Brock University

THIS THESIS WAS PRENSENTED AND DEFENDED

IN THE PRESENCE OF A BOARD OF EXAMINERS AND PUBLIC

ON JUNE 23, 2023

AT ÉCOLE DE TECHNOLOGIE SUPÉRIEURE

ACKNOWLEDGMENTS

I would like to express my sincere gratitude to Professor Georges El-Saikaly and Professor Omar Chaallal, my research directors, for their exceptional support and invaluable mentorship during my doctoral program. I have been blessed with their confidence and guidance throughout my research and have been grateful for working alongside these two professors.

I would also like to thank Mr. Jonathan Auger, Mr. John Lescelleur (senior technicians) and Mr. Juan Mauricio Rios (technician) at École de technologie supérieure for their assistance in performing the laboratory tests. Their collaboration in my experimental program has greatly facilitated my research project and is much appreciated.

The financial support of the Natural Sciences and Engineering Research Council of Canada (NSERC) and the Fonds de Recherche du Québec – Nature et Technologie (FRQNT) through operating grants is gratefully acknowledged. Also, many thanks go to Sika-Canada, Inc. (Pointe-Claire, QC) for contributing to the cost of materials in regard to the experimental program.

Finally, I can never forget the perpetual love, support, and encouragement that I have received from my family until the completion of my studies.

Comportement d'adhérence PRF-béton sous charges cycliques de fatigue des structures en béton armé renforcées à l'aide de composites en PRF collés en surface

Abbas FATHI

RÉSUMÉ

Les structures en béton armé telles que les poutres de pont sont soumises, pendant leur durée de vie utile, à des charges cycliques de fatigue, principalement sous la forme des charges de trafic. Ces structures sont sujettes à des dommages progressifs et peuvent subir une rupture par cisaillement, qui se caractérise souvent par une rupture fragile sans aucun avertissement préalable. Par conséquent, la réhabilitation des structures en béton armé déficientes en cisaillement nécessite l'application de systèmes de renforcement appropriés. L'utilisation de composites en PRF collés en surface (PRF-CS) présente de nombreux avantages et constitue une technologie prometteuse pour le renforcement en cisaillement des structures en béton armé. Cependant, la performance des structures en béton renforcées à l'aide de PFR-CS peut être fortement influencée par l'adhérence à l'interface PRF-béton, car le décollement interfacial peut entraîner une défaillance prématurée du système de renforcement. Peu d'études ont été menées sur le comportement d'adhérence PRF-béton des structures en béton renforcées à l'aide de PRF-CS sous chargement cyclique de fatigue, et par conséquent, d'autres recherches connexes contribueront à une meilleure compréhension de ce domaine de recherche complexe.

La présente recherche vise à examiner le comportement d'adhérence en fatigue à l'interface PRF-béton des structures en béton renforcées à l'aide de PRF-CS. À cette fin, dans la première phase de cette recherche, une revue de la littérature est effectuée afin d'identifier les paramètres influents sur le mécanisme d'adhérence en fatigue à l'interface PRF-béton. En effet, il est indiqué que les PRF en carbone (PFRC) peuvent fournir une meilleure résistance à la fatigue que d'autres composites en PRF, tels que les PRF en verre et en aramide.

Une étude expérimentale est menée dans la deuxième phase de cette recherche pour combler les lacunes existantes dans la littérature concernant le comportement d'adhérence PRF-béton. Une série d'essais d'arrachement en cisaillement sur de joints collés PFRC-béton à double rangée est conçue pour évaluer le comportement interfacial en fonction de différentes variables, telle que le type de composite en PRF (lamelle en PRFC vs tissu en PRFC), le rapport largeur PRF-béton (largeur FRP collé en surface sur largeur du béton), et la longueur d'adhérence du PRF sous chargement statique et cyclique. Les résultats de ce programme expérimental démontrent la performance supérieure du système de renforcement à l'aide de tissus en PRFC comparé aux lamelles en termes de résistance ultime sous chargement statique et durée de vie en fatigue sous chargement cyclique. De plus, l'augmentation du rapport de largeur PFRC-béton s'est avérée améliorer le comportement d'adhérence par rapport au mode de rupture par décollement sous les deux conditions de chargement. En ce qui concerne la longueur d'adhérence des PRFC, d'autres discussions sont présentées pour évaluer ce

paramètre sur le comportement d’adhérence, en mettant l’accent sur la détermination de la longueur d’adhérence effective sous les conditions de chargement statique et cyclique.

En incorporant les résultats expérimentaux actuels et les données de recherche disponibles dans la littérature, des études analytiques sont menées pour développer les deux modèles suivants : 1) une relation contrainte d’adhérence -glissement sous chargement statique ; et 2) un modèle de prédiction de la durée de vie en fatigue de l’adhérence PRFC-béton sous chargement cyclique. Les deux modèles se sont révélés satisfaisants lorsqu'ils ont été validés par rapport à la base de données sélectionnée et peuvent constituer un outil efficace pour prédire le comportement d’adhérence à l'interface PFRC-béton des structures en béton renforcées en cisaillement à l’aide de PRFC.

Mots clés: Structures en béton armé, tissu en PRFC, lamelle en PRFC, renforcement en cisaillement, chargement cyclique de fatigue, comportement d’adhérence, interface PRF-béton, rapport largeur PRF-béton, longueur d’adhérence, relation contrainte d’adhérence-glissement, modèle de prédiction de la durée de vie en fatigue.

Bond behavior of FRP-to-concrete under cyclic fatigue loading of RC structures strengthened with EB-FRP composites

Abbas FATHI

ABSTRACT

Reinforced concrete (RC) structures such as bridge girders are subjected, during their service life, to cyclic fatigue loading, mainly in the form of traffic loads. These structures are prone to progressive damage and may experience shear failure, which is often characterized by brittle rupture without any prior warning. Hence, retrofitting RC structures deficient in shear calls for the application of appropriate strengthening systems. The use of externally bonded (EB) fiber reinforced polymer (FRP) composites features numerous advantages and is a promising technology for shear strengthening of RC structures. However, the performance of EB-FRP retrofitted concrete structures can be highly influenced by the bond at FRP-to-concrete interface, as interfacial debonding can lead to the premature failure of the strengthening system. Limited investigations have been carried out on the FRP-to-concrete bond behavior of EB-FRP strengthened concrete structures under cyclic fatigue loading, and therefore, further related research will contribute to a better understanding of this complex research area.

The present research study aims to investigate the fatigue bond behavior at the FRP-to-concrete interface of EB-FRP strengthened RC structures. To this end, in the first phase of this study, a literature-review is conducted to identify the parameters affecting the fatigue bond mechanism at the FRP-to-concrete interface. Indeed, it is indicated that carbon FRPs (CFRPs) can provide better fatigue resistance than other FRP composites, such as glass and aramid FRPs.

An experimental investigation is conducted in the second phase of this study to fill existing gaps in the literature regarding the FRP-to-concrete bond behavior. A series of double-lap shear tests on CFRP-to-concrete bonded joints are designed to evaluate the interfacial behavior as a function of different variables, such as the FRP composite type (CFRP laminate vs. CFRP fabric sheet), the FRP-to-concrete width ratio (bonded FRP width to concrete width), and the FRP bond length under both monotonic and cyclic loading. The results of this experimental program demonstrate the superior performance of the CFRP composite bonding system using fabric sheet over the CFRP laminate in terms of bond ultimate resistance under monotonic loading and bond fatigue life under cyclic loading. Furthermore, increasing the CFRP-to-concrete width ratio was found to improve the bond behavior against the debonding failure mode under both loading conditions. As for the bond length, further discussions are presented to evaluate this parameter on the bond behavior, with emphasis on determining the effective bond length under both monotonic and cyclic loading conditions.

By incorporating the current experimental results and research data available in the literature, analytical studies are conducted to develop the following two models: 1) a bond stress-slip relationship under monotonic loading; and 2) a fatigue-life prediction model of CFRP-to-concrete bond under cyclic loading. Both models are shown to perform satisfactorily when validated against the selected database and can be an effective tool for predicting the bond

behavior at the CFRP-to-concrete interface of concrete structures strengthened in shear with CFRP composites.

Keywords: RC structures, CFRP sheet, CFRP laminate, shear strengthening, cyclic fatigue loading, bond behavior, FRP-to-concrete interface, FRP-to-concrete width ratio, bond length, bond-slip relationship, fatigue-life prediction model.

TABLE OF CONTENTS

Page

INTRODUCTION 1

CHAPTER 1 RESEARCH DESCRIPTION 5
1.1 Context 5
1.1.1 Shear failure and FRP strengthening technique 5
1.1.2 EB-FRP configurations 8
1.1.3 Debonding failure mode 9
1.1.4 Bond behavior at FRP-to-concrete interface 11
1.1.5 Fatigue life of EB-FRP retrofitted structures 12
1.1.6 Low and high cycle fatigue 13
1.2 Problem Statement 14
1.3 Research objectives 15
1.3.1 Main objective 15
1.3.2 Specific objectives 15
1.4 Methodology 16

CHAPTER 2 RESEARCH BACKGROUND 21
2.1 Design Considerations 21
2.1.1 Fatigue state limit of EB-FRP strengthened bridge structures 21
2.1.2 Fatigue stress limit of steel reinforcement 22
2.1.3 Fatigue stress limit of FRP and concrete 23
2.2 Literature Review 24
2.2.1 Experimental studies of the performance of EB-FRP shear-strengthened RC beams under fatigue loading 25
2.2.2 Bond-slip behavior of FRP-to-concrete interface under monotonic loading 33

CHAPTER 3 ON BOND-SLIP OF EB-FRP/CONCRETE INTERFACE IN SHEAR UNDER FATIGUE LOADING: REVIEW AND SYNTHESIS OF EXPERIMENTAL STUDIES AND MODELS 77
3.1 Abstract 77
3.2 Introduction 78
3.3 Design code provisions 82
3.4 Fatigue behavior of FRP/concrete interface under cyclic loading 83
3.4.1 Bond-slip models of FRP/concrete interface 83
3.4.2 FRP/concrete bond fatigue life models 96
3.4.3 Concrete compressive strength 98
3.4.4 Bond length 100
3.4.5 FRP-to-concrete width ratio 102
3.4.6 Fatigue loading amplitude 102
3.5 Finite-element analysis of EB-FRP/concrete interface under fatigue loading 103

3.5.1 FE modeling of the FRP/concrete bond 104
3.5.2 Numerical parametric studies on the FRP/concrete bond 105
3.6 Synthesis and discussion 108
3.7 Research needs 109
3.8 Conclusions 110
3.9 Acknowledgements 112

CHAPTER 4 EXPERIMENTAL AND ANALYTICAL STUDY OF BOND STRESS-SLIP BEHAVIOR AT THE CFRP-TO-CONCRETE INTERFACE 113
4.1 Abstract 113
4.2 Practical application 114
4.3 Introduction 114
4.4 Research significance 118
4.5 Experimental program 118
4.5.1 Test set-up 118
4.5.2 Specimen preparation 120
4.5.3 CFRP ratio and strain gauge configuration 123
4.6 Experimental results 124
4.6.1 Failure modes 125
4.6.2 Bond strength of the CFRP-to-concrete interface 127
4.6.3 Bond stress-slip curves 128
4.6.4 Bond stress-slip models 131
4.6.5 Modified bond-slip model 136
4.6.6 Global bond stress-slip curves 143
4.6.7 Effect of CFRP bond length 145
4.6.8 Effective bond length of specimens 146
4.6.9 Strain distributions along the bonded CFRP 149
4.6.10 Effect of CFRP type 151
4.6.11 Effect of CFRP width 153
4.7 Conclusions 153
4.8 Data availability statement 155
4.9 Acknowledgments 155

CHAPTER 5 FATIGUE BEHAVIOR IN THE CARBON-FIBRE-REINFORCED POLYMER-TO-CONCRETE BOND BY CYCLIC PULL-OUT TEST: EXPERIMENTAL AND ANALYTIAL STUDY 157
5.1 Abstract 157
5.2 Introduction 158
5.3 Research significance 162
5.4 Experimental program 163
5.4.1 Specimen preparation 165
5.4.2 CFRP width and strain gauge positions 167
5.4.3 Fatigue loading application 169
5.5 Experimental results 169

5.5.1 Failure modes 170
5.5.2 Bond-energy dissipation during fatigue loading 173
5.5.3 Bond stress-slip relationship 176
5.5.4 Strain distribution during cyclic loading 182
5.5.5 Fatigue performance of CFRP type (laminate vs. sheet) with varying bond length 185
5.5.6 Effect of CFRP-to-concrete width ratio 187
5.5.7 Bond fatigue-life model 187
5.6 Conclusions 192
5.7 Data availability statement 194
5.8 Acknowledgments 194

CONCLUSIONS 195

RECOMMENDATIONS 201

LIST OF BIBLIOGRAPHICAL REFERENCES 203

LIST OF TABLES

Page

Table 2.1 Summarized details of experimental studies on EB-CFRP shear-strengthened RC beams under fatigue loading from selected research studies 32

Table 2.2 Summarized details derived from experimental investigations on the monotonic bond behavior of FRP-to-concrete interface 55

Table 2.3 Summarized details of experimental studies regarding the behavior of FRP-to-concrete interface under fatigue loading condition 74

Table 3.1 Details of experimental investigations on the fatigue behavior of FRP/concrete bond along with the investigated parameters 84

Table 3.2 Available bond-slip models under static loading 85

Table 4.1 Experimental details of specimens 119

Table 4.2 CFRP properties used in the experimental program 122

Table 4.3 Maximum double-lap load-carrying capacity of specimens along with the corresponding predictions according to the existing models 128

Table 4.4 Database of tested specimens for the modified bond-slip model 138

Table 4.5 Calculation of bond-slip parameters based on the exiting models 141

Table 4.6 Effective bond-length relations and predicted results for the specimens 147

Table 5.1 Experimental details of specimens 164

Table 5.2 Mechanical properties of CFRP composites and epoxy adhesives 167

Table 5.3 Experimental results of specimens during cyclic testing 170

Table 5.4 Database of specimens used for the modified bond fatigue-life model 189

LIST OF FIGURES

Page

Figure 1.1 Shear failure of an RC beam 6

Figure 1.2 Idealized stress-strain curves of various FRP composites vs. steel 7

Figure 1.3 Bridge strengthening with EB-FRP systems 7

Figure 1.4 Wrapping schemes for EB FRP composites: a) complete wrapping; b) U-wrapping; and c) side bonding 8

Figure 1.5 Overlapped L-shaped laminates 8

Figure 1.6 FRP debonding failure in an EB-FRP strengthened RC beam 9

Figure 1.7 Modes of cracking pattern 10

Figure 1.8 Cracking mode of an EB-FRP strengthened RC beam 10

Figure 1.9 Bond-slip behavior in an FRP-to-concrete bonded joint 11

Figure 1.10 Schematic S-N curve of steel (in tension) and concrete (in compression) 12

Figure 1.11 S-N curve in LCF and HCF conditions 13

Figure 1.12 Methodology of the doctoral research project 18

Figure 1.13 Experimental program identified within the doctoral research 19

Figure 1.14 CFRP composites used in the experimental program 19

Figure 1.15 MTS loading machine 20

Figure 2.1 CL-W Truck 22

Figure 2.2 Different experimental set-up for the investigation of FRP-to-concrete bond: a) beam test; b) single pull-out test; c) double pull-out test 34

Figure 2.3 Possible failure modes of FRP-to-concrete interface 35

Figure 2.4 Concrete cover failure mode 35

Figure 2.5 Variation of effective bond length with respect to the FRP stiffness 43

Figure 2.6 NES single-lap pull-out test setup....48

Figure 2.7 CFRP anchorage system with CFRP rope....52

Figure 2.8 Phases of fatigue cracking along the interface....58

Figure 2.9 Damage quantity model for the CFRP-to-concrete interface....65

Figure 2.10 Proposed bond stress-slip model under fatigue load....69

Figure 2.11 Modeling of the concrete/CFRP interface with: a) solid element; b) interface element....71

Figure 2.12 Bond-slip behavior affected by fatigue damage....73

Figure 3.1 Schematic S-N curves of concrete and steel....80

Figure 3.2 Existing bond-slip models under static loading....86

Figure 3.3 Envelope-base bond-slip curve of a specimen tested by Ko and Sato (2007) under cyclic loading....87

Figure 3.4 Cyclic bilinear bond-slip model proposed by HM Diab et al. (2009)....89

Figure 3.5 Constitutive bond-slip model of Concrete/FRP interface under fatigue loading by Loo et al. (2012)....90

Figure 3.6 Bond-slip curves of a tested specimen under different number of load cycles (*n*) by K. Li et al. (2018)....93

Figure 3.7 Bond-slip model curves of a specimen from Group B (considering loading amplitude and concrete strength as variables)....94

Figure 3.8 Bond-slip model curves of a specimen from Group C (considering bond length and FRP-to-concrete width ratio as variables)....94

Figure 4.1 Schematic of double-lap pull-out test set-up (dimensions in mm): a) top view; b) side view....120

Figure 4.2 Test specimen (Specimen L-200-25)....122

Figure 4.3 Configuration of strain gauge locations on CFRP with: a) 50 mm bond length; b) 100 mm bond length; c) 150 mm bond length; and d) 200 mm bond length....124

Figure 4.4 Failure modes of specimens bonded with CFRP laminate (Series 1)....126

Figure 4.5 Failure modes of specimens bonded with CFRP sheet (Series 2 and 3)....126

Figure 4.6 Experimental maximum loads resisted by the specimens vs. the corresponding predictions from bond strength models....127

Figure 4.7 Schematic strain gauge locations on bonded CFRP 129

Figure 4.8 Schematic strain-displacement relationship....130

Figure 4.9 Local bond stress-slip curves of specimens: a) L-200-25; b) S-200-75; and c) S-200-112 132

Figure 4.10 Local bond stress-slip models along with the bond-slip curve: a) Series 1 specimens; b) Series 2 specimens; and c) Series 3 specimens....134

Figure 4.11 Average bilinear bond-slip curves: a) Series 1 specimens; b) Series 2 specimens; and c) Series 3 specimens 137

Figure 4.12 Predictions of maximum local bond stress versus experimental database....142

Figure 4.13 Predictions of bond slip at the maximum shear stress versus experimental database....142

Figure 4.14 Predictions of ultimate bond slip at failure versus experimental database....143

Figure 4.15 Global bond stress-slip curves related to the tested Specimens of: a) Series 1; b) Series 2 and c) Series 3....144

Figure 4.16 Maximum double-lap load gained by specimens with different bond lengths....146

Figure 4.17 Strain distributions along the bonded length at different ratios of the maximum bond capacity for: a) L-200-25; b) S-200-75; and c) S-200-112....150

Figure 4.18 Applied load vs. displacement of specimens bonded with CFRP laminate and 75 mm-wide sheet 152

Figure 5.1 Scheme of cyclic testing set-up (dimensions in mm): a) top view; b) side view 164

Figure 5.2 Cyclic testing configuration (Specimen CL-100-25)....166

Figure 5.3 Strain gauge positions on CFRP composites for specimens with different L_b (dimensions in mm): a) L_b = 50 mm; b) L_b = 100 mm; c) L_b = 150 mm; d) L_b = 200 mm....168

Figure 5.4 Failure modes of specimens with CFRP laminate during cyclic loading 172

Figure 5.5 Failure modes of specimens with CFRP sheet under post-fatigue monotonic loading 173

Figure 5.6 Displacement vs. load cycle ratio of specimens with laminate under fatigue loading 174

Figure 5.7 Displacement vs. load cycle ratio of specimens with: a) 75 mm-wide sheet; b) 112 mm-wide sheet 175

Figure 5.8 Local bond-slip curves of Specimen CL-200-25 during cyclic loading along the bond length: a) Interval $\varepsilon_5 - \varepsilon_6$; b) Interval $\varepsilon_4 - \varepsilon_5$; c) Interval $\varepsilon_3 - \varepsilon_4$; d) Interval $\varepsilon_2 - \varepsilon_3$; e) Interval $\varepsilon_1 - \varepsilon_2$; f) Interval $\varepsilon_0 - \varepsilon_1$.....177

Figure 5.9 Local bond-slip curves of specimen bonded with sheet: a) Specimen CS-200-75; b) Specimen CS-200-112 181

Figure 5.10 Strain distribution along the bonded length of specimens: a) Specimen CL-200-25; b) Specimen CS-200-75; c) Specimen CS-200-112 183

Figure 5.11 Fatigue life and post-fatigue residual capacity of specimens with respect to the bond length 186

Figure 5.12 Predicted fatigue life of specimens by the modified model versus experimental data 191

Figure 5.13 Predicted fatigue life of specimens by Zhu et al. (2016) model versus experimental data 192

LIST OF ABREVIATIONS

ACI	American Concrete Institute
ASCE	American Society of Civil Engineers
ASTM	American Society for Testing and Materials
AFRP	Aramid Fiber Reinforced Polymer
BFRP	Basalt Fiber Reinforced Polymer
CFRP	Carbon Fiber Reinforced Polymer
CSA	Canadian Standards Association
DLA	Dynamic Loading Allowance
EB	Externally Bonded
FRP	Fiber Reinforced Polymer
FEA	Finite Element Analysis
FIB	Fédération Internationale du Béton
GFRP	Glass Fiber Reinforced Polymer
HCF	High Cycle Fatigue
HM	High Modulus
HS	High Strength
JCI	Japanese Concrete Institute
LCF	Low Cycle Fatigue
NES	Near End Supported
RC	Reinforced Concrete

LIST OF SYMBOLS

a	Endurance limit of FRP-to-concrete bond corresponding to 2 million load cycles
a_d	Debonding length
b_c	Concrete width
b_f	FRP width
E_c	Concrete elastic modulus
E_f	FRP elastic modulus
f_c' , f_{cm}	Cylindrical concrete compressive strength
f_{cu}	Cubic concrete compressive strength
f_f	FRP tensile strength
$f_{s.y}$	Steel yielding stress
f_t	Concrete tensile strength
$f_{u,b}$	Ultimate monotonic load-carrying capacity (kN)
$F_{\max}$	Maximum double-lap load ($F_{\max}$= 2 P_{ult})
G_c , G_f , $G_{f,s}$	Interfacial fracture energy
G_{int}	Interfacial shear modulus
H_{beam}	Beam height
k_b	Parameter related to the FRP-to-concrete width ratio (b_f/b_c)
K_b	Bond stiffness
K_0 , K_{b0}	Cyclic stiffness of the bond at cycle 1 (time zero)
K_t , $K_{b,t}$	Cyclic stiffness of the bond at load cycle n (time t)
K_{un}	Unloading bond stiffness

$K_{un,0}$, $K_{un.1}$	Unloading bond stiffness at cycle 1 (time zero)
$K_{un,t}$, $K_{un.i}$	Unloading bond stiffness at load cycle n (time t)
l_b , L_b	FRP length
l_e	Effective bond length
L_{beam}	Beam length
n	Number of load cycles
n_f	Number of FRP layers
N , N_f	Maximum number of load cycles until bond failure
N_b	Predicted number of load cycles until bond failure
$N_{\max}$	Maximum number of load cycles
$P_{\max}$	Upper limit of cyclic loading (kN)
$P_{\min}$	Lower limit of cyclic loading (kN)
P_u	Applied pull-out load
P_{ult}	Ultimate monotonic load-carrying capacity (kN)
$P_{\text{ult,1}}$	Calibrated monotonic ultimate load-carrying capacity (kN)
$P_{\text{ult,2}}$	Post-fatigue monotonic ultimate load-carrying capacity (kN)
s , s_i	Local bond slip (mm)
$s_{b.max}$	Slip corresponding to the maximum applied average bond stress ($\tau_{b.max}$)
$s_{b,t}$, s_{eu}	Cycle-dependent bond slip on the envelope bond-slip curve
s_f	Total slippage of FRP
s_{peak} , s_0	Bond slip at the maximum bond shear stress (mm)
s_{ult}	Ultimate bond stress (mm)

$s_{\mathrm{ult},0}$	Ultimate bond stress at load cycle 1 (time zero) (mm)
$s_{\mathrm{ult},t}$	Cycle-dependent ultimate bond slip at load cycle n (time t) (mm)
s_{un}	Bond unloading residual slip
S , S_f	Relative cyclic load amplitude
S_a , $S_{f.a}$	Relative mean cyclic load
S_b	Stress ratio ($S_{\max}/S_{\mathrm{ult}}$)
$S_{\max}$, $S_{f.max}$	Maximum stress applied to the CFRP sheet during cyclic loading
$S_{\min}$, $S_{f.min}$	Minimum stress applied to the CFRP sheet during cyclic loading
S_r , ΔS	Cyclic loading range ($S_{max} - S_{min}$)
S_{ult} , $S_{f.u}$	Ultimate stress in the CFRP sheet at midspan under monotonic loading
t	Cyclic loading time (in seconds)
t_f	FRP thickness
t_{int}	Interfacial thickness
T	Relative cyclic load amplitude
x_i	Distance of strain gauge from the free end of FRP
Δx_i	Distance between the two consecutive strain gauges at the two ends of each interval
β_w	Parameter related to the FRP-to-concrete width ratio (b_f/b_c)
ε_0	Strain at the free end of FRP
ε_i	Strain measured by the strain gauge
ε_f	FRP tensile elongation
τ , τ_i	Local bond stress (MPa)
$\tau_{b.max}$	Maximum applied average bond stress

$\tau_{b.ult}$	Average bond stress at the maximum load cycle
$\tau_{b,t}$, τ_{eu}	Cycle-dependent bond stress on the envelope bond-slip curve
$\tau_{f,\text{ave}}$	Average global bond stress (MPa)
τ_{max}	Maximum bond stress (MPa)
$\tau_{max.0}$	Maximum cyclic bond stress at cycle 1 (time zero) (MPa)
$\tau_{max.t}$	Maximum cyclic bond stress at load cycle n (time t) (MPa)
$\tau_{m,\text{peak}}$	Maximum peak bond stress during cyclic loading (MPa)
φ	Creep fatigue coefficient

INTRODUCTION

Many reinforced concrete (RC) structures such as RC bridge girders are expected to resist high number of fatigue load cycles that can be applied in the form of traffic loads during their service-life. Rehabilitation of existing structures to withstand cyclic fatigue loads has always been a major concern for engineers. A common failure mode that can be triggered by fatigue loading is shear failure which often occurs in an abrupt manner and without warning. This mode of failure is characterized by diagonal cracks that mostly initiate from near the supports and propagate to the loading point. The use of externally bonded (EB) fiber reinforced polymer (FRP) composites is widely accepted as an effective retrofitting technique for RC structures deficient in shear because of their numerous advantages such as high strength to weight ratio, corrosion resistance, fatigue resistance, lightweight and ease of application. One challenge of using EB-FRP retrofitting system on concrete surfaces centers around the bonding mechanism at FRP-to-concrete interface. Indeed, the occurrence of debonding failure, which is often observed in EB-FRP strengthened concrete structures, leads to the premature failure of FRP composites. To that end, investigation on the bond behavior of FRP-to-concrete interface can result in a better understanding of EB-FRP strengthened structures and therefore enhance the application of such retrofitting techniques. The existing publications regarding the use of EB-FRP strengthening system on concrete structures are mainly focused on the monotonic loading condition and therefore the fatigue behavior of such rehabilitated structures has not received adequate investigation. The present research project intends to incorporate up-to-date findings surrounding the bond fatigue behavior of FRP-to-concrete interface and look further into the complex interlaminar bonding mechanism of EB-FRP concrete structures during fatigue loading through an experimental program. The following chapters present an overview of the content discussed in this study:

- Chapter 1 gives a description of the context, problem statement, research objectives and methodology identified for the current project.

- Chapter 2 discusses the relevant design considerations and related findings derived from the literature regarding the behavior EB-FRP shear-strengthened RC structures.

- Chapter 3 presents a state-of-the-art article entitled “On bond-slip of EB-FRP/concrete interface in shear under fatigue loading: Review and Synthesis of experimental studies and models” which focuses on the influencing parameters affecting the interaction between FRP composites and concrete in EB-FRP shear-strengthened concrete structures under fatigue loading. Further discussions regarding the modeling of FRP-to-concrete bond stress-slip relationship and existing bond fatigue-life models are also included in this article.

- Chapter 4 presents a research investigation entitled “Experimental and Analytical Study of Bond Stress-Slip Behavior at the CFRP-to-Concrete Interface” which reports the results of an experimental program on a series of CFRP-to-concrete bonded joints under monotonic loading. Indeed, the bond behavior at CFRP-to-concrete interface is evaluated with respect to the affecting variables of CFRP type, bond length and CFRP-to-concrete width ratio. Also, through an analytical study based on the existing research data (from literature) as well as the current test results, a bond stress-slip model is proposed to capture the CFRP-to-concrete interfacial behavior under monotonic loading.

- Chapter 5 presents an article entitled “Fatigue Behavior of CFRP-to-Concrete Bond by Cyclic Pull-out Test: Experimental and Analytical Study” which incorporates the experimental observations regarding the fatigue behavior of CRRP-to-concrete bond. The influence of affecting parameters including CFRP composite type, bond length and CFRP-to-concrete width ratio on the fatigue bond behavior is examined and the experimental conclusions are presented accordingly. In addition, a bond fatigue-life prediction model (S-N model) is developed based on a database comprised of the experimental data in literature as well as the results of current study. The bond S-N model is then shown to perform well at predicting the long-term performance of CFRP-to-concrete bond during load cycles.

- Finally, the conclusions drawn from the current thesis project as well as the research recommendations for possible further investigation are summarized at the end.

CHAPTER 1

RESEARCH DESCRIPTION

1.1 Context

Many of the existing bridge structures in Canada and worldwide have been designed according to the initial design codes in which the permitted loads did not correspond with the increased service loads as a result of higher traffic volume nowadays. According to the Canadian National Highway System, out of over 8,000 bridges in Canada, 60% are more than 30 years old, around 4% are rated as being in poor condition, and 80% require some sort of retrofitting (Azim & Gül, 2019). Indeed, many of the deficient RC bridge structures have lost their resisting capacity due to the concrete deterioration phenomenon and corrosion of steel reinforcement. Hence, rehabilitation of these structures that are approaching the end of their service fatigue life is a major concern for civil engineers.

1.1.1 Shear failure and FRP strengthening technique

Shear failure of RC beams is mainly characterized by a single major diagonal crack along with several shear cracks, as indicated in Figure 1.1. This can also be accompanied by tension cracks due to the combined effects of flexural (bending) and shearing action. One of the most efficient ways for strengthening RC beams in shear is by using fiber reinforced polymer (FRP) composites. FRP materials generally have higher tensile strength compared to steel elements, as shown in Figure 1.2 (Carolin, 2003; El-Saikaly, 2015). Among FRP composites, carbon FRPs (CFRPs) can provide a relatively better performance in terms of stiffness (with high modulus “HM” CFRP) and tensile capacity (with high strength “HS” CFRP) in comparison with glass and aramid fibers (Carolin, 2003; Siddika, Al Mamun, Ferdous, & Alyousef, 2020). Also, the long-term fatigue resistance of CFRP materials has been reported to be superior to that of other FRP types (Z. Wu, Kim, Diab, & Wang, 2010). As far as the application of FRP system goes, these composites can be externally bonded to deficient RC beams for shear

strengthening purposes. In fact, externally bonded (EB) FRP strengthening technique has received significant attention among researchers for its numerous advantages such as high strength to weight ratio, corrosion resistance, fatigue resistance, lightweight and ease of handling (Aidoo, Harries, & Petrou, 2004; Kim & Heffernan, 2008). FRP composites can also be easily tailored into a variety of shapes and geometry, which makes them great retrofitting tools for existing bridge structures (Figure 1.3).

Figure 1.1 Shear failure of an RC beam
Taken from El-Saikaly and Chaallal (2015-b)

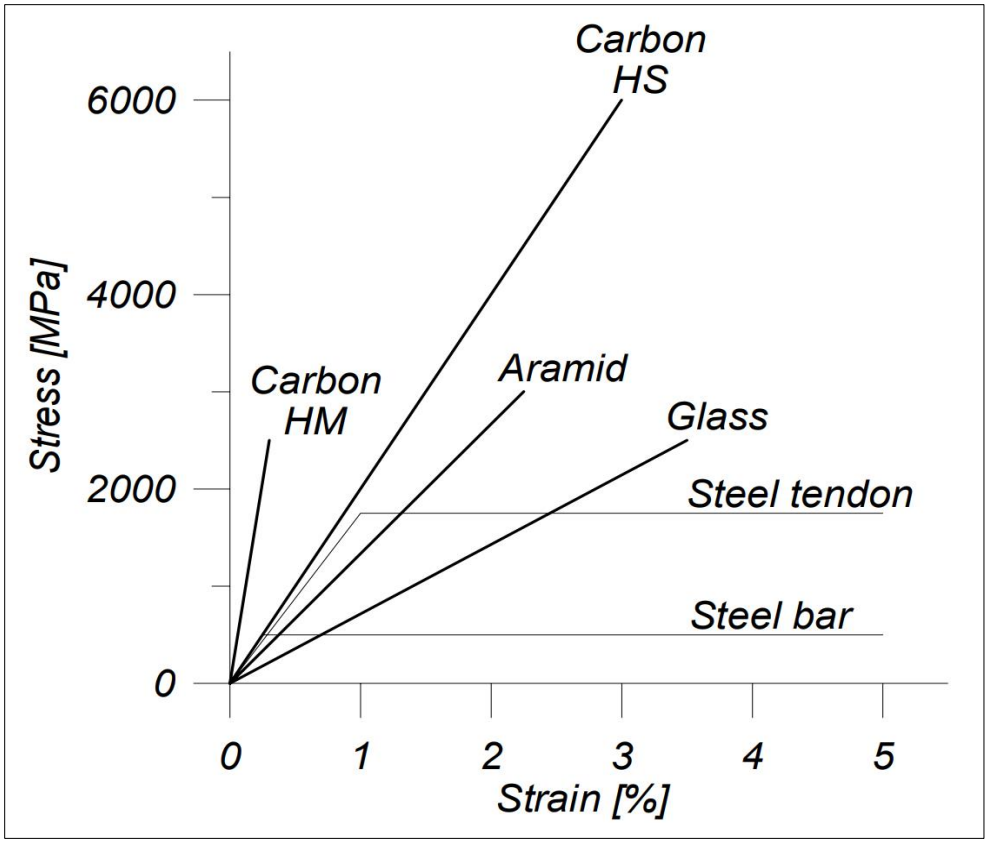

Figure 1.2 Idealized stress-strain curves of various FRP composites vs. steel
Taken from Carolin (2003)

Figure 1.3 Bridge strengthening with EB-FRP systems
Taken from Siddika et al. (2020)

1.1.2 EB-FRP configurations

A variety of FRP wrapping schemes have been used and investigated for shear strengthening of RC beams. Some of the most common schemes include complete wrapping, U-wrapping, side-bonding, as shown in Figure 1.4. Although, the full-wrapping FRP configuration is deemed to be the most effective retrofitting configuration, it is not generally practical in terms of construction limitations on real-world structural beams (Bae, Murphy, Mirmiran, & Belarbi, 2013). To that end, many FRP anchorage techniques have been introduced to improve the effectiveness of EB-FRP systems, such as L-shaped FRP laminates overlapped to the soffit of the beam (see Figure 1.5), which has been studied by El-Saikaly, Chaallal, and Benmokrane (2018).

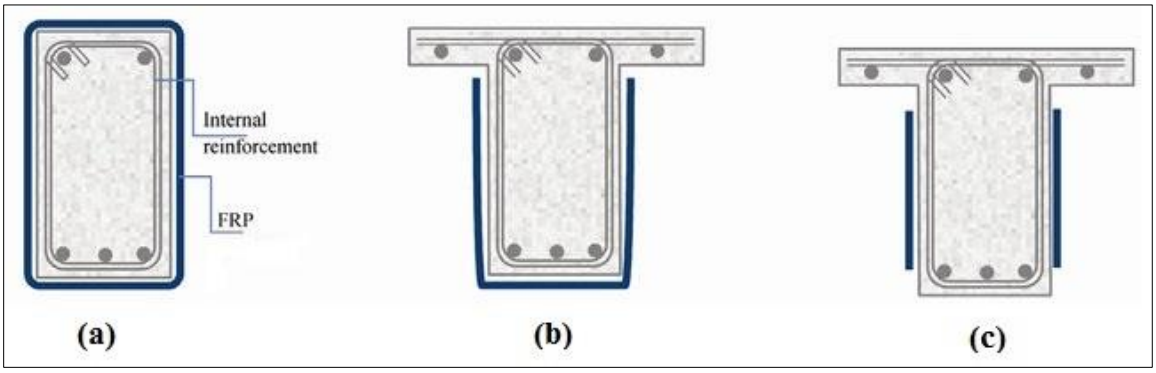

Figure 1.4 Wrapping schemes for EB FRP composites: a) complete wrapping; b) U-wrapping; and c) side bonding
Taken from Belarbi and Acun (2013)

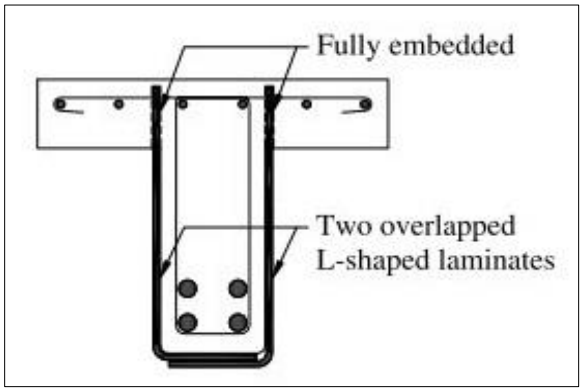

Figure 1.5 Overlapped L-shaped laminates
Taken from El-Saikaly et al. (2018)

Observations of using EB-FRP strengthening configurations show that bonding FRP composites to the tension faces of RC beams generally increases the flexural capacity and similarly, FRP retrofitting the lateral faces of the beam can enhance the shear capacity of the structure (Banjara & Ramanjaneyulu, 2019).

1.1.3 Debonding failure mode

EB-FRP shear-strengthened RC structures can undergo different failure modes including the debonding failure that typically occurs at the interface between FRP and the concrete substrate, as illustrated in Figure 1.6. Indeed, FRP debonding failure leads to the premature failure of the retrofitted structure by hindering the FRP materials from reaching their full capacity, and preventing their contribution to the shear resistance of the structure (El-Saikaly et al., 2018).

Figure 1.6 FRP debonding failure in an EB-FRP strengthened RC beam
Taken from El-Saikaly and Chaallal (2015-b)

The debonding failure of FRP-to-concrete interface in EB-FRP strengthened concrete structures can also be studied through the fracture mechanics criteria in terms of cracking propagation. In general, the cracking patterns can be divided in three modes according to fracture mechanics (see Figure 1.7), which include: Mode I) opening mode in which the tensile stress is normal to the plane of the crack; Mode II) shearing mode in which the shear stress is parallel to the plane of the crack and the movement of crack surfaces is perpendicular to the

crack front; and Mode III) tearing mode in which the shear stress is parallel to the plane of the crack and the movement of crack surfaces is also parallel to the crack front (Chaves, Da Silva, De Moura, Dillard, & Esteves, 2014; Xu et al., 2021). Indeed, the behavior of EB-FRP strengthened RC beams at service can be represented through mixed mode (I+II) fracture in terms of applied loading and cracking mechanism, as shown in Figure 1.8 (Chaves et al., 2014; Lee & Lopez, 2020).

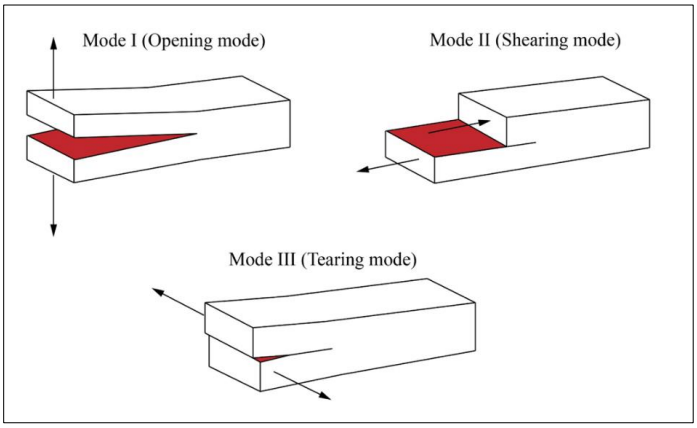

Figure 1.7 Modes of cracking pattern
Taken from Xu et al. (2021)

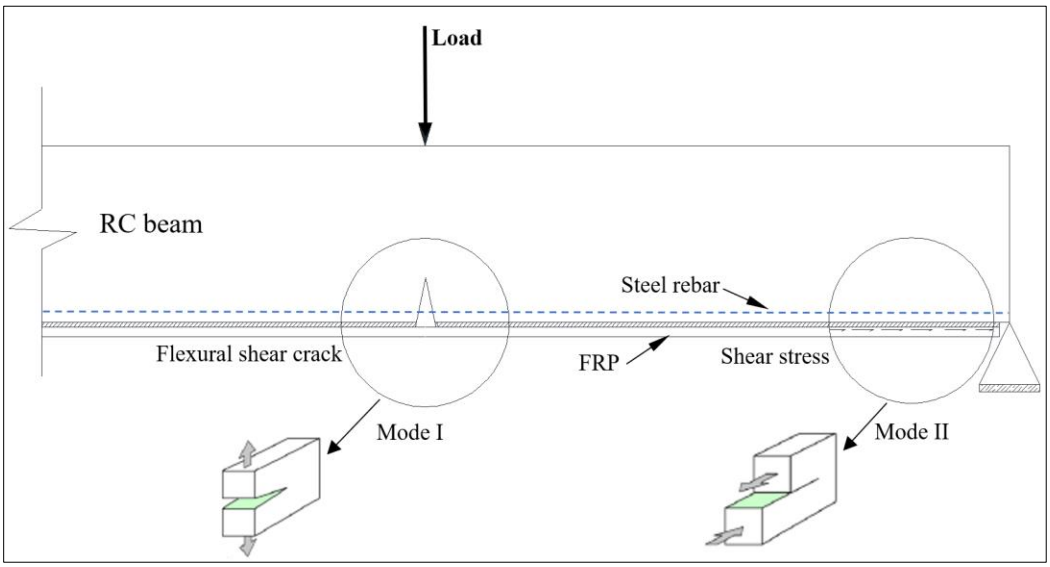

Figure 1.8 Cracking mode of an EB-FRP strengthened RC beam
Adapted from Lee and Lopez (2020)

1.1.4 Bond behavior at FRP-to-concrete interface

Since the performance of EB-FRP shear-strengthened RC structure depends greatly on the bonding mechanism of FRP composites on concrete surface, the study of FRP-to-concrete bond behavior can lead to an in-depth understating of such retrofitted structures. Indeed, some of the influencing parameters on the bond behavior of FRP-to-concrete interface include concrete strength, concrete surface preparation, FRP bond length, FRP-to-concrete width ratio, FRP material properties and thickness, anchorage systems, applied adhesive epoxy and environmental conditions (Abdalla, Mirghani, & Hawileh, 2020; De Lorenzis, Miller, & Nanni, 2001; Emmanuel Ferrier, Quiertant, Benzarti, & Hamelin, 2010; Maeda, Asano, Sato, Ueda, & Kakuta, 1997; Mazzotti, Savoia, & Ferracuti, 2008; McSweeney & Lopez, 2005; Nakaba, Kanakubo, Furuta, & Yoshizawa, 2001; C. Yuan, Chen, Pham, & Hao, 2019; P. Zhang et al., 2020). In fatigue loading conditions, the bond performance can also be greatly affected by the applied loading level in addition to the aforementioned variables (Bizindavyi, Neale, & Erki, 2003; Carloni, Subramaniam, Savoia, & Mazzotti, 2012; HM Diab, Wu, & Iwashita, 2009; Ko & Sato, 2007; K. Li, Cao, & Wang, 2015; K. Li, Cao, Yang, & Zhu, 2018; Xie, Wei, Huang, Zhang, & Chen, 2019; W. Zhang, 2018; Zheng, Huang, Chen, & Tan, 2015; Zhou, Fernando, & Dai, 2021; Zhu, Wang, Kang, & Li, 2016).

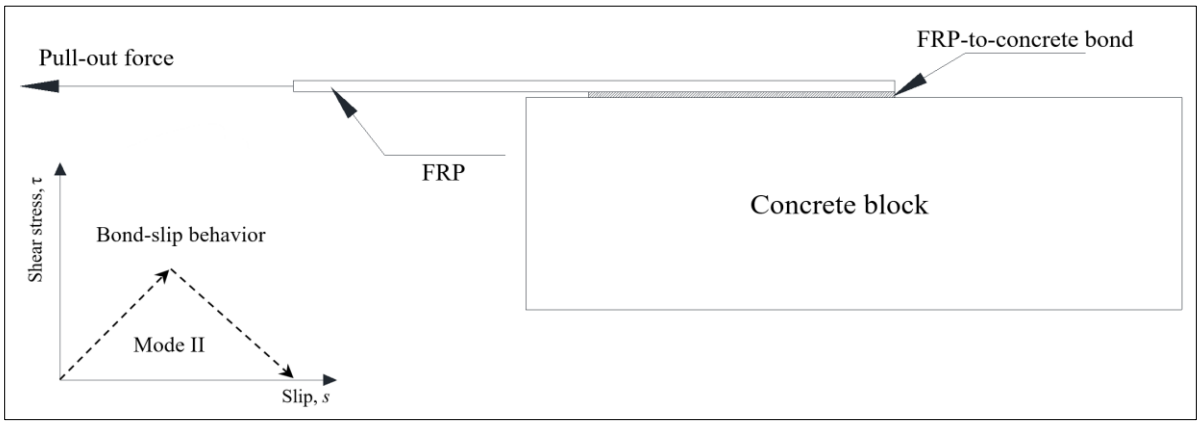

Figure 1.9 Bond-slip behavior in an FRP-to-concrete bonded joint

The bond behavior of FRP-to-concrete interface is generally investigated through pull-out tests in which a tensile load is applied to FRP-to-concrete bonded joints until the occurrence of

debonding failure (see Figure 1.9). Since, debonding occurs in the form of FRP composites sliding over concrete surface, Mode II fracture can be employed to represent the bond behavior. Indeed, bond stress-slip curves can be used to characterise the FRP-to-concrete bond behavior, which comprise of an ascending branch followed by a descending branch (Lu, Teng, Ye, & Jiang, 2005; Nakaba et al., 2001; Neubauer & Rostasy, 1999).

1.1.5 Fatigue life of EB-FRP retrofitted structures

The fatigue life of an FRP strengthened structure is defined as the number of fatigue load cycles that the structure can withstand at a particular stress level and is represented in the S-N curve of Wöhler in terms of stress versus the number of load cycles (typically in log).

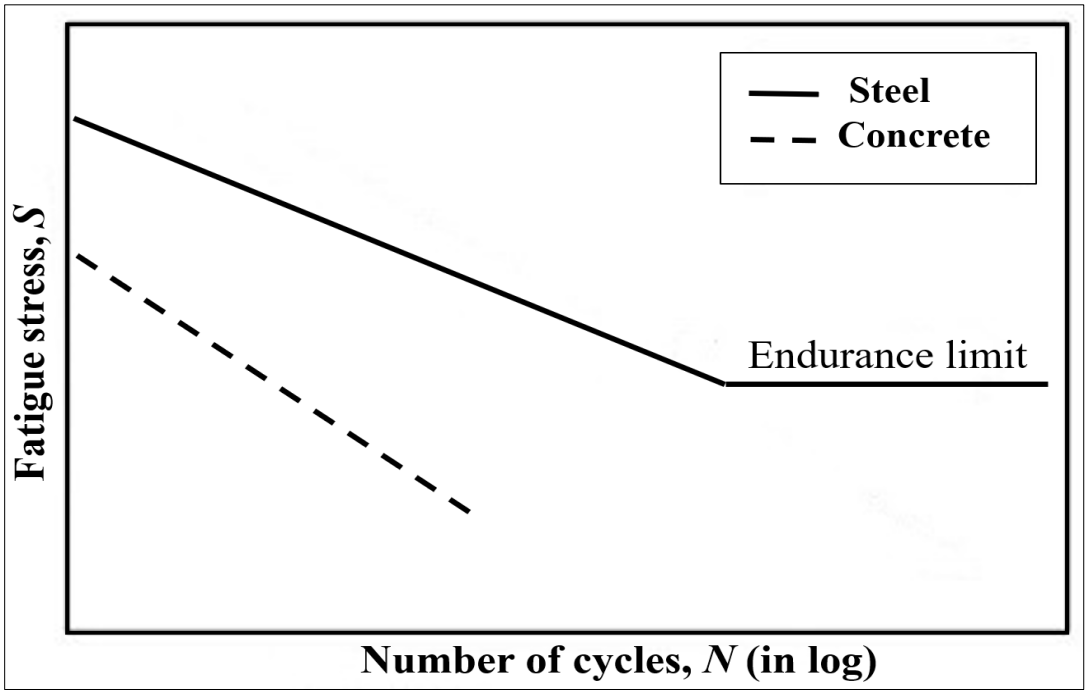

Figure 1.10 Schematic S-N curve of steel (in tension) and concrete (in compression)

Figure 1.10 indicates the S-N curves of steel versus concrete. As far as the fatigue life of steel goes, there is a downward trend in the S-N curve until a stress level at which the curve continues horizontally along the N axis (i.e., endurance limit). In other words, steel tends to resist an indefinite number of load cycles at its endurance limit. However, the S-N curve of

concrete appears to drop to its fatigue strength (Oudah & El-Hacha, 2013). More specifically, no endurance limit is observed in the fatigue life of concrete under 10 million load cycles. The fatigue strength of concrete in compression, tension or flexure under 10 million load cycles is reported to be approximately 55% of its monotonic strength according to the guidelines in ACI 215R (1974). As for FRP materials, a typical carbon FRP (CFRP) composite can exhibit an endurance limit of 60 to 70 percent of its initial monotonic ultimate strength, as stated in ACI 440.2R (2017).

1.1.6 Low and high cycle fatigue

A structure can undergo different number of fatigue load cycles during its service life. When the number of load cycles leading to failure of a material is low, the term low cycle fatigue (LCF) is used. On the other hand, in high cycle fatigue (HCF) loading condition, the material tends to reach its fracture point at higher number of cycles. Figure 1.11 indicates the stress levels versus the number of load cycles to failure in both LCF and HCF conditions. As can be seen, the material strains in HCF condition are mainly in the elastic region while under LCF loading, the material is expected to exhibit inelastic deformations (Homan, 2018). It is also noteworthy that structures in real-life situations, such as bridges, are likely to fail under HCF conditions. This is because the majority of the load applied to bridge structures stems from the low amplitudes of traffic (Karunananda, Ohga, Dissanayake, & Siriwardane, 2011).

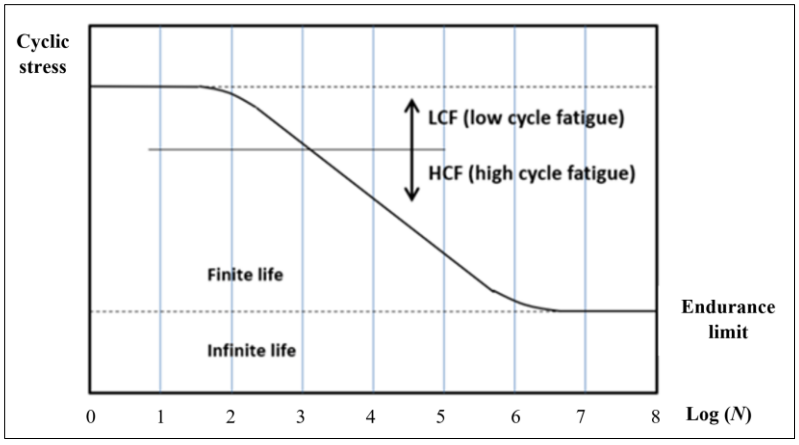

Figure 1.11 S-N curve in LCF and HCF conditions
Adapted from Homan (2018)

1.2 Problem Statement

A review of existing literature implies that investigation on the behavior of FRP-strengthened RC structures in shear under fatigue loading has not been as much documented as that under monotonic loading conditions. In addition, the bond fatigue behavior at FRP-to-concrete interface may require further assessment with respect to the influencing parameters, so that reliable bond-slip models, validated with experimental data, can be proposed to better characterise the interfacial interaction of FRP-to-concrete bond. To that end, the current research aims to address the following gaps in the field of EB-FRP strengthening of concrete structures, with a focus on the bond fatigue behavior of FRP-to-concrete interface:

- Most of the studies regarding the FRP-to-concrete bond behavior in EB-FRP shear-strengthened RC structures have been conducted under monotonic loading and limited investigation has been carried out on the fatigue performance EB-FRP retrofitting systems on RC structures.

- Existing literature lacks a comprehensive state-of-the-art research review incorporating the up-to-date findings regarding the bond behavior of FRP-to-concrete interface under fatigue loading as well as the numerical modelling of bond fatigue behavior.

- The FRP-to-concrete bond behavior needs to be further examined with respect to the influencing parameters and their contribution in governing the bond performance (e.g., bond strength, bond-slip relationship, and effective bond length) needs to be determined.

- There is a need for a reliable FRP-to-concrete bond-slip model that can capture the shear interaction between concrete and FRP with reasonable accuracy under both monotonic and fatigue loading conditions.

- The fatigue life of FRP-to-concrete bond in EB-FRP strengthened concrete beams has not been adequately investigated. Thus, reliable S-N relationships of the bond need to be developed to predict the fatigue life of such rehabilitated structures.

1.3 Research objectives

With respect to the research gaps in the field of EB-FRP shear-strengthening of RC structures, the current research study is intended to pursue the following main and specific objectives:

1.3.1 Main objective

- To investigate the bond behavior of FRP-to-concrete interface in EB-FRP shear-strengthened concrete structures under both monotonic and cyclic loading through an experimental program.

1.3.2 Specific objectives

- To identify the influencing parameters affecting the bond behavior of FRP-to-concrete interface in EB-FRP shear-strengthened RC beams.

- To evaluate the FRP-to-concrete bond behavior with respect to the influencing parameters through pull-out shear tests under both monotonic and cyclic loading conditions.

- To develop new bond-slip models of FRP-to-concrete interface, validated with adequate research data and capable of characterising the interfacial interaction between FRP composites and concrete (under monotonic loading).

- To establish a S-N relationship of Wöhler to predict the fatigue life of FRP-to-concrete bond and thereby determine the service life of RC structures strengthened in shear with EB-FRP composites.

1.4 Methodology

An overview of the methodology for the current research project is shown in Figure 1.12. A review of the latest studies in the field of shear strengthening of RC structures with EB-FRP reinforcement is required for pursuing the objectives specified in this research. To this end, a literature review is first conducted to identify the influencing parameters on the bond behavior of FRP-to-concrete interface and determine the research gaps in this area. Following that, an experimental investigation is carried out to investigate the CFRP-to-concrete bond behavior under both monotonic and fatigue loading. Indeed, a series of double-lap pull-out shear tests are performed on CFRP-to-concrete bonded joints. These tests are targeted to evaluate the effect of the influencing parameters of bond length, CFRP composite type (laminate vs. fabric sheet) and CFRP width on the bond behavior of specimens under both monotonic and cyclic loading. The testing outline as well as the evaluating variables are shown in Figure 1.13.

As can be seen, the bonding performance of two different types of EB-CFRP strengthening systems is evaluated on a total of 24 concrete blocks (250 mm × 150 mm × 150 mm). Figure 1.14 shows the two CFRP composite types used in the experimental program, which include: 1) SikaWrap Hex -103C (cured with Sikadur -300 Epoxy), referred to as CFRP sheet; and 2) Sika CarboDur S512 as CFRP laminate. The CFRP width, b_f, of all laminates (Sika CarboDur) is set to be 25 mm. In order to conduct a rational comparison between the performance of the two EB-CFRP strengthening systems, the two CFRP composites (laminate and sheet) are designed to reach the same FRP tensile stiffness ($f_f \times t_f \times b_f$). To that end, the equivalent width of CFRP sheet (SikaWrap Hex -103C cured with Sikadur -300) can be taken as 75 mm. Also, four different bond length values of 50 mm, 100 mm, 150 mm and 200 mm are selected for the specimens. It is, in fact, anticipated that the effective bond length of specimens is achieved within the range between 50 mm and 200 mm during the experiments based on the existing models (ACI 440.2R, 2017; J. F. Chen & Teng, 2001; CSA S806, 2012; *fib* TG5.1, 2019; JCI, 2003; Maeda et al., 1997; Neubauer & Rostasy, 1999; Niedermeier, 1996; Pellegrino, Tinazzi, & Modena, 2008; Z. Wu, Islam, & Said, 2009; H. Yuan, Teng, Seracino, Wu, & Yao, 2004). It should be noted that in order to investigate the effect of CFRP-to-

concrete width ratio (b_f/b_c) on the bond behavior, two different widths of 75 mm and 112 mm are allocated to the specimens with CFRP sheet which correspond to the two CFRP-to-concrete width ratios of 0.5 and 0.75, respectively, in the current experiments. An MTS machine, as shown in Figure 1.15 is used to apply pull-out forces to the specimens and all data will be captured by the strain gauges that are affixed along the CFRP.

During the monotonic testing, the ultimate load-carrying capacity of each CFRP-to-concrete bonded specimen is determined, and the failure modes are observed. Test results will be mainly presented in terms of bond stress-slip relationship and strain distribution curves along the bonded length. Furthermore, the effect of above-mentioned parameters are examined on the bonding mechanism of CFRP-to-concrete interface under monotonic loading condition.

Upon revealing the monotonic results, the cyclic testing program (LCF with the loading rate of 3 Hz and up to 2 million load cycles) is initiated to discover the fatigue life of CFRP-to-concrete bonded joints. The long-term performance of specimens is examined through the observation of fatigue failure modes as well as strain distribution profiles along the bond length during load cycles. Furthermore, a post-fatigue monotonic testing is performed on CFRP-to-concrete bonded joints enduring over 2 million cycles for the purpose of evaluating their residual capacity and interfacial responses.

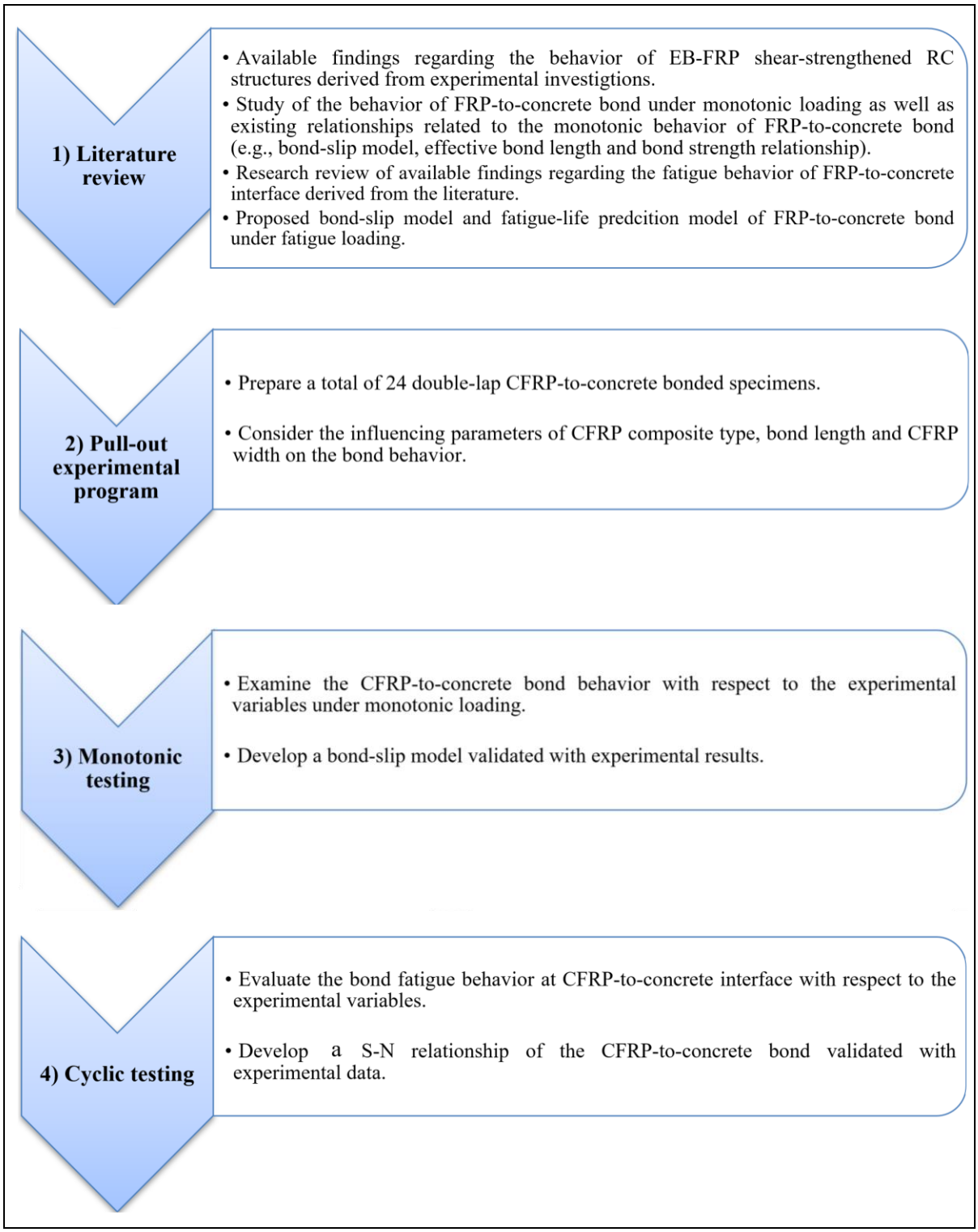

Figure 1.12 Methodology of the doctoral research project

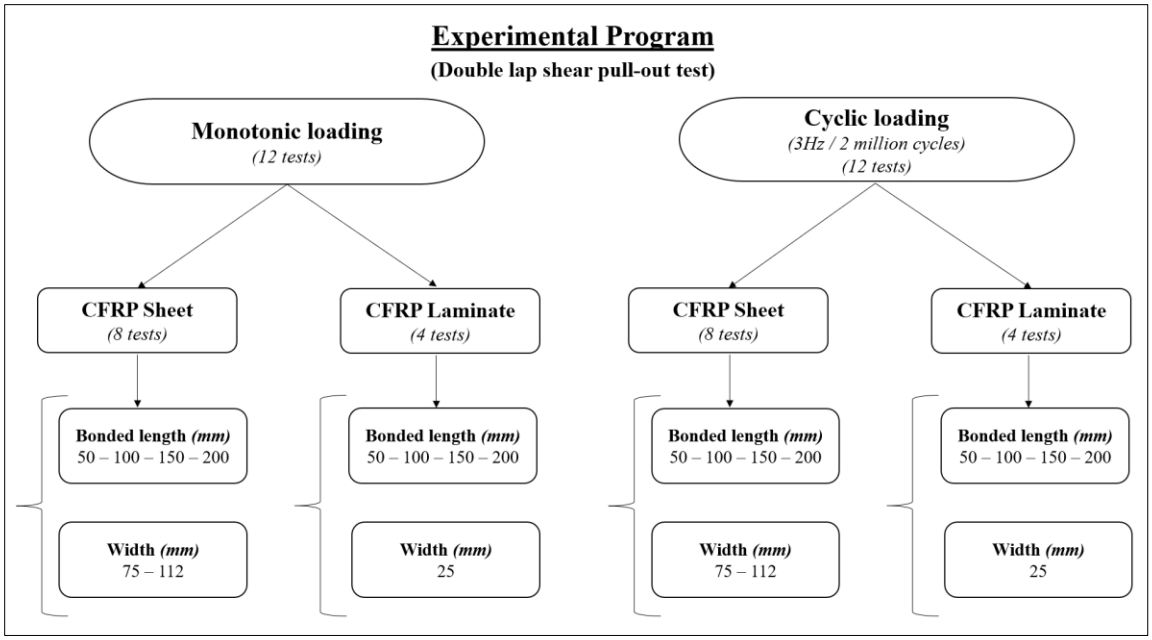

Figure 1.13 Experimental program identified within the doctoral research

Figure 1.14 CFRP composites used in the experimental program

Figure 1.15 MTS loading machine

CHAPTER 2

RESEARCH BACKGROUND

2.1 Design Considerations

For FRP-strengthened RC structures to withstand fatigue loading during their service life, certain design considerations need to be taken to ensure their long-term performance. To this end, the fatigue state limits of EB-FRP strengthened RC bridge structures, as well as fatigue stress limits of individual structural components (i.e., steel, concrete and FRP materials), derived from available design codes, are summarised in the following.

2.1.1 Fatigue state limit of EB-FRP strengthened bridge structures

Regarding the fatigue service-load condition of a structure under daily traffic (e.g., bridge structure), the typical upper and lower loading limits ($P_{\max}$ and $P_{\min}$) can be determined using the following equation (Chaallal, Boussaha, & Bousselham, 2010; El-Saikaly & Chaallal, 2015-c; El-Saikaly et al., 2018):

$$P_{\max} = P_{\text{mean}}(1 + DLA) \quad , \quad P_{\min} = P_{\text{mean}}(1 - DLA) \tag{2.1}$$

As can be noted, the loading limits evolve with respect to the mean load value, P_{mean}, estimated to be 50% of the ultimate load-carrying capacity of the structure (i.e., $P_{\text{mean}} = 0.5\, P_{\text{ult}}$), corresponding to the passage of a standard vehicle at a crawling speed. Also, DLA is the dynamic loading allowance that is ranged between 0.25 and 0.4 depending on the axle number of CL-W Truck used on the structure (see Figure 2.1), as stated in CSA S6 (2019).

Also, according to *fib* TG5.1 (2019), the fatigue damage on EB-FRP strengthened RC members is not considered to be significant if the applied service loading range lies between 30% and 60% of the load required to induce the first yield of the member. Indeed, structural damage can

occur when the maximum applied load exceeds 60% of the member's yield capacity (*fib* TG5.1, 2019).

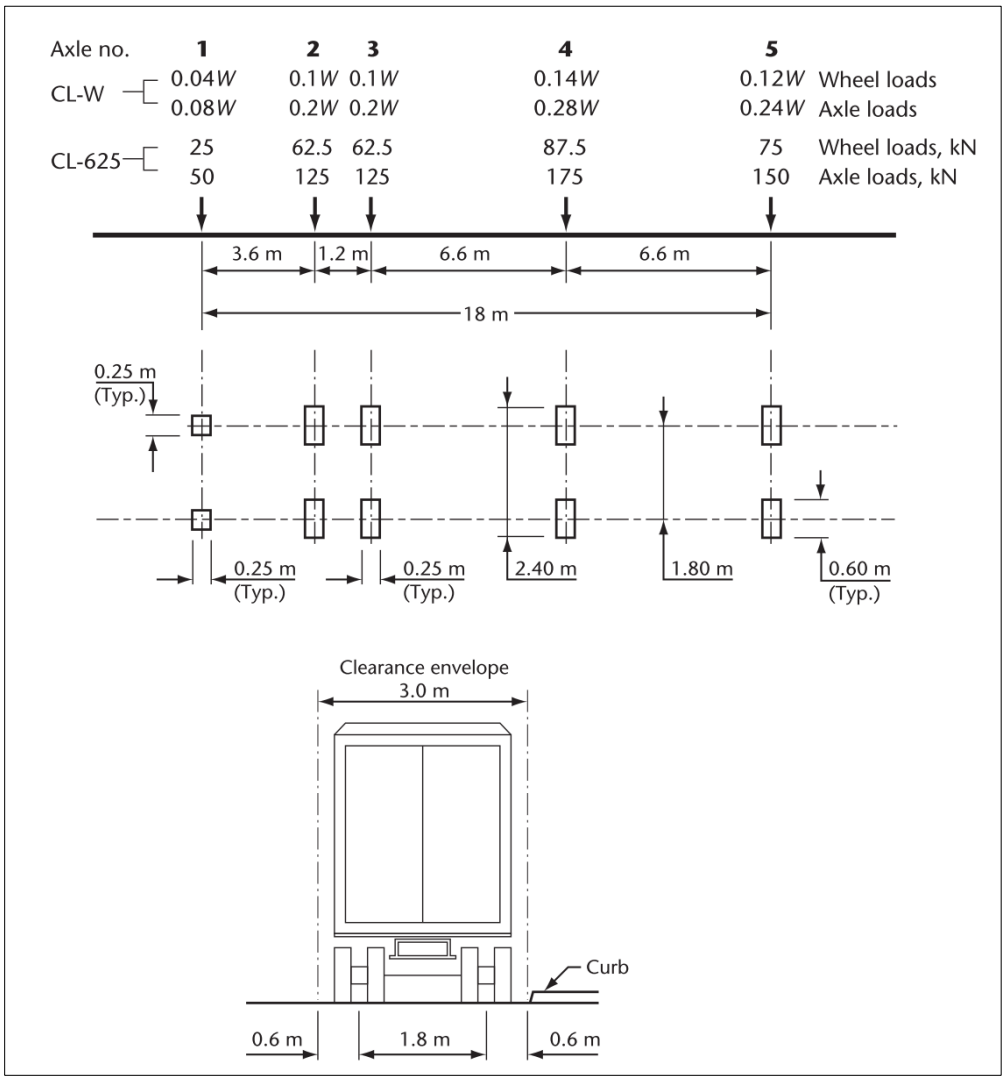

Figure 2.1 CL-W Truck
Taken from CSA S6 (2019)

2.1.2 Fatigue stress limit of steel reinforcement

It is well-established that the fatigue resistance of internal steel reinforcing bars in EB-FRP strengthened RC structures, in flexure, is the dominant factor in the establishment of the fatigue life of such structures (Barnes & Mays, 1999; Brena, Benouaich, Kreger, & Wood, 2005;

Ekenel & Myers, 2009; Heffernan & Erki, 2004; Masoud, Soudki, & Topper, 2001; Siddika et al., 2020; Toutanji, Zhao, Deng, Zhang, & Balaguru, 2006). Based on the recommendations found in *fib* TG5.1 (2019), the criteria for designing the strengthened structures in fatigue condition is to keep the allowable stress range limit of steel reinforcement the same as that permitted in the corresponding unstrengthened structure.

The stress range of straight steel reinforcement (S_r) must conform to the following relations according to ACI 215R (1974) and AASHTO (2017):

$$S_r = \begin{cases} 161 - 0.33\,S_{\min} & \text{(in MPa)} \\ 24 - 0.33\,S_{\min} & \text{(in ksi)} \end{cases} \tag{2.2}$$

where $S_{\min}$= algebraic minimum stress level in steel reinforcement, tension positive, compression negative, under service load and S_r= steel stress range. It is noteworthy that according to the specifications in ACI 215R (1974), the permissible steel stress range of reinforcing bars (S_r) is equal to 138 MPa, whereas CSA S6 (2019) suggests that the highest stress range limit in steel longitudinal reinforcement does not exceed 125 MPa. The guidelines in ACI 440.2R (2017) also mention that to avoid inelastic deformations of RC structures strengthened in flexure with EB-FRP under cyclic service loads, the fatigue stress level of reinforcing bars should be kept below 80% of their yield stress. Because the fatigue stress limit of steel stirrups in FRP-strengthened RC beams has not been specified in the current design guidelines, experimental results of research studies have shown that the stress limit of transverse steel reinforcement under fatigue conditions can be considered equal to that of the longitudinal steel bars (Barnes & Mays, 1999; El-Saikaly & Chaallal, 2015-a).

2.1.3 Fatigue stress limit of FRP and concrete

According to ACI 440.2R (2017), the fatigue stress limit of FRP reinforcement must be kept below the sustained plus cyclic stress limit, which is 20%, 30%, and 55% of the ultimate FRP strength for glass FRP (GFRP), aramid FRP (AFRP), and CFRP respectively, whereas the CSA

S6 (2019) specifications state that the maximum stress limits for GFRP, AFRP, and CFRP under fatigue conditions should be taken equal to 25%, 35%, and 65% of the FRP capacity respectively.

Considering the fatigue stress limit of concrete, it is specified in ACI 215R (1974) that the design criterion for RC structures in flexure under fatigue loading should be to limit the concrete stress range to 40% of its compressive strength. Moreover, the guidelines in ACI 440.2R (2017) state that the compressive stress limit of concrete needs to be 60% of its strength in RC structures strengthened with EB-FRP under cyclic service loads.

Since the weak link at the FRP/concrete interface of FRP-strengthened RC structures is the concrete substrate, the bond strength of the interface between concrete and FRP is greatly affected by the tensile strength of concrete. Therefore, the effectiveness of an externally bonded FRP system is mainly governed by the tensile strength and soundness of concrete (ACI 440.2R, 2017). It is recommended that the minimum required tensile strength of concrete in EB-FRP applications be greater than 1.5 MPa (CSA S6, 2019; *fib* TG5.1, 2019).

2.2 Literature Review

A review of the existing investigations in the field of EB-FRP shear-strengthening of RC structures under fatigue loading is presented in the following sections. Furthermore, the up-to-date findings related to the behavior of FRP-to-concrete interface are analyzed in this chapter. To that end, the reported experimental observations regarding the performance of EB-FRP shear-strengthened RC beams under cyclic loading with respect to the investigated parameters are first discussed. Following that, the state-of-the-knowledge on the bond behavior at FRP-to-concrete interface is presented in which the influencing parameters on the bond mechanism, bond-slip relationships and bond fatigue-life models are discussed in detail.

2.2.1 Experimental studies of the performance of EB-FRP shear-strengthened RC beams under fatigue loading

It has been widely accepted that using FRP composites results in increasing the fatigue life of strengthened RC beams in flexure (Aidoo et al., 2004; Barnes & Mays, 1999; Papakonstantinou, Petrou, & Harries, 2001; Shahawy & Beitelman, 1999). Indeed, the fatigue resistance of steel longitudinal bars has been reported to be the dominant factor in determining the fatigue life of RC beams strengthened with EB-FRP in flexure (Harries (2005) H Diab and Wu (2008) Y. Dong, Ansari, and Karbhari (2011) Oudah and El-Hacha (2013) Xin Wang, Sayed Ahmed, and Wu (2014) Al-Qaralleh and Toutanji (2018). As for shear strengthening RC beams under fatigue loading, experimental studies have shown that the application of EB-FRP retrofitting systems results in enhancing the long-term performance and shear resistance of such structures during load cycles (El-Saikaly & Chaallal, 2015-a; El-Saikaly et al., 2018; Farghal, 2014). As far as the fatigue failure mode of EB-FRP strengthened RC structures in shear goes, different failure patterns have been inspected during experimental investigations which include crushing of concrete struts, debonding of FRP from concrete, yielding and fracture of longitudinal tensile steel bars, and steel stirrup rupture (Chaallal et al., 2010; El-Saikaly & Chaallal, 2015-b).

Experimental investigations on the shear performance of RC beams retrofitted with FRP composites have been mainly conducted in the form of three-point or four-point bending test-setup (Bae et al., 2013; Chaallal et al., 2010; Czaderski & Motavalli, 2004; J. Dong, Wang, & Guan, 2012; El-Saikaly & Chaallal, 2015-a, 2015-b; El-Saikaly et al., 2018; Farghal, 2014; Williams & Higgins, 2008). The available research studies regarding the shear strengthening of RC beams with EB-FRP techniques are discussed in the following:

Czaderski and Motavalli (2004)

Czaderski and Motavalli (2004) conducted an experimental investigation in the shear-strengthening behavior of RC beams using CFRP L-shaped plates under 5 million cycles of

fatigue loading. Moreover, a design model was proposed for the performance of CFRP L-shaped plates in shear-strengthening the RC structures. On the basis of the experimental observations, the following conclusions were made: 1) no damage was apparent to the CFRP L-shaped plates during 5 million load cycles of the fatigue experiment. 2) the applied cyclic stresses resulted in an increase in the strain levels of CFRP L-shaped plates as well as the beam deflection. 3) the CFRP strain accumulation mainly occurred in the initial stage of the fatigue loading experiment unlike the beam deflection that experienced an approximate constant increase.

Williams and Higgins (2008)

An experimental investigation was carried out by Williams and Higgins (2008) through a field inspection of an in-service bridge RC deck girder (RCDG) to evaluate the fatigue behavior of RC T-beams retrofitted in shear using externally bonded CFRP under repeated loads. In addition, laboratory tests were conducted on five specimens, including two control specimens loaded monotonically and three ones subjected to fatigue loading with varying load amplitudes up to 1 million cycles. The aforementioned investigation led to the following conclusions: 1) according to the observations on the behavior of all tested specimens, it was revealed that the ultimate strength capacity of fatigue specimens did not undergo a significant change compared to that of the unfatigued specimens; 2) use of vertical CFRP strips resulted in a decrease in the service stress level of steel stirrups. However, no reduction was observed in the flexural steel stress level; and 3) it was recommended that the field inspection of bridge girders be done on the terminating edges of CFRP strips at the deck stem interface for the observation of debonding occurrences.

Chaallal et al. (2010)

The fatigue performance of CFRP strengthened RC beams was investigated through an experimental study involving six laboratory tests by Chaallal et al. (2010). Their experimental program consisted of specimens with no FRP (control), 1 layer and 2 layers of CFRP sheets

labeled as “0L”, “1L” and “2L”, respectively. The existence of internal steel stirrups was specified in the specimens with the symbol “S” where “S0” specimens had no stirrups and “S1” specimens were reinforced with steel stirrups. All specimens were subjected to an upper limit of 5 million load cycles. Test observations indicated that the existence of CFRP contributed to extending the fatigue life of RC beams under cyclic loads. It was also demonstrated that specimens with two layers of CFRP ended in failure well below 5 million load cycles unlike the one CFRP-layered specimens that survived through the whole duration of 5 million cycles and their failure mode was a combination of concrete strut crushing, FRP debonding and transverse steel reinforcement yielding. This could be due to the higher loading amplitude applied to specimens or the higher FRP rigidity that might have made changes to the stress distribution process among the influencing structural components. Finally, it was observed that the presence of steel stirrups extended the fatigue life of beams (for both un-retrofitted and retrofitted with CFRP) when compared to the corresponding specimens without transverse steel reinforcement.

J. Dong et al. (2012)

An experimental study was conducted by J. Dong et al. (2012) on the shear fatigue behavior of RC beams retrofitted with FRP sheets. To that end, 5 rectangular RC beams were prepared and tested under four-point cyclic loading set-up. As for FRP strengthening, CFRP and GFRP sheets were bonded with two different vertical and diagonal fiber orientations to the beam longitudinal direction. It was observed that the EB-FRP system performed well at increasing the shear fatigue resistance of the RC beam when compared to the unstrengthened beam (reference beam). Furthermore, EB-FRP strengthened beams showed fewer shear cracks and higher rigidity in comparison with the reference beams. As for the FRP configurations, the diagonal fiber arrangement was seen to outperform the vertical arrangement in terms of improving the shear capacity and beams stiffness under fatigue loading.

Bae et al. (2013)

Bae et al. (2013) carried out an experimental research program on the shear strengthening of RC beams using FRP sheets under cyclic loading. They tested three specimens: one unstrengthened beam subjected to monotonic loading, one shear-strengthened beam with FRP under monotonic loading and one FRP shear-strengthened specimen under cyclic loading. Taking into consideration the assumption that many existing RC beams that need shear retrofitting are deficient in shear capacity due to the lack of sufficient steel stirrups, the applied load range was set to cause yielding of some stirrups from the outset of cycling loading in the test. On the basis of observations from the experiments, it was concluded that CFRP sheets resulted in a 26.3% increase in shear capacity of the strengthened beam compared to the unstrengthened one. Moreover, it was seen that the location of FRP strips with respect to the shear critical crack has a major effect on the stress level of the FRP, which is one of the challenges for developing an analytical model for calculating the FRP shear contribution using the effective strain concept. It was also suggested that in order to prevent the occurrence of debonding failure at FRP/concrete interface in normal strength concrete blocks, the interfacial stress level of CFRP strip be limited to less than 1.5 MPa or 25% of the ultimate FRP/concrete interfacial strength.

Farghal (2014)

Farghal (2014) conducted an experimental investigation on the fatigue performance of RC T-shaped beams strengthened in shear with CFRP composites. The two CFRP strengthening configurations of side-bonded, and U-wrap were used. Also, the effect of transverse steel reinforcement was examined. It was observed that using EB-CFRP shear strengthening systems enhanced the fatigue life of RC beams. Furthermore, the use of U-jacket CFRP configurations changed the failure mode from brittle to the desirable ductile mode. As for the effect of steel stirrups on the long-term performance of strengthened beams, the fatigue life of the tested beams was seen to improve with the presence of transverse steel reinforcement.

El-Saikaly and Chaallal (2015-a)

El-Saikaly and Chaallal (2015-a) investigated the fatigue performance of RC beams strengthened in shear using L-shaped CFRP laminates through a number of experimental tests on specimens with various stirrup spacing values. The cyclic loading range was set between 35% and 65% of the monotonic capacity of each specimen. It was found that L-shaped FRP laminates contributed to an improvement in the fatigue life of strengthened beams in comparison with the unstrengthened counterparts. According to their observations, the fatigue degradation of specimens increased at a relatively significant rate during the initial loading cycles (within 0.5 million cycles) and then the damage accumulation occurred very slowly up to the imminent failure of the beam. Taking the effect of transverse steel reinforcement ratio into account, it was observed that specimens with lower stirrup spacing values showed more cumulative fatigue degradation or damage compared to the ones with higher stirrup spacing values, which is due to their higher capacity to resist applied fatigue loading. Furthermore, comparisons between the performance of the strengthened and unstrengthened specimens revealed that lower strain was experienced by the transverse steel reinforcement of strengthened beams than that of the unstrengthened beams, which corroborates the occurrence of stress redistribution between transverse reinforcing steel and EB FRP composites under fatigue loading. Finally, it was concluded that L-shaped FRP laminates performed satisfactorily for their resistance against debonding during fatigue loading and for their effective contribution in changing the shear failure mode of the beam with steel stirrups from brittle to ductile mode under post-fatigue monotonic loading.

El-Saikaly and Chaallal (2015-b)

In another experimental study done by El-Saikaly and Chaallal (2015-b), nine laboratory tests were conducted to investigate the fatigue behavior of RC T-beams retrofitted in shear with EB CFRP sheets and evaluate the possibility of using the EB CFRP shear strengthening systems for two purposes: (i) upgrading the service load applied to RC structures (category A); and (ii) rehabilitating the existent RC structures with no increase in applied load (Category B). During

the experimental tests a variety of specimen types including unstrengthened specimens (Control), specimens with CFRP plies (U-wrap) and specimens with different steel stirrup spacing values were loaded to an upper limit of 6 million fatigue cycles. According to the results derived from the tests, it was concluded that using EB FRP technique led into a substantial increase in the fatigue life of specimens whose behavior was examined for the purpose of repairing (Category B). Furthermore, the beams tested for the purpose of upgrading (Category A) exhibited a satisfactory performance when subjected to higher cyclic loads in comparison with the control specimens. The authors also suggested that an upper stress limit (i.e., 200 MPa) for steel stirrups in unstrengthened RC beams be specified in the current guidelines to avoid steel stirrup rupture under fatigue loading. Moreover, shear-strengthened specimens with steel stirrups of Category A exhibited a flexural fatigue failure by rupture of longitudinal steel. Therefore, the longitudinal steel may be the weakest link and should be looked with caution for extended service life of shear-strengthened RC structures with EB-FRP, as already observed by other researchers but for strengthening in flexure. Finally, it was observed that the existence of steel stirrups significantly reduced the shear contribution ratio of CFRP sheets in the specimens; this is attributable to the existence of stress redistribution between the internal transverse steel reinforcement and the EB CFRP composites, which is not yet captured in the design equations of guidelines.

El-Saikaly and Chaallal (2015-c)

During an experimental investigation on six T-shaped RC beams by El-Saikaly and Chaallal (2015-c) , the performance of two EB-CFRP shear-strengthening configurations (i.e., laminate vs. sheet) was examined under fatigue loading and post-fatigue monotonic loading. The reported observations include: a) the application of both EB-CFRP systems successfully prevented the debonding failure during the entire cyclic loading (i.e., 6 million cycles); b) the majority of fatigue damage accumulation, which was represented by the beam deflection at mid-span, took place in the initial load cycles (i.e., during the first 0.5 million cycles); c) the use of L-shaped CFRP laminates on RC beams has shown to be more effective in resisting the fatigue loading in terms of cyclic deflection and fatigue damage accumulation, when compared

to the performance of specimens strengthened with U-wrapped CFRP sheets; and d) The existence of inverse interaction between the EB-CFRP composites and steel stirrups was evidenced through the reduced shear contribution of CFRPs in beams with internal shear reinforcement under both fatigue and post-fatigue monotonic loading conditions.

El-Saikaly et al. (2018)

El-Saikaly et al. (2018) conducted an experimental investigation on the effectiveness of an innovative shear-strengthening technique of RC beams known as EB-CFRP closed stirrups under fatigue loading to reproduce the advantage of a full-wrap scheme. Their experimental program consisted of unstrengthened specimens (control specimens), specimens shear-strengthened with EB L-shaped CFRP laminates and anchoring ropes (EB L-shaped FRP closed stirrups or EBL CS) and specimens retrofitted with EB L-shaped CFRP laminates fully embedded along the beam web (EB L-shaped CFRP full embedment or EBL FE). The effect of transverse steel reinforcement was also taken into consideration in the tests by applying specimens with no steel stirrups and two different spacing values. Observations from the tests demonstrated that the use of shear-strengthening systems either by EBL CS or EBL FE resulted in a development in the ductile behavior of the beam and transformed the shear failure behavior from brittle to a more ductile mode under monotonic loads. Furthermore, it was observed that the L-shaped strengthening techniques performed well in preventing the premature CFRP debonding failure throughout the whole duration of fatigue loading and led into an increase in the load carrying capacity of strengthened beams compared to control specimens. Further assessment of experimental results revealed that addition of transverse steel reinforcement reduced the rate of growth of the strain levels in CFRP laminates under fatigue loading, which is attributed to the stress redistribution between steel stirrups and EB FRP composites. Finally, a comparison between the performance of EBL CS and EBL FE strengthening systems showed that L-shaped CFRP closed stirrups exhibited a better performance than full-embedded L-shaped CFRP laminates in reducing the internal steel stirrup strain levels and improving its shear behavior under cyclic loading.

Table 2.1 summarizes the details of experimental investigations on the fatigue performance of EB-FRP shear-strengthened RC beams under fatigue cyclic loading, from selected research studies discussed above.

Table 2.1 Summarized details of experimental studies on EB-CFRP shear-strengthened RC beams under fatigue loading from selected research studies

Authors	Czaderski and Motavalli (2004)	Williams and Higgins (2008)	Chaallal et al. (2010)	J. Dong et al. (2012)	Bae et al. (2013)	Farghal (2014)
Number of laboratory tests	1	5	6	5	3	12
Fatigue loading condition						
Loading configuration	Four-point bending	Three-point bending	Three-point bending	Four-point bending	Three-point bending	Four-point bending
Beam section	T-beam	T-beam & IT-beam	T-beam	Rectangular beam	T-beam	T-beam
L_{beam} (mm)	4000	7315 & 6280	4520	1700	10058	2300
H_{beam} (mm)	500	1219	406	300	934	320
$(a/d)_{beam}$	2.9	3.6	3	≈ 2	3.3	2.5
FRP type	CFRP L-shaped laminate	CFRP laminate	CFRP fabric sheet	CFRP & GFRP fabric sheet	CFRP fabric strip	CFRP fabric strip
Cyclic loading application						
Maximum number of load cycles (million)	5	1	5	1	2	1
Frequency (Hz)	4.4	1 & 1.25	2	5	1	4.16
Lower bound load	39% P_{ult}	var	35% P_{ult}	15% P_{ult}	30% P_{ult}	14 KN
Upper bound load	59% P_{ult}	var	65% P_{ult}	40% P_{ult}	60% P_{ult}	50% P_{ult}
Influencing parameters						
Applied Load range		✓				
FRP configuration				✓		✓
FRP ratio			✓			
Steel stress level					✓	
Steel stirrup ratio			✓			✓

Table 2.1 Summarized details of experimental studies on EB-CFRP shear-strengthened RC beams under fatigue loading from selected research studies (Continue)

Authors	Number of laboratory tests	Fatigue loading condition						Cyclic loading application				Influencing parameters				
		Loading configuration	Beam section	L_{beam} (mm)	H_{beam} (mm)	$(a/d)_{beam}$	FRP type	Maximum number of load cycles (million)	Frequency (Hz)	Lower bound load	Upper bound load	Applied Load range	FRP configuration	FRP ratio	Steel stress level	Steel stirrup ratio
El-Saikaly and Chaallal (2015-a)	6	Three-point bending	T-beam	4520	406	3	CFRP L-shaped laminate	6	3	35% P_{ult}	65% P_{ult}	✓				✓
El-Saikaly and Chaallal (2015-b)	9	Three-point bending	T-beam	4520	406	3	CFRP fabric sheet	6	3	35% P_{ult}	65% P_{ult}	✓				✓
El-Saikaly and Chaallal (2015-c)	6	Three-point bending	T-beam	4520	406	3	CFRP laminate and fabric sheet	6	3	35% P_{ult}	65% P_{ult}		✓			✓
El-Saikaly et al. (2018)	9	Three-point bending	T-beam	4520	406	3	CFRP L-shaped laminate	6	3	35% P_{ult}	65% P_{ult}		✓			✓

Note: L_{beam} = beam length, H_{beam} = beam height, $(a/d)_{beam}$ = shear span-to-depth ratio of the beam, P_{ult}= ultimate monotonic shear capacity of the beam.

2.2.2 Bond-slip behavior of FRP-to-concrete interface under monotonic loading

Since the shear strengthening performance of EB-FRP systems on RC beams can be compromised by the debonding mechanism at FRP-to-concrete interface, especially under fatigue loading, it is of great importance to investigate the FRP-to-concrete bond behavior and examine the affecting parameters on the interaction between FRP and concrete. Experimental research into the FRP-to-concrete bond behavior has been generally conducted in three test

set-ups which include beam test and single or double pull-out test, as shown in Figure 2.2. Indeed, in cases where only the pure shear effect is considered, the two pull-out single and double-lap shear tests can be adopted to investigate the interfacial behavior between FRP and concrete (Mukhtar & Faysal, 2018). Depending on the loading condition, the possible failure modes that can occur in FRP-to-concrete bonded specimens include 1) concrete surface failure; 2) FRP plate rupture; 3) FRP delamination failure; 4) adhesive failure; 5) FRP-to-adhesive interfacial failure; and 6) concrete-to-adhesive interfacial failure (J. F. Chen & Teng, 2001), as shown in Figure 2.3. However, it has been reported that the major FRP-to-concrete debonding failure mode observed during monotonic testing is due to the rupture of concrete surface beneath the FRP composite, namely, concrete cover separation, (J. F. Chen & Teng, 2001; Nakaba et al., 2001). In fact, this mode of failure occurs due to the fracture of a thin layer of concrete aggregates (see Figure 2.4), which is the weakest link among the FRP-adhesive-concrete bond elements under monotonic loading conditions.

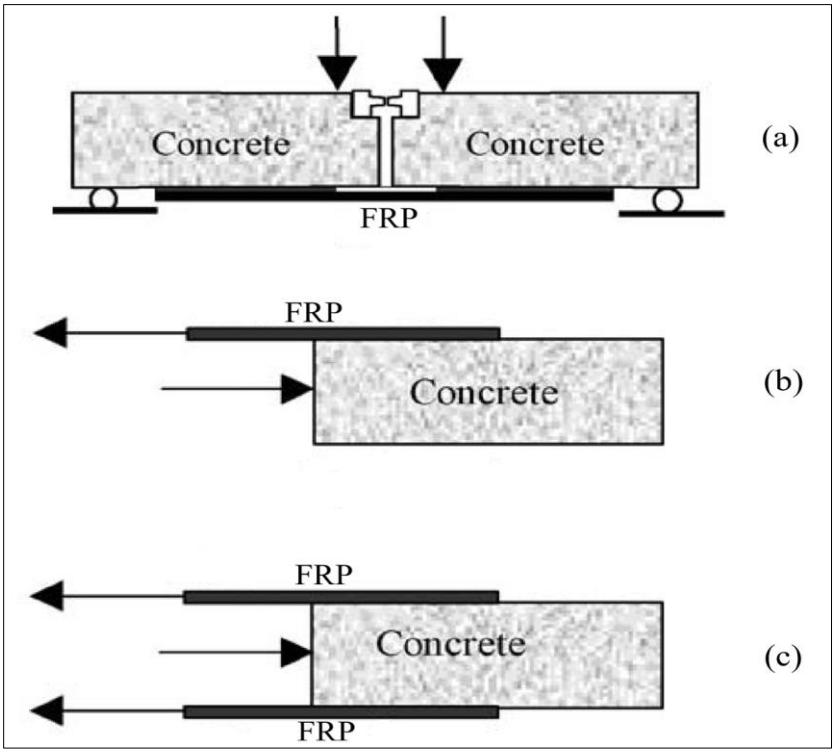

Figure 2.2 Different experimental set-up for the investigation of FRP-to-concrete bond: a) beam test; b) single pull-out test; c) double pull-out test
Adapted from Yao, Teng, and Chen (2005)

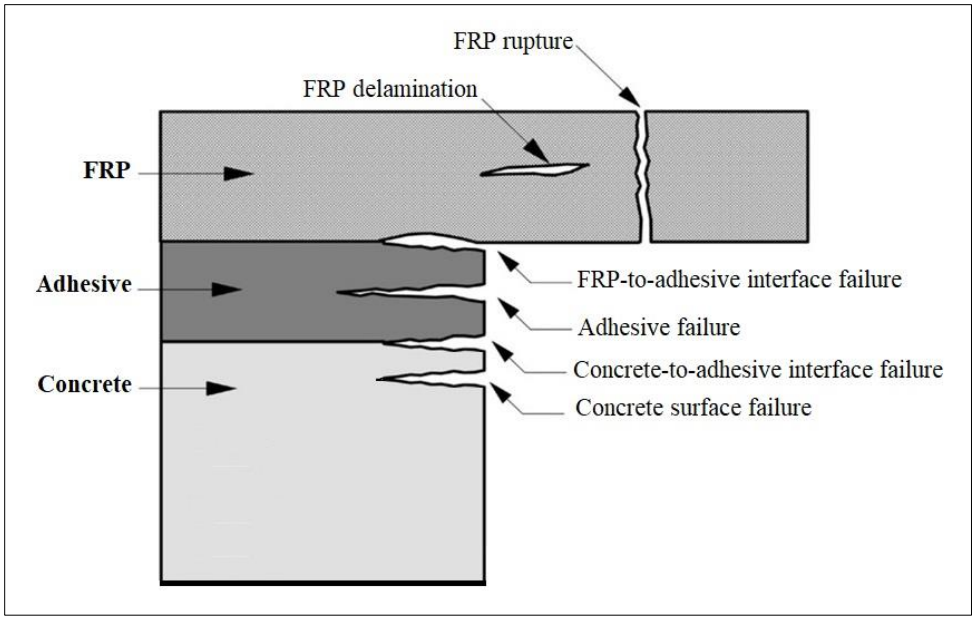

Figure 2.3 Possible failure modes of FRP-to-concrete interface
Adapted from Zhao and Zhang (2007)

Figure 2.4 Concrete cover failure mode

Through the inspection of FRP-to-concrete bond-slip as well as the shear stress, bond-stress slip models can be formulated which are generally used to visualize the behavior of FRP-to-concrete interface.

2.2.2.1 Bond strength prediction model

Several models can be found in the guidelines regarding the behavior of FRP-to-concrete bond under monotonic loading. For a typical FRP-to-concrete bonded joint, the maximum monotonic load at debonding failure, namely bond strength, is dependent on the influencing parameters of FRP bond length, FRP stiffness, concrete strength and FRP-to concrete width ratio, b_f/b_c.

Based on guidelines found in *fib* TG5.1 (2019), the bond ultimate strength, P_{ult}, can be determined using the following equations:

$$P_{\text{ult}} = \begin{cases} b_f\sqrt{2\, n_f E_f t_f G_f} & l_b \geq l_e \\ b_f\sqrt{2\, n_f E_f t_f G_f}\ \times \frac{l_b}{l_e}\left(2 - \frac{l_b}{l_e}\right) & l_b < l_e \end{cases} \tag{2.3}$$

where l_b is the FRP length and l_e is the effective bond length, required to gain the maximum bond capacity. b_f is the FRP width (in mm), $n_f E_f t_f$ is the FRP stiffness (in MPa.mm), and G_f is the fracture energy (in N/mm) and can be obtained as follows:

$$G_f = k^2 \times {k_b}^2 \times {f_c'}^{(2/3)} \quad , \quad k_b = \sqrt{\frac{2-(b_f/b_c)}{1+(b_f/b_c)}} \tag{2.4}$$

where k is a parameter that can be taken as 0.25 or 0.17 for mean value and 5% characteristic value, respectively. k_b is the FRP-to-concrete width factor and f_c' is the compressive strength of concrete cylinder. Furthermore, based on the guidelines found in Japan Concrete Institute, (JCI, 2003), three other bond strength models have been proposed as follows:

Izumo (JCI, 2003) model :

$$P_{\text{ult}} = \begin{cases} (3.8\, {f_c'}^{(2/3)} + 15.2)\, b_f l_b\, n_f E_f t_f\ \times 10^{-3} & \text{for carbon FRP} \\ (3.4\, {f_c'}^{(2/3)} + 69)\, b_f l_b\, n_f E_f t_f\ \times 10^{-3} & \text{for aramid FRP} \end{cases} \tag{2.5}$$

Sato (JCI, 2003) model :

$$P_{\text{ult}} = (b_f + 2\Delta b)\, l_b\, (2.68 \times {f_c}'^{0.2}\, n_f E_f t_f \times 10^{-5}) \tag{2.6}$$

Iso (JCI, 2003) model :

$$P_{\text{ult}} = b_f l_b (0.93 \times {f_c}'^{0.44}) \tag{2.7}$$

Where Δb is the working width of concrete and can be equal to as 3.7mm (Iso (JCI 2003)). Also, note that the FRP bond length, l_b, can not exceed the effective bond length (i.e., $l_b \leq l_e$) in the above-mentioned equations. A review of literature reveals that other bond strength models have also been proposed to predict the ultimate load-carrying capacity of FRP-to-concrete bonded joints (J. F. Chen & Teng, 2001; Khalifa, Gold, Nanni, & MI, 1998; W. Li, Li, Ren, Leung, & Xing, 2015; Lu et al., 2005; Maeda et al., 1997; Neubauer & Rostasy, 1999; Niedermeier, 1996; Yang, Yue, & Hu, 2001). These bond strength models are summarized in the following:

Niedermeier (1996) model :

$$P_{\text{ult}} = \begin{cases} 0.78 \times b_f \sqrt{2G_f n_f E_f t_f} & l_b \geq l_e \\ 0.78 \times b_f \sqrt{2G_f n_f E_f t_f}\, \dfrac{l_b}{l_e}\left(2 - \dfrac{l_b}{l_e}\right) & l_b < l_e \end{cases} \tag{2.8}$$

$$G_f = c_f {k_b}^2 f_t \quad , \quad k_b = \sqrt{1.125 \times \frac{2 - b_f/b_c}{1 + b_f/400}}$$

Where f_t is the concrete tensile strength (in MPa) and c_f is a parameter determined in a linear regression analysis of test results and can be equal to 0.204 (mm).

Maeda et al. (1997) model :

$$P_{\text{ult}} = \begin{cases} b_f\ l_e(110.2 \times 10^{-6}\ n_f E_f t_f) & l_b \geq l_e \\ b_f\ l_b(110.2 \times 10^{-6}\ n_f E_f t_f) & l_b < l_e \end{cases} \quad (2.9)$$

Khalifa et al. (1998) model :

$$P_{\text{ult}} = \begin{cases} b_f\ l_e \times 110.2 \times 10^{-6}\ \times (f_c'/42)^{2/3} n_f E_f t_f & l_b \geq l_e \\ b_f\ l_b \times 110.2 \times 10^{-6}\ \times (f_c'/42)^{2/3} n_f E_f t_f & l_b < l_e \end{cases} \quad (2.10)$$

Neubauer and Rostasy (1999) model :

$$P_{\text{ult}} = \begin{cases} 0.64 \times k_b b_f \sqrt{n_f E_f t_f f_t} & l_b \geq l_e \\ 0.64 \times k_b b_f \sqrt{n_f E_f t_f f_t} \times \dfrac{l_b}{l_e}\left(2 - \dfrac{l_b}{l_e}\right) & l_b < l_e \end{cases} \quad (2.11)$$

$$k_b = \sqrt{1.25 \times \frac{2 - b_f/b_c}{1 + b_f/400}}$$

J. F. Chen and Teng (2001) model :

$$P_{\text{ult}} = \begin{cases} 0.427 \times k_b \sqrt{f_c'}\ b_f\ l_e & l_b \geq\ l_e \\ 0.427 \times k_b \sqrt{f_c'}\ b_f\ l_e \times \sin(\dfrac{\pi l_b}{2\ l_e}) & l_b <\ l_e \end{cases} \quad (2.12)$$

$$k_b = \sqrt{\frac{2 - b_f/b_c}{1 + b_f/b_c}}$$

Yang et al. (2001) model :

$$P_{\text{ult}} = \begin{cases} (0.5 + 0.08\sqrt{n_f E_f t_f/(100\, f_t)}\,) \times\ l_e\ b_f(0.5\, f_t) & l_b \geq l_e \\ (0.5 + 0.08\sqrt{n_f E_f t_f/(100\, f_t)}\,) \times\ l_b\ b_f(0.5\, f_t) & l_b < l_e \end{cases} \quad (2.13)$$

Lu et al. (2005) model :

$$P_{\text{ult}} = \begin{cases} b_f\sqrt{2\, n_f E_f t_f G_f} & l_b \geq l_e \\ b_f\sqrt{2\, n_f E_f t_f G_f} \times \frac{l_b}{l_e}\left(2 - \frac{l_b}{l_e}\right) & l_b < l_e \end{cases} \quad (2.14)$$

$$G_f = 0.308\, {k_b}^2\, \sqrt{f_t} \quad , \quad k_b = \sqrt{\frac{2.25 - b_f/b_c}{1.25 + b_f/b_c}}$$

Karbhari, Niu, and Sikorsky (2006) model :

$$P_{\text{ult}} = \begin{cases} 1.135 \times {f_c}'^{(0.095)}\, b_f\sqrt{n_f E_f t_f} & l_b \geq l_e \\ 1.135 \times {f_c}'^{(0.095)} b_f\sqrt{n_f E_f t_f}\ \frac{l_b}{l_e}(2 - \frac{l_b}{l_e}) & l_b < l_e \end{cases} \quad (2.15)$$

W. Li et al. (2015) model :

$$P_{\text{ult}} = \begin{cases} b_f k_b\sqrt{n_f E_f t_f}\ (0.015 f_{cu} + 1) & l_b \geq l_e \\ b_f k_b\sqrt{n_f E_f t_f} \times \frac{l_b}{l_e}\left(2 - \frac{l_b}{l_e}\right)(0.016 f_{cu} + 0.79) & l_b < l_e \end{cases} \quad (2.16)$$

$$k_b = \sqrt{\frac{2 - b_f/b_c}{1 + b_f/b_c}}$$

Where f_{cu} is the compressive strength of concrete cube (in MPa).

2.2.2.2 Effective bond length

The effective bond length, l_e, is the minimum length at which, the FRP-to-concrete bond reaches its full capacity in terms of the maximum bond resistance. In other words, any increase in length after the effective bond length does not enhance the bond load-carrying capacity. The existing design codes recommend the following equations to determine the effective bond length:

Sato (JCI, 2003) model :

$$l_e = 1.89\ (n_f E_f t_f)^{0.4} \tag{2.17}$$

Iso (JCI, 2003) model :

$$l_e = 0.125\ (n_f E_f t_f)^{0.57} \tag{2.18}$$

ACI 440.2R (2017) model :

$$l_e = \frac{23300}{(n_f E_f t_f)^{0.58}} \tag{2.19}$$

CSA S806 (2012) model :

$$l_e = \frac{25350}{(n_f E_f t_f)^{0.58}} \tag{2.20}$$

***fib* TG5.1 (2019) model :**

$$l_e = \begin{cases} \dfrac{\pi}{k_b}\sqrt{\dfrac{n_f E_f t_f}{8\,{f_c}'^{2/3}}} & \text{for mean value} \\ \dfrac{0.25\pi}{0.17 k_b}\sqrt{\dfrac{n_f E_f t_f}{8\,{f_c}'^{2/3}}} & \text{for 5\% characterstic value} \end{cases} \tag{2.21}$$

Several other relationships have also been proposed by researchers to calculate l_e which are as follows:

Niedermeier (1996) model :

$$l_e = \sqrt{\frac{n_f E_f t_f}{4 f_t}} \tag{2.22}$$

Maeda et al. (1997) model :

$$l_e = e^{6.13 - 0.58 \ln(n_f E_f t_f)} \qquad (n_f E_f t_f \text{ in GPa.mm}) \tag{2.23}$$

Neubauer and Rostasy (1999) model :

$$l_e = \sqrt{\frac{n_f E_f t_f}{2\, f_t}} \tag{2.24}$$

J. F. Chen and Teng (2001) model :

$$l_e = \sqrt{\frac{n_f E_f t_f}{{f_c}'^{0.5}}} \tag{2.25}$$

H. Yuan et al. (2004) model :

$$l_e = \rho + \frac{1}{2\,\lambda_1} \ln \frac{\lambda_1 + \lambda_2 \tan(\rho\lambda_2)}{\lambda_1 - \lambda_2 \tan(\rho\lambda_2)} \tag{2.26}$$

$$\rho = \frac{1}{\lambda_2} \arcsin \left[0.99 \sqrt{\frac{s_{\text{ult}} - s_{\text{peak}}}{s_{\text{ult}}}} \right]$$

$$\lambda_1 = \sqrt{\frac{\tau_{\max}}{s_{\text{peak}} \times n_f E_f t_f}} \quad , \quad \lambda_2 = \sqrt{\frac{\tau_{\max}}{(s_{\text{ult}} - s_{\text{peak}}) \times n_f E_f t_f}}$$

Where $\tau_{\max}$ is the maximum bond stress, s_{peak} is the bond slip corresponding to the maximum stress and s_{ult} is the ultimate bond stress.

Karbhari et al. (2006) model :

$$l_e = \frac{0.6485 \sqrt{n_f E_f t_f}}{{f_c}'^{0.095}} \tag{2.27}$$

Pellegrino et al. (2008) model :

$$l_e = \sqrt{\frac{n_f E_f t_f}{2.15\, f_t}} \quad , \quad l_e \leq 140mm \tag{2.28}$$

Z. Wu et al. (2009) model :

$$l_e = 0.395\, \frac{(n_f E_f t_f)^{0.54}}{{f_c}'^{0.09}} \tag{2.29}$$

W. Li et al. (2015) model :

$$l_e = 1.222 \sqrt{\frac{n_f E_f t_f}{f_{\text{cu}}^{0.56}}} \tag{2.30}$$

As can be seen the available effective bond length models all express l_e as a function of FRP stiffness, $n_f E_f t_f$. Therefore, the performance of different effective bond length relationships can be visualized with respect to the variable of $n_f E_f t_f$ for a typical FRP-to-concrete bonded joint. Figure 2.5 indicates the effective bond length with respect to the variations of $n_f E_f t_f$ calculated from the available models. As for the equations with other affecting variables, the mean concrete compressive strength, f_c', was taken to be equal to 30 MPa and the FRP-to-concrete width ratio, b_f/b_c, was assumed to be 0.5.

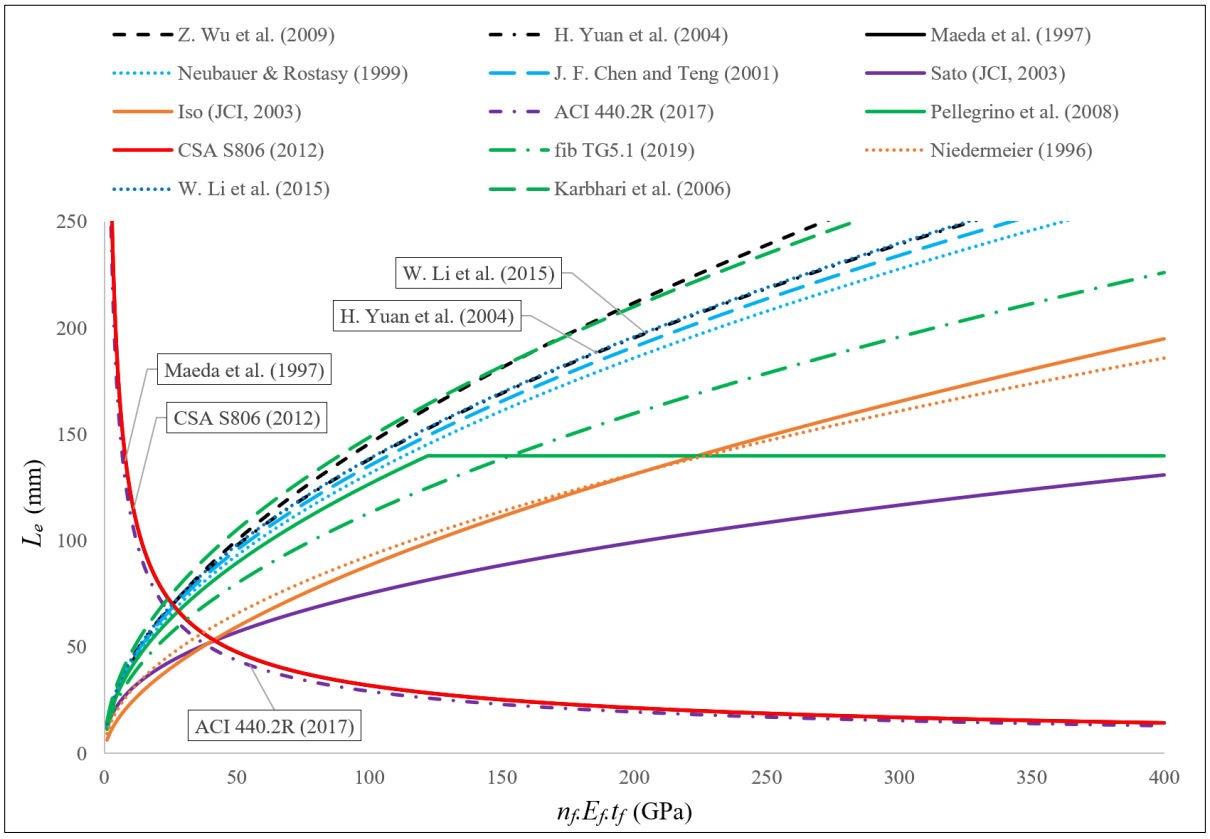

Figure 2.5 Variation of effective bond length with respect to the FRP stiffness

Some of the summarized research findings regarding the monotonic behavior of FRP-to-concrete in terms of bond-slip relationship as well as the influencing parameters are presented in the following:

Neubauer and Rostasy (1999)

In an analytical study by Neubauer and Rostasy (1999) regarding the interlaminar behavior of CFRP bonded concrete structures, a relationship for the local bond stress, τ, vs. bond slip, *s*, was proposed. The bond-slip model was based on the fracture mechanics theory and is expressed as follows:

$$\tau = \begin{cases} \tau_{\max}\left(\frac{s}{s_{\text{peak}}}\right) & s \le s_{\text{peak}} \\ 0 & s > s_{\text{peak}} \end{cases} \qquad (2.31)$$

$$\tau_{\max} = 1.8\, k_b f_t \quad , \quad s_{\text{peak}} = 0.202\, k_b \quad , \quad k_b = \sqrt{1.25 \times \frac{2 - b_f/b_c}{1 + b_f/400}}$$

Nakaba et al. (2001)

The FRP-to-concrete bond behavior was studied experimentally by Nakaba et al. (2001). A series of double-lap FRP-to-concrete joints were designed to study the affecting factors of FRP laminate type (carbon vs. aramid), adhesive thickness and concrete strength. It was observed that the bond behavior was not significantly affected by the adhesive thickness. However, increasing the FRP stiffness led to an improvement in the bond load carrying capacity. As for the local bond shear stress, the FRP type did not seem to affect the maximum interfacial stress, while increasing the concrete strength resulted in higher peak stresses at the FRP-to-concrete bond. Based on Popovic's equation, the following local bond stress, τ, vs. bond slip, *s*, relationship was also proposed:

$$\tau = \tau_{\max}\left(\frac{s}{s_{\text{peak}}}\right)\left[3/(2 + (\frac{s}{s_{\text{peak}}})^3)\right] \qquad (2.32)$$

$$\tau_{\max} = 3.5\, f_c'^{0.19} \quad , \quad s_{\text{peak}} = 0.065$$

De Lorenzis et al. (2001)

An experimental investigation was CFRP-to-concrete bond behavior. Upon performing carried out by De Lorenzis et al. (2001) on flexural tests on CFRP-bonded concrete beams, it was revealed that increasing the bond length after the effective bond length did not improve the ultimate load resistance of CFRP-to-concrete interface. As for the failure mode, the specimens mainly failed due to the concrete-to-adhesive interfacial failure with very little damage on the concrete cover. This was reported to indicate the reliance of bond failure mode on the number of CFRP plies used. It was also observed that the influence of concrete strength and CFRP width were not significant on bond strength. However, it was found that the concrete surface preparation can significantly change the bond load carrying capacity. A linear bond stress-slip model was also proposed as follows (De Lorenzis et al., 2001):

$$\tau = K_{\text{int}} \times s \tag{2.33}$$

$$K_{\text{int}} = G_{\text{int}}/t_{\text{int}} \quad , \quad \tau_{\max} = 0.0182\ (n_f t_f E_f)^{0.5}$$

where K_{int} is the slip modulus of interface, G_{int} is the interfacial shear modulus and can be equal to $74.86\ ksi$ $(515.8\ MPa)$ and t_{int} is interfacial thickness.

Toutanji and Ortiz (2001)

Another experimental study was conducted by Toutanji and Ortiz (2001) to evaluate the effects of surface preparation (water jet treatment vs. sandblasting treatment) and FRP type (glass vs. carbon) on the FRP-to-concrete bond behavior. It was seen that the surface treatment by water jet outperformed sandblasting treatment in terms of bond strength. Furthermore, specimens bonded with carbon FRPs reached a higher average tensile stress compared to those with glass FRPs. In addition, using CFRPs with higher elastic modulus improved the bonding resistance.

Monti, Renzelli, and Luciani (2003)

Following a numerical investigation on the nonlinear behavior at the FRP/adhesive/concrete interface, the following equations were proposed by Monti et al. (2003) to predict the relationship between the bond slip (in mm) and local shear stress (in MPa):

$$\tau = \begin{cases} \tau_{\max}\left(\frac{s}{s_{\text{peak}}}\right) & s \le s_{\text{peak}} \\ \tau_{\max}\left(\frac{s_{\text{ult}} - s}{s_{\text{ult}} - s_{\text{peak}}}\right) & s > s_{\text{peak}} \end{cases} \tag{2.34}$$

$$\tau_{\max} = 1.8\, k_b f_t \quad , \quad s_{\text{peak}} = 2.5\, \tau_{\max}\,(n_f t_f / E_f + 50/E_c)$$

$$s_{\text{ult}} = 0.33 k_b \quad , \quad k_b = \sqrt{1.5 \times \frac{2 - b_f/b_c}{1 + b_f/100}}$$

Where, E_c is the concrete elastic modulus (in MPa).

Savoia, Ferracuti, and Mazzotti (2003)

Savoia et al. (2003) conducted an analytical study of nonlinear bond-slip law for FRP-to-concrete interface. Their research led to the following bond-slip model.

$$\tau = \tau_{\max}\left(\frac{s}{s_{\text{peak}}}\right)\left[2.86/(1.86 + (\frac{s}{s_{\text{peak}}})^{2.86})\right] \tag{2.35}$$

$$\tau_{\max} = 3.5\, f_c'^{0.19} \quad , \quad s_{\text{peak}} = 0.051$$

Lu et al. (2005)

Through a combined numerical and analytical investigation on the FRP-to-concrete bond behavior, Lu et al. (2005) developed the following bilinear bond-slip model that was validated against a considerable size of data base derived from the literature (i.e., 253 pull-out tests).

$$\tau = \begin{cases} \tau_{\max}\left(\dfrac{s}{s_{\text{peak}}}\right) & s \le s_{\text{peak}} \\ \tau_{\max}\left(\dfrac{s_{\text{ult}} - s}{s_{\text{ult}} - s_{\text{peak}}}\right) & s_{\text{peak}} < s \le s_{\text{ult}} \\ 0 & s > s_{\text{ult}} \end{cases} \tag{2.36}$$

$$\tau_{\max} = 1.5\, k_b f_t \quad , \quad s_{\text{peak}} = 0.0195\, k_b f_t \le 0.06$$

$$s_{\text{ult}} = 2G_f/\tau_{\max} \quad , \quad G_f = 0.308\, {k_b}^2 \sqrt{f_t} \quad , \quad k_b = \sqrt{\frac{2.25 - b_f/b_c}{1.25 + b_f/b_c}}$$

The proposed bond slip model showed great agreement with the existing test data and was reported to be applicable for normal-adhesive FRP-to-concrete bonded joints, i.e., with the adhesive shear stiffness of greater than or equal to 2.5GPa/mm.

McSweeney and Lopez (2005)

McSweeney and Lopez (2005) performed a series of single-lap pull-out tests on CFRP-to-concrete bonded joints to examine the effects of concrete strength, CFRP bonded length and width and CFRP thickness on the bond behavior. It was observed that the bond ultimate load-carrying capacity can significantly increase by increasing the bond length until the effective bond length. However, it was seen bond ultimate strength was not affected by the change in concrete strength. As for the impact of FRP width and thickness, increasing either of these two variables was reported to enhance the bond resistance. Nevertheless, the bond failure load did not seem to double after doubling either of the two variables.

Yao et al. (2005)

An experimental program consisting of near end supported (NES) single-lap pull-out specimens was carried out by Yao et al. (2005) in which a portion of the height of concrete prism was subjected to tensile loading, as shown in Figure 2.6. The tests included varying bond lengths, FRP widths and height of concrete free edge, h_c, and loading offset, δ. The dominant failure mode occurred in the form of concrete cover separation and the failure load results agreed well with the J. F. Chen and Teng (2001) bond strength model. It was concluded that

the adopted test-setup showed a reliable performance at investigating the FRP-to-concrete bond behavior.

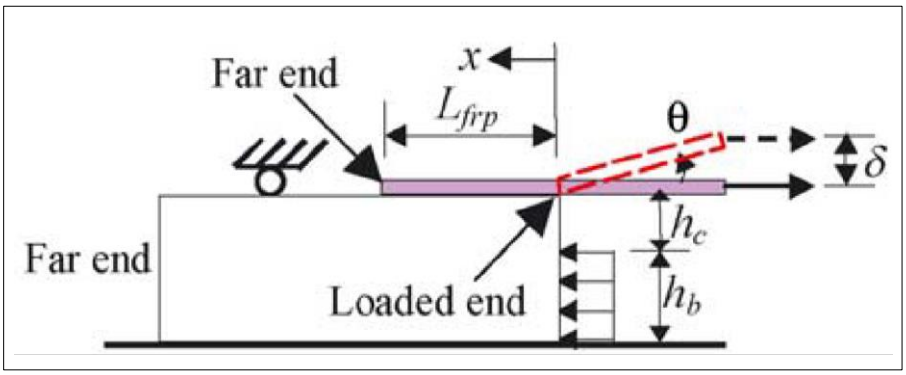

Figure 2.6 NES single-lap pull-out test setup
Taken from Yao et al. (2005)

Mazzotti et al. (2008)

During another experimental study by Mazzotti et al. (2008) regarding the behavior of CFRP-bonded concrete prisms with different CFRP bonded lengths and bonded widths, it was found that the ultimate loads reached by the specimens were not affected by the variable of CFRP bonded width. However, the bond-slip behavior was seen to change with varying FRP widths, as increasing this variable resulted in a decrease in the peak shear stresses of the FRP-to-concrete interface.

Pellegrino et al. (2008)

Pellegrino et al. (2008) conducted an experimental study of CFRP-to-concrete bond behavior and performed both double-lap and bending test setup. The influence of FRP stiffness on the bond-slip behavior was included in their investigation which led to the development of the following bond-slip model:

$$\tau = \begin{cases} \tau_{\max}\left(\frac{s}{s_{\text{peak}}}\right) & s \le s_{\text{peak}} \\ \tau_{\max}\left(\frac{s_{\text{ult}} - s}{s_{\text{ult}} - s_{\text{peak}}}\right) & s > s_{\text{peak}} \end{cases} \tag{2.37}$$

$$\tau_{\max} = 3.1\,(n_f t_f E_f)^{0.32} \quad , \quad s_{\text{peak}} = 0.075\,/(n_f t_f E_f)^{0.2}$$

$$s_{\text{ult}} = 10.5\,/(n_f t_f E_f)^{0.6} \quad , \quad (n_f t_f E_f \text{ in GPa , mm })$$

Emmanuel Ferrier et al. (2010)

Following a double-lap pull-out experimental investigation by Emmanuel Ferrier et al. (2010), the effects of curing conditions (temperature), FRP properties (type, stiffness, and thickness) and adhesive properties (stiffness and thickness) on the CFRP-to-concrete interfacial behavior were evaluated. It was observed that the bond load carrying capacity did not change significantly with respect to the curing conditions. However, better bonding performance (i.e., higher bond strength and lower peak shear stress) was reported to be achieved by a combined increase of FRP elastic modulus and adhesive thickness.

Woo and Lee (2010)

In an experimental study by Woo and Lee (2010), the effects of bond length, FRP width and concrete strength on the CFRP-to-concrete interfacial behavior was inspected. It was indicated that increasing the bond length beyond the effective bond length did not result in any increase in the failure load of the specimen. However, it could help provide some warning time before the occurrence of the bond failure. It was also observed that increasing the FRP width could improve the bond behavior in terms of the bond ultimate load-carrying capacity. As for the parameter of concrete compressive strength, it was reported that the influence of this variable on the bond behavior was insignificant.

Pan and Wu (2014)

Upon an analytical investigation on the debonding mechanism of FRP-bonded concrete blocks, Pan and Wu (2014) developed a bond-slip model which is comprised of a linear ascending segment, followed by a nonlinear softening segment. The proposed bond slip model is expressed on the following:

$$\tau = \begin{cases} k_{\text{adh}}.\, s & s \le s_{\text{peak}} \\ \tau_{\max}\, e^{-\beta(s - s_{\text{peak}})} & s > s_{\text{peak}} \end{cases} \quad (2.38)$$

Where k_{adh} is a parameter dependent on the properties of adhesive. And β is a variable that can be expressed by the material properties of interfacial fracture energy (G_f) and is equal to: $\beta = 1.8\, \tau_{\max}/G_f$.

W. Li et al. (2015)

The coupling effect of concrete strength and bond length on the behavior of CFRP-to-concrete interface has been studied experimentally by W. Li et al. (2015). It was observed that increasing the concrete strength led to greater bond strengths in specimens with the same bond lengths. This was reported to be attributed to the concrete surface failure as the dominant failure mode of specimens. Furthermore, the increment of bond failure load was shown to have an increasing trend with increasing concrete strength. As for the bond length lower than the effective bond length, a direct relationship was seen to exist between this variable and the bond strength. However, the increment of failure load was seen to decrease with increasing bond length.

Mohammadi and Wan (2015)

The effect of experimental boundary conditions on the bond-slip behavior of FRP-to-concrete interface was studied by Mohammadi and Wan (2015) through several single-lap pull-out tests. The concrete blocks were fixed in constraints with different heights with respect to the concrete

height. Based on the results derived from both experimental and numerical analyses, it was revealed that the height of the constraint, h_b, plays a significant role in single-lap shear tests as increasing h_b can increase the bond strength of FRP-to-concrete interface.

Huo et al. (2016)

Huo et al. (2016) carried out an experimental study to determine the effect of impact loading on CFRP-to-concrete bond. It was revealed that the failure mode under impact loading (i.e., dynamic) was concrete cover separation which is similar to the dominant failure mode under monotonic loading. However, results regarding the strain distribution shows that variations of strains along the bond length is much higher under impact loading in comparison with the corresponding values under monotonic loading. As a result, the dynamic effective bond length was found to be lower that the monotonic effective bond length. Furthermore, the ultimate bond strength was reported to be dependent on the rate of applied loading. Finally, a bond stress-slip (τ, s) model for CFRP-to-concrete interface under dynamic loading was proposed, as follows:

$$\tau = \begin{cases} \tau_{d,\max}\left(\dfrac{s}{s_{d,\text{peak}}}\right) & s \le s_{d,\text{peak}} \\ \tau_{d,\max}\left(\dfrac{s_{d,ult} - s}{s_{d,\text{ult}} - s_{d,\text{peak}}}\right) & s_{d,\text{peak}} < s \le s_{d,\text{ult}} \\ 0 & s > s_{d,\text{ult}} \end{cases} \tag{2.39}$$

Where $\tau_{d,\max}$, $s_{d,\text{peak}}$ and $s_{d,\text{ult}}$ are the maximum bond shear stress, corresponding slip at maximum bond stress and ultimate slip under dynamic loading, respectively and can be achieved by multiplying the dynamic increase factor (DIF) by the same variables ($\tau_{\max}$, s_{peak} and s_{ult}) under monotonic loading. It is noteworthy that DIF can also be found in (CEB-FIP, 1993).

Godat, Prowt, and Chaallal (2016)

Godat et al. (2016) carried out an investigation (both experimental and numerical) on the CFRP-to-concrete bond behavior with respect to the influencing parameters of concrete strength, FRP width and anchorage system. The experimental specimens were prepared by using L-shaped CFRP plates anchored with CFRP ropes, as shown in Figure 2.7. Therefore, the effect of CFRP rope length, as the anchorage parameters, was observed during the study. It was concluded increasing the CFRP width enhanced the bond ultimate load. However, the effect of this variable was found to be negligible on the anchored specimens. As for the performance of the anchorage system, results showed that increasing the CFRP rope length resulted in an increase in the bond load-carrying capacity. Also, it was reported that the influence of concrete strength would be insignificant on the FRP-to-concrete bond behavior in conditions where the applied FRP laminate had a narrow width and high thickness.

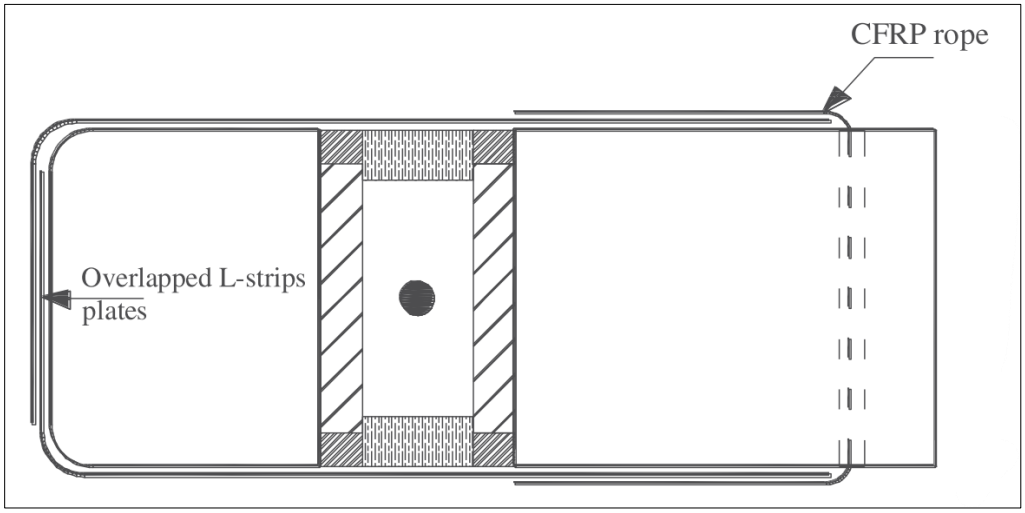

Figure 2.7 CFRP anchorage system with CFRP rope
Taken from Godat et al. (2016)

Sun, Jirsa, and Ghannoum (2016)

The influencing parameters of FRP width, concrete width and anchorage application on the CFRP-to-concrete bond behavior was studied experimentally by Sun et al. (2016). It was seen

that using wider CFRP strips could contribute to higher local peak strains but lower average shear stresses within the bond. Furthermore, increasing the concrete strength resulted in an increase in the bond strength of CFRP-to-concrete interface. However, this increase was observed to be little for the unanchored specimens.

Sun, Peng, and Yu (2017)

Sun, Peng, and Yu (2017) performed a numerical research study on the FRP-to-concrete bond behavior, evaluating the effects of bond length, FRP width, thickness, and elastic modulus. On the basis of exiting data from the literature, the following bilinear bond-slip model was also proposed:

$$\tau = \begin{cases} \tau_{\max}\left(\frac{s}{s_{\text{peak}}}\right) & s \le s_{\text{peak}} \\ \tau_{\max}\left(\frac{s_{\text{ult}} - s}{s_{\text{ult}} - s_{\text{peak}}}\right) & s_{\text{peak}} < s \le s_{\text{ult}} \\ 0 & s > s_{\text{ult}} \end{cases} \tag{2.40}$$

$$\tau_{\max} = 1.35 + 0.25\, k_b f_t + 0.62\, f_t$$

$$s_{\text{peak}} = 0.016 - 0.0046\, k_b f_t + 0.11\, k_b$$

$$s_{\text{ult}} = -0.06 + (0.88 - 0.23\, {k_b}^2) {f_t}^{-0.5} {k_b}^{0.5}$$

$$k_b = \sqrt{\frac{1.9 - b_f/b_c}{0.9 + b_f/b_c}} \quad , \quad f_t = 0.62\sqrt{f_c'}$$

Lin, Wu, and Smith (2017)

Following a numerical analysis, Lin et al. (2017) developed an FRP width factor, k_b, that incorporated the affecting parameters of concrete strength, FRP stiffness, and both FRP and concrete widths. The proposed width factor model, expressed in the following, was compared with the existing models (Brosens & Van Gemert, 1999; J. F. Chen & Teng, 2001; Lu et al., 2005; Neubauer & Rostasy, 1999; Y.-F. Wu & Jiang, 2013) and was shown to perform superior in terms of accuracy.

$$k_b = 1 + {f_c'}^{0385}\left[8\left(t_f E_f\right)^{-0.438} + 0.001\right]\left(1 - \frac{b_f}{b_c}\right)^{0.5} / (1 + 0.01\ {b_f}^{1.7}) \quad (2.41)$$

C. Yuan et al. (2019)

An experimental study was conducted by C. Yuan et al. (2019) on single-lap concrete specimens bonded with hybrid FRPs (basalt "BFRP" and carbon) to evaluate the effect of FRP stacking order and FRP stiffness on the bond behavior. Specimens with a combination of different layers of CFRPs and BFRPs were prepared. It was concluded that increasing the FRP stiffness improved the bond strength. As for the effect of FRP stacking order, it was shown that the best bond performance can be achieved in terms of bond strength when one ply of CFRP is attached directly to the concrete before bonding the upper BFRP layer.

P. Zhang et al. (2020)

The FRP-to-concrete bond behavior was investigated in another study P. Zhang et al. (2020) by using GFRP plates. Their experimental program consisted of double-lap pull-out specimens with different GFRP surface roughness and FRP-to-concrete interface surface types. It was concluded that the bond performance can be affected by the FRP surface roughness. As for the bond surface type, it was observed that using shear key anchorage can enhance the bond load-carrying capacity as well as restrict the interfacial slippage. Furthermore, increasing the concrete strength was reported to improve the bond resistance for cases where no interface anchorage was used.

C. Yuan et al. (2020)

An experimental study was carried out by C. Yuan et al. (2020) on the dynamic bond behavior of basalt FRP-bonded concrete specimens during which the influence of concrete strength and varying applied loading rate was investigated. Results showed that increasing either the concrete strength or loading rate resulted in an increase in the interfacial shear resistance of the bond. Also, it was observed that the failure mode of specimens occurred in the form of concrete

cover rupture at loading rates below 3 m/s, whereas the specimens were seen to fail at the concrete-adhesive interface when the loading rate was higher than 3 m/s. Furthermore, in cases where the failure mode was concrete cover rupture, the factor of concrete strength played a significant role on the bonding resistance.

The details of experimental studies regarding the bond behavior of FRP-to-concrete interface under monotonic loading, as discussed above, are summarized in Table 2.2.

Table 2.2 Summarized details derived from experimental investigations on the monotonic bond behavior of FRP-to-concrete interface

No.	Research	Test set-up	Number of specimens	FRP type	Influencing parameters on the bond behavior									
					Concrete strength	Bond length	FRP width	FRP stiffness	FRP thickness	FRP type	Epoxy properties	Surface preparation	Bonding condition (Anchorage)	Loading condition
1	Nakaba et al. (2001)	Double lap	36	CFRP & AFRP	✓					✓	✓			
2	De Lorenzis et al. (2001)	Beam test	18	CFRP	✓	✓	✓		✓			✓		
3	Toutanji and Ortiz (2001)	Double lap	12	GFRP & CFRP						✓		✓		
4	McSweeney and Lopez (2005)	Single lap	42	CFRP	✓	✓	✓		✓					
5	Yao et al. (2005)	Single lap	72	CFRP		✓	✓						✓	
6	Mazzotti et al. (2008)	Single lap	8	CFRP		✓	✓							
7	Pellegrino et al. (2008)	Double lap & beam test	39	CFRP		✓		✓						
8	Emmanuel Ferrier et al. (2010)	Double lap	36	CFRP & AFRP		✓		✓	✓	✓	✓	✓		

Table 2.2 Summarized details derived from experimental investigations on the monotonic bond behavior of FRP-to-concrete interface (Continue)

No.	Research	Test set-up	Number of specimens	FRP type	Influencing parameters on the bond behavior									
					Concrete strength	Bond length	FRP width	FRP stiffness	FRP thickness	FRP type	Epoxy properties	Surface preparation	Bonding condition (Anchorage)	Loading condition
9	Woo and Lee (2010)	Single lap	54	CFRP	✓	✓	✓							
10	W. Li et al. (2015)	Single lap	20	CFRP	✓	✓								
11	Mohammadi and Wan (2015)	Single lap	6	CFRP									✓	
12	Huo et al. (2016)	Beam test	23	CFRP										✓
13	Godat et al. (2016)	Double lap	16	CFRP	✓		✓						✓	
14	Sun et al. (2016)	Beam test	26	CFRP	✓		✓	✓					✓	
15	C. Yuan et al. (2019)	Single lap	24	Hybrid (CFRP/ BFRP)				✓		✓			✓	
16	P. Zhang et al. (2020)	Double lap	48	GFRP	✓					✓	✓		✓	
17	C. Yuan et al. (2020)	Single lap	42	BFRP	✓									✓

2.2.2.3 Bond-slip behavior of FRP-to-concrete interface under cyclic loading

As discussed earlier, the bond behavior at FRP-to-concrete interface has a major role in governing the long-term performance of EB-FRP shear-strengthened RC structures subjected to fatigue loading. Therefore, the following investigations have been carried out to determine the fatigue bond-slip behavior as well as the bond fatigue life of FRP-to-concrete interface.

Furthermore, the research findings derived from experimental studies regarding the effect of influencing parameters on the bond fatigue behavior are presented in the following.

Bizindavyi et al. (2003)

Bizindavyi et al. (2003) investigated the fatigue behavior of FRP-to-concrete bonded joints by performing as series of single-lap shear tests. In their study, the effect of FRP bond length and width and applied cyclic stress was evaluated. The fatigue testing of specimens indicated three interfacial cracking phases along the bonded region (see Figure 2.8) as follows: Phase 1) cracking initiates from the interfacial region close to loaded end (region I) within the concrete substrate, which takes place during the first 10-15% of the specimen's fatigue life; Phase 2) cracking propagates gradually along the concrete-adhesive interface (region II) towards the free end which leads to the growth of fatigue debonding during approximately 50-75% of the bond fatigue life; Phase 3) rapid propagation of interfacial cracking takes place in the from of concrete shearing (region III) until the total failure of the specimen, which occupies 10-15% of the specimen's fatigue life. Indeed, it was observed that specimens that were subjected to the maximum cyclic load level near the monotonic load-carrying capacity mainly failed due to FRP rupture. Furthermore, test results showed that that increasing the FRP width resulted in reducing the bond slip. A bond S-N model was also proposed based on the data derived from the experiment as follows:

$$\ln S_r = c_1 - c_2 \ln N_f \tag{2.42}$$

where, S_r is the applied cyclic loading range (i.e., $S_r = S_{\max} - S_{\min}$), N_f is the maximum number of load cycles until bond failure. And c_1 and c_2 are coefficients that can be obtained from fitting the test data.

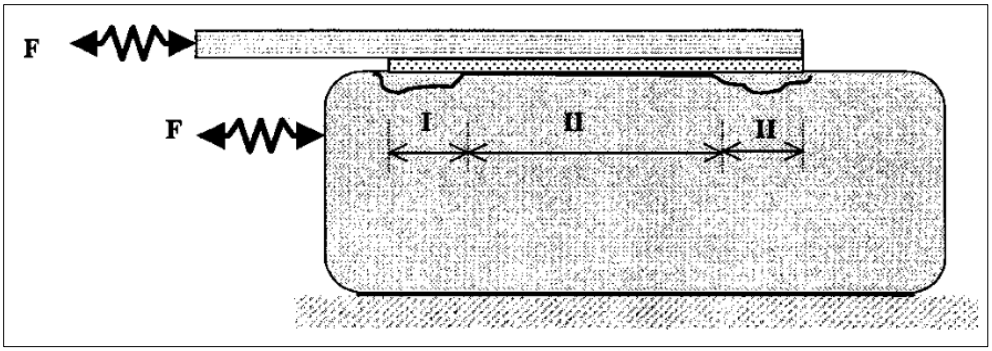

Figure 2.8 Phases of fatigue cracking along the interface
Taken from Bizindavyi et al. (2003)

E Ferrier, Bigaud, Hamelin, Bizindavyi, and Neale (2005)

Results of an experimental research program including both single and double-lap tests were presented by E Ferrier et al. (2005), during which the fatigue behavior of CFRP-to-concrete was investigated. It was observed that application of higher cyclic stress resulted in shortening the fatigue life of CFRP-to-concrete bond. It was also reported that the fatigue failure of FRP-to-concrete joint was mainly triggered by the damage of epoxy adhesive. Finally, the results showed that, unlike the bond, the FRP stiffness did not seem to undergo degradation due to the application of fatigue loading.

Ko and Sato (2007)

An experimental double shear pull-out test was performed on 54 specimens by Ko and Sato (2007) to investigate the bond-slip behavior of FRP-to-concrete interface under cyclic loading with respect to the three variables of FRP type（aramid, carbon, and polyacetal), number of sheet layers (single and double) and loading hysteresis. It was observed that the main failure mode occurred due to peeling of FRP from the concrete substrate. Also, a local bond-slip model was developed which was based on the envelopes of bond stress-slip relationships under cyclic loading. The model was obtained based on the bond stress-slip formulation presented by Popovics (1973) and showed good agreement with the overall test results. The proposed cyclic bond stress-slip model is expressed in the following and involves the empirical parameters of

maximum bond stress, $\tau_{\max}$, slip corresponding to the maximum bond stress, s_{peak} and the curve characteristic constant, α.

$$\tau = \frac{\tau_{\max}\, \alpha s}{s_{\text{peak}}} \Big/ \left[(\alpha + 1) + \left(\frac{s}{s_{\text{peak}}}\right)^{\alpha}\right] \tag{2.43}$$

Furthermore, the following equation was used to formulate the relationship between the unloading stiffness, K_{un}, and bond unloading residual slip, s_{un}, according to their test results.

$$K_{\text{un}} = 0.56\, {s_{\text{un}}}^{1.90} \tag{2.44}$$

Yun, Wu, and Tang (2008)

Through an experimental study by Yun et al. (2008), the use of different anchorage systems was investigated on CFRP-to-concrete bonded joints under fatigue loading. It was observed that using a proposed hybrid bonded FRP system, in which mechanical fasteners are affixed on to the bonded CFRP sheets, could improve the fatigue bond resistance in terms of stiffness and strength degradation under load cycles. Furthermore, the residual bond slip was found to reduce by using the proposed anchorage technique. Also, test observations indicated that much of the bond energy dissipation occurs during the initial load cycle of fatigue loading. This was reported to be due to the occurrence of initial microcracking at the beginning of cyclic loading. Finally, the post-fatigue monotonic bond strength was seen to be unaffected by the fatigue loading amplitude.

HM Diab et al. (2009)

HM Diab et al. (2009) carried out an analytical study on the shear behavior of FRP/concrete interface under fatigue loading and proposed a prediction methodology for the determination of fatigue debonding phenomenon at the FRP-to-concrete interface. Indeed, a nonlinear

interfacial constitutive law was employed to achieve the rate of the debonding growth per loading cycle ($\frac{\mathrm{d}a_d}{\mathrm{d}n}$) that can be expressed as follows:

$$\frac{\mathrm{d}a_d}{\mathrm{d}n} = m_1 \left(\frac{G_{f,\max}}{G_{f,s}}\right)^{m_2} \times \eta \tag{2.45}$$

Where, a_d is the debonding length, n is the number of cycles. m_1 and m_2 are parameters that are obtained from the regression analysis of the experimental tests. $G_{f,\max}$ and $G_{f,s}$ are the maximum strain-energy release rate and the quasi-static fracture energy, respectively. Finally, η is the fatigue debond growth coefficient which is used to consider the reduction of debonding propagation rate with the increase in the debonding length, a_d. The reliability of the proposed methodology was assessed through a set of double-lap shear tests, and it was shown that the model agreed well with the experimental results. Furthermore, their experimental investigation revealed that the concrete/FRP interface is likely to resist debonding failure provided that the applied fatigue load is limited to maximum 30% of the monotonic bond capacity between concrete and FRP materials. Also, the following cyclic bilinear bond-slip model was proposed to characterize the fatigue behavior of the CFRP/concrete interface:

$$\tau = \begin{cases} \dfrac{\tau_{\max,t}}{s_{\text{peak}}} s & 0 \le s \le s_{\text{peak}} \\ \dfrac{\tau_{\max,t}}{s_{\text{ult},t} - s_0}(s_{\text{ult},t} - s) & s_{\text{peak}} < s \le s_{\text{ult}.t} \end{cases} \tag{2.46}$$

$$\tau_{\max,t} = \frac{\tau_{\max,0}}{1 + \varphi \cdot \kappa}$$

$$s_{\text{ult},t} = \frac{\tau_{\max,0} \times s_{\text{peak}}}{\tau_{\max,t}}$$

$$K_{b,t} = \frac{K_{b,0}}{1 + \varphi \cdot \kappa}$$

$$\varphi = \begin{cases} 0.046(t)^{0.4} & t \le 2000 \\ 1.2(1 - \exp(-t/1200) & t > 2000 \end{cases}$$

Where, t is the cyclic loading time (in seconds), $\tau_{\max,0}$ and $\tau_{max,t}$ are the cyclic bond strengths of the adhesive at time zero and time t, respectively, $K_{b,0}$ and $K_{b,t}$ are the cyclic stiffness values of the bond at time zero and time t, respectively, $s_{\mathrm{ult},t}$ is the cycle-dependent ultimate slip (at time t), φ is the creep fatigue coefficient, and κ is a frequency-dependent factor that is equal to 1 for a frequency of 5 Hz. As can be seen, the cyclic dependent bilinear model takes into account the degradation of interfacial stiffness under fatigue loading by adopting a simple creep-fatigue coefficient, φ, in the equations.

Z. Wu et al. (2010)

Z. Wu et al. (2010) presented a literature review on the long-term performance of FRP-to-concrete bond under fatigue loading. On the basis of research findings, the following conclusions were reported: 1) The fatigue behavior of FRP-to-concrete bonded joints are significantly governed by the performance of epoxy resin; 2) carbon FRPs have demonstrated superior fatigue resistance in comparison with other FRP types; 3) Exposure to environmental conditions such moisture and temperature have adverse effects on the long-term performance of epoxy adhesives; 4) increasing the FRP bonded length improves the fatigue performance of FRP-to-concrete; 5) increasing the adhesive stiffness decreases the effective bond length; and 6) the fatigue failure mode of FRP-to-concrete bond is affected by the applied fatigue loading level. Also, it was recommended that the cyclic loading level be less than 30 % of the bond monotonic capacity to avoid debonding failure.

Carloni et al. (2012)

Carloni et al. (2012) carried out an experimental investigation on the shear debonding mechanism of the interface between concrete and FRP under fatigue loading. They performed seven direct shear tests under both monotonic-quasi static and fatigue loading conditions. It was observed that the load carrying capacity of the specimen under monotonic loading seems to be the same as that under fatigue loading provided that the FRP bonding length is larger than the stress transfer zone associated with the quasi-static cohesive crack. Furthermore,

assessment of the variations in the slope of the load-slip response of the FRP/concrete interface indicated that the bond stiffness was seen to reduce during fatigue loading. As far as the fatigue loading amplitude is concerned, at higher values, the fatigue life of the concrete/FRP interface is mainly dominated by crack initiation. However, at lower fatigue load limits, crack propagation played the main role in determining the bond fatigue strength.

Carloni and Subramaniam (2013)

An experimental study of the fatigue cracking behavior at the interfacial elements of FRP-epoxy-concrete interface was conducted by Carloni and Subramaniam (2013). It was reported that fatigue cracking propagation tends to occur more at the FRP-epoxy interface rather than the epoxy-concrete interface. Furthermore, the cohesive stress transfer zone under fatigue loading, which determines the effective bond length, was found to be lower than that under monotonic loading. Similarly, the fracture energy during cyclic loading was reported to be smaller than that under monotonic loading, which is attributed to the lower tensile load applied to the FRP-to-concrete bond.

Daud, Cunningham, and Wang (2015)

During an experimental single-lap pull-out tests on CFRP-to-concrete bonded specimens, Daud et al. (2015) studied the behavior of CFRP-to-concrete bond under fatigue and post-fatigue monotonic loading. The effect of fatigue loading and CFRP properties including FRP stiffness and thickness on the bond fatigue behavior was considered. Observations showed the concrete cover shearing as the dominant failure mode during tests. Furthermore, the post-fatigue results revealed that the bond underwent strain reductions, and therefore the bond post-fatigue residual capacity reduced during the cyclic loading. Finally, the effect of concrete strength was seen to be negligible on the bond post-fatigue residual strength, while the CFRP stiffness was reported to play a dominant role in terms of bond energy degradations. As for the effect of fatigue loading amplitude, the fatigue life of the CFRP-to-concrete bond was found to be significantly dependent on this factor.

K. Li et al. (2015)

An experimental investigation on the bond behavior of CFRP/concrete interface under fatigue loading condition was conducted by K. Li et al. (2015). The fatigue endurance of the CFRP/concrete bond was evaluated with respect to the four influencing variables of loading amplitude, concrete strength, ratio of FRP to concrete width and bond length. Test observations showed that the debonding failure mode was more likely to occur in the form of concrete cover separation when the applied maximum fatigue load was greater than or equal to 70% of the bond monotonic load-carrying capacity and in cases where the maximum fatigue load was lower than 70% of monotonic bond strength, debonding mainly took place within the epoxy adhesive. It was also found that increasing the concrete strength led into an increase in the fatigue life of the FRP/concrete interface. Likewise, increased bond length contributed to a higher bond fatigue endurance of FRP/concrete. Although, increasing the bond length when it is more than the effective bond length does not affect the monotonic bond strength of FRP/concrete interface. Test results also revealed that the fatigue life of FRP/concrete interface was seen to reduce following an increase in either the loading amplitude or the CFRP-to-concrete width ratio. Moreover, a prediction model was proposed for the fatigue life of FRP/concrete interface that took account of the concrete strength (f_{cu}) and CFRP-to-concrete width ratio (b_f/b_c) as follows:

$$S/(1-S_a) = 1.90 - 0.0902\left\{\frac{0.0902\ln N_f}{[(2.06\times10^{-3}f_{cu})+0.872]\left[1.094-\left(0.382b_f/b_c\right)\right]}\right\} \quad (2.47)$$

$$\text{for} \quad S/(1-S_a) > 1.90 - \left\{\frac{1.90-(0.3/0.7)}{[(2.06\times10^{-3}f_{cu})+0.872]\left[1.094-\left(0.382b_f/b_c\right)\right]}\right\}$$

$$N_f > 2 \text{ million} \quad (2.48)$$

$$\text{for} \quad S/(1-S_a) \leq 1.90 - \left\{\frac{1.90-(0.3/0.7)}{[(2.06\times10^{-3}f_{cu})+0.872][1.094-(0.382b_f/b_c)]}\right\}$$

In the above equations, S and S_a denote the relative cyclic stress amplitude and relative mean stress applied at the CFRP sheet at the mid-span, respectively, that could be obtained as follows:

$$S = \frac{S_{\max} - S_{\min}}{S_{\text{ult}}} \quad ; \quad S_a = \frac{S_{\max} + S_{\min}}{2\, S_{\text{ult}}} \tag{2.49}$$

where, S_{ult} = ultimate stress in the CFRP sheet at midspan achieved from the monotonic test and $S_{\max}$ and $S_{\min}$ are the maximum and minimum stress applied to the CFRP sheet at midspan during the fatigue test, respectively.

Zheng et al. (2015)

An experimental investigation was performed by Zheng et al. (2015) to examine the bond fatigue behavior in concrete specimens bonded with CFRP laminates, exposed to hygrothermal environmental condition. In addition, three different loading upper-bound limits were applied to the specimens. It was observed that exposure to hygrothermal treatment tends to shorten the fatigue life of CFRP-to-concrete bond. As for the bond damage accumulation during load cycles, observations showed three stages of damage which include: Stage I) rapid decrease of bond stiffness, K_b, during the initial cycles (i.e., 3% of the number of load cycles to failure, N_f); Stage II) gradual and stable decrease of K_b during 95% N_f; and Stage III) sudden rapid decrease of K_b during the final load cycles until the bond failure (i.e., 2% N_f). Furthermore, the following model was proposed to characterize the damage quantity, D_{kn}, of the CFRP-to-concrete bond at load cycle n in hygrothermal conditions:

$$D_{kn} = \begin{cases} y_{\text{I}} \left(\frac{n}{N_{\text{I}}}\right) & n \le N_{\text{I}} \\ D_{kN_{\text{I}}} + y_{\text{II}} \left(\frac{n - N_{\text{I}}}{N_{\text{II}} - N_{\text{I}}}\right) & N_{\text{I}} < n \le N_{\text{II}} \\ D_{kN_{\text{II}}} + y_{\text{III}} \left(\frac{n - N_{\text{II}}}{N_f - N_{\text{II}}}\right) & N_{\text{II}} < n \le N_f \end{cases} \tag{2.50}$$

Where $D_{kN_{\mathrm{I}}}$ and $D_{kN_{\mathrm{II}}}$ are damage quantities at load cycles $n = N_{\mathrm{I}}$ and $n = N_{\mathrm{II}}$, respectively. Also, y_{I}, y_{II} and y_{III} are the slopes of lines related to the three stages of bond damage accumulation, as shown in Figure 2.9. Finally, a bond fatigue-life model was proposed based on the experimental results of specimens with hydrothermal pre-treatment, as follows:

$$P_{\max}/P_{\mathrm{ult}} = 1.65 - 0.1671 \log N_f \tag{2.51}$$

It may be noted that according to the proposed S-N model, the CFRP-to-concrete interface is expected to endure 2 million load cycles when the maximum applied load is less than (or equal to) approximately 59% of the bond ultimate monotonic load-carrying capacity.

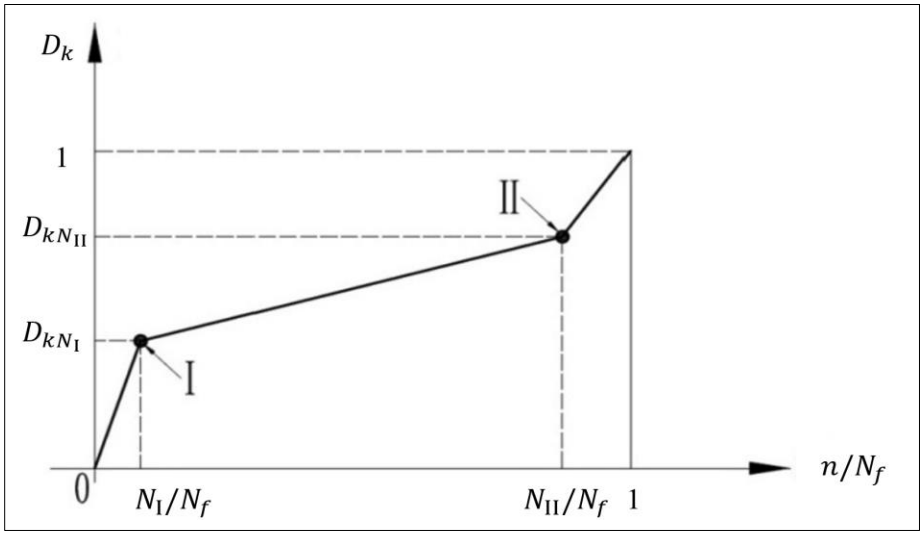

Figure 2.9 Damage quantity model for the CFRP-to-concrete interface
Taken from Zheng et al. (2015)

Zhu et al. (2016)

Zhu et al. (2016) carried out an experimental program on nine concrete specimens strengthened with CFRP to study the bond slip behavior of CFRP/concrete interface under fatigue loading conditions with respect to the concrete strength and fatigue loading amplitudes. The results

showed that as the concrete strength increases the failure mode tends to occur in a way that the CFRP sheets detach from the epoxy resin in the specimen. Also, based on the observations, the following conclusions were made: 1) an upward trend appears in the fatigue life of specimens as the concrete strength increases, and a downward trend is apparent with an increase in the fatigue load amplitude; 2) the concrete strength and fatigue loading amplitude do not have any considerable effect on the effective bond length of CFRP sheet under cyclic loading, although it is suggested that more research is needed to prove this conclusion; 3) an increase in the number of load cycles results in a degradation in the bond stress-slip curve, meaning that as load cycles increase, a reduction occurs in the shear stress levels corresponding to the same slip value. On the basis of a regression analysis with respect to the test results, the following equation was proposed for the calculation of maximum bond shear stress during load cycles, $\tau_{\max}$.

$$\tau_{\max} = \gamma k_b\,(1.085 - 0.648\,S)(0.2233 f_{cu} - 2.1433) e^{(38.46-112\,S)\frac{n}{N_f}} \qquad (2.52)$$

$$k_b = \sqrt{\frac{2.25 - b_f/b_c}{1.25 + b_f/b_c}} \quad , \quad \gamma = 0.005 f_{cu} + 0.7 \le 1$$

As can be noted the above equation took account of the effect of concrete strength, f_{cu}, and applied fatigue loading ($S = S_{\max}/S_{\text{ult}} - S_{\min}/S_{\text{ult}}$). However, this equation was achieved based on limited experimental data. In addition, the following fatigue-life prediction model of the CFRP-to-concrete bond was proposed.

$$\ln N_f = -31.646\,(S - 0.8683)\,(0.0021 f_{cu} + 0.8724) \qquad (2.53)$$

K. Li et al. (2018)

K. Li et al. (2018) carried out an investigation on the bond-slip relationship between CFRP sheets and concrete in EB FRP strengthened beams under cyclic loading. They carried out four series of tests in which four different influencing parameters were taken into consideration. The CFRP to concrete width ratio and CFRP bond length were evaluated in A and B specimen

groups and the two other parameters of loading amplitude and concrete strength were examined in C and D specimen groups. The test results revealed that the debonding load level remained almost unchanged with increasing the CFRP bond length, under the condition that the FRP bond length is longer than the effective bond length. Moreover, it was discovered that increase in the bond length resulted in increased number of cycles to FRP failure, as more loading cycles were needed for the delamination of the CFRP sheets from the concrete. Observations of the bond-slip curve demonstrated that the slope of the ascending segment of the curve decreases as the number of cycles increases without causing a noticeable change in the amount of slip corresponding to the maximum bond shear stress. Furthermore, it was concluded that increase in the concrete strength decreases the rate of slope reduction of the ascending range of bond-slip curve and increasing either of the two parameters of CFRP to concrete width ratio or load level makes the reduction rate increase under cyclic loading. Finally, through an analytical study, the following bond-slip model was proposed for the concrete/FRP interface under cyclic loading:

$$\tau = \begin{cases} \dfrac{\tau_{max,t}}{s_{\text{peak}}} s & 0 \le s \le s_{\text{peak}} \\ \dfrac{\tau_{max,t}}{s_{\text{ult},t} - s_{\text{peak}}} (s_{\text{ult},t} - s) & s_{\text{peak}} < s \le s_{\text{ult},t} \\ \tau = 0 & s > s_{\text{ult},t} \end{cases} \tag{2.54}$$

It has been reported that the local slip (s_{peak}) caused by maximum shear stress is remained constant during the cyclic loading. However, the maximum shear stress, $\tau_{\text{max},t}$, and ultimate bond slip capacity ($s_{\text{ult},t}$) are both dependent on the number of load cycles. Given that the interfacial fracture energy remains constant during load cycles, the following relationship can be found between these variables at cycle n (i.e., $\tau_{\text{max},t}$ and $s_{\text{ult},t}$) and those at the first load cycle (i.e., $\tau_{\text{max},0}$ and $s_{\text{ult},0}$), meaning, $s_{\text{ult},t} \times \tau_{\text{max},t} = \tau_{\text{max},0} \times s_{\text{ult},0}$.

In order to take into consideration, the fatigue degradation phenomenon of the concrete/FRP interface, the variable maximum shear stress ($\tau_{\text{max},t}$) at the load cycle n can be determined with respect to the bond stiffness parameter $K_{b,t}$ which is, in fact, the slope of the ascending

segment of the bond-slip curve as varied with the number of load cycles. Hence, the following equations need to be applied:

$$\tau_{\max,t} = K_{b,t}\, s_{\text{peak}} \tag{2.55}$$

$$K_{b,t} = \frac{K_{b,0}}{1 + c_k (n)^{b_k}}$$

$$c_k = 0.0007 \times e^{2.919 \times {S_c}^2}$$

$$b_k = (0.873 S_c + 0.0198)(1.208 - 0.00337 f_{cu}) \left(0.619 \frac{b_f}{b_c} + 0.838\right)$$

$$S_c = \frac{S}{1 - S_a}$$

As can be noted, S_c is the cyclic load parameter and is function of relative load range, (i.e., $S = P_{\max}/P_{\text{ult}} - P_{\min}/P_{\text{ult}}$) and relative mean cyclic load, (i.e., $S_a = P_{\max}/2P_{\text{ult}} + P_{\min}/2P_{\text{ult}}$).

W. Zhang (2018)

In another research study, W. Zhang (2018) investigated the fatigue behavior of the bond between concrete and CFRP by performing a series of double lap shear tests under fatigue loading. They also developed a bond stress-slip model of the FRP/concrete interface for strengthened beams subjected to cyclic loading. It was concluded that the increasing trend in the number of load cycles resulted in an increase in the residual slip of the FRP/concrete interface. Furthermore, test observations revealed that the locations of the unloading stiffness and the unloading slip on the envelop curve affects significantly on the shape of the loading curve. The following equations were developed to determine the cycle-dependent variables of bond slip, $s_{b,t}$, and bond stress, $\tau_{b,t}$, as shown in Figure 2.10, based on the envelope bond-slip curve, of specimens reinforced with high-strength (HS) type CFRP plate.

$$\frac{\tau_{b,t}}{\tau_{max}} = \frac{s_{b,t}}{s_{\text{peak}}} \times \frac{m}{(m-1) + (s_{b,t}/s_{\text{peak}})^m} \tag{2.56}$$

where, the maximum bond stress during fatigue loading, τ_{max}, is equal to 2.19 MPa and the corresponding bond slip, s_{peak} is equal to 0.0604 mm. Also, m is the curve characteristic constant and is equal to 3.44. In addition, the following equations were proposed for the calculation of $s_{b,t}$ and the unloading bond stiffness, $K_{\text{un},t}$, at different load cycles, n.

$$s_{b,t} = 0.046\ \text{EXP}(0.26 \log(n)) \tag{2.57}$$

$$\frac{K_{\text{un},t}}{K_{\text{un},0}} = 1.25 - 0.20 \log(n)$$

where, $K_{\text{un},0}$ is the unloading stiffness at the first load cycle.

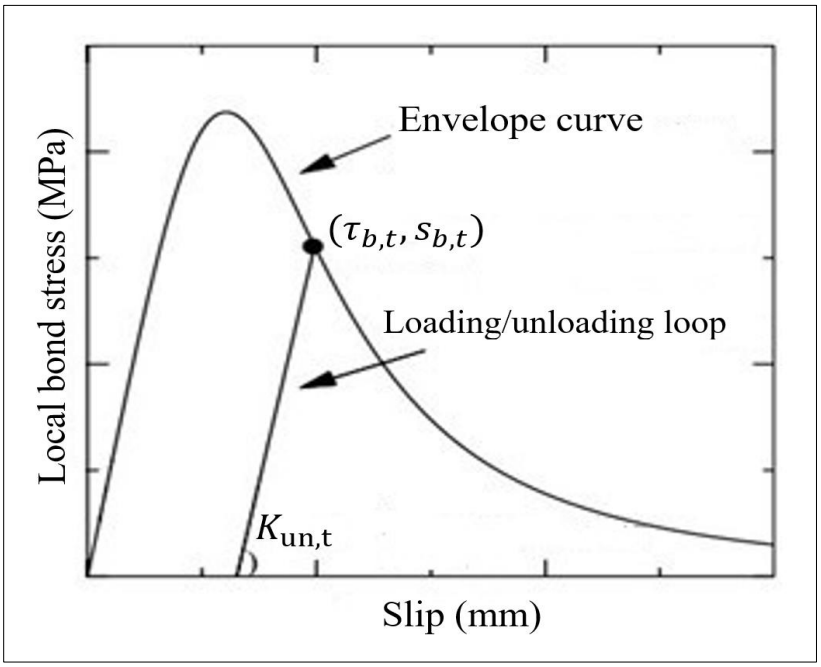

Figure 2.10 Proposed bond stress-slip model under fatigue load
Adapted from W. Zhang (2018)

Al-Saoudi, Al-Mahaidi, Kalfat, and Cervenka (2019)

A finite element (FE) analysis was performed by Al-Saoudi et al. (2019) on the fatigue performance of concrete blocks bonded with CFRP laminates with a focus on the effect of applied cyclic loading. The numerical results were also shown to be correlated with their experimental data derived from a single shear pull-out test program. In order to model the tensile fatigue behavior of the concrete, a parameter known as Beta fatigue was introduced in the FE program of ATENA and the fatigue life of the specimens were evaluated with respect to four different values of Beta fatigue, including 0.05, 0.08, 0.1 and 0.15. Also, the interaction between the concrete and the CFRP laminate was simulated by using two techniques. In the first method, a solid element with a perfect bond was applied to represent the adhesive between the concrete and CFRP, while in the second technique, an interface element was defined between the two components. It was revealed that using the former technique exhibited a more realistic behavior of the specimen under fatigue loading. Both of the aforementioned techniques are illustrated in Figure 2.11. It was shown that the numerical simulations led to similar responses observed experimentally in terms of failure modes. Furthermore, as for the numerical evaluation of structural fatigue performance goes, it was found that by adopting the Beta fatigue factor equal to 0.15, the highest correlation was achieved between the numerical results and test observations in terms of strain measurements and number of cycles to fatigue failure. Finally, it was reported that a concrete specimen with EB CFRP laminate would not undergo fatigue failure provided that the maximum stress level is set to be lower than 75% of its ultimate monotonic capacity.

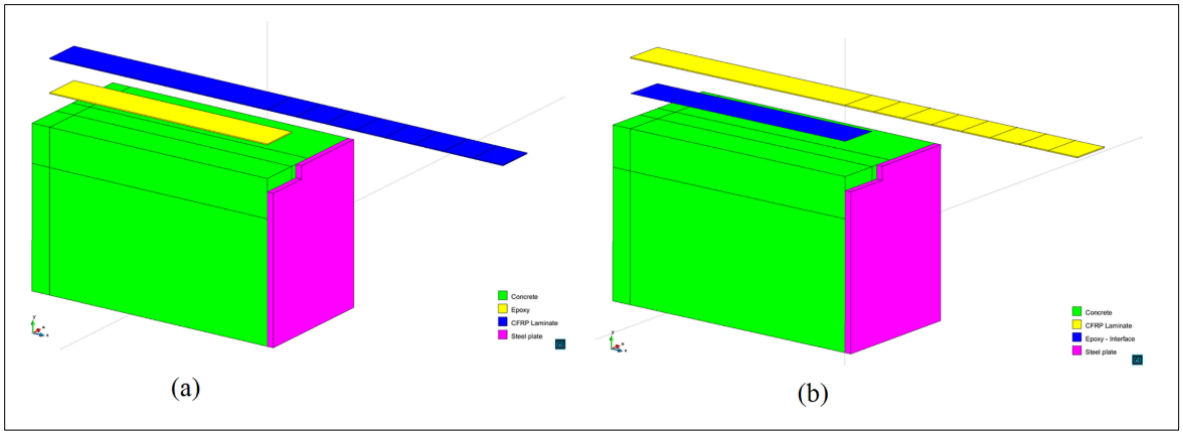

Figure 2.11 Modeling of the concrete/CFRP interface with: a) solid element; b) interface element
Taken from Al-Saoudi et al. (2019)

Chalot, Michel, and Ferrier (2019)

Another experimental study of the bond fatigue behavior was performed by Chalot et al. (2019) through a series of CFRP-to-concrete double-lap bonded specimens under cyclic loading. Different cyclic loading rates along with two different CFRP types including unidirectional CFRP (Composite A) and bidirectional CFRP (Composite B) were used in their experiments. Observations of the bond fatigue behavior showed that all specimens behaved similarly in terms of the fatigue failure mode (CFRP peel-off failure) regardless of the CFRP type or loading amplitude. Furthermore, the following S-N model of CFRP-to-concrete bond was proposed on a basis of analytical study, which includes the two variables of loading rate, $P_{\max}/P_{\text{ult}}$ and the number of loading cycles at failure, N_f:

$$P_{\max}/P_{\text{ult}} = 0.925 - 0.051 \log N_f \tag{2.58}$$

Xie et al. (2019)

Xie et al. (2019) carried out a study regarding the fatigue behavior of basalt FRP composites bonded to concrete beams and evaluated the effect of marine exposure on the bond behavior. It was observed that exposure to simulated-ocean environment decreased the ultimate

monotonic capacity of BFRP-to-concrete bond. Also, the effective bond length was seen to reduce after undergoing the saltwater condition under fatigue loading. As for the fatigue failure mode, specimens without the exposure of wet-dry cycling failed as a result adhesive failure. However, the failure mode of specimens changed to BFRP rupture after being exposed to marine conditions. Finally, an empirical S-N model was proposed for the BFRP-to-concrete interface as expressed in the following:

$$P_{\max}/P_{\text{ult}} = 1.16 - 0.088 \log N_f \tag{2.59}$$

Zhou et al. (2021)

Zhou et al. (2021) conducted a cyclic pull-out experimental program on CFRP-to-concrete one-side bonded specimens and evaluated the fatigue performance of two types of CFRP laminate from two suppliers (SikaCarborDur vs. MasterBrace) along with the effect of concrete strength and loading amplitude on the bond behavior. It was observed that the failure mode of specimens with SikaCarborDur CFRP occurred mainly due to the failure of CFRP-to-adhesive interface regardless of the concrete strength and loading amplitude, whereas the failure mode of specimens with MasterBrace changed from the concrete cover failure, under fatigue loading with the upper level higher than (or equal to) 65% of the bond monotonic capacity, to adhesive failure when the maximum applied load level was less than 65% of the bond strength. Furthermore, increasing the load cycles resulted in a decrease in the bond stiffness of CFRP-to-concrete interface. As for the fatigue bond-slip behavior, the peak cyclic bond stress was seen to increase until a threshold after which it follows a decreasing trend due to the bond fatigue damage accumulation during load cycles, as shown in Figure 2.12.

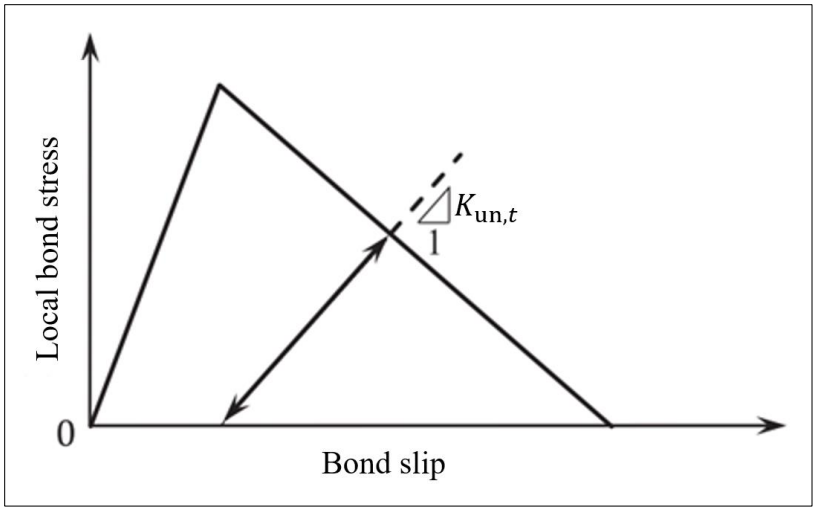

Figure 2.12 Bond-slip behavior affected by fatigue damage
Adapted from Zhou et al. (2021)

Min et al. (2023)

Min et al. (2023) conducted an analytical study of the debonding behavior of CFRP-to-concrete bonded joint under fatigue loading. It was concluded that the fatigue debonding growth was dependent on the fatigue load range. A prediction model, validated by an experimental single-lap study, was proposed for measuring the fatigue debonding growth rate, $\frac{\mathrm{d}a_d}{\mathrm{d}n}$, as follows:

$$\frac{\mathrm{d}a_d}{\mathrm{d}n} = 10^{9.3}(S_a \times S/2)^{11.3}[383.54\,(a_d + 26.78)^{-1.12}] \tag{2.60}$$

Table 2.3 shows the summarized details of the previously discussed studies on the effect of different influencing factors on the FRP/concrete interface in fatigue loading condition.

Table 2.3 Summarized details of experimental studies regarding the behavior of FRP-to-concrete interface under fatigue loading condition

No.	Research study	Test set-up	Number of specimens	FRP composite type	Influencing parameters on the bond fatigue behavior									
					Concrete strength	Bond length	FRP width	FRP stiffness	FRP thickness	FRP type	Epoxy properties	Environmental condition	Bonding condition (Anchorage)	Loading amplitude
1	Bizindavyi et al. (2003)	Single lap	46	CFRP & GFRP		✓	✓			✓				✓
2	E Ferrier et al. (2005)	Single & double lap	15	CFRP				✓			✓			✓
3	Ko and Sato (2007)	Double lap	54	CFRP AFRP & Polyacetal					✓	✓				✓
4	Yun et al. (2008)	Double lap	13	CFRP									✓	✓
5	HM Diab et al. (2009)	Double lap	17	CFRP		✓								✓
6	Carloni et al. (2012)	Single lap	7	CFRP										✓
7	Carloni and Subramaniam (2013)	Single lap	6	CFRP										✓
8	Daud et al. (2015)	Single lap	24	CFRP					✓	✓				✓
9	K. Li et al. (2015)	Beam test	19	CFRP	✓	✓	✓							✓
10	Zheng et al. (2015)	Double lap	17	CFRP								✓		✓
11	Zhu et al. (2016)	Beam test	9	CFRP	✓									✓

Table 2.3 Summarized details of experimental studies regarding the behavior of FRP-to-concrete interface under fatigue loading condition (Continue)

No.	Research study	Test set-up	Number of specimens	FRP composite type	Influencing parameters on the bond fatigue behavior									
					Concrete strength	Bond length	FRP width	FRP stiffness	FRP thickness	FRP type	Epoxy properties	Environmental condition	Bonding condition (Anchorage)	Loading amplitude
12	K. Li et al. (2018)	Beam test	15	CFRP	✓	✓	✓							✓
13	W. Zhang (2018)	Double lap	15	CFRP	✓					✓				✓
14	Al-Saoudi et al. (2019)	Single lap	6	CFRP										✓
15	Chalot et al. (2019)	Double lap	39	CFRP						✓				✓
16	Xie et al. (2019)	Beam test	26	BFRP								✓		✓
17	Zhou et al. (2021)	Single lap	13	CFRP	✓					✓				✓
18	Min et al. (2023)	Single lap	11	CFRP										✓

CHAPTER 3

ON BOND-SLIP OF EB-FRP/CONCRETE INTERFACE IN SHEAR UNDER FATIGUE LOADING: REVIEW AND SYNTHESIS OF EXPERIMENTAL STUDIES AND MODELS

Abbas Fathi [1], Georges El-Saikaly [2], Omar Chaallal [3]

[1,2,3] Department of Construction Engineering, École de Technologie Supérieure
1100 Notre-Dame St. West, Montreal, Quebec, Canada H3C 1K3

Article published in Journal of Civil Engineering and Construction, Volume 11, Issue 1, February 2022.

3.1 Abstract

Reinforced concrete (RC) structures subjected to cyclic fatigue loading are prone to progressive damage. Among the types of structural damage, those leading to shear deficiencies can result in sudden rupture of structures without warning. Hence, RC structures deficient in shear urgently need retrofitting. The use of externally bonded (EB) fiber-reinforced polymer (FRP) composites presents many advantages and is a very promising technology for shear strengthening of RC structures. This paper encompasses a wide range of research findings related to the interaction between concrete and FRP under fatigue loading. The behavior of the bond between FRP and concrete plays a major role in the failure mode of FRP shear-strengthened structures especially under fatigue. Therefore, it is of interest to characterize the FRP/concrete interaction using appropriate models with respect to the influencing parameters. The paper will first discuss existing design guidelines and considerations related to the fatigue behavior of RC structures. A thorough review of available literature on EB-FRP/concrete bond in shear under cyclic fatigue loading will then be presented, with a focus on proposed bond-slip models and finite element studies of the FRP/concrete interface under fatigue loading.

Keywords: Fatigue loading; Bond-slip models; Shear; Reinforced concrete structures; Fiber-reinforced polymer (FRP); FRP/concrete interface; Finite element analysis (FEA)

3.2 Introduction

Many reinforced concrete (RC) structures such as bridge girders are expected to resist high numbers of cycles of fatigue loading, mainly due to traffic loads, during their life span. Many existing bridge structures in Canada and worldwide were designed according to old design codes in which the design loads did not consider the increased service loads caused by higher present-day traffic volume (Chaallal et al., 2010; El-Saikaly & Chaallal, 2015-b). Indeed, out of over 8,000 bridges reported on by the Canadian National Highway System, 60% are more than 30 years old, about 4% are rated as being in poor condition, and 80% need some sort of retrofitting (Azim & Gül, 2019). In the United States, reports also show that out of 615,002 bridges, about 9% are classified as structurally deficient (FHWA, 2017). A large proportion of RC bridge structures show considerable signs of damage due to concrete deterioration, corrosion of steel reinforcement, and lack of sufficient load-carrying capacity according to current design guidelines (Chaallal et al., 2010). Therefore, rehabilitation of such structures to withstand cyclic fatigue loads has always been a major concern for engineers. Shear failure, which is a common failure mode that can be caused by fatigue loading, often occurs suddenly and without warning. This mode of failure is characterized by diagonal tension cracks that are mainly due to the combined effects of flexural (bending) and shearing action. The use of externally bonded (EB) fiber-reinforced polymer (FRP) composites to strengthen deficient RC beams is widely accepted. EB-FRP composites present many advantages such as high strength-to-weight ratio, corrosion resistance, fatigue resistance, light weight, and ease of application (Aidoo et al., 2004; Kim & Heffernan, 2008; Oudah & El-Hacha, 2013).

The fatigue life (fatigue strength) of an EB-FRP strengthened RC structure is defined as the number of load cycles leading up to the structural failure. Indeed, the stress level in the steel reinforcement is known as the main component that determines the fatigue life of RC structures EB-FRP strengthened, particularly in flexure. Therefore, the fatigue life of a structure is generally represented by an S-N curve, which is in terms of stress versus the logarithm of the number of load cycles. Experimental investigations have revealed that the fatigue life of FRP strengthened RC structures depend on their failure modes. The most common failure modes

that have been observed in EB-FRP shear-strengthened RC structures under fatigue loading include crushing of concrete struts, debonding of FRP from concrete, yielding and fracture of longitudinal tensile steel bars, and steel stirrup rupture (Chaallal et al., 2010; El-Saikaly & Chaallal, 2015-b). However, it is widely accepted that the fatigue life of FRP strengthened RC beams in flexure is typically governed by the fatigue strength of the internal steel reinforcement. Indeed, it is reported that fracture of the steel reinforcement is the dominant failure mode in such structures (Oudah & El-Hacha, 2013). As far as the fatigue strength of steel goes, a downward trend appears in the S-N curve until a stress level, known as the endurance limit, beyond which the curve progresses horizontally along the N-axis. Therefore, steel tends to resist an indefinite number of load cycles at its endurance limit. For concrete, however, the curve seems to drop to its fatigue strength, as shown in Figure 3.1 (Oudah & El-Hacha, 2013). More specifically, no endurance limit has been observed in the fatigue life of concrete under ten million cycles of fatigue load, but its fatigue strength in compression, tension, or flexure under the same number of load cycles has been found to be approximately 55% of its static strength. This level of residual strength is in fact the ultimate load reached by the specimens under quasi-static loading condition after they experienced 10 million cycles (ACI 215R, 1974). As for the fatigue performance of FRP composites, carbon FRP (CFRP) has been found to have the longest fatigue life among FRP materials (Z. Wu et al., 2010). Moreover, a typical CFRP composite can exhibit an endurance limit of 60% to 70% of its initial static ultimate strength (ACI 440.2R, 2017).

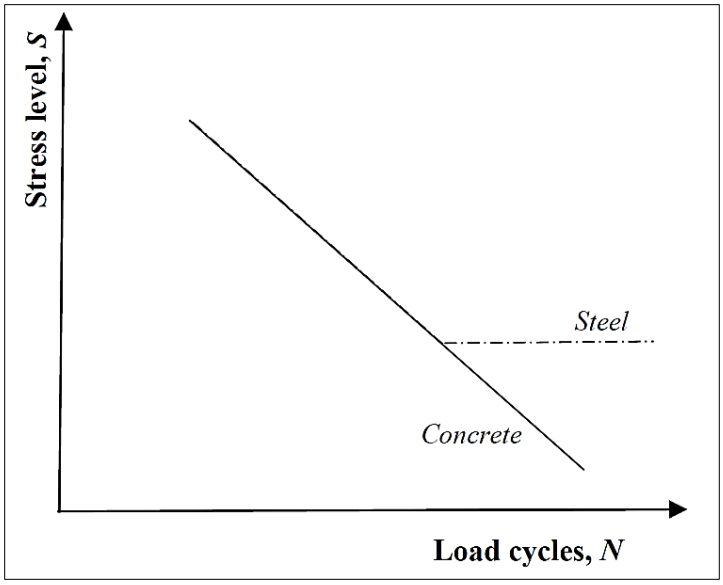

Figure 3.1 Schematic S-N curves of concrete and steel

Through extensive research investigations on the fatigue behavior of RC beams strengthened in flexure with EB-FRP, researchers have developed numerous S-N models to determine the fatigue failure of internal longitudinal tensile reinforcement, which has been known to be the governing factor in the fatigue life of EB-FRP strengthened RC beams in flexure (Barnes & Mays, 1999; Brena et al., 2005; Harries, 2005; Heffernan & Erki, 2004; Masoud et al., 2001; Toutanji et al., 2006).

Considering the performance of an EB-FRP shear-strengthened RC beam under fatigue loading, the FRP/concrete bond behavior can have a significant effect on the fatigue strength of the structure because premature debonding at the interface prevents the EB-FRP from attaining its full capacity. Hence, it is of great interest to evaluate the fatigue life of RC structures strengthened in shear with EB-FRP in terms of the behavior of the FRP/concrete bond and to investigate the influencing parameters affecting the interlaminar interaction between FRP and concrete.

Despite considerable research on shear strengthening of RC beams using EB-FRP systems under monotonic loading, the fatigue behavior of EB-FRP shear-strengthened RC structures has not been fully documented. Kim and Heffernan (2008) presented the state of the art on the

fatigue performance of FRP-strengthened RC structures in flexure. Various fatigue-related parameters were investigated, including applied load range, FRP bond behavior, crack propagation, environmental effects, and failure modes. Another state-of-the-art review was published by Oudah and El-Hacha (2013), in which a parametric study was carried out on the fatigue behavior of RC structures strengthened in flexure with FRP composites. Furthermore, a few other literature reviews have been published on the fatigue behavior of FRP-strengthened RC beams (Danraka, Mahmod, Oluwatosin, & Student, 2017; H Diab & Wu, 2008; Z. Wu et al., 2010). It is noteworthy that these studies focused on the flexural performance of RC structures strengthened with EB-FRP under cyclic fatigue loading. In contrast, investigations related to shear behavior were not considered in previous literature reviews.

Prior investigations on the fatigue behavior of concrete/FRP bond have demonstrated the reliance of the resistance of FRP strengthened concrete structures on the bond failure mechanism, thereby making it necessary to determine the bond-slip model of concrete/FRP interface in such structures (Lu et al., 2005; Zhou et al., 2021). An accurate bond-slip model needs to take into account all the influencing parameters including concrete strength, FRP bonded length, FRP-to-concrete width ratio, and fatigue loading amplitude. A review of related literature shows that a bond-slip model with the ability to consider all the aforementioned factors under fatigue conditions has yet to be developed. The aim of this paper is to introduce all the proposed models related to the bond behavior at FRP/concrete interface and identify the pros and cons of each of them. Furthermore, the application of bond-slip models in finite element modeling (FEM) of FRP/concrete interface is evaluated through reported numerical studies. Based on the existing gaps identified herein, further investigations could be conducted on the FRP/concrete bond behavior under fatigue loading.

The state of our knowledge is presented in the following sections to shed light on the fatigue behavior of EB-FRP shear-strengthened RC structures by examining bond behavior. To that end, this paper is organized into several sections covering a wide range of aspects, which include: i) a review of existing design codes related to the fatigue life of concrete as well as FRP composites; ii) research findings regarding the fatigue behavior of the bond at the

FRP/concrete interface; and iii) a review of finite-element simulations of the FRP/concrete bond under fatigue loading. Finally, the gaps and shortcomings in the available published research are identified, along with recommendations for further investigation.

3.3 Design code provisions

The fatigue stress limits of concrete and FRP materials are specified in many design code provisions. The stress in FRP should not exceed the maximum applied stress, including sustained and cyclic loading. For example, the maximum stress specified by ACI 440.2R (2017) is equal to 20%, 30%, and 55% of ultimate FRP strength for glass FRP (GFRP), aramid FRP (AFRP), and CFRP, respectively, whereas these stress limits are 25%, 35%, and 65% according to CSA S6 (2019).

For RC structures under flexural fatigue loading, ACI 215R (1974) limits the stress range of concrete to 40% of its compressive strength, whereas according to ACI 440.2R (2017), the compressive stress in concrete should be limited to 60% of its strength for RC structures strengthened with EB-FRP under cyclic service load.

On the basis of experimental observations, an EB-FRP strengthened RC member is exposed to fatigue damage when the cyclic load range is over 60% of its monotonic yield capacity (*fib* TG5.1, 2019). Furthermore, in EB-FRP strengthened RC structures, the bond strength at the FRP/concrete interface is greatly affected by the tensile strength of the concrete substrate. The concrete substrate is the weakest link in the FRP/concrete interface, and its tensile strength and soundness govern the effectiveness of externally bonded FRP systems (ACI 440.2R, 2017). Therefore, it is recommended that the minimum required tensile strength of concrete in EB-FRP applications be greater than 1.5 MPa (ACI 440.2R, 2017; CSA S6, 2019; *fib* TG5.1, 2019).

3.4 Fatigue behavior of FRP/concrete interface under cyclic loading

The FRP/concrete interface plays a major role in the shear performance of EB-FRP strengthened RC structures under fatigue loading. The FRP/concrete bond can be affected by numerous parameters including concrete strength, FRP bonded length, FRP-to-concrete width ratio and fatigue loading amplitude. An investigation by Ko and Sato (2007) on the bond behavior of different FRP materials including carbon, aramid, and polyacetal revealed that concrete specimens bonded with carbon FRP (CFRP) materials featured superior performance in terms of load-carrying capacity and initial stiffness compared to those strengthened with aramid and polyacetal FRPs. Increasing FRP stiffness by using multiple layers was also reported to increase the maximum bond strength (Ko & Sato, 2007). In addition, the FRP/concrete bond is likely to undergo fatigue failure when the adhesive is exposed to temperatures higher than its glass transition temperature or as a result of freezing and thawing (Z. Wu et al., 2010). Furthermore, exposure to a hygrothermal environment (high temperature and moisture) can shorten the fatigue life of the CFRP-concrete interface and result in aggressive decay of the bond behavior (Zheng et al., 2015). Since the fatigue failure mode of RC structures shear-strengthened with EB-FRP depends on the FRP/concrete interaction, research has been carried out to develop bond-slip models for the FRP/concrete interface under cyclic loading considering various influencing factors such as concrete strength, FRP-to-concrete width ratio, fatigue loading amplitude, and bond length. Table 3.1 presents details of experimental investigations that were conducted to evaluate the behavior of bond between EB-FRP and concrete under fatigue loading. In the following sections, the proposed bond-slip models as well as the fatigue life models of FRP-to-concrete interface are presented. In addition, the influencing parameters of the bond between EB-FRP and concrete in fatigue loading conditions are thoroughly discussed.

3.4.1 Bond-slip models of FRP/concrete interface

A number of bond-slip models have been proposed to characterize the interfacial behavior of FRP/concrete bond under static loading. Table 3.2 lists the proposed local bond slip models

under static loading reported in the literature. Figure 3.2 shows the developed bond-slip curves for an FRP bonded concrete specimen under static loading with the following properties: f_c'= 30 MPa, f_t= 2.9 MPa, b_f= 75 mm, b_c=150 mm, t_f= 0.13 mm, E_f= 230 GPa, E_c= 32.5 GPa. The aforementioned symbols are defined in Table 3.2.

Table 3.1 Details of experimental investigations on the fatigue behavior of FRP/concrete bond along with the investigated parameters

Authors	**Number of specimens**	**Test specifications**		**Fatigue loading condition**				**Influencing parameters**						
		Pull-out Test set-up	**FRP system**	**Maximum number of load cycles**	**Frequency (Hz)**	**Lower bound load**	**Upper bound load**	**Concrete strength**	**FRP to concrete width ratio**	**Loading amplitude**	**Bond length**	**FRP type**	**FRP ratio**	**Environmental condition**
Bizindavyi et al. (2003)	46	Single lap shear	FRP laminates	-	1	var	var		✓	✓	✓	✓		
Ko and Sato (2007)	54	Double lap shear	CFRP sheets	-	-	-	-					✓	✓	
HM Diab et al. (2009)	17	Double lap shear	CFRP sheets	3 million	5	10% $f_{u,b}$	30-80% $f_{u,b}$			✓				
Carloni et al. (2012)	7	Single lap shear	CFRP sheets	-	1	var	var			✓				
K. Li et al. (2015)	21	Four-point bending	CFRP sheets	2 million	2.5	15% $f_{u,b}$	45-80% $f_{u,b}$	✓	✓	✓	✓			
Zheng et al. (2015)	17	Double lap shear	CFRP laminates	-	10	var	var			✓				✓
Zhu et al. (2016)	9	Four-point bending	CFRP sheets	2.5 million	2.5	15% $f_{u,b}$	var	✓		✓				
K. Li et al. (2018)	15	Four-point bending	CFRP sheets	-	2.5	15% $f_{u,b}$	var	✓	✓	✓	✓			
W. Zhang (2018)	15	Double lap shear	CFRP laminates	1 million	1	10% $f_{u,b}$	50-90% $f_{u,b}$			✓				
Xie et al. (2019)	26	Four-point bending	BFRP sheets	2 million	10	var	var			✓				✓

Note: $f_{u,b}$= Static bond capacity

Table 3.2 Available bond-slip models under static loading

Authors	Bond-slip models
Neubauer and Rostasy (1999)	$\tau = \begin{cases} \tau_{max}\left(\frac{s}{s_0}\right) & s \le s_0 \\ 0 & s > s_0 \end{cases}$ $\tau_{max} = 1.8\,\beta_w f_t \quad , \quad s_0 = 0.202\,\beta_w \quad , \quad \beta_w = \sqrt{1.25 \times \frac{2-b_f/b_c}{1+b_f/400}}$
De Lorenzis et al. (2001)	$\tau = K_{int} \times s$ $K_{int} = G_{int}/t_{int} \quad , \quad \tau_{max} = 0.0182\,(n_f t_f E_f)^{0.5} \quad , \quad (n_f t_f E_f$ in MPa , mm)
Nakaba et al. (2001)	$\tau = \tau_{max}\left(\frac{s}{s_0}\right)\left[3/(2+(\frac{s}{s_0})^3)\right]$ $\tau_{max} = 3.5\,f_c'^{0.19} \quad , \quad s_0 = 0.065$
Monti et al. (2003)	$\tau = \begin{cases} \tau_{max}\left(\frac{s}{s_0}\right) & s \le s_0 \\ \tau_{max}\left(\frac{s_{ult}-s}{s_{ult}-s_0}\right) & s > s_0 \end{cases}$ $\tau_{max} = 1.8\,\beta_w f_t \quad , \quad s_0 = 2.5\,\tau_{max}\,(n_f t_f/E_f + 50/E_c)$ $s_{ult} = 0.33\beta_w \quad , \quad \beta_w = \sqrt{1.5 \times \frac{2-b_f/b_c}{1+b_f/100}}$
Savoia et al. (2003)	$\tau = \tau_{max}\left(\frac{s}{s_0}\right)\left[2.86/(1.86+(\frac{s}{s_0})^{2.86})\right]$ $\tau_{max} = 3.5\,f_c'^{0.19} \quad , \quad s_0 = 0.051$
Lu et al. (2005)	$\tau = \begin{cases} \tau_{max}\left(\frac{s}{s_0}\right) & s \le s_0 \\ \tau_{max}\left(\frac{s_{ult}-s}{s_{ult}-s_0}\right) & s_0 < s \le s_{ult} \\ 0 & s > s_{ult} \end{cases}$ $\tau_{max} = 1.5\,\beta_w f_t \quad , \quad s_0 = 0.0195\,\beta_w f_t \le 0.06$ $s_{ult} = 2G_f/\tau_{max} \quad , \quad G_f = 0.308\,{\beta_w}^2\sqrt{f_t} \quad , \quad \beta_w = \sqrt{\frac{2.25-b_f/b_c}{1.25+b_f/b_c}}$
Pellegrino et al. (2008)	$\tau = \begin{cases} \tau_{max}\left(\frac{s}{s_0}\right) & s \le s_0 \\ \tau_{max}\left(\frac{s_{ult}-s}{s_{ult}-s_0}\right) & s > s_0 \end{cases}$ $\tau_{max} = 3.1\,(n_f t_f E_f)^{0.32} \quad , \quad s_0 = 0.075/(n_f t_f E_f)^{0.2}$ $s_{ult} = 10.5/(n_f t_f E_f)^{0.6} \quad , \quad (n_f t_f E_f\ in\ GPa\ ,\ mm)$

Note:
τ_{max}: Maximum interfacial shear stress
s_0: Peak slip at which shear stress reaches maximum
s_{ult}: Ultimate slip value
$n_f t_f E_f$: FRP stiffness
E_c: Concrete elastic modulus
K_{int}: Slip modulus of the interface, $K_{int} = 1386\ ksi/in$ (376 MPa/mm)
f_c': Concrete cylinder compressive strength
f_t: Concrete tensile strength
β_w: Width ratio factor
b_f/b_c: FRP-to-concrete width ratio
G_f: Fracture energy
G_{int}: Interfacial shear modulus, $G_{int} = 74.86\ ksi$ (515.8 MPa)
t_{int}: Interfacial thickness

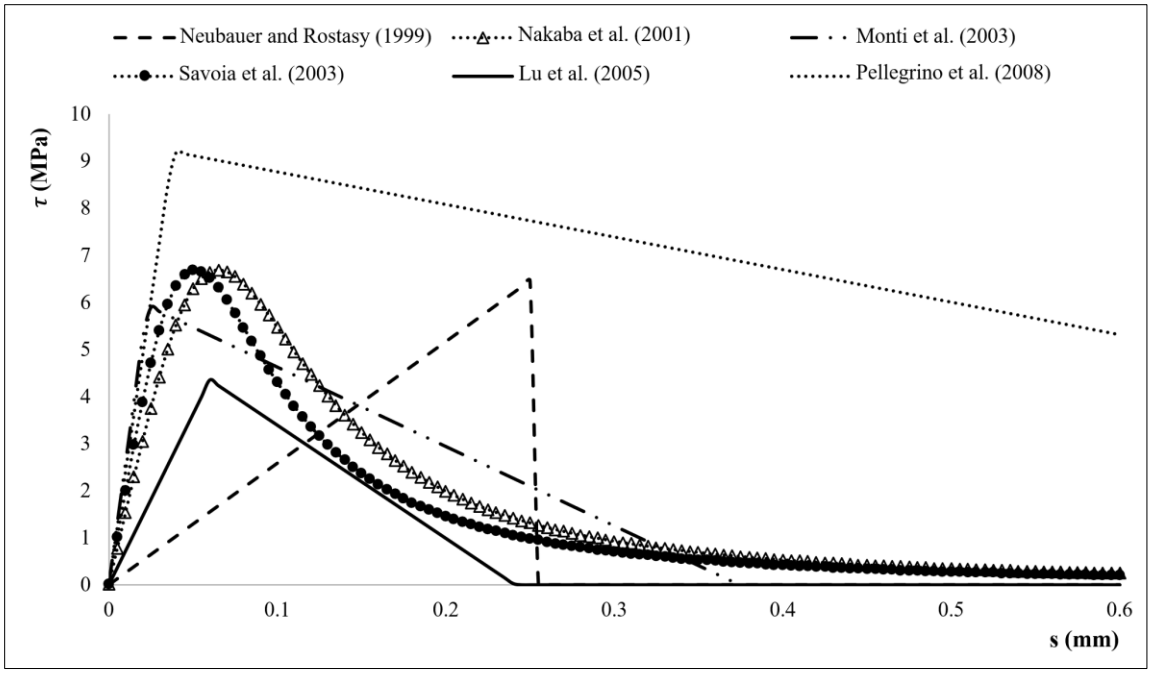

Figure 3.2 Existing bond-slip models under static loading

Ko and Sato (2007) developed a bond stress-slip model under cyclic loading based on Popovics (1973) that agreed well with their own experimental results of double shear pull-out tests on 54 specimens. Indeed, two cyclic loading conditions (Cyclic 1 and 2) were considered in their experiments. During both cyclic loading conditions, a limited number of unload/reload paths were set. For Cyclic 1, the unloading loads corresponded to the maximum monotonic load capacity as well as the maximum monotonic displacement, whereas for Cyclic 2 condition, unloading of specimens was performed according to the maximum slips reached at each strain gauge location. Figure 3.3 depicts the bond-stress curve of a tested specimen based on the envelopes derived from the cyclic hysteresis of the interfacial stress-slip relation. The proposed model, expressed in Eq. (3.1) and Eq. (3.2), involved several empirical parameters, including the maximum bond stress, τ_{max} , the corresponding slip, s_0, the curve characteristic constants, c, c_2, c_3, the unloading stiffness, K_{un}, the ultimate slip, s_{ult}, the friction stress, τ_{fp}, the negative friction stress, τ_{fn} and the unloading slip s_{un}:

$$\tau = \frac{\frac{\tau_{max} \times c \times s}{s_0}}{\left[(c+1) + \left(\frac{s}{s_0}\right)^c\right]} \quad (3.1)$$

$$K_{un} = c_2 \times {s_{un}}^{c_3} \quad (3.2)$$

Where, τ and s are the bond stress and slip of the FRP/concrete interface, respectively. Also, the constant values of c, c_2 and c_3 can be found from the experimental data in Ko and Sato (2007). Despite the fact that the results predicted by the model and the experimental data showed a good agreement, the proposed model was nevertheless developed on the basis of a limited number of loading/unloading repetitions. In addition, a linear approximation was adopted for the unload/reload path in the model for simplicity, which is inconsistent with the actual oval-shaped curves featured in the experiments (Ko & Sato, 2007).

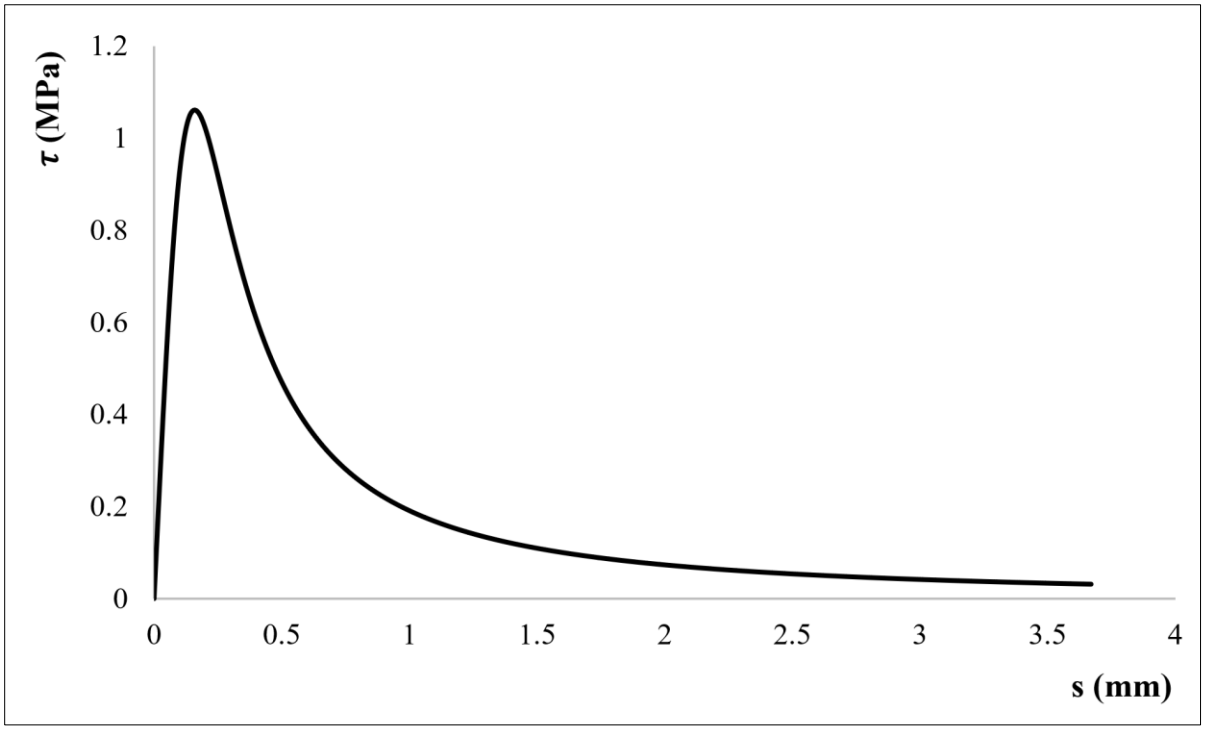

Figure 3.3 Envelope-base bond-slip curve of a specimen tested by Ko and Sato (2007) under cyclic loading

The following cyclic bilinear bond-slip model, as stated in Eqs. (3.3)–(3.7) and illustrated in Figure 3.4 was proposed by HM Diab et al. (2009) to characterize the fatigue behavior of the CFRP/concrete interface:

$$\tau = \begin{cases} \dfrac{\tau_{max.t}}{s_0} s & 0 \le s \le s_0 \\ \dfrac{\tau_{max.t}}{s_{ult.t} - s_0}(s_{ult.t} - s) & s_0 < s \le s_{ult.t} \end{cases} \tag{3.3}$$

$$\tau_{max.t} = \frac{\tau_{max.0}}{1 + \varphi \cdot \alpha} \tag{3.4}$$

$$s_{ult.t} = \frac{\tau_{max.0} \times s_0}{\tau_{max.t}} \tag{3.5}$$

$$K_{bt} = \frac{K_{b0}}{1 + \varphi \cdot \alpha} \tag{3.6}$$

$$\varphi = \begin{cases} 0.046(t)^{0.4} & t \le 2000 \\ 1.2(1 - \exp(-t/1200) & t > 2000 \end{cases} \tag{3.7}$$

Where, t is the cyclic loading time (in seconds), $\tau_{max.0}$ and $\tau_{max.t}$ are the cyclic bond strengths of the adhesive at time zero and time t, respectively, K_{b0} and K_{bt} are the cyclic stiffness values of the bond at time zero and time t, respectively, $s_{ult.t}$ is the cyclic ultimate slip (at time t), φ is the creep fatigue coefficient, and α is a frequency-dependent factor that is equal to 1 for a frequency of 5 Hz. As can be seen, the cyclic dependent bilinear model successfully takes into account the degradation of interfacial stiffness under fatigue loading by adopting a simple creep-fatigue coefficient (φ) in the equations. It should be noted that the model presented above was developed for the case of simple shear pull-out test. However, it has been argued that in actual debonding phenomenon, failure occurs due to the combined effects of shear and normal stresses near the cut-off points of bonded FRP (Z. Wu et al., 2010).

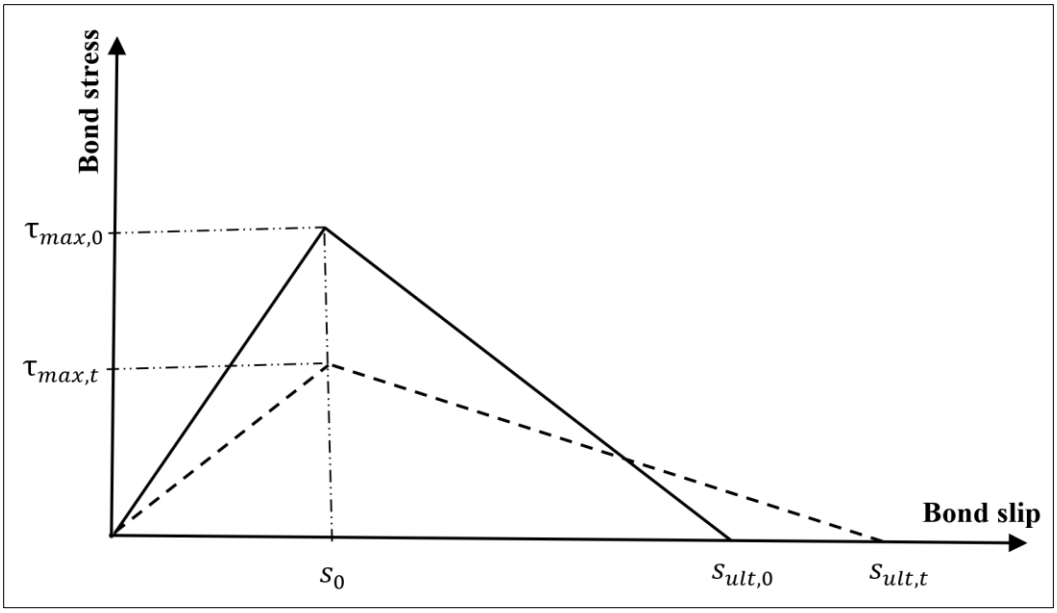

Figure 3.4 Cyclic bilinear bond-slip model proposed by HM Diab et al. (2009)

By examining the interfacial behavior of concrete and FRP in EB-FRP flexural strengthened RC beams under cyclic loading, Loo, Foster, and Smith (2012) proposed a bond-slip model for concrete/FRP interaction. The proposed model, illustrated in Figure 3.5, can be expressed by the following equations:

$$s_{b.max} = \frac{\tau_{b.max}}{E_{b0}}[1 + K_a \times M(\log n)^b \times (\frac{\Delta\tau_b}{\tau_{b.ult}})^h] \tag{3.8}$$

$$E_b = E_{b0}[1 + K_2 \times \mu(\log n)^\beta \times \left(\frac{\Delta\tau_b}{\tau_{b.ult}}\right)^\lambda] \tag{3.9}$$

Where, $s_{b.max}$ is the slip (in mm) corresponding to the maximum applied average bond stress ($\tau_{b.max}$), $\Delta\tau_b$ is the difference between the average bond stress at maximum cyclic load and the average stress at minimum load cycle, $\tau_{b.ult}$ is the average bond stress at the maximum load cycle, N_b, leading to bond failure (in *N/mm*^{2}), n is the number of load cycles, E_b and E_{b0} are the moduli of elasticity of the bond (in *N/mm*^{2}) at cycle n and at the first loading cycle, respectively, and $K_a = K_1 \log(n)$ and K_2 are factors defining the relationship between average bond stress and bonding length. By validating these equations with the limited literature data,

the following parameters were determined: $M = 1.068$, $b = 1.402$, $h = 2.612$, $\mu = -190.3$, $\beta = 0.990$ and $\lambda = 8.797$. Based on numerical results, the proposed FE model showed good agreement with experimental results in terms of beam displacements at maximum loads, CFRP strains, and the number of load cycles to failure.

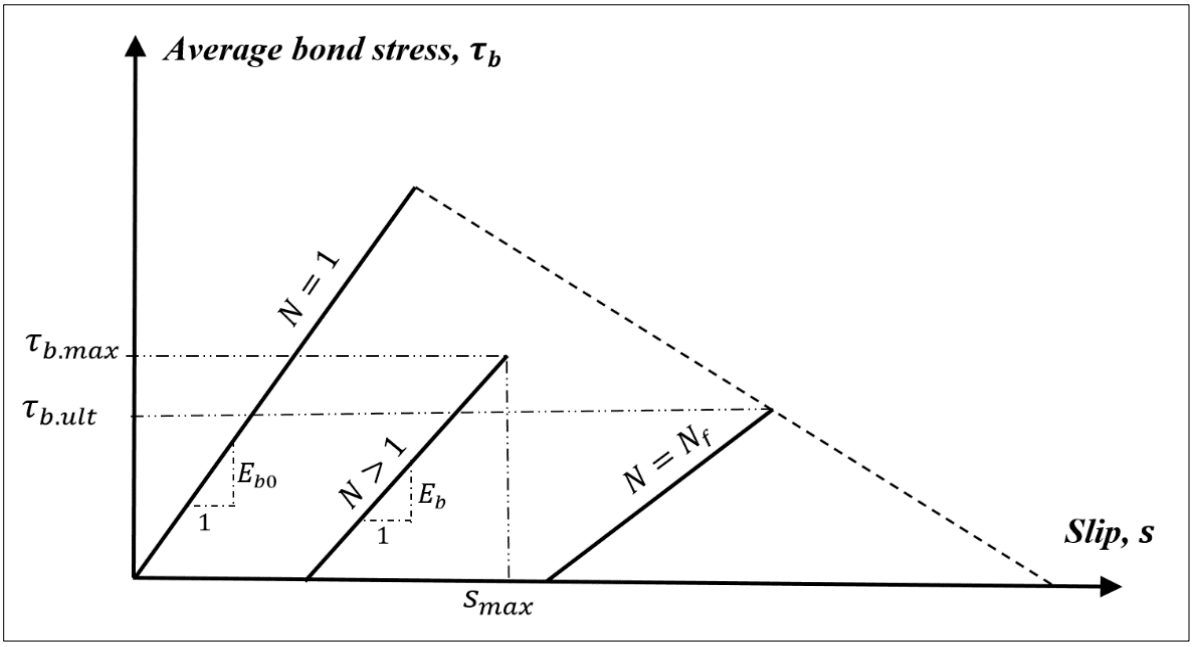

Figure 3.5 Constitutive bond-slip model of Concrete/FRP interface under fatigue loading by Loo et al. (2012)

Based on a regression analysis with limited experimental data, another bond stress-slip relationship was proposed by considering the effects of concrete strength and load amplitude under fatigue loading (Zhu et al., 2016), as follows:

$$\tau_{max} = \gamma\beta_w(1.085 - 0.648T)(0.2233f_{cu} - 2.1433)e^{(38.46-112T)\frac{n}{N}} \qquad (3.10)$$

Where, τ_{max} is the maximum shear stress of the CFRP/concrete interface, f_{cu} is the concrete cubic compressive strength, and n and N are the number of fatigue loading cycles and the fatigue life of specimens, respectively. T is the ratio of the applied fatigue loading amplitude, $P_{max} - P_{min}$, to the monotonic capacity, P_u, $(\frac{P_{max}-P_{min}}{P_u})$ for each specimen, β_w is the

coefficient related to the ratio of the CFRP and concrete specimen's widths, b_f/b_c, and the coefficient γ can be expressed as:

$$\beta_w = \sqrt{\frac{2.25 - b_f/b_c}{1.25 + b_f/b_c}} \qquad ; \qquad \gamma = 0.005 f_{cu} + 0.7 \leq 1 \tag{3.11}$$

The proposed nonlinear bond-slip relationship successfully took into consideration the effect of fatigue degradation on the FRP/concrete bond behavior due to cyclic loading when calculating the maximum bond shear stress. However, in their experimental data analysis based on which the above-mentioned bond-slip model was developed, the effect of CFRP-to-concrete width ratio was not considered as a variable despite its demonstrated influence on the bond property of FRP/concrete interface as evidenced by reported experimental studies (K. Li et al., 2018).

Also, an analytical study along with an experimental investigation by K. Li et al. (2018) led to a bond-slip model for the concrete/FRP interface under cyclic loading, as expressed in Eqs. (3.12) – (3.20):

$$\tau = \begin{cases} \dfrac{\tau_{max.t}}{s_0} s & 0 \leq s \leq s_0 \\ \dfrac{\tau_{max.t}}{s_{ult.t} - s_0}(s_{ult.t} - s) & s_0 < s \leq s_{ult.t} \\ \tau = 0 & s > s_{ult.t} \end{cases} \tag{3.12}$$

$$s_{ult.t} = \frac{2G_f}{\tau_{max.t}} \tag{3.13}$$

$$G_f = {\beta_w}^2 (0.029 f_{cu} - 0.2668) \tag{3.14}$$

$$\tau_{max.t} = K_t \, s_0 \tag{3.15}$$

$$K_t = \frac{K_0}{1 + c_k \times n^{b_k}} \tag{3.16}$$

$$c_k = 0.0007 \times e^{2.919 \times {S_c}^2} \tag{3.17}$$

$$b_k = (0.873 \times S_c + 0.0198)(1.208 - 0.00337 \times f_{cu})(0.619 \times \frac{b_f}{b_c} + 0.838) \tag{3.18}$$

$$S_c = \frac{T}{1 - S_a} \tag{3.19}$$

$$S_a = \frac{P_{max} + P_{min}}{2P_u} \tag{3.20}$$

Where, s_0 and $s_{ult.t}$ are the slip corresponding to the maximum shear stress ($\tau_{max.t}$) and the ultimate slip within the load cycles, respectively, K_0 and K_t are the slopes of the ascending segment of the bond-slip curve at the initial load cycle and cycle n, respectively, G_f is the interfacial fracture energy, c_k , b_k are coeffcients obtained from the test results. S_c is the cyclic load level, which is a function of the applied loading amplitude-to-ultimate load capacity ratio (T) and the average cyclic loading-to-ultimate load capacity ratio (S_a). It has been reported that the local slip at the maximum interfacial shear stress (s_0) remains constant during the load cycles. However, the maximum cyclic shear stress ($\tau_{max.t}$) and the maximum cyclic slip ($s_{ult.t}$) are both dependent on the number of load cycles, thereby keeping the interfacial fracture energy (G_f) unchanged during cyclic loading. During the experimental testing, the performance of a series of specimens within four groups (A, B, C and D) was observed. The effects of loading amplitude and concrete strength were taken into consideration in group A and B, whereas in groups C and D, the bond length and FRP-to-concrete width ratio (b_f/b_c) were chosen as the variables. Figure 3.6 shows the bond-slip curves of a specimen (from group D) with respect to different number of load cycles, n, (0, 420, 2500 and 6500) obtained from the proposed model. It can be understood from the cyclic bond-slip curve that the slope of the ascending segment decreases as the number of cycles increases without causing a noticeable

change in the amount of slip corresponding to the maximum bond shear stress (s_0). The bond-slip curves derived from the two models developed by Zhu et al. (2016) and K. Li et al. (2018) are illustrated in Figure 3.7 and Figure 3.8 under different number of load cycles for specimens selected from group B and group C, with the following properties: f_{cu}= 35.3 MPa, b_f/b_c= 0.25 mm, γ= 0.8765, T= 0.5, N= 88300, for the specimen from group B and f_{cu}= 62.2 MPa, b_f/b_c= 0.35 mm, γ= 1, T= 0.55, N= 20680, for the specimen from group C. As can be observed from the two figures, the results from both models tend to agree more with group-B specimens compared to group-C specimens. This is attributed to the fact that the parameter of FRP-to-concrete width ratio was considered in specimens from group B when developing the bond-slip model. Therefore, the superiority of the developed bond-slip model against the previous proposed models was that the effect of the CFRP-to-concrete width ratio was taken into account when deriving the bond-slip curves. In addition, the bilinear bond-slip model was reported to be simpler and more efficient for identifying the fatigue interfacial behavior of CFRP/concrete bond (K. Li et al., 2018).

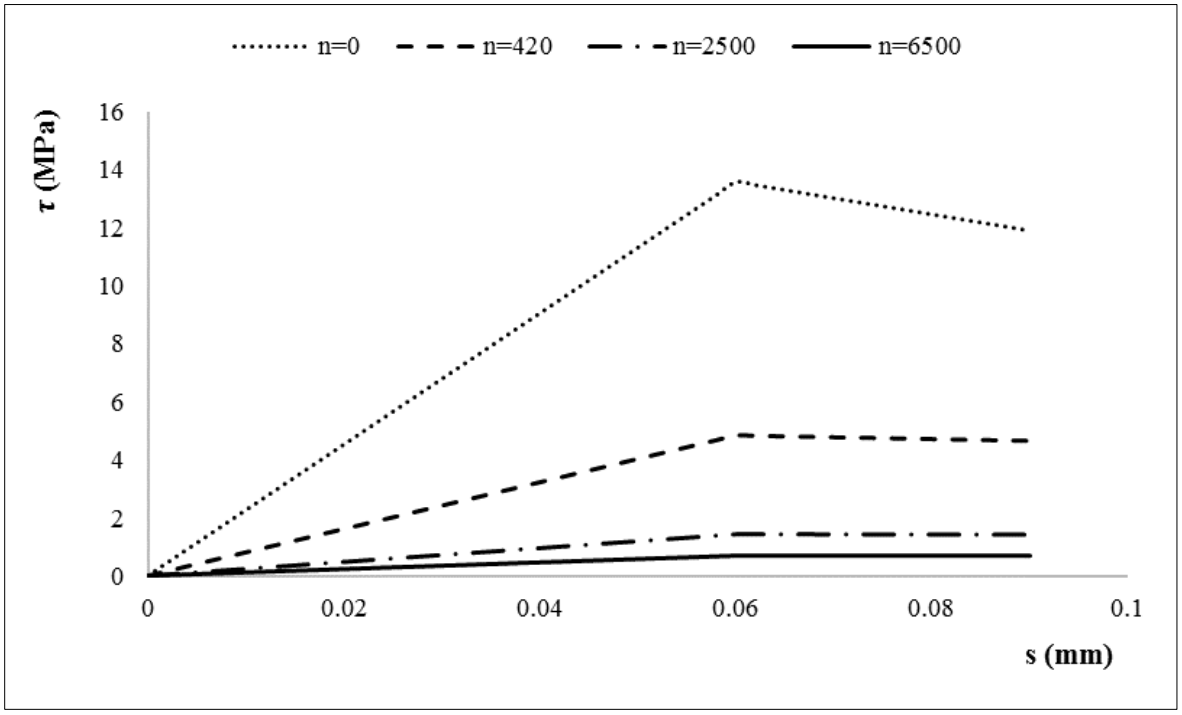

Figure 3.6 Bond-slip curves of a tested specimen under different number of load cycles (*n*) by K. Li et al. (2018)

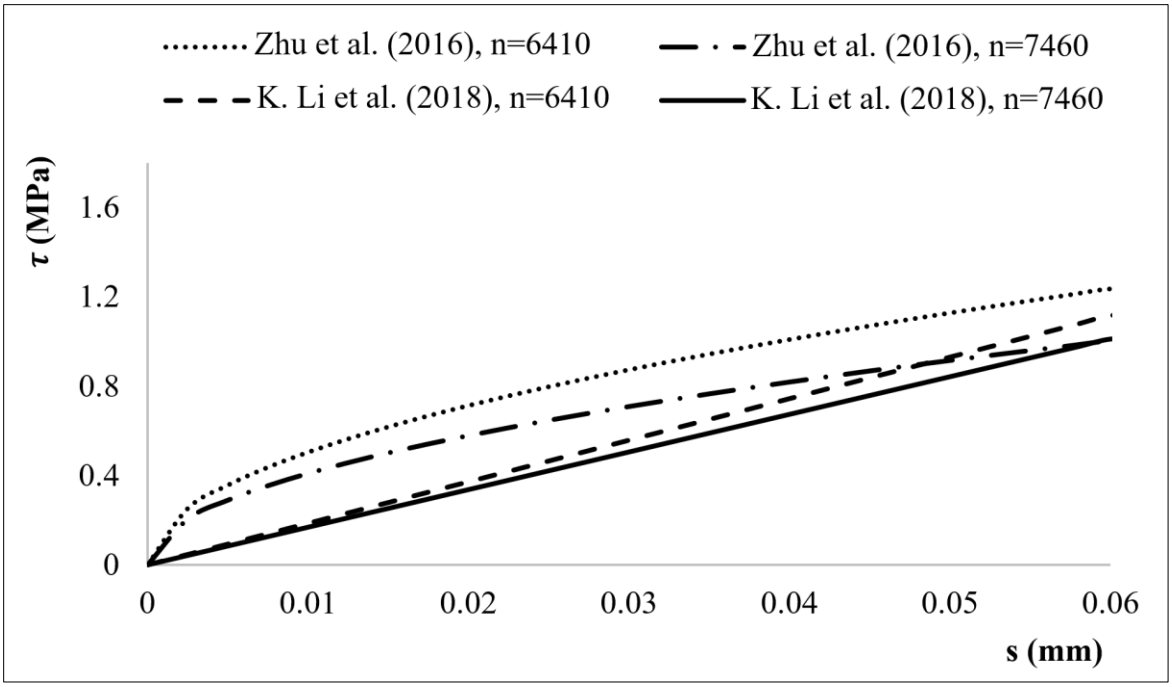

Figure 3.7 Bond-slip model curves of a specimen from Group B (considering loading amplitude and concrete strength as variables)

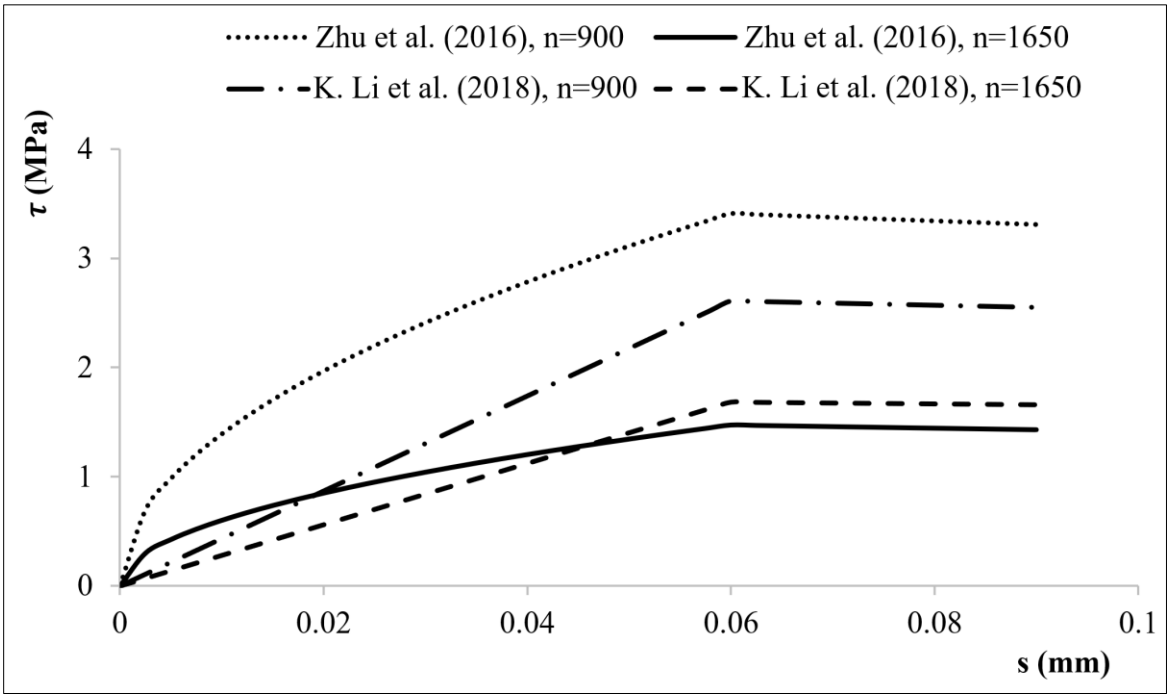

Figure 3.8 Bond-slip model curves of a specimen from Group C (considering bond length and FRP-to-concrete width ratio as variables)

W. Zhang (2018) carried out some research to develop a bond stress-slip model and proposed the following equations to determine the local bond stress-slip relationship of specimens reinforced with high-strength (HS) CFRP plate. The proposed model, which was based on the model first presented by Popovics (1973), showed good agreement with their own experimental results from a series of double-lap fatigue shear tests:

$$s_{eu} = 0.046\ \mathrm{EXP}(0.26\log(n)) \tag{3.21}$$

$$\frac{K_{un.i}}{K_{un.1}} = 1.25 - 0.20\log(n) \tag{3.22}$$

$$\tau_{eu} = \tau_{max}\frac{s_{eu}}{s_0} \times \frac{m}{(m-1) + (^{s_{eu}}/_{s_0})^m} \tag{3.23}$$

Where s_{eu} and τ_{eu} are the slip and stress values on the envelope curve, respectively, n is the number of fatigue cycles, $K_{un.i}$ and $K_{un.1}$ are the unloading stiffness at cycle n and the unloading stiffness during the first cycle, respectively, which can be determined by the unloading slope from the envelope curve, τ_{max} and s_0 are the maximum bond stress and the corresponding slip, respectively and m is the curve characteristic constant which is equal to 3.44. The proposed model showed good agreement with the experimental results of specimens strengthened with HS CFRP plates. However, the applicability of the aforementioned model on other types of CFRP reinforcement requires further investigation.

Considering the cyclic bond-slip models discussed above, it is fair to say that the model developed by K. Li et al. (2018), expressed in Eqs. (3.12) – (3.20), has successfully taken into account the influencing factors, in particular FRP-to-concrete width ratio, and is able to predict interfacial shear stress of FRP-to-concrete bond under fatigue loading with adequate accuracy. However, it seems that the proposed model was developed using limited experimental data and a wider range of test results is needed to corroborate its effectiveness.

3.4.2 FRP/concrete bond fatigue life models

A fatigue life model was proposed by Bizindavyi et al. (2003) in the form of the following power-law relationship for FRP/concrete bonded members:

$$\Delta S = (N_b \times C_b)^{-\omega} \tag{3.24}$$

Where, ΔS is the cyclic mean bond stress range, and can be obtained from the maximum and minimum applied stresses, $S_{max} - S_{min}$, N_b is the number of cycles to the bond failure, and C_b and ω are constants obtained from test data. In their experimental investigation, which led to the aforementioned S-N model, two different FRP types of Glass FRP (GFRP) and Carbon FRP (CFRP) were applied to the specimens. It was observed from the S-N curves that the fatigue life of the FRP/concrete interface can be reduced by either increasing the applied stress level or decreasing the bond length.

Following an analytical investigation of the shear behavior of the FRP/concrete interface under fatigue loading, HM Diab et al. (2009) proposed a prediction methodology to determine the fatigue life of the FRP/concrete interface. A nonlinear interfacial constitutive law was proposed to calculate the rate of debonding growth per loading cycle ($\frac{\mathrm{d}a_d}{\mathrm{d}n}$), which can be expressed as follows:

$$\frac{\mathrm{d}a_d}{\mathrm{d}n} = m_1 \left(\frac{G_{max}}{G_c}\right)^{n_1} \beta_d \tag{3.25}$$

Where a_d is the debonding length, n is the number of cycles, m_1 and n_1 are parameters obtained from regression analysis of experimental tests, and G_{max} and G_c are the maximum strain-energy release rate and the quasi-static fracture energy, respectively. Finally, β_d is the fatigue debonding growth coefficient, which is used to account for the reduction in debonding propagation rate with increasing debonding length, a_d.

K. Li et al. (2015) proposed a prediction model for the fatigue life of the FRP/concrete interface that takes into account the concrete cube compressive strength (f_{cu}) and the CFRP-to-concrete width ratio (b_f/b_c) as follows:

$$S_f/(1-S_{f.a}) = 1.90 - 0.0902\left\{\frac{0.0902\ln N_b}{[(2.06\times10^{-3}f_{cu})+0.872][1.094-(0.382b_f/b_c)]}\right\} \quad (3.26)$$

$$\text{for} \quad S_f/(1-S_{f.a}) > 1.90 - \left\{\frac{1.90-(0.3/0.7)}{[(2.06\times10^{-3}f_{cu})+0.872][1.094-(0.382b_f/b_c)]}\right\}$$

$$N_b > 2\ million \quad (3.27)$$

$$\text{for} \quad S_f/(1-S_{f.a}) \le 1.90 - \left\{\frac{1.90-(0.3/0.7)}{[(2.06\times10^{-3}f_{cu})+0.872][1.094-(0.382b_f/b_c)]}\right\}$$

In Eqs. (3.26) and (3.27), N_b represents the fatigue life of the FRP/concrete interface, and S_f and $S_{f.a}$ are the stress amplitude and related mean stress of the CFRP sheet at the mid-span of the four-point bending test, respectively and are given by:

$$S_f = \frac{S_{f.max}-S_{f.min}}{S_{f.u}} \quad ; \quad S_{f.a} = \frac{S_{f.max}+S_{f.min}}{2S_{f.u}} \quad (3.28)$$

Where $S_{f.u}$ = ultimate stress in the CFRP sheet at mid-span obtained from the monotonic test and $S_{f.max}$ and $S_{f.min}$ are the maximum and minimum stress in the CFRP sheet at the mid-span (in the four-point bending test setup), obtained from the fatigue test, respectively. Hence, as can be understood from the prediction model, by measuring the applied stresses to CFRP and calculating the ratio $S_f/(1-S_{f.a})$, the fatigue life of CFRP-to-concrete interface (N_b) can be determined (K. Li et al., 2015).

An S-N relationship of the CFRP/concrete bond was proposed by Zheng et al. (2015) based on an experimental program including a series of double-lap shear tests on specimens with hygrothermal pre-treatment in which the temperature and relative humidity of environmental chambers were set according to the considerations stated in Zheng et al. (2015). It should be

noted that by using Eq. (3.29), the CFRP/concrete bond fatigue strength (S_b) was determined as 59% of static bond strength within 2 million load cycles (N_b):

$$S_b = 1.65 - 0.167 \log N_b \tag{3.29}$$

In an experimental study by Xie et al. (2019), the fatigue behavior of the interface between basalt-FRP (BFRP) sheets and concrete under marine environmental conditions (i.e., environment with large temperature variations and over repeated wet-dry cycles) was investigated. The following empirical equation was proposed to determine the fatigue life of the BFRP/concrete bond:

$$S_b = 1.16 - 0.088 \log N_b \tag{3.30}$$

Where S_b is the stress ratio of BFRP and N_b is the number of cycles at which fatigue failure of the BFRP/concrete interface occurs. It is noteworthy that the measured fatigue strength of the BFRP/concrete interface with exposure to marine conditions was approximately 60% of its ultimate monotonic load-carrying capacity.

It can be understood from the S-N models discussed above that the interface between the FRP and concrete tends to comply with a different fatigue life relationship depending on various conditions, namely, Glass or Carbon FRP-to-concrete bond, bond in hygrothermal environment and also Basalt FRP-to-concrete interface. Hence, when applying the fatigue life model at the interface between FRP and concrete, it is of importance to ensure that the model corresponds to the right condition and predicts the fatigue behavior of the bond accordingly.

3.4.3 Concrete compressive strength

The influence of concrete compressive strength on the bond behavior of the FRP/concrete interface has been investigated through many experimental studies. Experimental investigations on the FRP-to-concrete bonded members have revealed different forms of

debonding failure including concrete cover separation and intermediate crack-induced debonding (C. Chen et al., 2019). In cases where the interfacial failure of the FRP/concrete bond is due to the concrete cover separation, it is reasonable to believe that increasing the concrete compressive strength could result in an enhancement in the ultimate load capacity of the bond between concrete and FRP under static loading (Abdalla et al., 2020). Likewise, results of another investigation showed that increasing the concrete compressive contributes to reaching higher cohesive stress at the FRP/concrete interface as well as delaying the activation of FRP strain under static loading (C. Chen & Cheng, 2019).

As far as fatigue loading is concerned, test observations have indicated that increasing the concrete strength extends the fatigue life of FRP/concrete interface (K. Li et al., 2015; Zhu et al., 2016). In an experimental study by K. Li et al. (2015), specimens with three concrete cube compressive strengths of 62.2, 35.3, and 25.1 MPa bonded with CFRP were tested under the same fatigue loading ratio ($P_{max}/P_{ult} = 0.65$). It was shown that increasing the concrete strength from 25.1 MPa to 35.3 MPa enhanced the number of load cycles to failure of CFRP/concrete interface by approximately 30% and an increase of about 90 % was also observed in the fatigue life of the bond between concrete and CFRP when the concrete strength of specimens increased from 35.3 MPa to 62.2 MPa. Similarly, it was reported by C. Chen and Cheng (2017) that concrete with a higher compressive strength, and hence a higher tensile strength, could help hinder the fatigue crack propagation and lower the distributed axial strain on the FRP reinforcement, thereby improving the performance of the bond between FRP and concrete. An experimental program was carried out by Zhu et al. (2016) on nine concrete beam specimens strengthened with EB-CFRP to study the bond-slip behavior of the CFRP/concrete interface under fatigue loading conditions for the same three concrete cube compressive strengths investigated by K. Li et al. (2015) (i.e., 25.1 MPa, 35.3 MPa, and 62.2 MPa). It was observed that debonding may occur in one of the three regions of concrete cover, interface between concrete and epoxy, and interface between CFRP and epoxy. Furthermore, it has appeared that as concrete compressive strength increases, the fatigue life of the CFRP/concrete interface reaches higher levels, leading to an improvement in the performance of the bonding system. In addition, the maximum interfacial shear stress at the first cycle was seen to rise with

an increase in the concrete strength. Indeed, an increase of about 40% and 230% in the shear stress of concrete/FRP interface was seen when the concrete strength increased from 25.1 MPa to 35.3 MPa and then from 35.3 MPa to 62.2 MPa, respectively. It may be of interest to note that higher concrete strength triggers the failure to occur as a result of CFRP sheet debonding from the epoxy resin rather than the concrete cover separation in the specimen (Zhu et al., 2016). Another study by K. Li et al. (2018) showed that variations in the concrete compressive strength can affect the bond-slip relationship of the FRP/concrete interface during the cyclic loading. Indeed, the slope of the ascending branch of the bond-slip curve tends to decrease at a lower rate during the load cycles, with an increase in the concrete strength.

3.4.4 Bond length

The effect of bond length on the fatigue behavior of the CFRP/concrete interface has been evaluated in many research studies. It was concluded in a research review that increasing FRP bond length enhances the fatigue life of the FRP/concrete interface (Z. Wu et al., 2010). In an experimental investigation by K. Li et al. (2015), the fatigue endurance of the CFRP/concrete bond was evaluated with respect to bond lengths of 60, 160, and 240 mm, where increased bond length contributed to higher bond fatigue endurance of the FRP/concrete interface. Indeed, test observations indicated that increasing the bond length from 60 mm to 160 mm resulted in an increase of about 338% in the fatigue life of CFRP/concrete interface, and when the bond length increased from 160 mm to 240 mm, the number of cycles to failure of specimens has almost tripled. It was reported that, when the bond length increases, the increase in the fatigue life of the bond between CFRP and concrete was attributed to the fact that more loading cycles were needed to delaminate the CFRP sheets from the concrete (K. Li et al., 2018). Similar experimental results were observed in an study by Bizindavyi et al. (2003), in which shorter bonded length seemed to reduce the fatigue life of the FRP/concrete interface by creating higher stress intensity levels at the FRP-to-concrete bond.

The effective bond length in FRP-strengthened concrete structures is defined as the minimum FRP bonded length at which the maximum force is transferred between the concrete substrate

and the EB-FRP composite (*fib* TG5.1, 2019). The effective bond length can be determined in experimental programs by taking the average of the bonded lengths of three specimens with the same load-carrying capacity at failure that have been tested constitutively, within a tolerance of 10% (CSA S806, 2012). In the case of monotonic loading, the effective bond length (l_e) can be obtained from the following equations according to existing guidelines:

$$l_e = \frac{23300}{(n_f \times E_f \times t_f)^{0.58}} \quad \text{(ACI 440.2R, 2017)} \tag{3.31}$$

$$l_e = \frac{25350}{(n_f \times E_f \times t_f)^{0.58}} \quad \text{(CSA S806, 2012)} \tag{3.32}$$

$$l_e = \frac{\pi}{\beta_w}\sqrt{\frac{n_f \times E_f \times t_f}{8\, {f_{cm}}^{2/3}}} \quad , \quad \beta_w = \sqrt{\frac{2-b_f/b_c}{1+b_f/b_c}} \quad \text{(}fib\text{ TG5.1, 2019)} \tag{3.33}$$

Where, n_f is the number of FRP layers, E_f and t_f are the elastic modulus and thickness of FRP, respectively, f_{cm} is the concrete mean compressive strength and b_f/b_c is the FRP-to-concrete width ratio.

It has been reported by K. Li et al. (2015) that the effective bond length obtained experimentally under fatigue loading with the frequency of 2.5 Hz is less than that under monotonic loading at a rate of 0.001 mm/s. This can be attributed to the fact that the debonding failure of the specimen initiates at a lower load level during fatigue loading in comparison with that under quasi-static loading. Moreover, the interfacial crack propagation tends to occur in the epoxy adhesive rather than in the concrete under the fatigue condition (Carloni & Subramaniam, 2013; Carloni et al., 2012; K. Li et al., 2015). It has also been experimentally observed that increasing the bond length beyond the effective bond length does not seem to affect either the debonding load level or the bond strength of the CFRP/concrete interface (K. Li et al., 2015; K. Li et al., 2018).

3.4.5 FRP-to-concrete width ratio

As discussed in the bond-slip models, the factor of FRP-to-concrete width ratio (b_f/b_c), included in some of the proposed bond slip models (see Eq. 3.11), plays a key role in determining the bond behavior of the FRP/concrete interface under fatigue loading; therefore, neglecting its effect could lower the accuracy of the bond-stress slip predictions obtained from the models. Considering the effect of FRP width on the fatigue behavior of the FRP/concrete interface, it has been experimentally observed that using narrower FRP laminates leads to higher slip values (Bizindavyi et al., 2003), which could be attributed to the greater stress concentration imposed on the FRP-to-concrete interface. Furthermore, a series of other experimental tests has revealed that the fatigue life of the FRP/concrete interface drops with increasing CFRP-to-concrete width ratio, which may be due to the fact that the interfacial bond capacity tends to increase at lower FRP-to-concrete ratios (K. Li et al., 2015). Another study by K. Li et al. (2018) also showed that increasing the CFRP-to-concrete width ratio in strengthened concrete specimens during a sequence of load cycles reduces the fatigue resistance of the CFRP/concrete interface and accelerates the reduction in the slope of the ascending segment of the corresponding bond-slip curve.

3.4.6 Fatigue loading amplitude

Test results on the effect of fatigue loading amplitude revealed that the fatigue life of the CFRP/concrete interface tends to decline with increasing loading amplitude (K. Li et al., 2015; Xie et al., 2019; Zheng et al., 2015). It has also been reported that at higher loads, the fatigue life of the concrete/FRP interface is dominated by crack initiation, whereas at lower fatigue load limits, crack propagation plays the main role in determining bond fatigue strength (Carloni et al., 2012). Experimental observations of cyclic single-lap shear tests conducted by Bizindavyi et al. (2003) revealed that CFRP-strengthened concrete specimens are likely to fail due to rupture of laminates at higher applied cyclic stresses, particularly when the maximum stress is close to the static load-bearing strength of the CFRP laminate. This effect was also observed on the bond performance of near-surface mounted (NSM) strips under fatigue

loading, where it has been demonstrated that the bond strength of NSM strips does not undergo a significant decrease provided that the upper applied load is less than 60% of the monotonic debonding load and that the stress amplitude of the FRP strip is kept below 250 MPa (*fib* TG5.1, 2019). Finally, an experimental study on the effect of fatigue loading amplitude by Zhu et al. (2016) showed that an increase in the number of load cycles leads to a degradation of the bond stress-slip curve, meaning that shear stress is reduced under the same slip condition.

3.5 Finite-element analysis of EB-FRP/concrete interface under fatigue loading

Finite-element analysis (FEA) provides a cost-effective tool to evaluate structural behavior by taking into account a wide spectrum of influencing parameters without having to perform time-consuming and costly experiments (ACI, 2018). Numerous studies have been carried out on the use of finite-element (FE) simulations of EB-FRP strengthened RC structures and particularly of FE modeling of the FRP/concrete interface under both static and fatigue loading. It has been reported that applying an appropriate model for the FRP/concrete bond as well as the interface between the internal steel and concrete in FRP shear strengthened RC beams could significantly alter the numerical responses, in particular, the shear capacity of the beam under static loading (G. Chen, Chen, & Teng, 2012). However, Loo et al. (2012) found that there is a negligible slippage between concrete and steel reinforcement in FRP strengthened RC structures during fatigue loading cycles. Hence, the FE modeling of steel/concrete interface does not affect the cyclic behavior of the structure as much as modeling of the bond between FRP and concrete. It should be noted that regarding numerical analysis of RC beams strengthened with EB-FRP under fatigue loading, researchers have investigated only the flexural behavior of structures, and to the authors' knowledge, there has been no investigation on FE modeling of the FRP/concrete interface in EB-FRP shear-strengthened RC beams under cyclic loading. Nevertheless, a few FE studies have been conducted on the fatigue behavior of the bond between concrete prisms and FRP materials in pull-out shear tests (Al-Saoudi et al., 2019; Daud, Cunningham, & Wang, 2017).

3.5.1 FE modeling of the FRP/concrete bond

The modeling of the FRP/concrete interface has a significant effect on the numerical results derived from FE simulations. It is now well established that assuming a perfect bond between EB-FRP and concrete under monotonic loading results in over-estimation of the shear resistance of shear-strengthened RC beams (ACI, 2018; G. Chen et al., 2012; Godat, Neale, & Labossière, 2007). The FE modeling of the interface between FRP and concrete under fatigue loading has been performed in a few studies, which led to an enhancement in the numerical results validated with the experimental observations. In a numerical investigation on the fatigue performance of EB-FRP strengthened RC beams in flexure by Xin Wang et al. (2014), the concrete/FRP bond behavior was defined using the bilinear bond-slip model proposed by Lu et al. (2005). As for the bond geometry modeling, contact elements (TARGE170 and CONTA174) in ANSYS were used. The contact elements were able to take into account the shear stresses between the two interfacial surfaces by applying a Coulomb friction model. Also, in FE simulations performed by Pathak and Zhang (2019) on EB-FRP strengthened RC beams in flexure under cyclic loading, the model developed by Loo et al. (2012) was adopted to characterize the bond-slip behavior of the interface between FRP and concrete. Spring elements in ANSYS were used to simulate the interfaces between concrete, adhesive and FRP. This two-node nonlinear element has no physical mass and dimension and can incorporate the cyclic bond-slip model for the interfacial behavior. Indeed, through the implementation of the cyclic bond-slip models in the FEA of FRP-strengthened RC structures, a more accurate prediction of the bond behavior was achieved.

In another study, the EB-CFRP/concrete interface was simulated based on the Mohr-Coulomb criterion with tension cut-off (Banjara & Ramanjaneyulu, 2019). Accordingly, the linear relationship between the interfacial stresses and the corresponding displacements in the tangential and normal directions ($\Delta v_1 \,.\, \Delta v_2 \,.\, \Delta u$) was expressed according to the following equation:

$$\begin{Bmatrix}\tau_1\\ \tau_2\\ \sigma\end{Bmatrix}=\begin{bmatrix}k_{tt} & 0 & 0\\ 0 & k_{tt} & 0\\ 0 & 0 & k_{nn}\end{bmatrix}\begin{Bmatrix}\Delta v_1\\ \Delta v_2\\ \Delta u\end{Bmatrix} \tag{3.34}$$

Where τ and σ are the shear and normal stresses, respectively and k_{tt} and k_{nn} are the initial elastic normal and shear stiffnesses, respectively. The numerical model successfully evaluated the fatigue life of RC beams with different levels of flexural deficiencies when compared to the corresponding experimental data.

Fatigue modeling of the EB-FRP/concrete interaction has also been investigated in numerical studies of shear pull-out tests. Daud et al. (2017) performed a numerical analysis on a single shear pull-out test and evaluated the interfacial behavior between the concrete block and the bonded CFRP plate under post-fatigue loading condition. The bond between the concrete and the EB-CFRP was represented using cohesive elements in which a traction separation model was applied. In another numerical investigation simulating a series of single shear pull-out tests of CFRP bonded concrete blocks under fatigue loading (Al-Saoudi et al., 2019), the interaction between the concrete and the CFRP laminate was modeled using two techniques. In the first technique, a solid element with a perfect bond was used to represent the adhesive between the concrete and the CFRP, whereas in the second, an interface element was assumed between the two components. It was concluded that using a solid element with a perfect bond exhibited more realistic specimen behavior under fatigue loading than using an interface element.

3.5.2 Numerical parametric studies on the FRP/concrete bond

Numerical investigations have been conducted to evaluate the influence of different parameters on the behavior of bond between FRP and concrete, specially in FRP strengthened RC beams, under both monotonic and fatigue loading. In a numerical study by Al-Rousan and Issa (2011) under fatigue loading, the effects of applied stress range, CFRP-to-concrete contact area, and number of CFRP layers on the flexural capacity and deflection of the strengthened beam were assessed. The applied load range corresponded to various ratios of steel yielding stress ($f_{s.y}$),

including $0.25f_{s.y}$–$0.35f_{s.y}$, $0.45f_{s.y}$–$0.65f_{s.y}$, $0.65f_{s.y}$–$0.90f_{s.y}$, and $0.45f_{s.y}$–$0.90f_{s.y}$. The stress range had a considerable influence on the structural behavior in terms of mid-span deflection, stiffness degradation, and failure mode, particularly for the fatigue stress range of $0.45f_{s.y}$–$0.90f_{s.y}$. Further numerical results proved that increasing either the CFRP contact area with concrete or the number of CFRP layers leads to an enhancement in stiffness and ultimate load capacity, as well as a reduction in mid-span beam deflection. Likewise, through nonlinear FEA of CFRP-strengthened RC beams in flexure under cyclic loading, Pathak and Zhang (2019) indicated that increasing the FRP thickness resulted in a decrease in beam deflection as well as FRP strain. However, in a numerical parametric study of the number of CFRP layers on the fatigue life of FRP strengthened RC beams by Banjara and Ramanjaneyulu (2019), it was shown that using three CFRP layers did not significantly increase the load-carrying capacity of beams over that achieved with two layers of CFRP.

According to the numerical results, it was also observed that carbon FRP (CFRP) strips exhibited a better performance in reducing beam deflection and increasing beam fatigue life when compared to glass FRP (GFRP) strips. Furthermore, the computational results demonstrated that beams strengthened with longer FRP sheets underwent less central deflection and showed lower FRP strain (Pathak & Zhang, 2019).

The effect of prestressing CFRP on the fatigue behavior of flexural strengthened RC beams was analyzed in a FE study by Guo, Wang, Huang, and Chen (2019). Various prestressing levels (0%, 10%, 15%, and 22%) were modelled by applying initial stress values to the CFRP laminates. Increasing the prestressing level resulted in enhanced beam fatigue life by reducing the stresses on the reinforcing bars. However, using prestressed laminates tended to increase damage to the CFRP/concrete interface, increasing thereby the possibility of debonding failure. Similar conclusions were made by Xiaomeng Wang, Zhou, Ai, Petrů, and Liu (2020) upon FEA of RC beams strengthened in flexure with prestressed hybrid FRP (HFRP), consisting of hybrid carbon and glass FRP (C/GFRP), under fatigue loading. It was stated that applying too much prestressing could lead to a large reversed arch and premature fracture of C/GFRP composites.

Environmental conditions can also affect the fatigue behavior of FRP-strengthened beams in flexure. Indeed, numerical observations have shown that hygrothermal conditions (high temperature, high humidity) can decrease the strength of the CFRP/concrete interface and increase the stress level of internal steel reinforcement, in turn leading to an accelerated rate of damage at the CFRP/concrete interface and at the main longitudinal steel reinforcement under fatigue loading (Y. Wang et al., 2020). It has also been observed that CFRP-strengthened beams in an indoor environment tend to fail as a result of steel reinforcing rupture under fatigue loading, whereas the failure mode of beams in hygrothermal environments was found to be debonding of the CFRP/concrete interface (Y. Wang et al., 2020).

An assessment of the effect of various design parameters such as concrete compressive strength, CFRP stiffness, CFRP-to-concrete width ratio, and CFRP bond length on the post-fatigue performance of the CFRP/concrete interface was conducted in a numerical investigation consisting of a single pull-out test (Daud et al., 2017). The study revealed that increasing the bond length increases the ultimate load capacity until the effective bond length is provided, after which the ultimate load tends to stabilize. As for variation in concrete compressive strength, higher concrete strength results in an increase in bond strength, provided that the failure mode is concrete surface separation (delamination) beneath the adhesive layer. However, specimens that failed because of CFRP rupture did not seem to be affected by the change in concrete strength. Finally, numerical observations indicated that an increase in the CFRP-to-concrete width ratio results in an increase in CFRP bond strength, which agreed with the corresponding experimental results.

Based on reported numerical results from FRP/concrete pull-out tests, it was also stated that shear-strengthened structures with EB-CFRP laminates are able to perform better in terms of fatigue resistance, provided that the maximum applied stress is less than 75% of the ultimate monotonic load capacity (Al-Saoudi et al., 2019).

3.6 Synthesis and discussion

Research studies of FRP/concrete interaction show that the debonding in EB-FRP strengthened concrete blocks mainly occur in the form of concrete surface separation. Hence, the FRP/concrete bond behavior is greatly affected by concrete compressive strength. Indeed, increasing the concrete compressive strength is likely to enhance the interfacial fatigue life as well as the bond strength. Similarly, bond length has been reported to affect the FRP/concrete interface. However, CFRP/concrete bond strength does not seem to be affected by increasing the CFRP bond length beyond the effective bond length derived from experimental tests. In contrast, by considering the effect of fatigue loading range, an inverse relationship between the applied load amplitude and the fatigue life of the FRP/concrete bond was revealed, meaning the FRP-to-concrete interface tends to fail at lower load cycles when subjected to higher amplitudes of fatigue loading. Furthermore, based on reported experimental results, increasing the number of load cycles results in reduced maximum shear stress of the FRP/concrete interface. However, that does not seem to affect the maximum apparent slip at the FRP/concrete interface.

Looking into the proposed bond-slip models under fatigue loading, it can be understood that a reliable model needs to take into account all the influencing parameters, including concrete compressive strength, bond length, FRP-to-concrete width ratio and fatigue loading amplitude. It can also be seen from the fatigue bond-slip models that the maximum interfacial shear stress tends to decrease with an increase in the number of load cycles. Furthermore, comparison between the proposed bond-slip models shows that when the FRP-to-concrete ratio is not considered as a factor affecting the fatigue behavior of FRP/concrete interface, the bond-slip model is not likely to provide accurate predictions of the bond behavior under fatigue loading. However, discrepancies between the few existing models may suggest the need for more investigations in this respect.

Available experimental studies of FRP/concrete bond behavior under fatigue loading revealed that the influence of concrete tensile strength has yet to be examined. Since the effect of

concrete tensile strength on bond behavior at the FRP/concrete interface is significant, an investigation of fatigue bond behavior with respect to concrete tensile strength seems to be necessary.

Based on reported numerical investigations, it could be concluded that FE analysis of EB-FRP strengthened RC structures is a reliable tool for predicting structural responses as well as evaluating influencing parameters under both monotonic and fatigue loading. A review of related research studies indicates that the accuracy of FE models of EB-FRP shear-strengthened RC beams depends greatly on the performance of the concrete/FRP interface model. Indeed, assuming a perfect bond at the FRP/concrete interface will lead to over-estimated structural predictions in terms of bond strength and load-carrying capacity. Hence, the FRP/concrete bond can contribute to highly realistic prediction of structural capacity when simulated by appropriate bond-stress slip models. Furthermore, numerical parametric studies under cyclic loading have indicated that the fatigue life of the FRP/concrete interface depends on a number of factors. These influencing parameters include applied load range, FRP-to-concrete width ratio, FRP bonded length, FRP thickness, FRP type and also environmental conditions. According to the observations from FRP bonded concrete pull-out tests, concrete compressive strength, FRP-to-concrete width ratio and FRP bond length (lower than the effective bond length) have significant influence on the bond strength between concrete and FRP, especially when the failure mode is concrete surface separation. Furthermore, by setting the applied stress level to its endurance limit (75% of the ultimate capacity), the long-term fatigue resistance of EB-FRP shear strengthened RC beams can be reached.

3.7 Research needs

Based on this review of research studies on the FRP/concrete bond behavior of EB-FRP shear-strengthened RC structures under fatigue loading, the following research gaps and needs were identified:

1) Since available studies regarding the fatigue life of the bond between FRP and concrete have been conducted based on limited data, more research studies are required to develop reliable S-N relationships corresponding to the fatigue life of the EB-FRP/concrete interface, especially in FRP shear-strengthened RC structures, by incorporating all the influencing factors.

2) Special attention must be devoted to the fatigue bond behavior of the FRP/concrete interface in shear-strengthened RC structures, and reliable bond stress-slip models should be proposed that fully capture the influencing parameters, especially under fatigue conditions similar to real-life situations.

3) Numerical investigations must be conducted to evaluate the performance of shear-strengthened RC structures with respect to the FRP/concrete bond under fatigue loading by considering various influencing factors, including concrete compressive strength, bond length, FRP ratio, and environmental conditions.

4) Research should be undertaken to evaluate the effect of environmental conditions as well as moisture on the fatigue performance of the FRP/concrete interface in FRP shear-strengthened RC beams.

5) Because concrete tensile strength is a key parameter affecting the interfacial behavior between concrete and FRP materials under fatigue loading, more research is required to evaluate its effect on FRP-strengthened RC beams, particularly in shear.

3.8 Conclusions

A state of knowledge has been presented with a focus on the fatigue behavior of the FRP/concrete bond in EB-FRP strengthened RC structures in shear, and a wide spectrum of related aspects were covered. These include the influencing parameters under cyclic loading, existing design guidelines, prior investigations of fatigue bond behavior at the FRP/concrete

interface, and numerical analyses of the FRP/concrete bond in EB-FRP strengthened RC structures under fatigue loading. Based on the reported literature, the following conclusions can be drawn:

1) CFRP composites have enhanced fatigue properties that can be used to increase the fatigue life of RC beams.

2) The bond at the CFRP/concrete interface is influenced by numerous variables under fatigue loading, including concrete strength, fatigue load amplitude, CFRP-to-concrete width ratio, and bond length.

3) Increasing the concrete compressive strength improves the bond behavior under fatigue loading by increasing the fatigue life of the interface. For instance, an increase of about 75 % in the concrete strength enhanced the fatigue life of the bond by around 90 %, as reported in the literature.

4) Increasing the bond length can result in an increase in the fatigue life of the FRP/concrete interface. For instance, increasing the bond length by around 166 % led to an increase of approximately 338 % in the fatigue life of the bond, according to the reported experimental data.

5) A hygrothermal environment (high temperature and high humidity) can have an adverse influence on the fatigue life of the CFRP/concrete bond in EB-FRP strengthened beams in flexure.

6) For all developed fatigue bond-slip models, the slope of the ascending section tends to decrease with increasing number of load cycles. Increasing the concrete compressive strength also decreases the rate of slope reduction of the ascending branch. In contrast, an increase in either the level of fatigue loading or the CFRP-to-concrete width ratio increases the rate of slope reduction.

7) Finite-element analysis (FEA) of EB-FRP strengthened RC structures under fatigue loading, when validated with literature data, is a reliable and cost-effective alternative to experimental investigation for evaluating the influencing parameters on structural performance.

8) The accuracy of FEA of EB-FRP strengthened RC beams relies on accurate concrete/FRP interface modeling.

9) Assuming a perfect bond between concrete and FRP leads to over-estimation of the predicted shear resistance. Using proper bond-slip models along with interfacial elements to simulate the FRP/concrete interface will enhance the accuracy of shear capacity predictions with respect to experimental data.

10) Based on numerical simulations, the fatigue behavior of the EB-FRP/concrete bond can be affected by design parameters as well as environmental conditions

3.9 Acknowledgements

We would like to acknowledge the Natural Sciences and Engineering Research Council of Canada (NSERC) and the Fonds de Recherche du Québec – Nature et Technologie (FRQNT) for their financial support through operating grants.

CHAPTER 4

EXPERIMENTAL AND ANALYTICAL STUDY OF BOND STRESS-SLIP BEHAVIOR AT THE CFRP-TO-CONCRETE INTERFACE

Abbas Fathi [1], Georges El-Saikaly [2], Omar Chaallal [3]

[1,2,3] Department of Construction Engineering, École de Technologie Supérieure
1100 Notre-Dame St. West, Montreal, Quebec, Canada H3C 1K3

Article published in Journal of Composites for Construction, American Society of Civil Engineers (ASCE), Volume 27, Issue 2, January 2023.

4.1 Abstract

The application of externally bonded (EB) carbon fiber reinforced polymer (CFRP) systems for strengthening existing structures such as reinforced concrete (RC) beams has been widely approved in the construction industry worldwide for its numerous benefits. The CFRP-to-concrete bond has a governing role in the reliability and effectiveness of EB-CFRP systems. Indeed, failure of the CFRP-to-concrete bond can lead to rupture of CFRP-strengthened structures. Hence, ongoing research into assessment of bond behavior at the CFRP-to-concrete interface helps to bring more insightful clarity to the use of EB-CFRP strengthening techniques. The aim of this study is to evaluate the bond behavior between CFRP and concrete by conducting a series of pull-out tests. The parameters considered include CFRP type (sheet vs. laminate), bonded length and bonded CFRP width. The results show that using CFRP fabric sheets can contribute to higher bond load-carrying capacity and ductility than CFRP laminates. Furthermore, through the analyses of database in the literature, a bilinear bond-slip model is proposed that takes into account the CFRP width factor. Through a comparison, it is shown that the proposed model performs well in terms of predicting the maximum local bond stress and CFRP slippage.

Keywords: Pull-out test; CFRP-to-concrete bond; Bond length; CFRP type; CFRP width; Bond-strength; Bond-slip models; Local and global bond stress-slip; Effective bond length.

4.2 Practical application

This research is aimed at investigating the use of CFRP composites for strengthening RC structures. The complexities regarding the behavior of CFRP-strengthened RC beams and columns, especially at the CFRP-to-concrete bond, have provoked the authors to conduct this experimental study. The testing program is intended to evaluate the effect of certain parameters on the bond behavior of CFRP-to-concrete interface. In addition, an analytical study is carried out to develop a model, capable of characterising the interfacial behavior in terms of bond shear stress and bond slip. The proposed model proved to perform well at predicting the bond-slip behavior by conducting a validation study. Findings obtained from this research can better familiarize civil engineers with the application of EB-CFRP strengthening techniques on concrete surfaces and possibly enhance the design of such retrofitting systems on deficient real-life RC structures.

4.3 Introduction

Much of today's infrastructure has undergone progressive damage and deterioration, which is a global concern among civil engineers. The need to sustain existing infrastructure calls for its rehabilitation through innovative strategies. The use of externally bonded (EB) fiber-reinforced polymer (FRP) composites to retrofit reinforced concrete (RC) structures has received worldwide acceptance. Some of the superior features of FRP composites over conventional steel strengthening systems include their high strength-to-weight ratio, corrosion resistance, lightweight and ease of application (Aidoo et al., 2004; Kim & Heffernan, 2008; Oudah & El-Hacha, 2013; Xin Wang et al., 2014). A common failure mode in EB-FRP strengthened concrete structures is debonding of the FRP systems from the concrete substrate which prevents the FRP composites from reaching their full tensile capacity.

Many research studies have examined the behavior of the FRP-to-concrete bond in EB-FRP strengthened concrete structures (J. F. Chen & Teng, 2001; Khalifa et al., 1998; Lu et al., 2005; Maeda et al., 1997; Neubauer & Rostasy, 1999; Niedermeier, 1996; Pellegrino et al., 2008; Z. Wu et al., 2009; Yang et al., 2001; H. Yuan et al., 2004). Relevant test observations have revealed that a typical FRP bonded concrete specimen under static loading can collapse due mainly to debonding of the concrete layer beneath the adhesive, namely, concrete cover separation (J. F. Chen & Teng, 2001; De Lorenzis et al., 2001; H. Yuan et al., 2004). Furthermore, two other failure modes that have reportedly been discovered include debonding of the adhesive between the concrete and FRP (FRP peeling from concrete) and rupture of FRP (Jianguo Dai, Ueda, & Sato, 2005; Daud et al., 2015). Note that loading conditions can also change the main failure mode of the FRP-to-concrete bond. In fact, when FRP-bonded concrete joints are subjected to cyclic loading, the dominant failure mode is most likely debonding of the adhesive (Fathi, El-Saikaly, & Chaallal, 2022; Zhou et al., 2021). As far as the numerical analysis of FRP-to-concrete bond behavior goes, it has been indicated that adopting a cohesive fracture modeling approach can well capture the debonding failure mechanism in EB-FRP strengthened RC beams by taking into account the interfacial damage propagation as well as concrete cracking (Al-Saawani, Al-Negheimish, El-Sayed, & Alhozaimy, 2022; De Maio, Greco, Leonetti, Blasi, & Pranno, 2022; Rabinovitch, 2014).

Experimental investigations into the behavior of FRP-to-concrete bond have been mostly conducted in the form of single or double pull-out shear tests. In fact, single pull-out tests can be accompanied by undesired normal stresses that might affect the results expected from a pure shear test (Emmanuel Ferrier et al., 2010; Mohammadi & Wan, 2015). Therefore, the double-lap shear test set-up has been deemed a better option for investigating bond behavior.

A wide range of parameters have been investigated to better understand the behavior of the FRP-to-concrete bond, including concrete strength, concrete surface preparation, FRP bond length, FRP-to-concrete width ratio, FRP material properties and thickness, applied adhesive epoxy and anchorage systems (Abdalla et al., 2020; De Lorenzis et al., 2001; Emmanuel Ferrier

et al., 2010; Maeda et al., 1997; Mazzotti et al., 2008; McSweeney & Lopez, 2005; Nakaba et al., 2001; C. Yuan et al., 2019; P. Zhang et al., 2020; Zhou et al., 2021).

The study by De Lorenzis et al. (2001) on carbon FRP (CFRP) bonded concrete specimens in a flexural test set-up showed that concrete surface preparation can affect the ultimate load capacity of specimens. Indeed, concrete surfaces roughened by chiseling performed better than sandblasted surfaces. Furthermore, their test results showed that more plies of CFRP laminate can improve bond capacity. Similar results regarding the effect of CFRP thickness were observed in the single-lap pull-out test performed by McSweeney and Lopez (2005). It was also reported that increasing CFRP width can enhance the ultimate load resisted by the bond (McSweeney & Lopez, 2005). However, a contradictory conclusion was reported by De Lorenzis et al. (2001), in which the CFRP bonded width had no effect on bond strength.

The two factors of FRP type and concrete strength were also evaluated in a series of double-lap pull-out tests performed by Nakaba et al. (2001). They concluded that the ultimate load-carrying capacity of the specimen can increase at higher FRP stiffness. The same conclusion has been reported in other related studies (Maeda et al., 1997; H. Yuan et al., 2004). However, based on experimental results by Nakaba et al. (2001), the FRP type does not seem to affect the maximum local bond stress, whereas increasing the concrete compressive strength enhances the maximum local stress at the FRP-to-concrete interface (Nakaba et al., 2001).

Following a series of double lap tests by Emmanuel Ferrier et al. (2010), regarding the effect of FRP elastic modulus and adhesive thickness on bond behavior, it was found that increasing these variables could improve bond resistance by lowering the maximum interfacial stress.

The effect of using a new CFRP rope anchorage technique on CFRP-to-concrete bond behavior was examined experimentally by Godat et al. (2016). Furthermore, concrete strength and CFRP laminate width were included in the study. It was found that increasing the CFRP width in the anchored specimens improved bond capacity. However, the effect of concrete strength was negligible on the bond when the new anchorage system was used (Godat et al., 2016).

The application of hybrid FRP (carbon/basalt) was studied by C. Yuan et al. (2019) in which different orientations of FRP layers were bonded to concrete specimens. It was found that the specimens bonded with hybrid FRPs had the same debonding failure mode as specimens bonded solely with CFRPs. As for the hybrid FRP layer orientation, it was reported that higher bond strength could be obtained by using one ply of CFRP before adding a single basalt FRP (BFRP) layer.

An investigation by P. Zhang et al. (2020) on surface treatment of concrete-to-FRP bonded joints found that surface roughness can also affect bond strength. Observations of double lap shear tests revealed that applying glass FRP (GFRP) with a transverse surface mat as well as using bond anchoring systems in the form of shear keys can maximize the load capacity of FRP bonded specimens.

The existence of opposing conclusions in the literature regarding the effect of CFRP width on bond strength has been the main impetus to assess this important parameter further through an experimental investigation. Moreover, it may be of interest to examine the bond performance of different CFRP types including CFRP laminate and fabric sheet on the concrete surface to find the most effective CFRP bonding configuration. To this end, an experimental program in the form of double-lap shear testing was conducted in this study to examine the behavior of the CFRP-to-concrete interface by applying two CFRP types (laminate vs. fabric sheet), different bonded lengths, and different CFRP widths. The test results were presented in terms of bond-slip relationships, and further discussions were included to assess the reliability of existing bond-slip models. On the basis of experimental data analyses in the literature, a modified bond-slip model is proposed and its performance is evaluated against the available models. Furthermore, the accuracy of existing effective bond-length relations was examined by studying the strain distribution along the bonded lengths of tested specimens. Finally, comparisons were made to evaluate the behavior of the CFRP-to-concrete bond with respect to the parameters mentioned and research conclusions are drawn accordingly.

4.4 Research significance

This paper intends to evaluate the bond behavior of CFRP-to-concrete interface with respect to the influencing parameters of CFRP types (fabric tissue vs. laminate), bonded length and CFRP width through an experimental program. In addition, an analytical study is carried out to develop a bilinear bond-stress slip model, capable of capturing the bond behavior of specimens bonded with CFRP fabric sheets as well as CFRP laminates. The reliability of available effective bond-length relationships as well as the recommendations aligned with the current study is also discussed.

4.5 Experimental program

An experimental program was conducted in this study with the aim of evaluating the CFRP-to-concrete bond behavior under static loading. The testing details are presented below.

4.5.1 Test set-up

A double pull-out shear test set-up was considered for the current study. The tests were performed on a total of 12 concrete blocks (three series) with the dimensions of 250 mm × 150 mm × 150 mm. Each specimen was bonded with CFRP made up of either fabric sheet, referred to hereafter as sheet, or laminate for each test. Four bond lengths, 50 mm, 100 mm, 150 mm and 200 mm were considered in each test series. Three CFRP bond widths were also considered. Concrete casting was performed three times. Hence, three slightly different concrete compressive strengths are associated with the experimental blocks. Details of the test specimens within each series (Series 1, 2 and 3) are presented in Table 4.1. Note that each specimen's label indicates the CFRP type (laminate "L" vs. fabric sheet "S"), bonded length and CFRP width. For instance, the label L-50-25 refers to a specimen bonded with CFRP laminate with a bond length and CFRP width of 50 mm and 25 mm, respectively. Figure 4.1 shows a schematic test set-up.

Table 4.1 Experimental details of specimens

Series	Number	Specimen label	Concrete compressive strength, f_c' (MPa)	CFRP type	Bond length (mm)	CFRP width (mm)
Series 1	1	L-50-25	51.9	Laminate	50	25
	2	L-100-25	44	Laminate	100	25
	3	L-150-25	51.9	Laminate	150	25
	4	L-200-25	44.9	Laminate	200	25
Series 2	5	S-50-75	44	Fabric sheet	50	75
	6	S-100-75	44	Fabric sheet	100	75
	7	S-150-75	44	Fabric sheet	150	75
	8	S-200-75	51.9	Fabric sheet	200	75
Series 3	9	S-50-112	44.9	Fabric sheet	50	112
	10	S-100-112	44.9	Fabric sheet	100	112
	11	S-150-112	44.9	Fabric sheet	150	112
	12	S-200-112	51.9	Fabric sheet	200	112

Note: Concrete compressive strengths are the average results of testing at least 3 concrete cylinders (diameter = 100 mm, height = 200 mm) from each concrete batch according to ASTM C39/C39-21 (ASTM, 2021) test method, with a standard deviation of < 0.5.

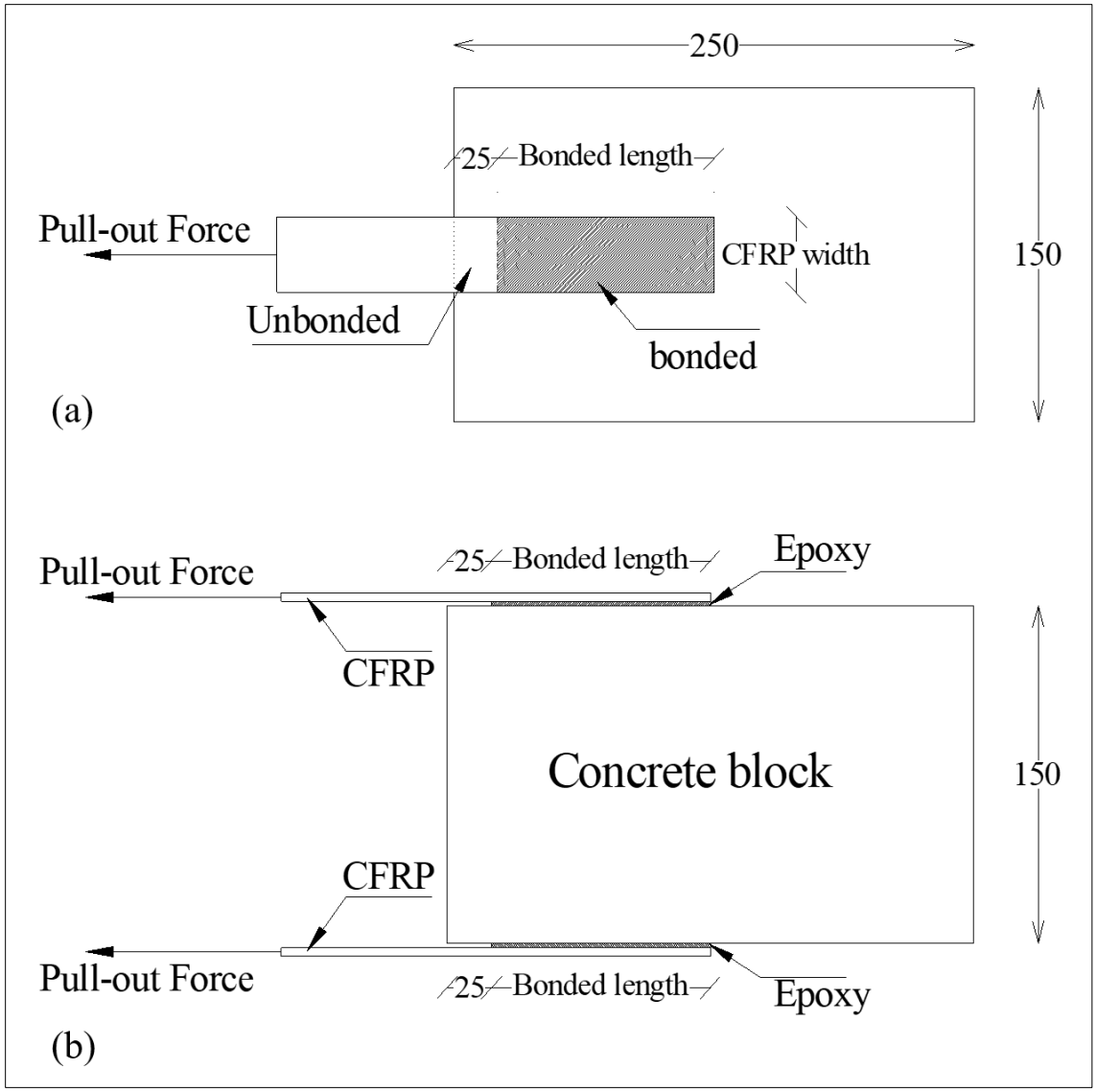

Figure 4.1 Schematic of double-lap pull-out test set-up (dimensions in mm): a) top view; b) side view

4.5.2 Specimen preparation

Before applying the CFRP, all bonding surfaces of concrete prisms were sandblasted to achieve a CSP (concrete surface profile) of 4. The CFRP was attached to the two opposite sides of the concrete block (Block A) using epoxy resin adhesive. Figure 4.2 shows an image of a specimen bonded with CFRP laminates (Specimen L-200-25) and prepared for the testing program. The

external tensile force was applied to the specimen through a concrete loading block (Block B), with dimensions of 500 mm × 150 mm ×150 mm.

To ensure that debonding occurred in Block A, the bonded length of Block B was set significantly higher, i.e., at least 2.5 times that of Block A ($L_{b.\text{Block B}} \geq 2.5 \times L_{b.\text{Block A}}$). Furthermore, adequate anchorage systems were used to prevent premature CFRP debonding failure on the loading block (Block B). To that end, two anchorage configurations were adopted on the loading blocks: 1) a confining full wrap of the loading block with CFRP sheet with the fiber orientation perpendicular to that of the anchored sheet or laminate; 2) use of an additional CFRP sheet layer attached to the loading block. Note that the two edges of the loading block, where the anchoring CFRP layer sheet was attached, were rounded to avoid premature failure of the anchorage system.

As mentioned earlier, the bond performance at the CFRP-to-concrete interface was evaluated using two different types of CFRP: CFRP laminate and CFRP sheet. Table 4.2 provides details of the material properties of CFRP products used in this experiment. Note that the technical properties (tensile strength, modulus and elongation) of CFRP fabric sheets, cured with the epoxy resin, were obtained from the average values minus 3 standard deviations of 24 sample coupons per test series according to ASTM D3039 (ASTM, 2008) tension test method, as stated in the product data sheet (SikaWrap). As for CFRP laminates, it is reported that property testing was performed at 23 °C (73 °F) and 50 % R.H. (relative humidity) (SikaCarboDur). To prepare the CFRP laminate, acetone cleaning was performed to remove any impurities from the laminate surface. Before bonding the CFRP to the blocks, the concrete surface was covered with one layer of epoxy paste adhesive, as recommended by the manufacturers (SikaCarboDur; SikaWrap).

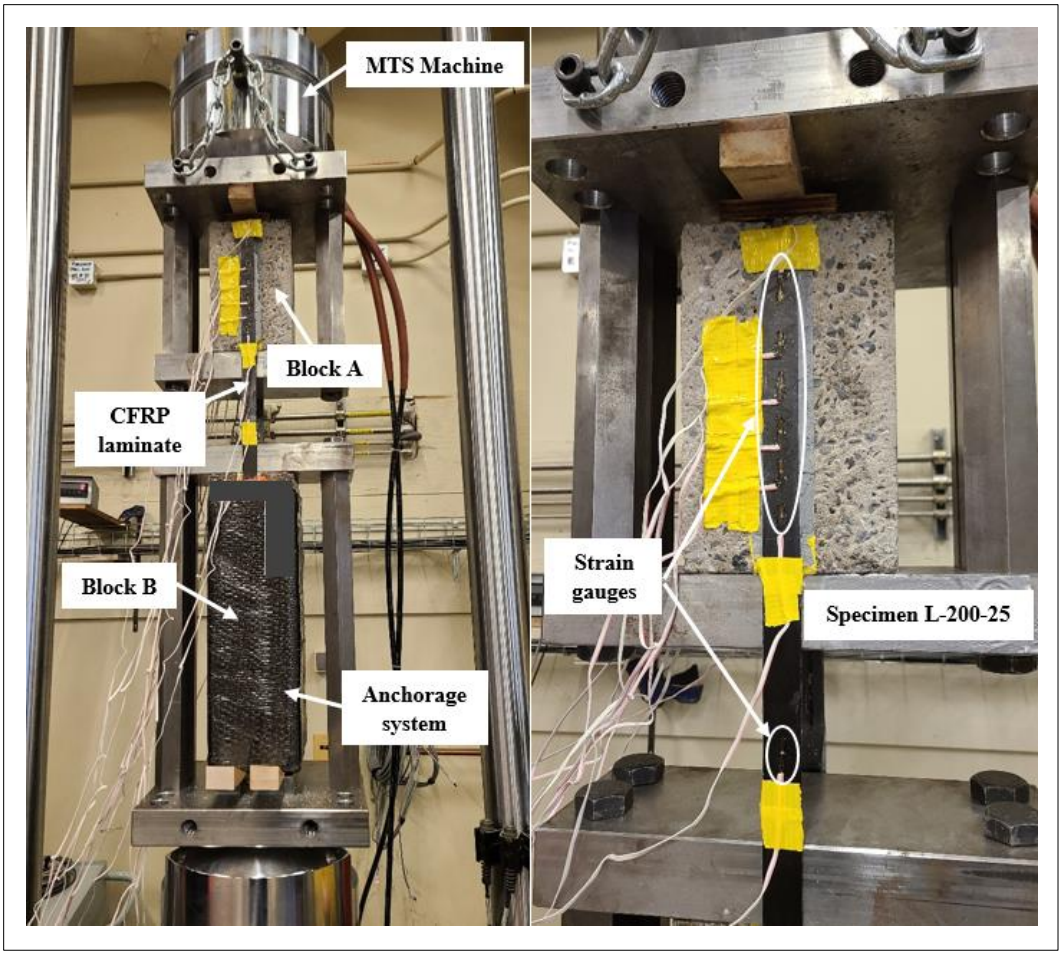

Figure 4.2 Test specimen (Specimen L-200-25)

Table 4.2 CFRP properties used in the experimental program

CFRP type	CFRP laminate	CFRP fabric sheet
Product name	SikaCarboDur- S512	SikaWrap-Hex 103C (cured with Sikadur-300 epoxy)
Tensile modulus, E_f (GPa)	165	71.7
Tensile strength, f_f (GPa)	2.8	1.1
Tensile elongation, ε_f	> 1.7 %	1.45 %
Thickness, t_f (mm)	1.2	1.016

4.5.3 CFRP ratio and strain gauge configuration

All CFRP laminates used in this study had the same width of 25 mm. To conduct a rational comparison between the performance of FRP laminate and fabric sheet, an equivalent width of 75 mm was assumed for the CFRP sheet. The choice of two CFRP widths, b_f, was based on the equivalent tensile strength attributed to CFRP in each of the configurations ($f_f \times t_f \times b_f$). Furthermore, to investigate the effect of CFRP-to-concrete width ratio (b_f/b_c) on the bond behavior of concrete blocks bonded with CFRP fabric sheet, two different widths, 75 mm and 112 mm, were used, corresponding to the two CFRP-to-concrete width ratios of 0.5 and 0.75, respectively.

Several strain gauges were affixed along the bonded length of CFRP on both sides of the concrete prism to measure the strain distribution and thereby the bond stress-slip behavior during quasi-static loading. Figure 4.3 shows the locations of strain gauges along the CFRP with different bond lengths. One strain gauge (Gauge #1) is installed on the unbonded area of CFRP, right at the midpoint between the two blocks (Blocks A and B); this can be used to measure slippage at the loaded end of the bonded CFRP. In other words, since the tensile load is distributed into the bonded area of CFRP, the strain captured on the unbonded zone, ε_1, represents the tension imposed at the loaded end and thereby can be used to calculate the bond slip of the interval between the loaded end and Gauge #2 (i.e., Interval loaded end-2).

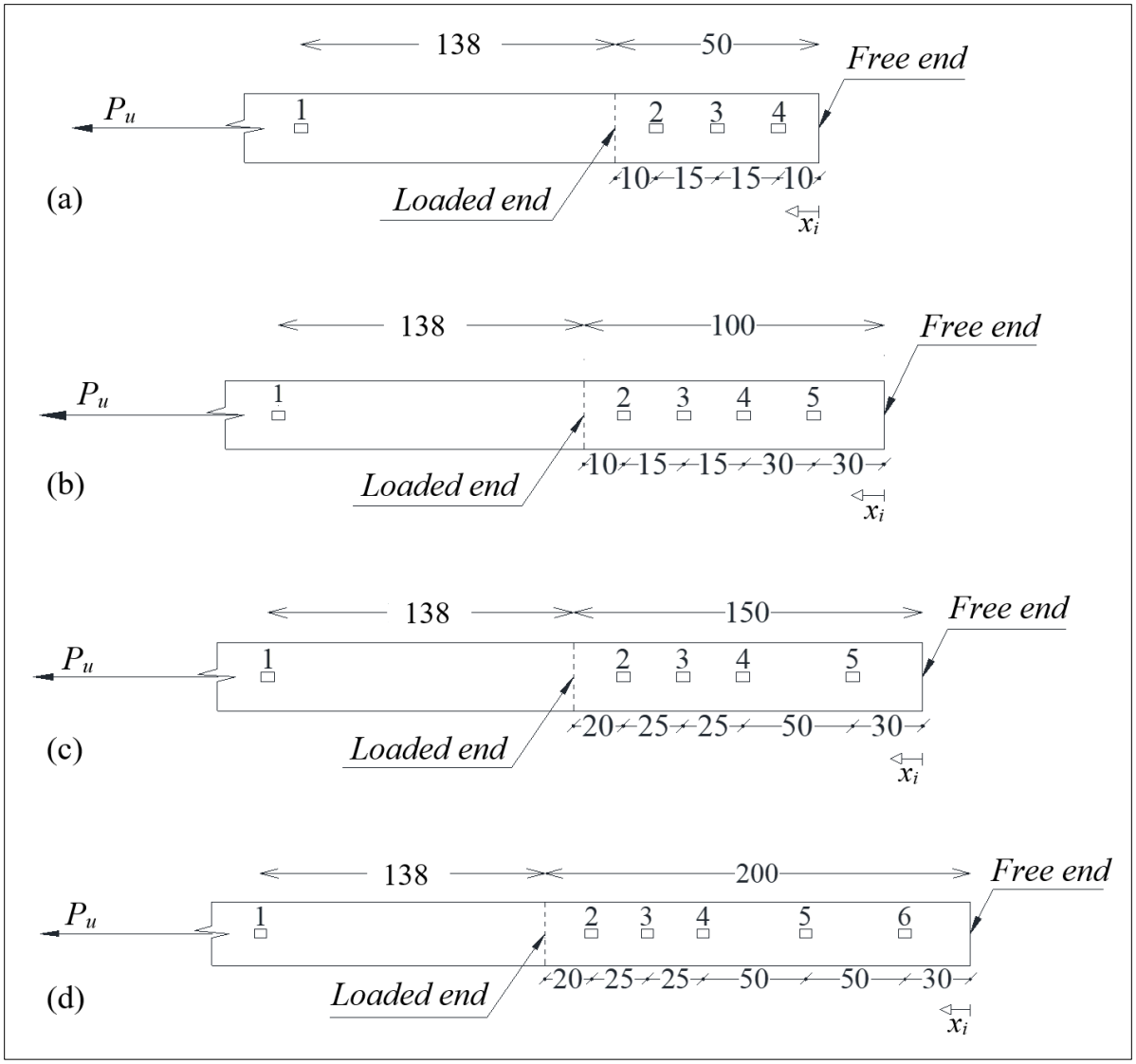

Figure 4.3 Configuration of strain gauge locations on CFRP with: a) 50 mm bond length; b) 100 mm bond length; c) 150 mm bond length; and d) 200 mm bond length

4.6 Experimental results

An MTS machine was used to apply tensile force to the specimens at a rate of 0.5 mm/min. Failure of the specimen in each test occurred when either of the two bonded sides debonded completely. Upon debonding failure, the test was stopped and data were extracted from the data acquisition system. Note that the experimental results in this study are based on the strain data from the side of the specimen that experienced debonding failure.

4.6.1 Failure modes

As discussed earlier, most prior experimental investigations on CFRP bonded concrete pull-out tests under static loading have agreed on the occurrence of debonding failure in the form of concrete surface separation (J. F. Chen & Teng, 2001; De Lorenzis et al., 2001; H. Yuan et al., 2004). In other words, failure of FRP-bonded concrete specimens under static loading is mainly governed by concrete failure a few millimeters beneath the concrete-to-adhesive interface.

4.6.1.1 Failure modes of specimens with CFRP laminate (Series 1)

Test observations of specimens bonded with laminate (Series 1) revealed that, as the loading increased, interfacial cracking propagated from the loaded end towards the free end of the bonded CFRP. Failure of the specimens occurred with abrupt total debonding of the CFRP-to-concrete interface on one side of the specimen. Figure 4.4 shows the failure patterns of Series 1 specimens. The ruptured concrete layer is visible on the debonded CFRP in all specimens except for Specimen L-50-25. The latter failed as a result of a combination of concrete surface rupture and CFRP peeling from the epoxy. This could be attributed to the small size of the bonded area ($L_b \times b_f$) of this specimen, which did not provide sufficient shear resistance at the link between the CFRP and the epoxy against the applied load and thereby leading into a simultaneous failure of both the CFRP-to-adhesive interface and the underlying concrete surface layer.

4.6.1.2 Failure modes of specimens bonded with CFRP sheet (Series 2 and 3)

During testing of the specimens bonded with CFRP sheet (Series 2 and 3), cracking sounds started to be emitted at higher applied loads unlike the specimens with laminate. Figure 4.5 shows the failure modes of specimens bonded with CFRP sheet. Much like the failure patterns in specimens of Series 1 (except for Specimen L-50-25), the existence of a concrete layer on

the debonded CFRP indicates that all specimens with CFRP sheet failed due to separation of the concrete cover beneath the bonded CFRP sheet.

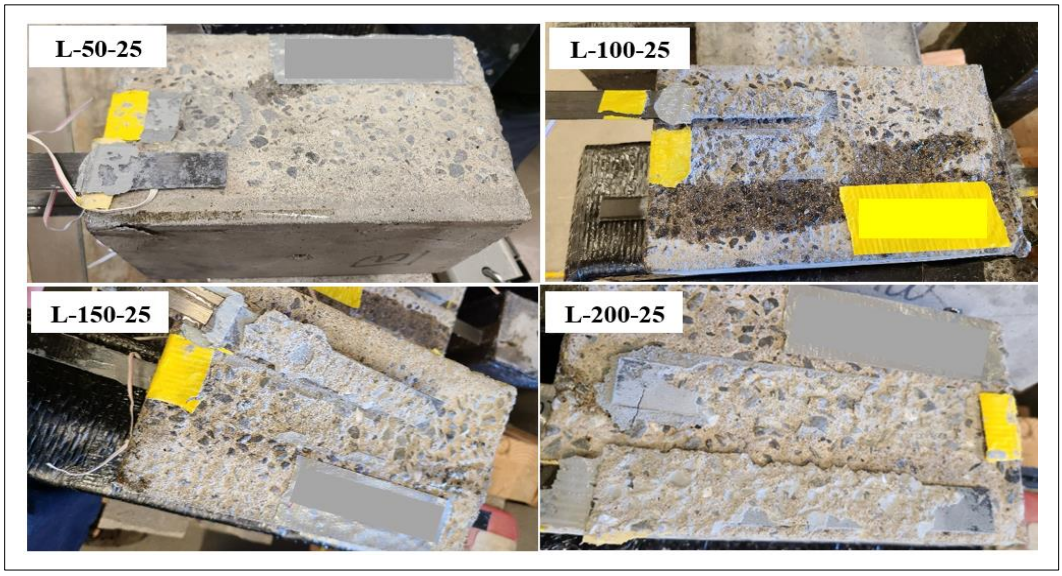

Figure 4.4 Failure modes of specimens bonded with CFRP laminate (Series 1)

Figure 4.5 Failure modes of specimens bonded with CFRP sheet (Series 2 and 3)

4.6.2 Bond strength of the CFRP-to-concrete interface

Table 4.3 presents the maximum double-lap loads ($F_{max} = 2\ P_{ult}$) reached by the specimens as well as those predicted by existing bond strength models. According to bond strength models, the parameters affecting the bond capacity include the concrete strength, FRP stiffness, bonded length and CFRP-to-concrete width ratio (J. F. Chen & Teng, 2001; Khalifa et al., 1998; Lu et al., 2005; Maeda et al., 1997; Neubauer & Rostasy, 1999; Niedermeier, 1996; Yang et al., 2001). Comparing the predicted failure loads of specimens according to the available models with test results (see Figure 4.6) reveals that the models developed by Khalifa et al. (1998) and Neubauer and Rostasy (1999) can provide the most reliable load-carrying capacity for the tested specimens. Indeed, the predictions made by these two models showed the correlation rates of $R^2 = 0.87$ and $R^2 = 0.84$, respectively, with the corresponding results achieved during the tests. In addition, Figure 4.6 shows that the model developed by Neubauer and Rostasy (1999) tends to overestimate the maximum bond strength whereas predictions of the model by Khalifa et al. (1998) are mostly underestimated versus the actual test results. Hence, the latter can be deemed a better model for its conservative performance at predicting the bond load-carrying capacity in this experiment.

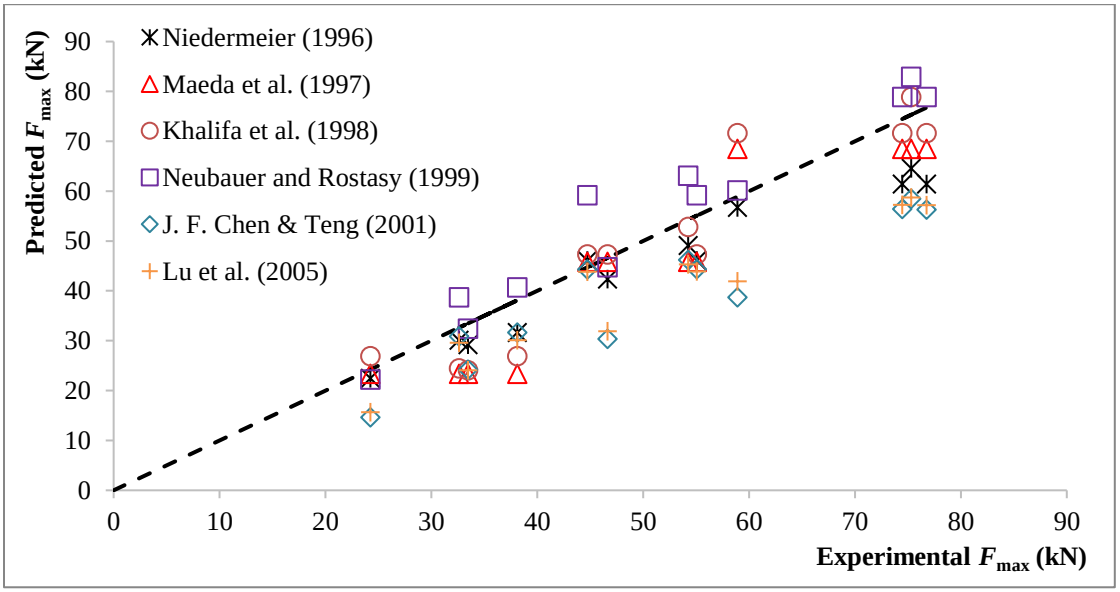

Figure 4.6 Experimental maximum loads resisted by the specimens vs. the corresponding predictions from bond strength models

Table 4.3 Maximum double-lap load-carrying capacity of specimens along with the corresponding predictions according to the existing models

Number	Specimen label	Maximum double-lap force upon failure, F_{max} (kN)	Niedermeier (1996)	Maeda et al. (1997)	Khalifa et al. (1998)	Neubauer and Rostasy (1999)	J. F. Chen and Teng (2001)	Lu et al. (2005)
1	L-50-25	24.2	22.4	23.3	26.9	22.2	14.6	15.6
2	L-100-25	33.5	29.2	23.3	24.1	32.4	24.2	24.1
3	L-150-25	38.1	31.7	23.3	26.9	40.6	31.6	30.1
4	L-200-25	32.6	30.1	23.3	24.4	38.7	30.8	29.6
5	S-50-75	46.6	42.3	45.8	47.3	44.7	30.3	31.8
6	S-100-75	44.7	46.1	45.8	47.3	59.2	44.2	43.8
7	S-150-75	55.1	46.1	45.8	47.3	59.2	44.3	43.9
8	S-200-75	54.2	49.1	45.8	52.8	63	46.2	45.3
9	S-50-112	58.9	56.7	68.4	71.6	60.1	38.7	41.9
10	S-100-112	76.8	61.4	68.4	71.6	78.8	56.3	57.1
11	S-150-112	74.5	61.4	68.4	71.6	78.8	56.4	57.2
12	S-200-112	75.3	64.5	68.4	78.8	82.9	58.5	58.7

4.6.3 Bond stress-slip curves

Through strain readings extracted from the gauges, the bond stress-slip curves could be derived. In general, the bond-slip, s_i, can be obtained as follows:

$$s_i = \int_0^{x_i} \varepsilon_i \, \mathrm{d}x \tag{4.1}$$

where ε_i is the strain value recorded by the gauge and x_i is the distance between the strain gauge and the free end of the CFRP, as shown in Figure 4.7. The bond slip is, in fact, equal to the relative displacement between the CFRP and the concrete layer underneath. However, the displacement of the concrete layer is reported to be trivial and therefore can be assumed to be zero (W. Zhang, 2018).

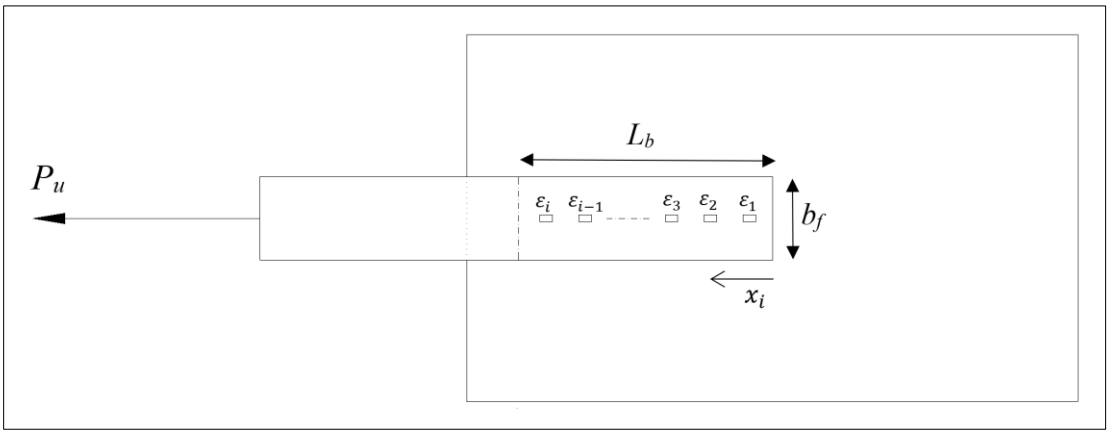

Figure 4.7 Schematic strain gauge locations on bonded CFRP

In the current study, the slippage between the CFRP and the concrete, s_i, was obtained through:

$$s_i = s_{i-1} + \frac{\Delta x_i}{2}(\varepsilon_0 + 2\varepsilon_{i-1} + \Delta\varepsilon_i) \tag{4.2}$$

where $\Delta\varepsilon_i$ is the difference between the strain values of two consecutive gauges ($\Delta\varepsilon_i = \varepsilon_i - \varepsilon_{i-1}$), Δx_i is the distance between the two consecutive strain gauges at the two ends of each interval ($\Delta x_i = x_i - x_{i-1}$). Assuming that the bond length is set to be greater than the effective bond length, ε_0 could be equal to zero. Note that the above equation for calculating s_i is based on the trapezoidal diagram of the strain-displacement relationship, which is shown schematically in Figure 4.8.

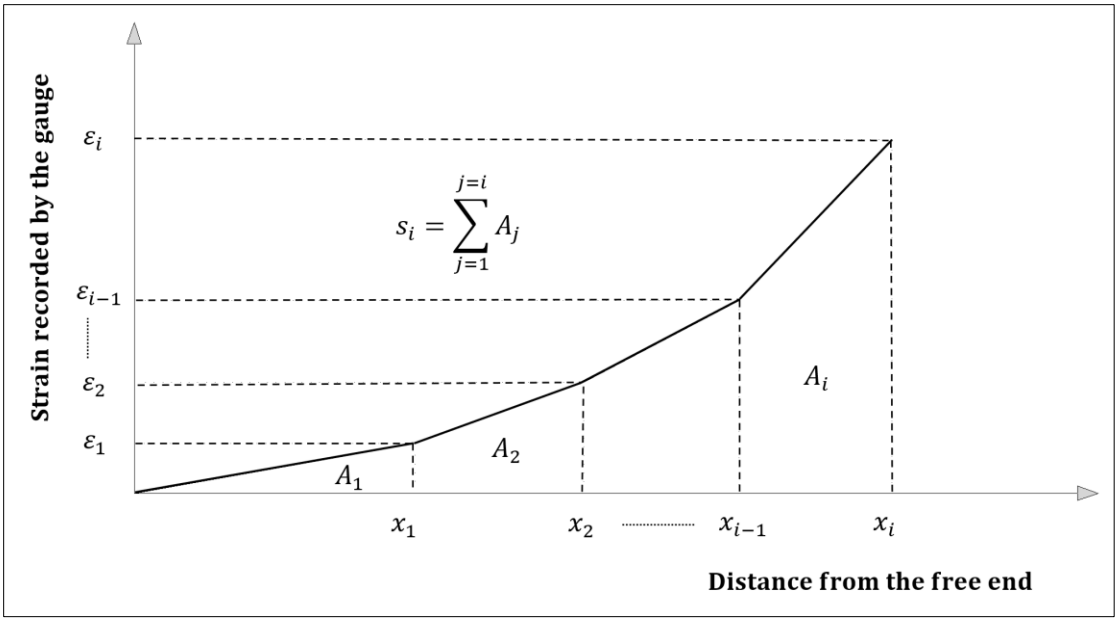

Figure 4.8 Schematic strain-displacement relationship

Figure 4.8 shows that the slip, s_i, is equal to the summation of the area under each division of the strain-distance curve, A_i.

As for bond shear stress, the following equation can be used to obtain the average shear stress, τ:

$$\tau = t_f E_f \frac{\mathrm{d}\varepsilon}{\mathrm{d}x} \tag{4.3}$$

Indeed, by using the relative strains captured by the two consecutive gauges in each interval ($\Delta\varepsilon_i = \varepsilon_i - \varepsilon_{i-1}$), as well as the distance between them, Δx_i, the average local stress of each bond interval, τ_i , can also be expressed as follows:

$$\tau_i = \frac{t_f E_f}{\Delta x_i} |\Delta\varepsilon_i| \tag{4.4}$$

Note that the global bond shear stress of the applied CFRP, $\tau_{f.\mathrm{ave}}$, can be estimated as the ratio of the pull-out force over the bonded area of CFRP to concrete, which is as follows:

$$\tau_{f,ave} = \frac{P_u}{L_b \times b_f} \tag{4.5}$$

Another option for calculating the average bond stress, $\tau_{f,ave}$, is to divide the sum of local bond stresses by the number of intervals, n, (i.e., $\frac{\sum_{i=1}^{i=n}\tau_i}{n}$). Note that the overall slip, s_f, is, in fact, the total accumulated elongation of CFRP over the bonded length, which can be calculated using Eq. (4.2).

4.6.4 Bond stress-slip models

By determining the bond-stress slip relationship, one can evaluate the behavior of the CFRP-to-concrete interface. A number of bond stress-slip models have been proposed to characterize the interfacial behavior of the CFRP-to-concrete bond under static loading (Lu et al., 2005; Monti et al., 2003; Nakaba et al., 2001; Neubauer & Rostasy, 1999; Pellegrino et al., 2008; Savoia et al., 2003; Sun, Peng, & Yu, 2017). In fact, a typical bond stress-slip curve consists of an ascending branch followed by a descending segment.

4.6.4.1 Analysis of local bond stress-slip relationships based on the test results

Figure 4.9 (a), (b) and (c) illustrates the local bond stress-slip curves of specimens L-200-25, S-200-75 and S-200-112, which are derived from the strain gauges along the bonded length. It can be understood that the bond stress-slip curve generally shows a linear ascending branch up to the maximum interfacial shear stress, followed by a nonlinear descending branch. However, the local bond slip curve of Interval 6-free end (in all three specimens) does not exhibit a nonlinear behavior. This is because the intervals outside the effective bond length (e.g., Interval 6-free end) do not seem to carry significant bond shear stresses and therefore show a linear

increase up to the maximum local stress. It can be seen that as the slip of the CFRP/concrete interface increases, local debonding grows along the bonded length until the total bond failure. Furthermore, it is observed that the local shear stress-slip curves of bond intervals closer to the loaded end (e.g., intervals loaded end-2, 2-3 and 3-4) experience higher local interfacial stresses in comparison with the intervals near the free end.

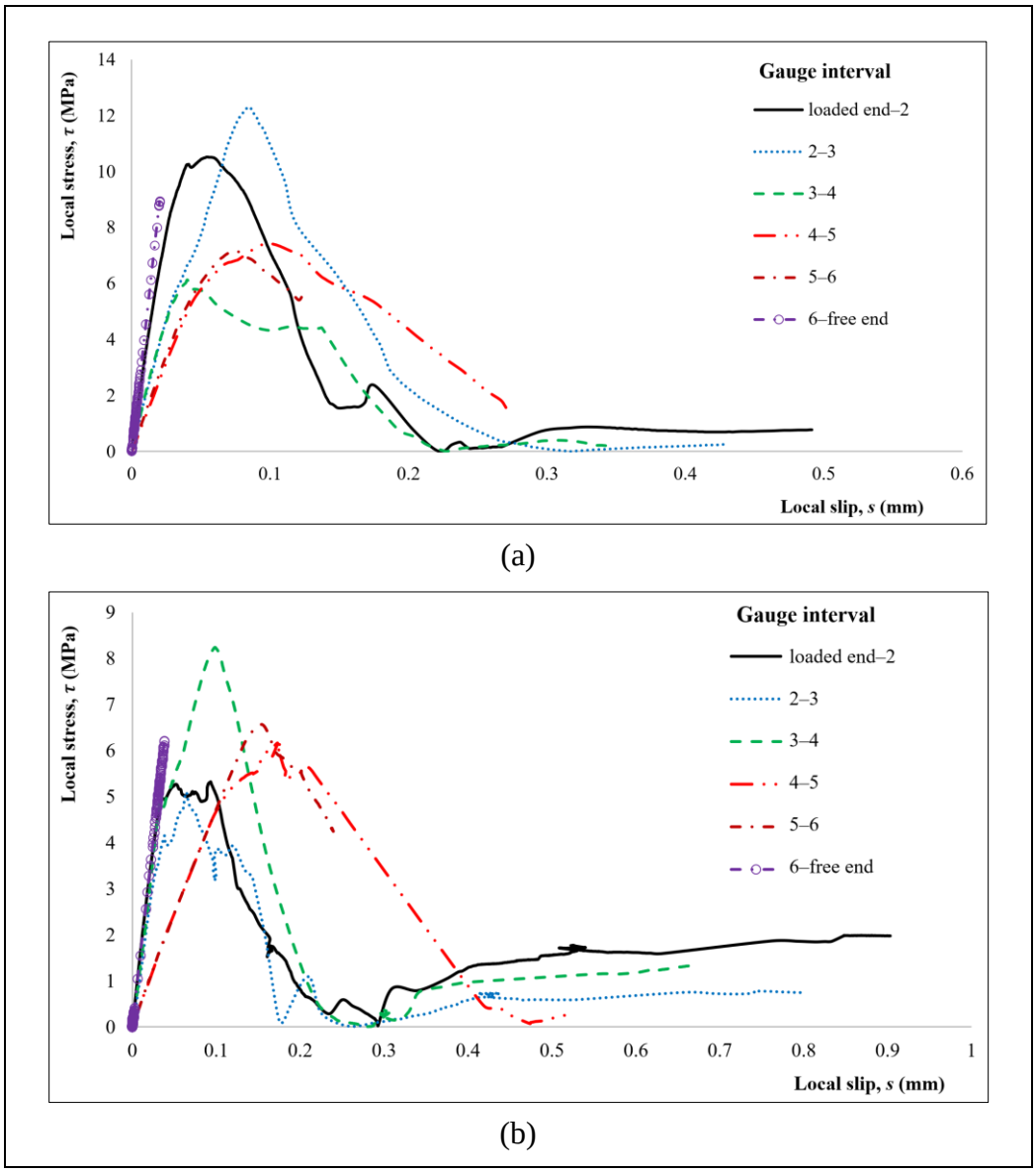

Figure 4.9 Local bond stress-slip curves of specimens: a) L-200-25; b) S-200-75; and c) S-200-112

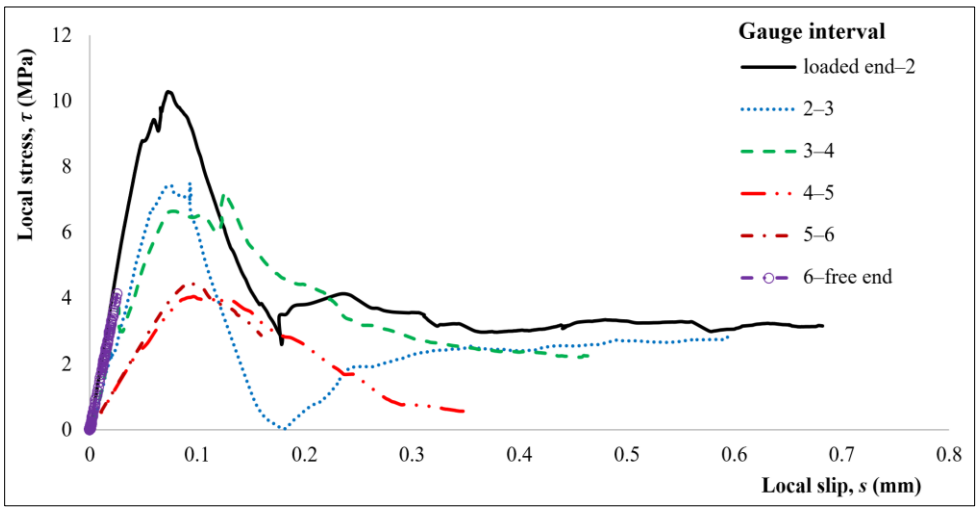

(c)

Figure 4.9 Local bond stress-slip curves of specimens: a) L-200-25; b) S-200-75; and c) S-200-112 (Continue)

It can be clearly understood that the local bond stress-slip relationship is dependent on the location of the interval along the bonded length (see Figure 4.9), which has also been reported in similar studies (JG Dai, Saito, Ueda, & Sato, 2005; Nakaba et al., 2001). The bond-slip relationship of the interval closest to the loaded end has been generally used to derive the existing bond slip models during pull-out tests (Jianguo Dai et al., 2005). This can be attributed to the fact that this interval is the first bonded region which receives the pull-out force and transfers the shear stresses to the concrete surface.

To evaluate the accuracy of the existing proposed bond slip models, Figure 4.10 (a), (b) and (c) presents the bond-slip curves of specimens in each of the test series as well as the corresponding curves drawn from the models. Specimens L-100-25, L-150-25 and L-200-25 from Series 1, Specimens S-100-75, S-150-75 and S-200-75 from Series 2 and Specimens S-100-112, S-150-112 and S-200-112 from Series 3 were selected for the comparison. The reason why specimens with 50 mm bonded lengths were excluded from the analyses is because these specimens did not seem to provide the shear resistance close enough to the ultimate bond capacity in each series. Note that the average local stress-slip values of both sides of each specimen, related to the interval closest to the loaded end (i.e., interval loaded end-2) is

presented in the figures. Also, the average concrete strength of selected specimens in each series was used in the bond-slip models for drawing the curves. As can be seen in these figures, the local bond-slip curves of Series 1 and Series 2 specimens show better agreement with the model proposed by Monti et al. (2003) in terms of the maximum local bond stress, τ_{max}. As for Series 3 specimens, the maximum local bond stresses appear to be higher than the corresponding predictions by all models except for that of Pellegrino et al. (2008), in which an overestimated value is depicted. Taking into consideration the average slippage corresponding to the maximum shear stress, s_{peak}, of all specimens (Series 1, 2 and 3), the models of Lu et al. (2005), Savoia et al. (2003) and Nakaba et al. (2001) showed the best performance at estimating this value. As for the ultimate bond slippage, s_{ult}, the predicted value of the model proposed by Lu et al. (2005) was the closest to the average ultimate slip of specimens bonded with CFRP laminate (Series 1). However, the average ultimate slippage of specimens bonded with CFRP sheets (Series 2 and 3) were more aligned with the predictions of the model by Monti et al. (2003).

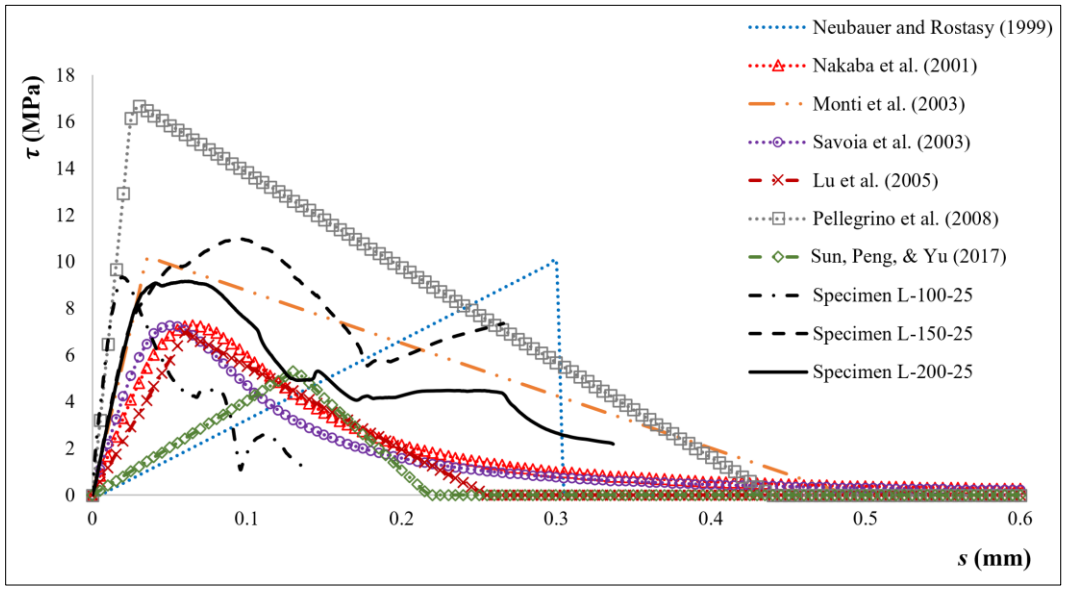

(a)

Figure 4.10 Local bond stress-slip models along with the bond-slip curve: a) Series 1 specimens; b) Series 2 specimens; and c) Series 3 specimens

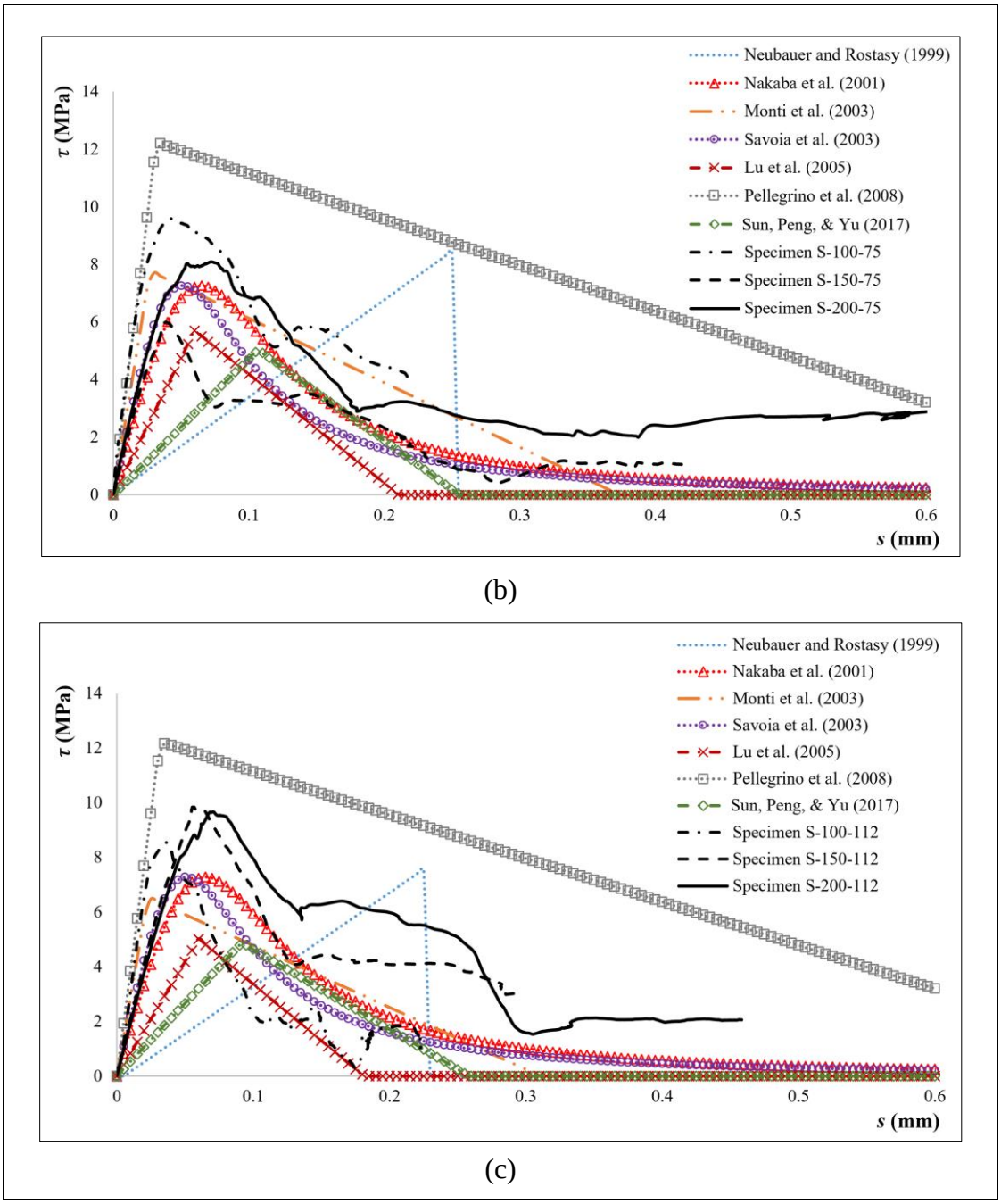

Figure 4.10 Local bond stress-slip models along with the bond-slip curve: a) Series 1 specimens; b) Series 2 specimens; and c) Series 3 specimens (Continue)

Overall, the bond-slip models proposed by Monti et al. (2003) and Lu et al. (2005) appear to perform relatively better in capturing the bond behavior of tested specimens in this study

among the abovementioned models. However, further modifications can be made to enhance the reliability of the bond-slip model to fit the current experimental results.

4.6.5 Modified bond-slip model

Among the selected bond stress-slip models, bilinear models were considered the most practical because of their simple implementation (Lu et al., 2005; Monti et al., 2003; Pellegrino et al., 2008; Sun, Peng, & Yu, 2017). Moreover, the ascending-descending curves drawn by these models were able to capture the bond behavior of CFRP-to-concrete interface with sufficient approximation. The three parameters of maximum local bond stress, τ_{max}, slip corresponding to the maximum stress, s_{peak}, and ultimate bond slip, s_{ult} control the overall performance of a typical bilinear bond slip model. Figure 4.11 (a), (b) and (c) show the bilinear bond-slip curves of tested specimens based on the average values of τ_{max}, s_{peak} and s_{ult} in each test series along with the corresponding bilinear curves drawn by the available models (Lu et al., 2005; Monti et al., 2003; Pellegrino et al., 2008; Sun, Peng, & Yu, 2017). It can be seen that the model by Pellegrino et al. (2008) overestimates the average predicted values of tested specimens in this study. An analysis was conducted in this study on the basis of the current experimental results along with the test results reported by Jianguo Dai et al. (2005), Pellegrino et al. (2008) and Sun, Peng, and Yu (2017). Table 4.4 summarizes the database for the analyses. It may be noted that since the experimental data scattering is inevitable, the database includes a portion of the specimens' data from the aforementioned studies that could contribute to the modified bond-slip model.

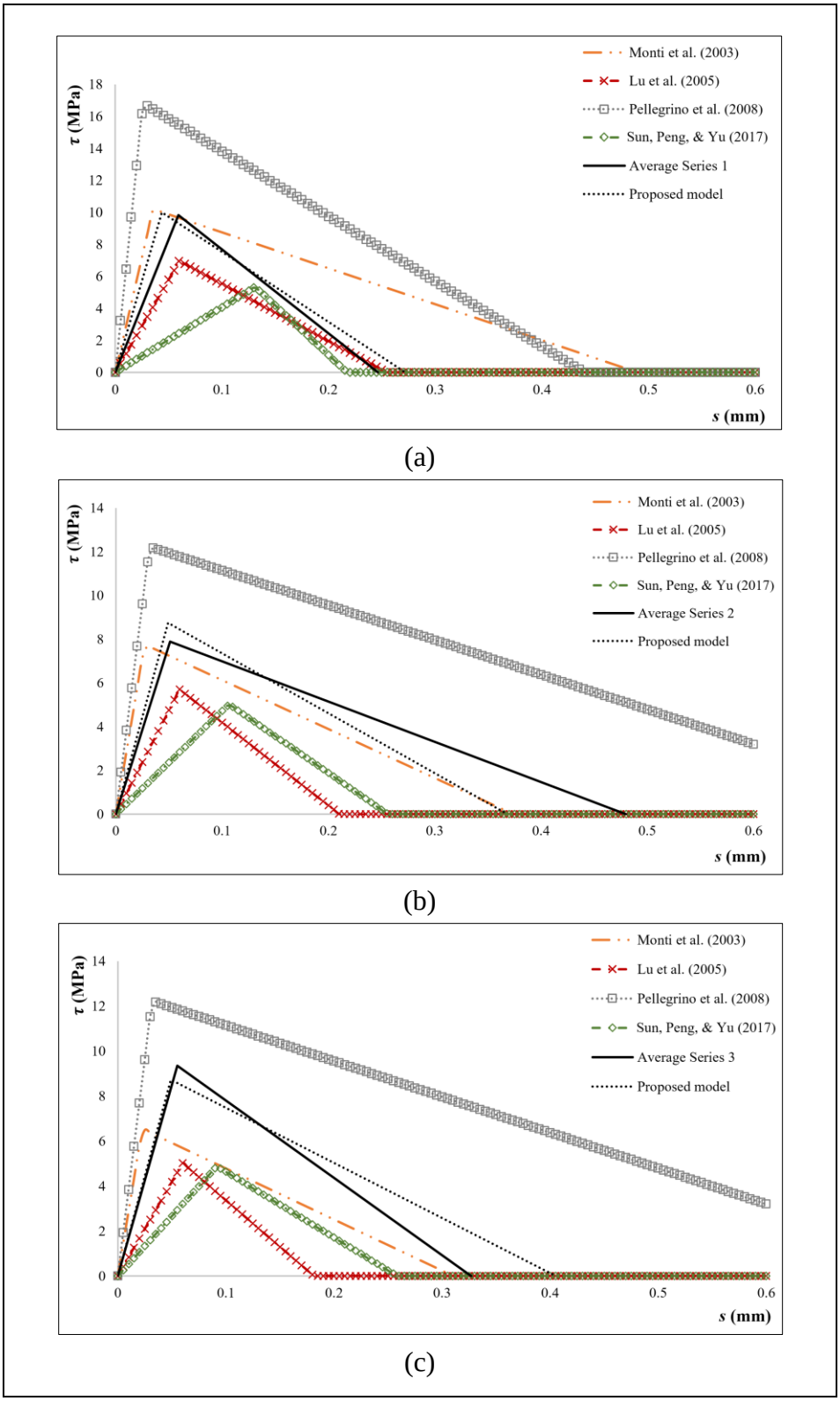

Figure 4.11 Average bilinear bond-slip curves: a) Series 1 specimens; b) Series 2 specimens; and c) Series 3 specimens

Table 4.4 Database of tested specimens for the modified bond-slip model

Research	No.	Specimen code	f'_c (MPa)	b_c (mm)	b_f (mm)	$n_f t_f E_f$ (mm.GPa)	τ_{max} (MPa)	s_{peak} (mm)	s_{ult} (mm)
This study	1	L-100-25	44	150	25	198	9.3	0.019	0.135
	2	L-150-25	51.9	150	25	198	11	0.096	0.266
	3	L-200-25	44.9	150	25	198	9.2	0.062	0.337
	4	S-100-75	44	150	75	73	9.6	0.042	0.220
	5	S-150-75	44	150	75	73	6.0	0.039	0.420
	6	S-200-75	51.9	150	75	73	8.1	0.072	0.798
	7	S-100-112	44.9	150	112	73	8.5	0.037	0.225
	8	S-150-112	44.9	150	112	73	9.8	0.057	0.299
	9	S-200-112	51.9	150	112	73	9.7	0.071	0.458
Sun, Peng, and Yu (2017)	10	B3L1.4XLa	37.2	152.4	76	54	5.9	0.203	N/A.
	11	B3L1.4XLb	37.2	152.4	76	54	3.3	0.056	0.305
	12	B3L1XLb	37.2	152.4	76	54	4.3	0.108	0.296
Pellegrino et al. (2008)	13	S1C1a	63	100	50	38	15.4	0.032	1.190
	14	S1C5c	58	100	50	64	15.5	0.036	0.885
	15	S2C1a	63	100	50	76	17.8	0.027	0.810
	16	S2C1c	58	100	50	76	18.9	0.031	0.859
	17	S3C1a	63	100	50	114	9.2	0.025	0.712
	18	S3C1b	58	100	50	114	10.1	0.022	0.668
	19	S3C1c	58	100	50	114	10.9	0.024	0.606
	20	S2C5a	63	100	50	129	18.9	0.046	0.671
	21	S2C5b	58	100	50	129	10.2	0.034	0.483
	22	S3C5a	63	100	50	193	23.7	0.019	0.352
	23	S3C5b	63	100	50	193	11.3	0.027	0.614
	24	S3C5c	58	100	50	193	22.9	0.030	0.466
Jianguo Dai et al. (2005)	25	CR1L1	35	400	100	25	5.6	0.064	N/A.
	26	CR1L1	35	400	100	25	7.2	0.066	N/A.
	27	CR1L1	35	400	100	25	6.8	0.053	N/A.
	28	CR1L2	35	400	100	51	5.6	0.069	N/A.
	29	CR1L2	35	400	100	51	6.7	0.061	N/A.
	30	CR1L2	35	400	100	51	6.1	0.077	N/A.
	31	CR1L3	35	400	100	76	5.4	0.064	N/A.

Table 4.4 Database of tested specimens for the modified bond-slip model (Continue)

Research	No.	Specimen code	f_c' (MPa)	b_c (mm)	b_f (mm)	$n_f t_f E_f$ (mm.GPa)	τ_{max} (MPa)	s_{peak} (mm)	s_{ult} (mm)
Jianguo Dai et al. (2005)	32	CR1L3	35	400	100	76	6.5	0.057	N/A.
	33	CR1L3	35	400	100	76	6.4	0.062	N/A.
	34	CR1L3	35	400	100	76	5.4	0.059	N/A.
	35	AR1L1	35	400	100	19	7.3	0.070	N/A.
	36	AR1L2	35	400	100	32	6.9	0.073	N/A.
	37	AR1L3	35	400	100	74	6.9	0.068	N/A.
	38	GR1L3	35	400	100	32	4.9	0.062	N/A.
	39	GR1L5	35	400	100	44	6.5	0.062	N/A.
	40	CR2L1	35	400	100	25	5	0.111	N/A.
	41	CR2L2	35	400	100	51	4.7	0.123	N/A.
	42	CR2L3	35	400	100	76	4.5	0.103	N/A.
	43	AR2L3	35	400	100	74	5.1	0.111	N/A.
	44	GR2L3	35	400	100	32	4.6	0.090	N/A.
	45	CR3L2	35	400	100	51	2.9	0.290	N/A.
	46	CR3L3	35	400	100	76	2.8	0.227	N/A.
	47	AR3L3	35	400	100	74	3.5	0.309	N/A.

4.6.5.1 Development of τ_{max}, s_{peak} and s_{ult} for the modified bilinear bond-slip model

Looking into the exiting bilinear models, it can be seen that the maximum bond shear stress, τ_{max} and the corresponding slip, s_{peak}, are directly correlated with the concrete tensile strength, f_t, as well as the width factor, k_b (Lu et al., 2005; Monti et al., 2003; Sun, Peng, & Yu, 2017). The ultimate bond slip, s_{ult}, is mainly presented as a function of k_b (Lu et al., 2005; Monti et al., 2003; Sun, Peng, & Yu, 2017). Indeed, the effect of FRP-to-concrete width ratio on the bond behavior has been well evidenced in relevant studies. Lin et al. (2017) has developed a width factor that takes into account the influencing variables including FRP stiffness, $n_f t_f E_f$, concrete compressive stress, f_c', and widths of concrete and bonded FRP.

Table 4.5 summarizes the equations for calculating the parameters of k_b, τ_{max}, s_{peak} and s_{ult} based on the aforementioned models. On the basis of data analyses of experimental results in Table 4.4, the following bilinear bond-slip model is proposed:

$$\tau = \begin{cases} \tau_{max}\left(\frac{s}{s_{peak}}\right) & s \le s_{peak} \\ \tau_{max}\left(\frac{s_{ult}-s}{s_{ult}-s_{peak}}\right) & s_{peak} < s \le s_{ult} \\ 0 & s > s_{ult} \end{cases} \quad (4.6)$$

$$\tau_{max} = 0.0492\ (k_b f_t)^{3.5585} \quad (4.7)$$

$$s_{peak} = 4.5314\ (k_b f_t)^{-3.12} \quad (4.8)$$

$$s_{ult} = 0.0005\ (k_b\ {f_t}^{-0.5})^{-9.284} \quad (4.9)$$

where the width factor, k_b, can be obtained through the model proposed by Lin et al. (2017) (see Table 4.5) and the concrete tensile strength, f_t, is equal to $0.62\sqrt{f_c'}$ according to ACI (2019). It is noteworthy that the proposed equations are obtained through a nonlinear regression analysis that best fits the available data. Indeed, by adopting a power-curve regression on the two variables of k_b and f_t, the closest approximation of the bond-slip parameters (τ_{max}, s_{peak} and s_{ult}) against actual test results can be achieved.

Figure 4.12, Figure 4.13 and Figure 4.14 illustrate the predicted parameters of τ_{max}, s_{peak} and s_{ult} based on Eq. (4.7)-(4.9) as well as the existing bilinear models versus the selected experimental database (Table 4.4). It can be found that the proposed equations are able to estimate the aforementioned parameters with better approximation in comparison with the available bilinear bond-slip models. The average predictions of τ_{max}, s_{peak} and s_{ult} through the proposed equations also show better agreement with the average test results of each series

in this study, compared to other models (see Figure 4.11 (a), (b) and (c)). More experimental data may be required to further assess the reliability of the proposed bond-slip model.

Table 4.5 Calculation of bond-slip parameters based on the exiting models

Researcher	**Equations of k_b, τ_{max}, s_{peak} and s_{ult}**
Monti et al. (2003)	$k_b = \sqrt{1.5 \times \frac{2 - b_f/b_c}{1 + b_f/100}}$ $\tau_{max} = 1.8\, k_b f_t$ $s_{peak} = 4.5\, k_b f_t\, (n_f t_f/E_f + 50/E_c)$ $s_{ult} = 0.33 k_b$
Lu et al. (2005)	$k_b = \sqrt{\frac{2.25 - b_f/b_c}{1.25 + b_f/b_c}}$ $\tau_{max} = 1.5\, k_b f_t$ $s_{peak} = 0.0195\, k_b f_t \leq 0.06$ $s_{ult} = 0.4107\, k_b\, {f_t}^{-0.5}$
Sun, Peng, and Yu (2017)	$k_b = \sqrt{\frac{1.9 - b_f/b_c}{0.9 + b_f/b_c}}$ $\tau_{max} = 1.35 + 0.25\, k_b f_t + 0.62\, f_t$ $s_{peak} = 0.016 - 0.0046\, k_b f_t + 0.11\, k_b$ $s_{ult} = -0.06 + (0.88 - 0.23\, {k_b}^2)\, {f_t}^{-0.5} {k_b}^{0.5}$
Lin et al. (2017)	$k_b = 1 + \frac{{f_c'}^{0.385} \left[8 \left(n_f t_f E_f\right)^{-0.438} + 0.001\right] \left(1 - \frac{b_f}{b_c}\right)^{0.5}}{(1 + 0.01\, {b_f}^{1.7})}$

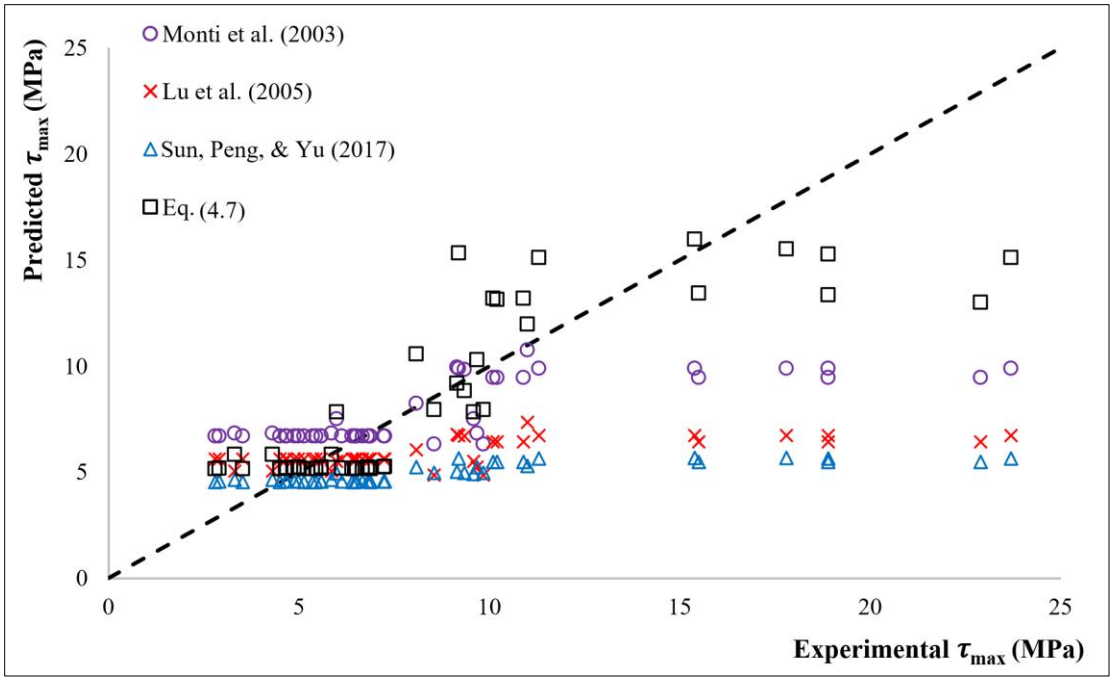

Figure 4.12 Predictions of maximum local bond stress versus experimental database

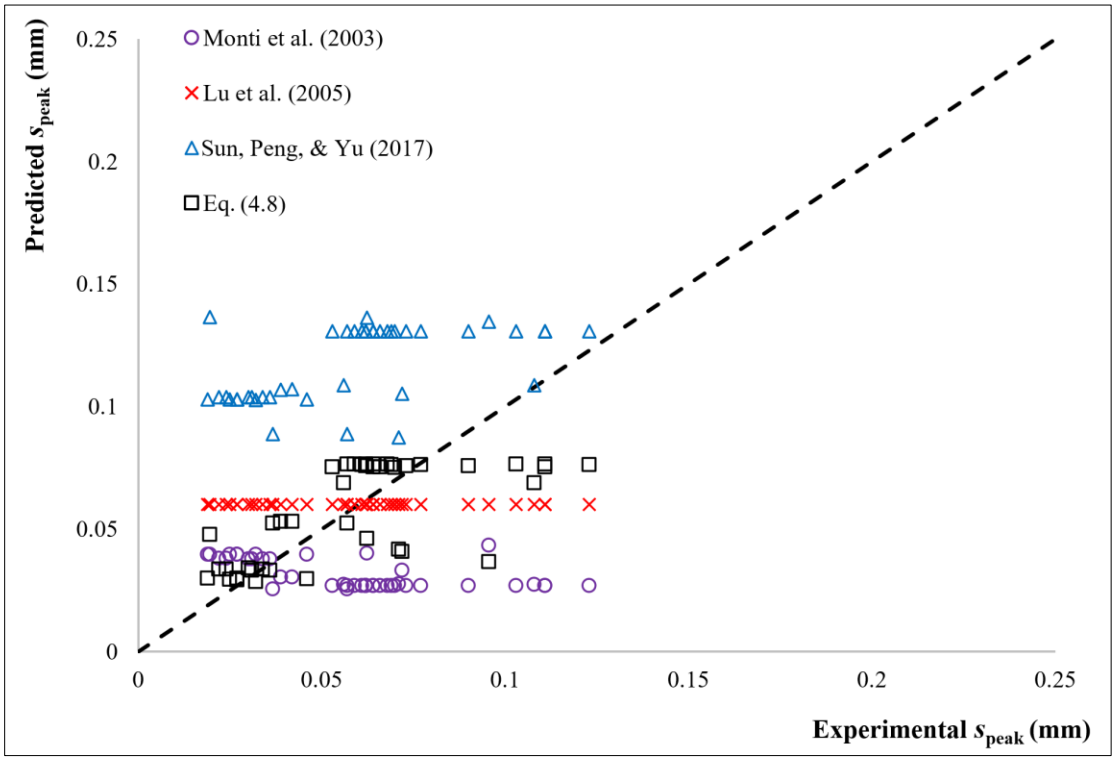

Figure 4.13 Predictions of bond slip at the maximum shear stress versus experimental database

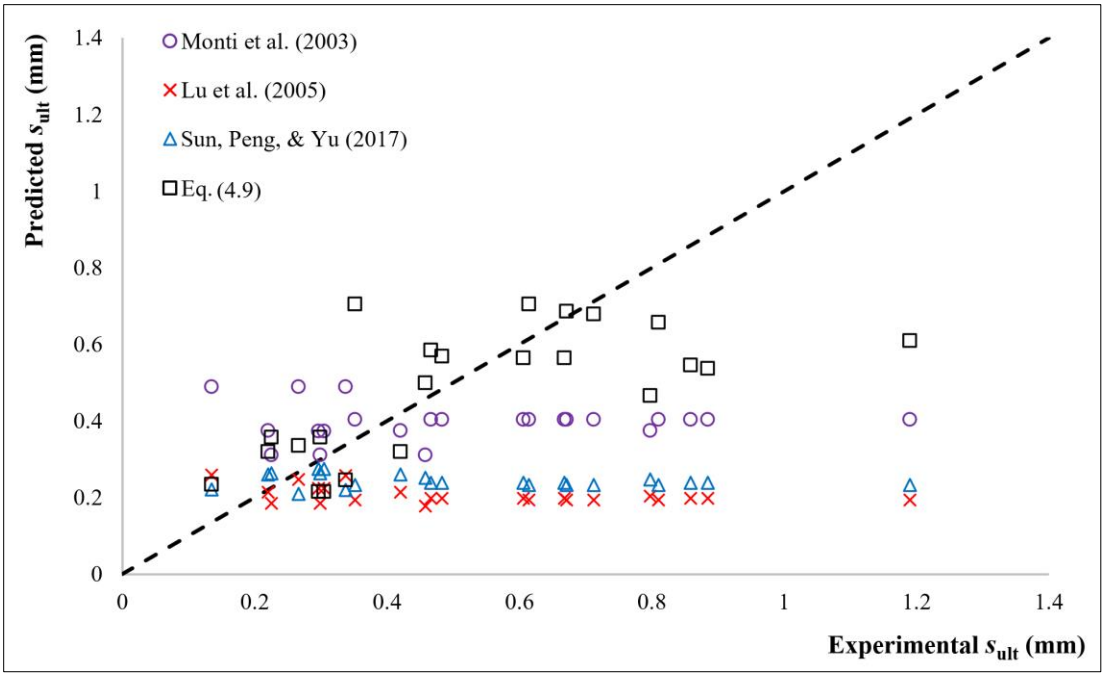

Figure 4.14 Predictions of ultimate bond slip at failure versus experimental database

4.6.6 Global bond stress-slip curves

Figure 4.15 shows the global bond stress-slip curves of specimens bonded with laminate and with sheet. As can be observed, the average bond stress decreased at greater bond length, as reported in similar experimental studies (Nakaba et al., 2001). Furthermore, observations of interfacial slips show that specimens with greater bond lengths can undergo higher bond slippage up to failure. This could corroborate the observation reported in the literature, that using a greater bond length can enhance bond ductility (Sun, Peng, Liu, & Qi, 2017).

Further detection of Figure 4.15 (a), (b) and (c) reveals that CFRP laminates in Series 1 specimens overall underwent higher average tensile stresses but lower total slippage when compared to CFRP sheets in Series 2 and 3 specimens. Similarly, when comparing the specimens with CFRP sheets (Series 2 vs. Series 3), it can be found that applying greater bonded area by increasing the CFRP sheet width can lead to lower average bond stress, as evidenced in Series 3 specimens (b_f=112 mm) versus Series 2 specimens (b_f=75 mm). This could also be attributable to the fact that interfacial stresses cannot be fully distributed

throughout the whole width of the bonded area, leading to lower average values (Nakaba et al., 2001).

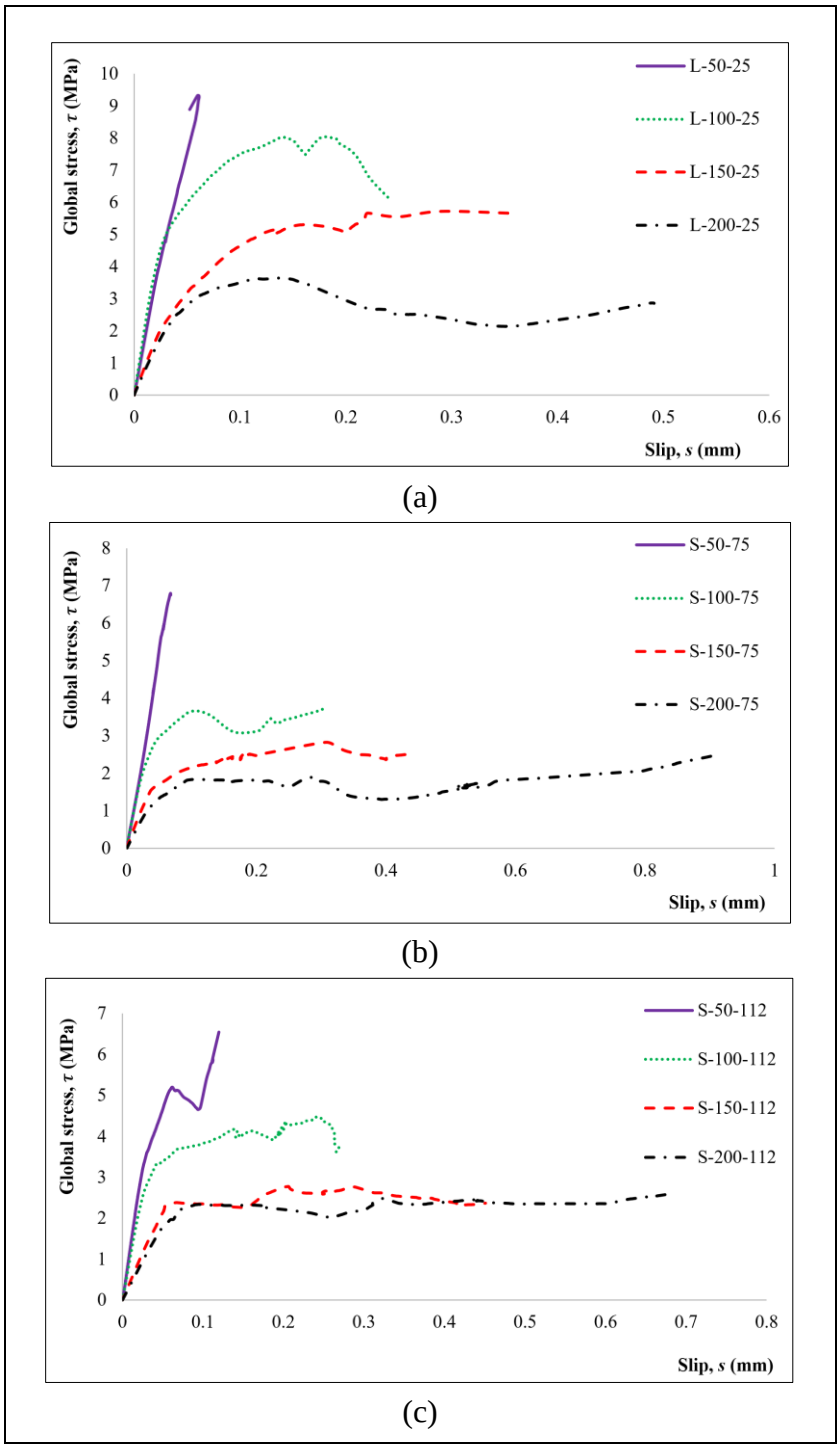

Figure 4.15 Global bond stress-slip curves related to the tested Specimens of: a) Series 1; b) Series 2 and c) Series 3

4.6.7 Effect of CFRP bond length

Figure 4.16 shows the double-lap maximum loads of specimens bonded with CFRP laminate and sheet with the bonded lengths investigated (50 mm, 100 mm, 150 mm and 200 mm). Increasing the bond length generally led to higher bond strength up to a threshold, known as the effective bond length, after which no increase in load was achieved during the tests. More specifically, in specimens bonded with CFRP laminate (Series 1), specimen L-150-25 endured the highest load until failure ($F_{\max} = 38.1$ kN) and no increase in the ultimate load was achieved in Specimen L-200-25 (with a greater bond length). Note that Specimen L-200-25 did not even achieve the same ultimate load as Specimen L-150-25. This could be attributed to the lower concrete strength of specimen L-200-25 compared to that of Specimen L-150-25. Similarly, the specimens with CFRP sheet (Series 2 and 3) exhibited an increase in ultimate load with increasing bonded length until the effective bond length. Indeed, test observations showed that two specimens, S-150-75 and S-100-112, reached maximum loads of 55.1 kN and 76.8 kN, respectively, among the specimens with the same CFRP width. The maximum double-lap load of Specimen S-100-75 ($F_{\max} = 44.7$ kN) was, however, slightly lower than that of Specimen S-50-75 ($F_{\max} = 45.6$ kN), which is contrary to the anticipated greater failure load of the former specimen considering its higher bond length. This unexpected result could be attributed to possible inaccuracies during laboratory testing including specimen preparation or CFRP alignment over the concrete block. Hence, it seems that the ultimate load of specimens bonded with CFRP sheet tends to stabilize after bonded lengths of 150 mm and 100 mm for Series 2 (75 mm-wide sheet) and Series 3 (112 mm wide sheet) specimens, respectively.

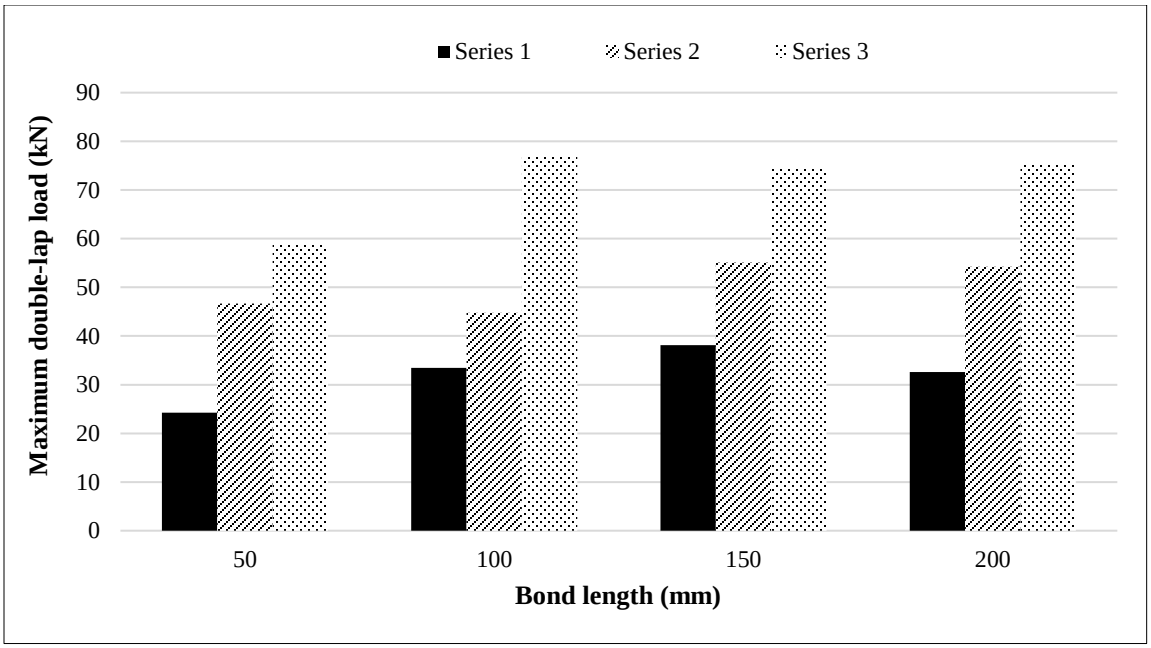

Figure 4.16 Maximum double-lap load gained by specimens with different bond lengths

4.6.8 Effective bond length of specimens

Research investigations on CFRP bonded concrete pull-out tests have clearly proved a direct relationship between CFRP bonded length and bond strength. However, an increase in bond strength can only be achieved with a bond length less than the effective bond length, after which there is no significant increase in bond capacity (J. F. Chen & Teng, 2001; Maeda et al., 1997; Neubauer & Rostasy, 1999; Pellegrino et al., 2008; Z. Wu et al., 2009). As a matter of fact, the existence of the effective bond length suggests that by increasing the tensile force at the loading end of CFRP, the active bonded area tends to shift towards the free end as a result of interfacial cracking propagation (Ben Ouezdou, Belarbi, & Bae, 2009; Nakaba et al., 2001). Related studies have discovered that the effective bond length depends on the FRP properties, i.e., tensile modulus, thickness and width and concrete strength. Table 4.6 presents some of the most practical models in the literature for calculating effective bond length, l_e, under static loading along with their predictions for the test specimens. Note that the average value of the three concrete compressive strengths used in the experiment was assumed to estimate the effective bond length (i.e., f_c' = 46.9 MPa).

Table 4.6 Effective bond-length relations and predicted results for the specimens

Effective bond-length models		**Predicted l_e (mm) for the specimens bonded with**	
		Laminate	**Sheet**
Niedermeier (1996)	$l_e = \sqrt{\frac{n_f E_f t_f}{4 f_t}}$	112.66	68.05
Maeda et al. (1997)	$l_e = e^{6.13 - 0.58 \ln(n_f E_f t_f)}$, $(E_f t_f \ in \ GPa.mm)$	21.39	38.38
Neubauer and Rostasy (1999)	$l_e = \sqrt{\frac{n_f E_f t_f}{2\ f_t}}$	159.33	96.24
J. F. Chen and Teng (2001)	$l_e = \sqrt{n_f E_f t_f / (f_c'^{1/2})}$	169.99	102.68
Sato (JCI, 2003)	$l_e = 1.89\ (n_f E_f t_f)^{0.4}$, $l_e \le L_b$	248.39	165.95
Iso (JCI, 2003)	$l_e = 0.125\ (n_f E_f t_f)^{0.57}$, $l_e \le L_b$	130.62	73.52
H. Yuan et al. (2004)	$l_e = a + \frac{1}{2\,\lambda_1} \ln \frac{\lambda_1 + \lambda_2 \tan(\lambda_2 a)}{\lambda_1 - \lambda_2 \tan(\lambda_2 a)}$ $\lambda_1 = \sqrt{\frac{\tau_{max}}{s_{peak} \times n_f E_f t_f}}$, $\lambda_2 = \sqrt{\frac{\tau_{max}}{(s_{ult} - s_{peak}) \times n_f E_f t_f}}$ $a = \frac{1}{\lambda_2} \arcsin\left[0.99 \sqrt{\frac{s_{ult} - s_{peak}}{s_{peak}}}\right]$	169.88	102.61
Pellegrino et al. (2008)	$l_e = \sqrt{n_f E_f t_f / (c_2\ f_t)}$ $l_e \le 140mm\ .\ c_2 = 2.15$	140.00	92.82

Table 4.6 Effective bond-length relations and predicted results for the specimens (Continue)

Effective bond-length models		**Predicted l_e (mm) for the specimens bonded with**	
		Laminate	**Sheet**
Z. Wu et al. (2009)	$l_e = 0.395 \frac{(n_f E_f t_f)^{0.54}}{f_c'^{0.09}}$	202.46	117.46
CSA S806 (2012)	$l_e = \frac{25350}{(n_f E_f t_f)^{0.58}}$	21.47	38.54
ACI 440.2R (2017)	$l_e = \frac{23300}{(n_f E_f t_f)^{0.58}}$	19.74	35.42
fib TG5.1 (2019)	$l_e = \frac{\pi}{k_b}\sqrt{\frac{n_f E_f t_f}{8 f_c'^{2/3}}}$, $k_b = \sqrt{\frac{2-b_f/b_c}{1+b_f/b_c}}$	163.93	$l_{e.1}$= 124.13 $l_{e.2}$= 146.53

Inspection of the available effective bond-length models reveals that some of the equations express a direct correlation between CFRP stiffness, $n_f E_f t_f$, and effective bond length (J. F. Chen & Teng, 2001; *fib* TG5.1, 2019; JCI, 2003; Neubauer & Rostasy, 1999; Niedermeier, 1996; Pellegrino et al., 2008; Z. Wu et al., 2009; H. Yuan et al., 2004), whereas others suggest an inverse relationship between these two parameters (ACI 440.2R, 2017; CSA S806, 2012; Maeda et al., 1997). This is why the predictions of the effective bond length by these two groups of models vary significantly. Furthermore, among the existing effective bond length relations, only *fib* TG5.1 (2019) considers the CFRP-to-concrete width factor, b_f/b_c, as a variable for measuring the effective bond length, which gives two values of $l_{e.1}$= 124.1 mm and $l_{e.2}$=146.5 mm for specimens with 75 mm-wide CFRP sheet and 112 mm-wide CFRP sheet, respectively.

As mentioned earlier, the effective bond length is in fact the active bonded region along which most of the interfacial shear stresses are transferred to the concrete layer. In other words, the bonded zone, in excess of the effective bonded length, does not contribute to the bond-stress

distribution and, in turn, the bond capacity (Ben Ouezdou et al., 2009). Considering the ultimate load resisted by specimens bonded with CFRP laminate (Series 1) leads to the conclusion that the effective bond length, l_e, should be between 100 mm and 150 mm because there is no increase in bond strength at a bond length greater than 150 mm. Using the same logic for specimens with CFRP sheet, the effective bond length is estimated to lie within the $100\ mm \leq l_e \leq 150\ mm$ range for Series 2 specimens and $50\ mm \leq l_e \leq 100\ mm$ for Series 3 specimens.

4.6.9 Strain distributions along the bonded CFRP

Figure 4.17 (a), (b) and (c) depicts the strain distribution of specimens, as captured by the gauges along the bonded length, at different ratios of ultimate load (P_{ult}). Increasing the tensile load clearly results in higher strain over the bond length. Furthermore, observations of the strain distribution at load levels closer to the ultimate load (e.g., 0.9 – 0.99 P_{ult}) reveal that the strain beyond a certain distance from the loaded end tends to vanish. Indeed, based on the concept of effective bond length, the strain distribution of bonded zones outside the effective bonded region is expected to be negligible (Ben Ouezdou et al., 2009; Yao et al., 2005). Hence, the effective bond length could also be obtained through strain readings over the bonded length of CFRP.

As for the specimen bonded with CFRP laminate (Specimen L-200-25), Figure 4.17 (a) shows that 90% -99% of the ultimate load (P_{ult}) was generally resisted over a length between 100 and 150 mm. This could indicate that the effective bond length of specimens bonded with CFRP laminate lies within this range. With reference to Specimen S-200-75 in Figure 4.17 (b), the strain distribution beyond the bond length of 150 mm exhibited lower values at 90%-99% P_{ult}. Therefore, the effective bond length of specimens with 75 mm-wide CFRP sheet could be determined to lie within the 100 mm – 150 mm range. Likewise, as for specimens with 112 mm-wide CFRP sheet (Specimen S-200-112 in Figure 4.17 (c)), the effective bond length seems to lie at a distance between 50 mm and 100 mm from the loaded end according to the strain distribution.

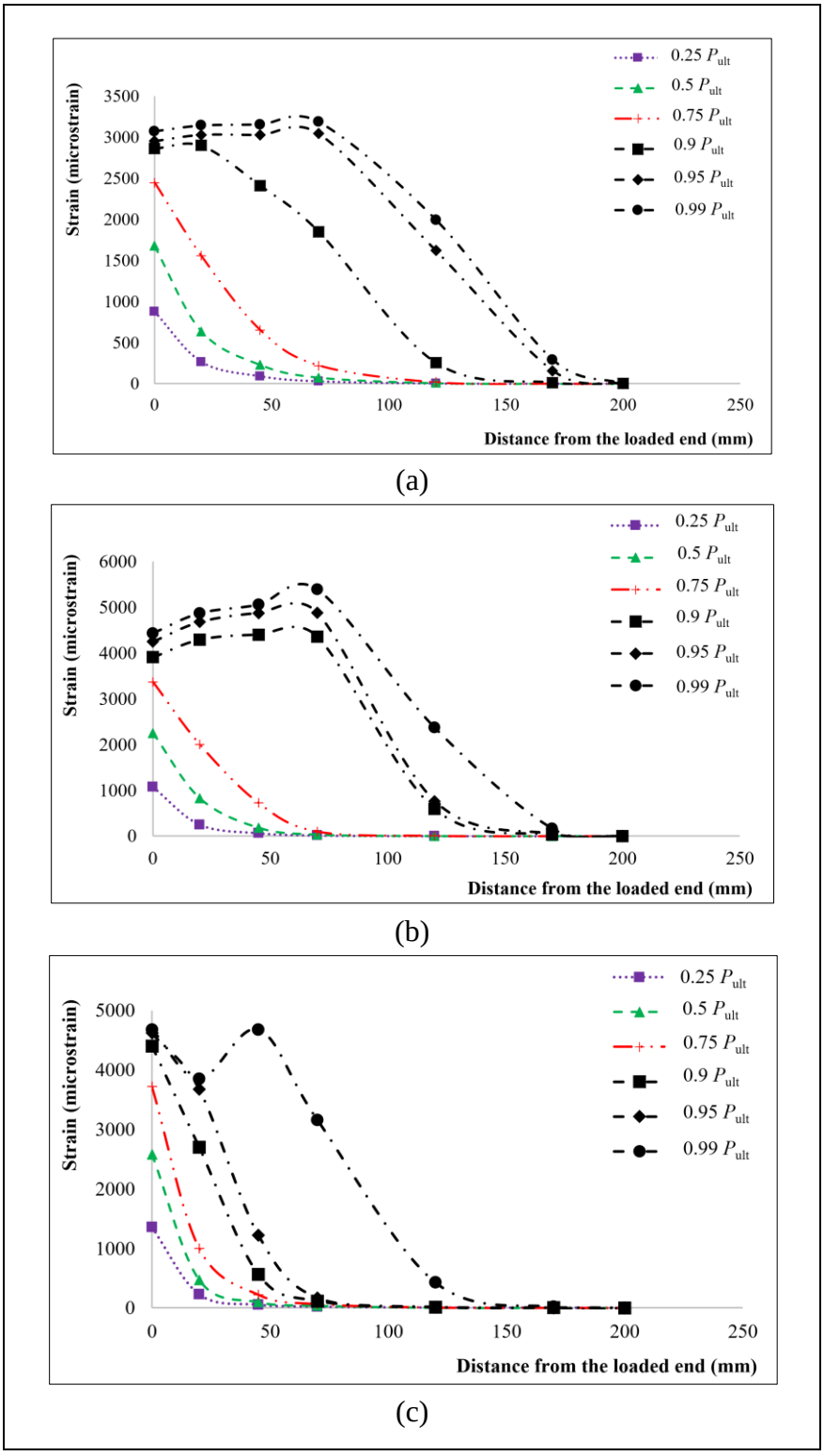

Figure 4.17 Strain distributions along the bonded length at different ratios of the maximum bond capacity for: a) L-200-25; b) S-200-75; and c) S-200-112

Based on the limited experimental results in the present study, it appears that the equations suggested by Niedermeier (1996), Neubauer and Rostasy (1999), J. F. Chen and Teng (2001), Iso (JCI, 2003), H. Yuan et al. (2004), Pellegrino et al. (2008) and *fib* TG5.1 (2019) may be better options for calculating l_e. The predictions of effective bond length by these models are closer to the anticipated effective bond lengths of specimens in this study. However, it should be noted that the influence of CFRP-to-concrete width ratio on effective bond length is evident based on the results obtained in this experiment. However, although the CFRP-to-concrete width ratio is included in the effective bond-length relation stated in *fib* TG5.1 (2019), the calculated l_e of specimens with 75 mm and 112 mm-wide CFRP sheet from this model did not entirely agree with the ranges cited above for the effective bond lengths of Series 2 and 3 specimens. To this end, more experimental data can help to see the proportional effect of CFRP width on the determination of effective bond length.

4.6.10 Effect of CFRP type

As noted earlier, the two widths of 25 mm for CFRP laminate and 75 mm for the CFRP sheet (Series 1 and 2) were selected to facilitate comparison between the two CFRP types (laminate vs. sheet). According to the experimental test results (see Table 4.3), using 75 mm-wide CFRP sheet instead of 25 mm-wide laminate can significantly increase the bond strength. More specifically, by comparing the ultimate loads gained by specimens with a bonded length of 150 mm (Specimen L-150-25 vs. S-150-75), which have obtained the maximum bond capacity in each test series, one can see that an increase of about 45 % was achieved in the load-carrying capacity of specimens with CFRP sheet over those with laminate. Since, the two CFRP composites were equally designed in terms of their ultimate tensile strength, it can be concluded that in cases where the main failure mode is the interfacial debonding failure and not CFRP rupture, the bonded area plays a significant role at determining the bond capacity. Hence, the greater bonded area of specimens with sheet led to a higher bond strength compared to those bonded with laminates.

4.6.10.1 Load-displacement relationship

Figure 4.18 shows the displacement versus applied load curves of Series 1 and 2 specimens. It is worth mentioning that displacement can be measured by adding the overall slip of bonded CFRP, s_f, to the elongation of the unbonded part (C. Yuan et al., 2019). Each curve features three regions, namely, the elastic region, the softening region, and the debonding region. Indeed, the load-displacement curve tends to behave linearly until it reaches the first plateau of applied force after which the curve exhibits a wavy pattern (the softening region). In this softening region, the bond undergoes loss of interfacial shear stress, while slip continues to increase. As micro-cracking propagates on the concrete surface, complete debonding of CFRP from concrete occurs at the failure load (Emmanuel Ferrier et al., 2010; Sun, Peng, Liu, et al., 2017; C. Yuan et al., 2019). Figure 4.18 also shows that specimens bonded with sheet achieved better performance than those bonded with CFRP laminate in terms of both bond capacity and ductility of the CFRP-to-concrete interface.

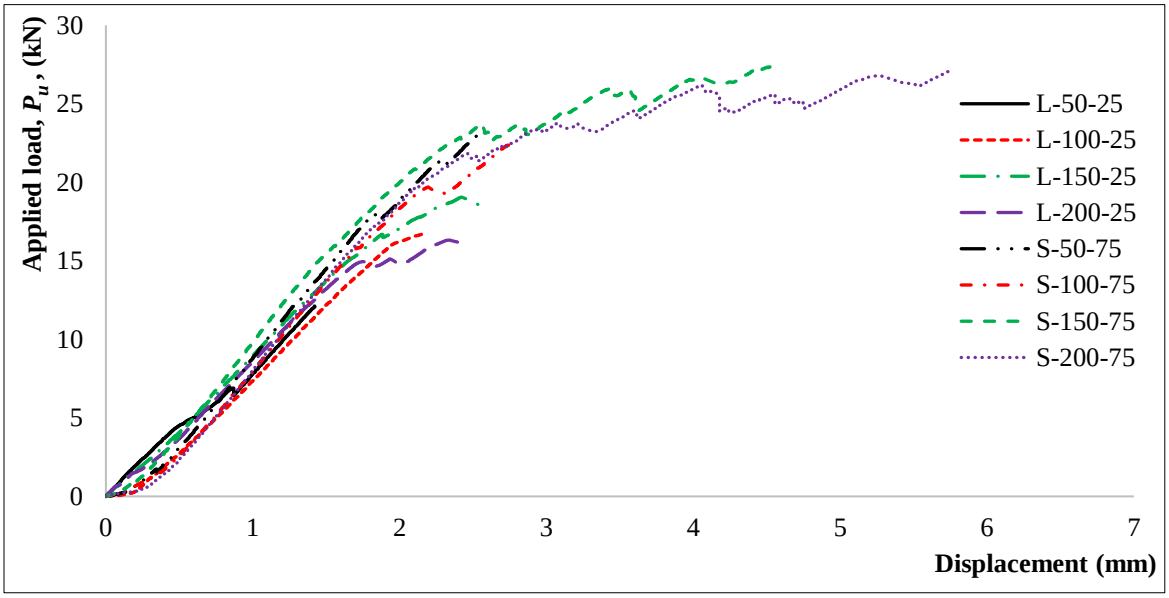

Figure 4.18 Applied load vs. displacement of specimens bonded with CFRP laminate and 75 mm-wide sheet

4.6.11 Effect of CFRP width

Test observations of the performance of specimens with 75 mm-wide sheet versus 112 mm-wide sheet (Series 2 vs. Series 3) show that CFRP width is an influencing factor on bond strength. Indeed, relevant research findings have confirmed that when the failure mode of the bond is concrete surface separation, the bonded CFRP width affects bond behavior (Brosens & Van Gemert, 1999; Ueda, Sato, & Asano, 1999). However, it has been reported that when bond failure tends to occur at the adhesive between CFRP and concrete, the CFRP width is not likely to affect the bond behavior (De Lorenzis et al., 2001). Considering the ultimate bond capacity of test specimens with CFRP sheet (Series 2 and 3), it is evident from the test results and the model predictions (Table 4.3) that increasing the CFRP-to-concrete bond width can contribute to higher bond resistance and thereby improves bond performance. For instance, at bond lengths of 150 mm and 200 mm, which were assumed to be greater than the effective bond lengths of Series 2 and 3 specimens, an increase of over 30 % was achieved in the load-carrying resistance of specimens with 112 mm-wide CFRP compared to the ones bonded with 75 mm-wide sheets. Therefore, it can be concluded that applying greater CFRP widths to specimens can result in higher bond strengths.

4.7 Conclusions

A double-lap pull-out test was performed to investigate the behavior of the bond between CFRP and concrete. The experimental program was intended to include the influencing parameters of CFRP type, bonded length and CFRP width. Upon capturing data from the strain gauges, bond-slip curves of the tested specimens were drawn, and the accuracy of existing bond-slip models was evaluated. A modified bilinear bond-slip model was proposed on the basis of the current test results along with the experimental data in the literature. The reliability of the proposed bilinear model in capturing the bond behavior was compared with the available bond-slip models. Furthermore, the performance of available effective bond-length relations as well as bond-strength models were assessed based on experimental results. The following conclusions are drawn on the basis of the findings of this study:

- The failure mode of CFRP bonded concrete specimens is debonding at the CFRP-to-concrete interface which occurs mainly in the form of concrete surface separation.

- Higher bond strength at the CFRP-to-concrete interface can be achieved by increasing the bonded length up to the effective bond length. The effective bond length of specimens with CFRP laminate was found to be greater than that of specimens bonded with CFRP sheet. This could be due to the higher stiffness of CFRP laminate compared to CFRP sheet which helps transmit interfacial stresses from CFRP laminate into the concrete over a greater bonded length before debonding.

- Applying CFRP fabric sheet can enhance bond load-carrying capacity compared to using CFRP laminate of equivalent width. This can be attributed to the greater width of CFRP fabric sheet compared to the width of the laminate, which provides a larger bonded area to carry the interlaminar shear stresses. Since, the applied CFRPs do not reach their full tensile capacity due to premature debonding failure, the bond behavior greatly depends on the bonded area rather than the type of CFRP element. Furthermore, using CFRP sheet instead of laminate can also increase the ductility of the CFRP-to-concrete bond.

- Increasing the CFRP-to-concrete width ratio leads to an increase in bond load-carrying capacity, whereas effective bond length seems to decrease when a wider CFRP sheet is used. It is noteworthy that the inverse relationship between effective bond length and CFRP width mentioned earlier was based on a limited data set.

- The modified bond-slip model was seen to perform well at estimating the maximum bond shear stress and bond slippage of test data in the literature when compared to the existing bilinear models. Further research may be necessary to examine the reliability of the proposed model.

- Of the existing effective bond-length relations, models that suggest a direct relationship between CFRP stiffness and effective bond length show more consistency with the current

experimental results. Furthermore, the CFRP-to-concrete width ratio appears to impact the effective bond length. Therefore, considering this parameter in the effective bond-strength model seems to be vital. More experimental research may be required to further assess the reliability of the models.

4.8 Data availability statement

Some or all data, models, or code that support the findings of this study are available from the corresponding author upon reasonable request including experimental results of concrete cylinder tests and pull-out tests.

4.9 Acknowledgments

Financial support of the Natural Sciences and Engineering Research Council of Canada (NSERC) and the Fonds de Recherche du Québec – Nature et Technologie (FRQNT) through operating grants is gratefully acknowledged. The authors thank Sika-Canada, Inc. (Pointe-Claire, QC) for contributing to the cost of materials. The efficient collaboration of J. Auger and J. Lescelleur (senior technicians) at École de technologie supérieure in conducting the tests is also acknowledged.

CHAPTER 5

FATIGUE BEHAVIOR IN THE CARBON-FIBRE-REINFORCED POLYMER-TO-CONCRETE BOND BY CYCLIC PULL-OUT TEST: EXPERIMENTAL AND ANALYTIAL STUDY

Abbas Fathi [1], Georges El-Saikaly [2], Omar Chaallal [3]

[1,2,3] Department of Construction Engineering, École de Technologie Supérieure
1100 Notre-Dame St. West, Montreal, Quebec, Canada H3C 1K3

Article published in Journal of Composites for Construction, American Society of Civil Engineers (ASCE), May 2023, (Fathi, El-Saikaly, & Chaallal, 2023-b).

5.1 Abstract

Today's construction industry has been more inclined to the practice of innovative rehabilitation techniques including externally bonded (EB) fiber-reinforced polymer (FRP) composites on existing reinforced concrete (RC) structures rather than traditional strengthening methods. Indeed, the higher fatigue resistance of carbon FRPs (CFRPs) has made them superior strengthening tools for structures subjected to fatigue loading, such as RC bridge girders against daily traffic loads. However, the performance of RC structures retrofitted with EB-CFRP composites can be highly influenced by the bonding mechanism at the CFRP-to-concrete interface. The occurrence of debonding failure at the CFRP-to-concrete interface can result in a premature failure of EB-CFRP retrofitting system and thereby leads to the rupture of the deficient structure. Therefore, an in-depth understanding of the bond behavior, especially under fatigue loading, can contribute to improve the efficiency of EB-CFRP strengthening techniques. To this end, this paper investigates the bond fatigue behavior through an experimental study. The parameters of CFRP composite type (laminate vs. fabric sheet), bond length and CFRP-to-concrete width ratio are considered herein to examine their effectiveness on the fatigue bond performance at the CFRP-to-concrete interface. The research results reveal that the CFRP composite system comprised of fabric sheet and the corresponding epoxy adhesive can perform better compared to the CFRP bonded joint with laminate in terms

of fatigue life and residual load-carrying capacity. Furthermore, a modified bond fatigue-life model (S-N model), validated with existing research data, is proposed that can successfully take into consideration the effect of fatigue loading, concrete compressive strength and CFRP-to-concrete width ratio.

Keywords: CFRP-to-concrete interface; Fatigue behavior; Pull-out test; Cyclic loading; CFRP composite type; bond length; CFRP-to-concrete width ratio; Bond fatigue-life model.

5.2 Introduction

Reinforced concrete (RC) structures, such as bridge girders, are continuously subjected to fatigue loading due to daily traffic. In fact, a typical RC bridge deck is likely to undergo up to 7×10^8 load cycles during its 120-year-lifespan (E Ferrier et al., 2005). Therefore, strengthening such structures via innovative methods can lead to their stability and sustainable performance. Externally bonding (EB) of concrete beams and columns using fiber reinforced polymer (FRP) composites offers an effective solution to retrofit infrastructures. Indeed, the superior advantages of using EB-FRP strengthening methods over the conventional steel reinforcement include higher tensile strength, light weight, corrosion resistance, ease of application, cost-effectiveness and high resistance to fatigue.

Among FRP composites, carbon FRPs (CFRPs) are known to have the highest strength and durability under fatigue conditions (Fathi et al., 2022). However, one of the main challenges of using CFRP strengthening systems, especially on concrete structures, is the bond mechanism at the CFRP-to-concrete interface. Indeed, the major failure mode of EB-CFRP bonded concrete joints is reported to occur by CFRP debonding. In the case of monotonic loading conditions, the concrete surface beneath the bonded CFRP composite tends to break primarily, thereby leading to the premature failure of CFRP bonding systems (J. F. Chen & Teng, 2001; De Lorenzis et al., 2001; H. Yuan et al., 2004). However, it has been observed that the bond failure mode is greatly dependent on the applied loading rate (C. Yuan et al., 2020). Indeed, experimental results of single-lap shear tests by C. Yuan et al. (2020) have

revealed that when the quasi-static (i.e., monotonic) loading rate is less than 3 m/s, fracture of the concrete cover triggers the debonding failure. However, at loading rates of 3 m/s or higher, the debonding failure tends to occur within the interface between concrete and adhesive, as opposed to the former case with the concrete cover failure.

As far as fatigue loading goes, some of the most observed failure modes of FRP-to-concrete interface during pull-out experimental investigations include concrete cover failure, failure of concrete-to-adhesive interface, cohesive failure of adhesive, failure of FRP-to-adhesive interface, FRP interlaminar failure and FRP rupture (Bizindavyi et al., 2003; Chalot et al., 2019; JG Dai et al., 2005; W. Zhang, 2018; Zhou et al., 2021; Zhu et al., 2016). Experimental observations of specimens under fatigue loading by K. Li et al. (2015) showed that the applied level of cyclic loading can govern the bond failure mode. Their experimental study showed that when the maximum cyclic load level applied to a CFRP-bonded concrete joint was equal to or greater than 70% of its ultimate monotonic capacity, P_{ult}, the fatigue failure occurred by debonding of concrete cover. In contrast, at cyclic load levels below that limit (i.e., $P_{\max} < 0.7\ P_{\mathrm{ult}}$), the typical failure mode was due to the peeling of CFRP sheet from the epoxy adhesive (i.e., failure of FRP-to-adhesive interface).

Through a research review, the authors have summarized some of the influencing parameters on the fatigue behavior of CFRP-to-concrete interface such as concrete strength, FRP-to-concrete width ratio, fatigue loading amplitude, bond length, FRP properties and environmental conditions (Fathi et al., 2022). Indeed, it is well-documented in the literature that increasing the bond length can improve the bond fatigue behavior in terms of the number of load cycles until failure (Bizindavyi et al., 2003; JG Dai et al., 2005; HM Diab et al., 2009; K. Li et al., 2015; K. Li et al., 2018; Mazzotti & Savoia, 2009; Z. Wu et al., 2010). However, the post-fatigue residual capacity of FRP-to-concrete bond has been reported to be unaffected by fatigue loading at bond lengths greater than the effective bond length (Carloni et al., 2012; K. Li et al., 2015). As for the effect of FRP-to-concrete width ratio, experimental results of Bizindavyi et al. (2003) showed that adopting a wider FRP sheet reduced the bond slip during load cycles and therefore enhanced the bond fatigue life. However, K. Li et al. (2015) reported

that an inverse relationship existed between the FRP-to-concrete width ratio and bond fatigue life.

The experimental study by E Ferrier et al. (2005) including both single-lap and double-lap pull-out tests showed that the fatigue behavior of CFRP-to-concrete interface was mainly governed by the adhesive bonding. Indeed, FRP properties did not have any significant effect on the bond fatigue behavior. Similar observations were also reported in the study by Chalot et al. (2019), in which the epoxy adhesive was found to be the weakest element in the FRP-to-concrete bonded joint under fatigue loading. Their experimental study, consisting of 39 double-lap shear tests, showed that the fatigue performance of two CFRP types, i.e., unidirectional fabric and bidirectional fabric, was similar during the cyclic tests. However, Daud et al. (2015) reported that the FRP stiffness properties seem to affect the fatigue behavior of FRP-to concrete bond. According to their investigation, the effect of concrete compressive strength on the bond fatigue resistance did not appear to be significant, although test results of K. Li et al. (2015) showed that increasing the concrete strength can extend the fatigue life of CFRP-concrete bonded specimens.

W. Zhang (2018) conducted a series of double-lap shear tests on CFRP-to-concrete bonded joints under fatigue loading. Two types of high-strength (HS) and high-stiffness (HE) CFRP laminates were used in the experiments and different loading amplitudes were applied to specimens. It was concluded that the bond residual slip (slippage caused by unloading) followed an increasing trend with the number of load cycles. Furthermore, a fatigue bond-slip model for the HS-type CFRP laminate, based on the envelope stress-slip curves, was proposed in their study.

Following an experimental investigation on the fatigue behavior of the bond between basalt FRP (BFRP) sheet and concrete, the effect of marine environmental exposure was studied by Xie et al. (2019). It was observed that the failure mode of specimens exposed to wet dry cycles occurred in the form of BFRP rupture rather than the interfacial debonding. Furthermore, it

was found that marine environmental conditions tend to reduce the effective bond length of specimens during fatigue loading.

Through another experimental work on the fatigue behavior of CFRP-concrete bonded joints by Al-Saoudi et al. (2019), it was seen that specimens bonded with 120×1.4 mm (width × thickness) CFRP laminates did not undergo any fatigue failure when subjected to a maximum cyclic load level less than 75% of their ultimate monotonic capacity. However, their results showed that the specimen tends to exhibit a very short fatigue life at a maximum cyclic load level equal to (or higher than) 85% of the monotonic bond capacity.

Finally, Zhou et al. (2021) carried out a series of single-lap shear tests on CFRP-to-concrete bonded joints with different concrete strengths, two types of CFRP laminate (Type SC vs. Type MC) and loading amplitudes. It was observed that specimens bonded with Type SC CFRP laminates mostly failed as a result of CFRP peel-off from the concrete surface, regardless of the concrete strength or applied loading amplitude, whereas the failure mode of specimens with Type MC laminates appeared to be dependent on the maximum fatigue loading. Indeed, the failure mode of MC CFRP-bonded specimens was due to the cohesive failure within the adhesive when subjected to a maximum cyclic load less than or equal to 65% of the bond load-carrying capacity. However, the main failure mode changed to the concrete cover separation when a maximum cyclic load higher than 65% of load-carrying capacity was applied.

The review of existing findings in literature shows that studies regarding the behavior of CFRP-to-concrete bond under fatigue loading are much less documented than those under monotonic loading (Fathi et al., 2022; Kim & Heffernan, 2008; Oudah & El-Hacha, 2013; Z. Wu et al., 2010). In this research, a shear pull-out test program is performed to investigate the bond fatigue behavior of CFRP-to-concrete interface. In order to avoid the undesirable normal stresses that might occur during shear test configurations such as single-lap set-up (Emmanuel Ferrier et al., 2010; Mohammadi & Wan, 2015), a double-lap test set-up is employed by the authors. Different series of specimens are prepared to incorporate the influencing parameters of CFRP composite system (fabric sheet vs. laminate), bond length, and CFRP-to-concrete

width ratio. Test results are mainly presented in terms of interfacial energy dissipation, bond-slip relationship, and strain evolution during load cycles. Furthermore, a database consisting of test results derived from the literature (including this study) is used to develop a modified bond fatigue-life model (S-N model). The proposed S-N model performs well in predicting the fatigue life of CFRP-to-concrete bonded joints, as well as their endurance limit corresponding to 2 million load cycles.

5.3 Research significance

Inspection of the limited work regarding the fatigue behavior of CFRP-to-concrete bonded systems shows that the effect of CFRP width on the fatigue behavior of CFRP-to-concrete interface has not been adequately documented and therefore requires further research. More specifically, it is important to examine the impact of CFRP-to-concrete width ratio on the bond fatigue life and assess the fatigue bonding mechanism with respect to this variable. The current study takes into consideration the effect of CFRP width factor as one of the experimental parameters to address this issue. Furthermore, the existence of contradictory observations in prior studies regarding the effect of FRP properties on the fatigue bond behavior has been an impetus to investigate the fatigue performance of different CFRP types together with the corresponding epoxy adhesive (referred to, herein, as CFRP composite system) during the experiment. As for the parameter of bond length, the primary objective is to observe the bond fatigue life with respect to this variable, with an emphasis on the effective bond length under both fatigue and post-fatigue monotonic loading conditions and compare with available relevant findings. Finally, a modified fatigue-life prediction model is presented for the CFRP-to-concrete bond, which takes into account the three influencing variables of fatigue loading amplitude, concrete compressive strength and CFRP-to-concrete width ratio. This model is validated against a considerable amount of database found in the literature (i.e., 68 specimens) and proves to predict the bond S-N relationship with great accuracy.

5.4 Experimental program

Three series of specimens were prepared to perform double-lap pullout tests under cyclic loading. Each specimen was comprised of a concrete block (250 mm × 150 mm × 150 mm) bonded with one layer of either CFRP fabric sheet, also referred to as sheet hereafter, or CFRP laminate (both made up of unidirectional carbon fibers). Figure 5.1 shows the scheme of the testing set-up, whereas Table 5.1 summarizes the specimen details of the three Series of the experimental program. The test variables include CFRP composite type (fabric sheet vs. laminate), bond length and CFRP width. Four bond lengths of 50 mm, 100 mm, 150 mm and 200 mm were considered. These four bond lengths were chosen because the bond strength of specimens in each series (Series 1, 2 and 3) was assumed to stabilize within the range between 50 mm and 200 mm based on the calculations of effective bond length (ACI 440.2R, 2017; J. F. Chen & Teng, 2001; CSA S806, 2012; *fib* TG5.1, 2019; Maeda et al., 1997; Neubauer & Rostasy, 1999; Niedermeier, 1996; Pellegrino et al., 2008; Z. Wu et al., 2009; H. Yuan et al., 2004). Note that each specimen label represents, in order, the type of CFRP (laminate "L" or sheet "S"), bond length and CFRP width. For instance, CL-50-25 refers to the specimen, bonded with CFRP laminate "L", with a bond length and CFRP width of 50 mm and 25 mm, respectively.

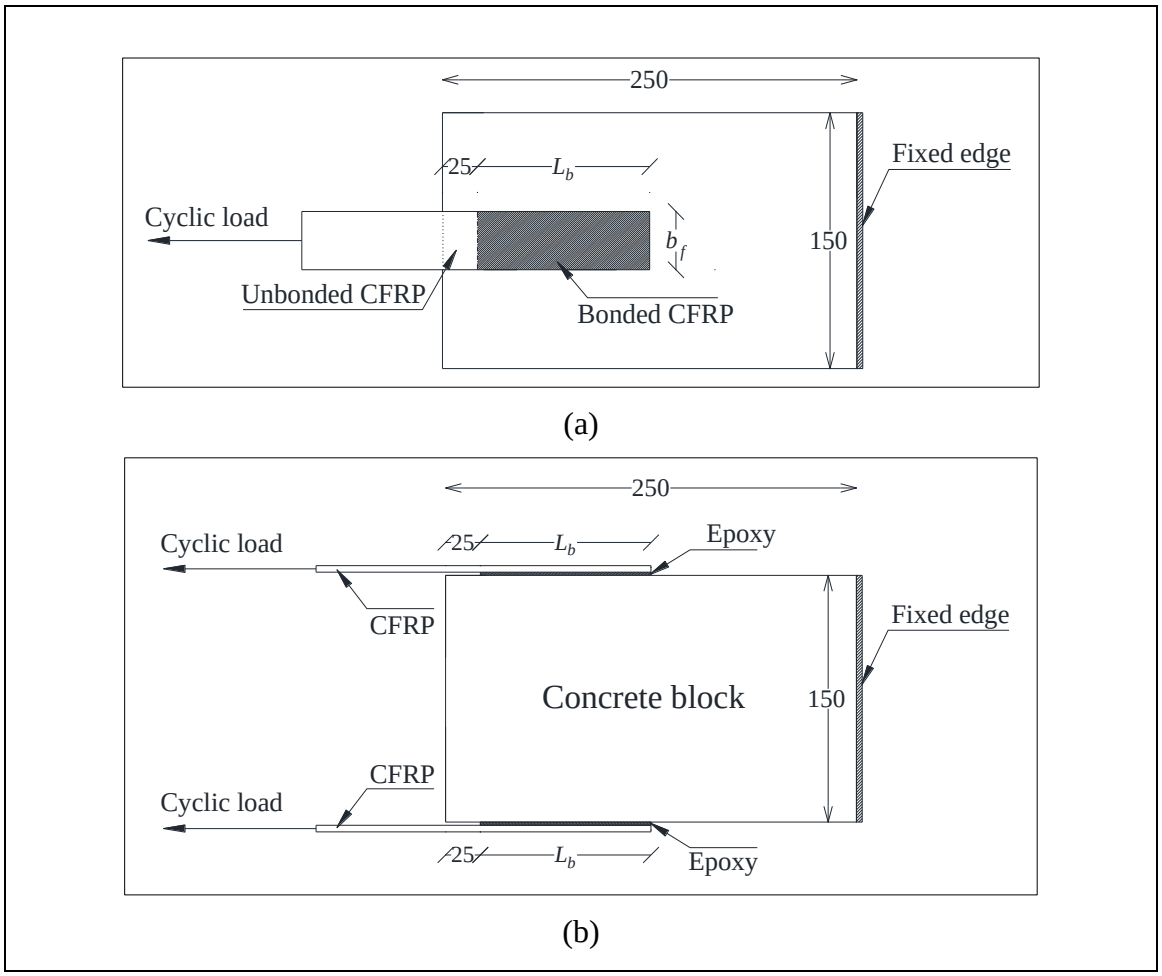

Figure 5.1 Scheme of cyclic testing set-up (dimensions in mm): a) top view; b) side view

Table 5.1 Experimental details of specimens

Series	Number	Specimen label	f'_c (MPa)	CFRP composite type	L_b (mm)	b_f (mm)	b_f / b_c
Series 1	1	CL-50-25	44	Sika CarboDur laminate	50	25	0.17
	2	CL-100-25	44	Sika CarboDur laminate	100	25	0.17
	3	CL-150-25	44	Sika CarboDur laminate	150	25	0.17
	4	CL-200-25	44	Sika CarboDur laminate	200	25	0.17
Series 2	5	CS-50-75	44.9	SikaWrap fabric sheet	50	75	0.5
	6	CS-100-75	44.9	SikaWrap fabric sheet	100	75	0.5
	7	CS-150-75	44.9	SikaWrap fabric sheet	150	75	0.5
	8	CS-200-75	44.9	SikaWrap fabric sheet	200	75	0.5
Series 3	9	CS-50-112	51.9	SikaWrap fabric sheet	50	112	0.75
	10	CS-100-112	51.9	SikaWrap fabric sheet	100	112	0.75
	11	CS-150-112	51.9	SikaWrap fabric sheet	150	112	0.75
	12	CS-200-112	51.9	SikaWrap fabric sheet	200	112	0.75

5.4.1 Specimen preparation

The concrete blocks were casted at three different times, using pre-mixed concrete products provided by a local supplier (Bomix). As a result, three slightly different concrete compressive strengths, f_c', of 44 MPa, 44.9 MPa and 51.9 MPa were allocated to the specimens (see Table 5.1). It should be noted that f_c' in each series was obtained from the average results of compression tests on at least three concrete cylinders (100mm × 200mm) according to ASTM C39/C39-21 (ASTM, 2021) with a standard deviation less than 0.5 MPa. The cubic compressive strength of concrete can also be taken as $f_{\mathrm{cu}} = 1.16\, f_c'$ in this study (Zabihi & Eren, 2014). Figure 5.2 shows the configuration of a typical specimen subjected to cyclic loading. As can be seen, a secondary larger concrete block (500 mm × 150 mm × 150 mm), also known as the loading block is used to apply tensile loads to the specimen. In order to avoid the possible premature debonding failure in the loading block, the following anchorage techniques were applied: a) extending the CFRP bonded length along the entire length of loading block; b) using an additional CFRP sheet stretched from the top of the loading block to anchor the ends of extended CFRP on both sides; and c) CFRP full-wrapping the lateral sides of loading block to provide a symmetric double-lap loading application. Note that prior to the application of CFRP composites, concrete blocks were sandblasted to reach a concrete surface profile (GSP) of 4, which provides a desired roughened surface for the application of epoxy adhesive. In fact, sandblasting was performed on every concrete surface that was bonded with CFRP composite, both for experimental blocks (250 mm × 150 mm × 150 mm) and loading blocks (500 mm × 150 mm × 150 mm). The top edges of the loading blocks were rounded before attaching the additional anchorage sheets. Also, in order to avoid stress concentration at the corners, a minimum length (gap) of 25 mm is left unbonded from the edges of each specimen.

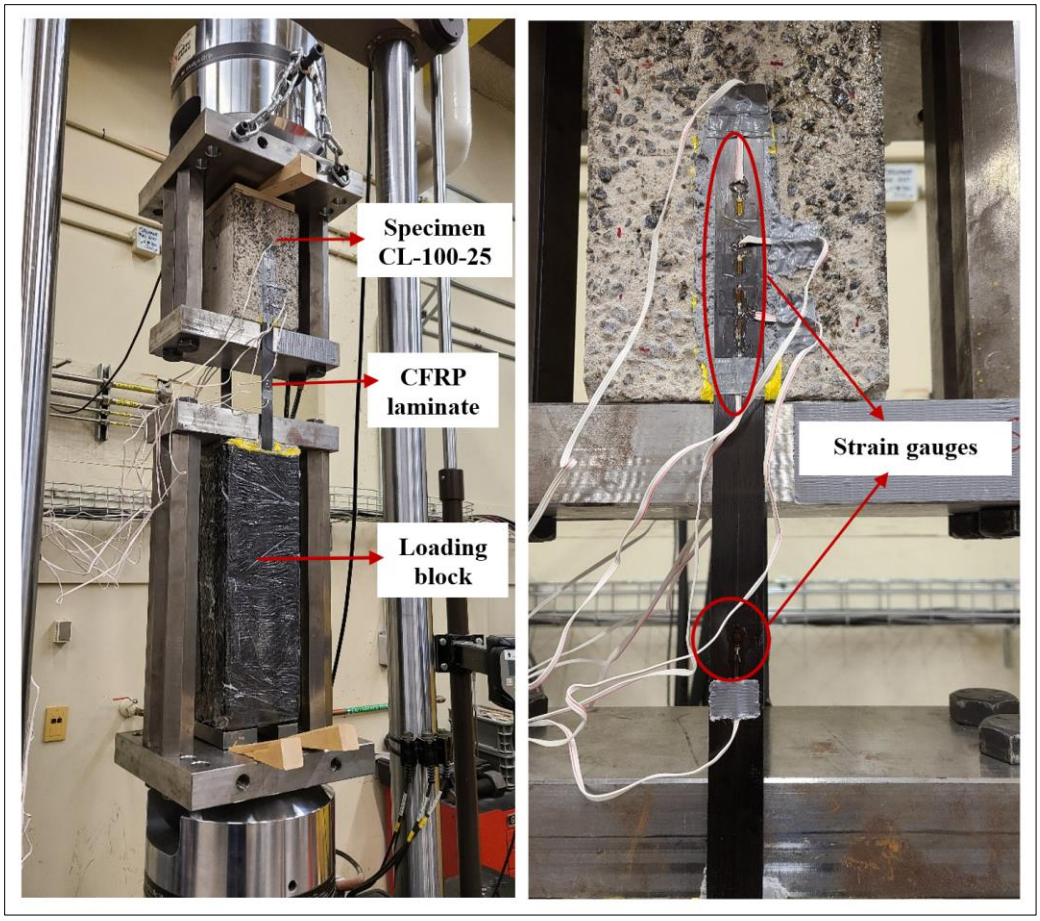

Figure 5.2 Cyclic testing configuration (Specimen CL-100-25)

Table 5.2 presents the mechanical properties of the CFRP composites along with the epoxy adhesives used in this experiment. It is noteworthy that the material properties are typically averages that have been obtained from laboratory testing condition at +23 °C (73 °F) and 50 % R.H. (relative humidity), as stated by the suppliers (Sika CarboDur; Sikadur -30; Sikadur -330; SikaWrap Hex -103 C). As far as the preparation of specimens with CFRP laminate goes, all laminates were first thoroughly cleaned with acetone on both surfaces. Also, prior to bonding the laminates, the concrete surfaces were covered with one layer of epoxy adhesive paste (Sika CarboDur; Sikadur -30).

The application of CFRP sheet to the concrete block was performed through a wet lay-up procedure, in accordance with the manufactures' instructions. Thus, all fabric sheets were first

impregnated with the corresponding epoxy resin (Sikadur -300). The impregnated sheets were then bonded to concrete surfaces that were already covered with a layer of epoxy adhesive, as recommended in the supplier's data sheet (Sikadur -330; SikaWrap Hex -103 C).

Table 5.2 Mechanical properties of CFRP composites and epoxy adhesives

Material type	**CFRP laminate**	**CFRP sheet**	**Epoxy adhesive for laminate**	**Epoxy adhesive for sheet**
Product name	Sika CarboDur S512	SikaWrap Hex -103 C (cured with Sikadur -300)	Sikadur -30	Sikadur -330
Elastic modulus (GPa)	165	71.7	4.5	3.8
Tensile strength (MPa)	2800	1110	24.8	30
Tensile elongation %	> 1.7	1.45	1	1.5
Thickness, t_f (mm)	1.2	1.016	-	-

5.4.2 CFRP width and strain gauge positions

All CFRP laminates were prepared to have the same width, b_f, of 25 mm. In order to carry out a comparison between the performances of the two CFRP composite types (laminate vs. sheet), an equivalent width of 75 mm was selected for the CFRP sheet in Series 2 specimens. The choice of these two CFRP widths (25 mm and 75 mm) was based on reaching the same CFRP tensile strength ($f_f \times t_f \times b_f$) in both configurations (laminate vs. sheet). Also, to evaluate the effect of CFRP-to-concrete width ratio on the bond fatigue behavior, a greater width of 112 mm was considered for specimens with CFRP sheet in Series 3. Hence, the two widths of 75 and 112 mm would correspond to the CFRP-to-concrete width ratios of 0.5 and 0.75, respectively.

Figure 5.3 shows the positions of strain gauges. As can be seen, all strain gauges were attached to the centerline of CFRP composite along the bonded length. The number of strain gauges and spacing between gauges may vary depending on the bonded length (see Figure 5.3), so that the strain distribution of CFRP-to-concrete interface can be well represented during load cycles. It may also be noted that one strain gauge is affixed to the midpoint of the unbonded

CFRP length. This gauge is targeted to capture the strains at the loaded end of CFRP, which can then be used to derive the cyclic bond stress-slip curves of the interval closest to the applied loading (e.g., Interval ε_3–ε_4 for L_b = 50 mm).

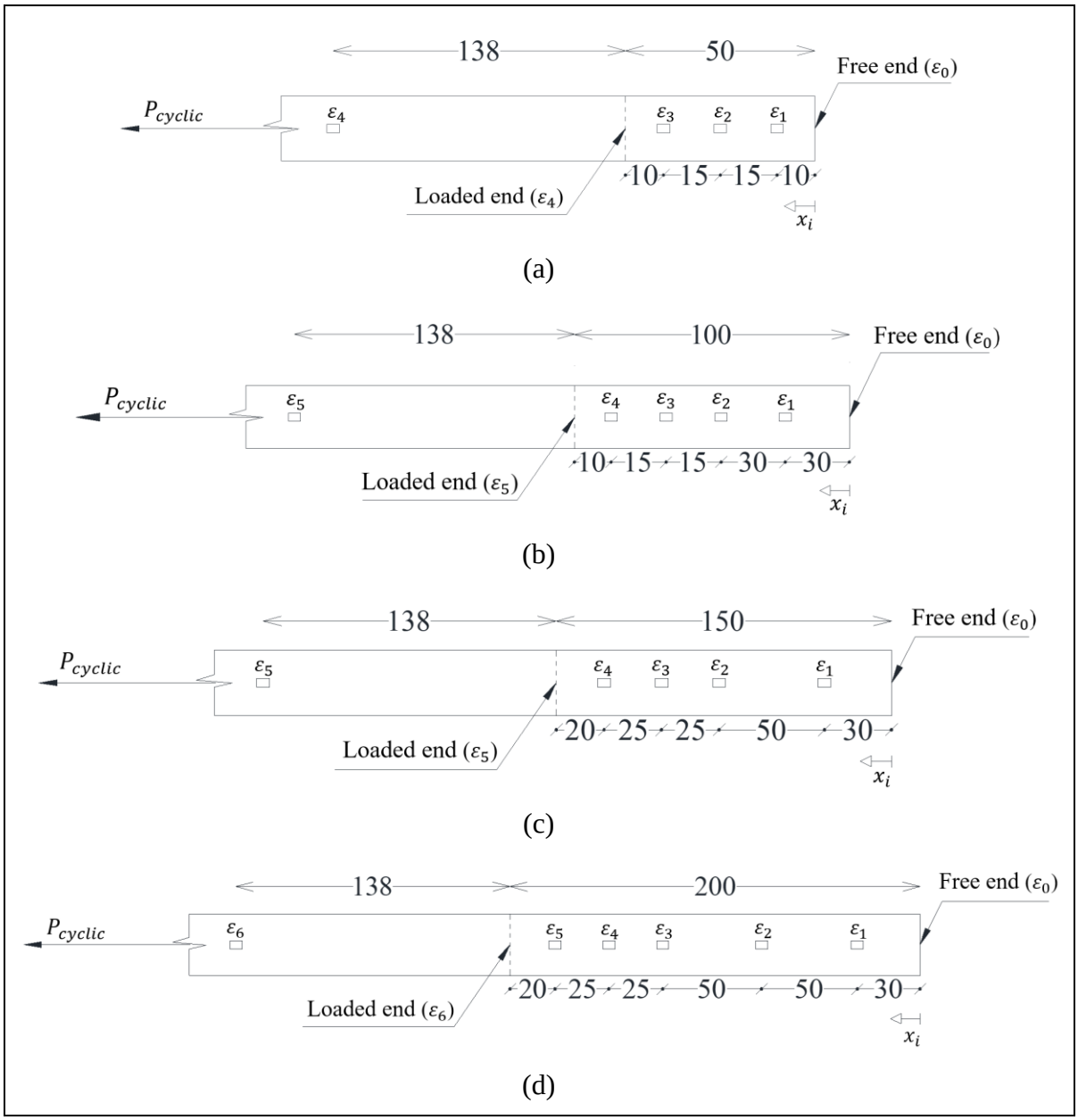

Figure 5.3 Strain gauge positions on CFRP composites for specimens with different L_b (dimensions in mm): a) L_b = 50 mm; b) L_b = 100 mm; c) L_b = 150 mm; d) L_b = 200 mm

5.4.3 Fatigue loading application

For each specimen in the test series, a companion specimen with the same specifications (CFRP composite type, bond length and width) was also prepared. This specimen was subjected to monotonic loading at a rate of 0.5 mm/min to determine the ultimate load-carrying capacity, P_{ult}, prior to fatigue testing. Comprehensive discussions regarding the experimental results of monotonic tests are presented in a separate study by the authors (Fathi, El-Saikaly, & Chaallal, 2023-a). It should be noted that the ultimate monotonic loads of specimens in each series were then calibrated ($P_{\text{ult},1}$) with respect to their bond length and concrete strength by using reliable bond-strength models that showed the highest agreement with the monotonic test results (Khalifa et al., 1998; Neubauer & Rostasy, 1999). As for the application of cyclic loading, the lower and upper levels of applied loads ($P_{\min}$ and $P_{\max}$) were set to be 35% and 65% of the monotonic load-carrying capacity of each specimen, respectively. These cyclic load ratios can be representative of the common service loading applied to structures like bridges during their service life (Chaallal et al., 2010; Ekenel & Myers, 2009; El-Saikaly & Chaallal, 2015-a, 2015-b; El-Saikaly et al., 2018). The fatigue testing was performed at a frequency of 3 Hz up to 2 million cycles. The reason for choosing the loading frequency as 3 Hz was that conventional real-life structures are typically cycled at a rate varying between 1 and 5 Hz (E Ferrier et al., 2005; W. Zhang, 2018). Note that the specimens that did not fail during fatigue loading were then subjected to post-fatigue monotonic loading (at the rate of 0.5 mm/min) until the total bond failure to assess their residual load-carrying capacity, $P_{\text{ult},2}$.

5.5 Experimental results

An MTS machine was employed to apply loading to the specimens. As for fatigue testing, the cyclic loading pattern was set in the form of sinewave. Each test was stopped when either the maximum 2 million load cycles were reached or until the debonding failure of the specimen. Due to the very high amount of recorded data during cyclic loading, the strain gauges were regulated to mainly capture the peaks and valleys in each cycle. This, in fact, helped to reduce the size of saved data. In cases where no fatigue failure was observed within 2 million load

cycles, post-fatigue monotonic loading was applied until the occurrence of debonding failure on either side of the specimen. Table 5.3 presents the results obtained for the three Series of the experimental program.

Table 5.3 Experimental results of specimens during cyclic testing

Series	**No.**	**Specimen label**	$P_{ult,1}$ (kN)	P_{min} (kN)	P_{max} (kN)	N_f	$P_{ult,2}$ (kN)	**Failure mode**
Series 1	1	CL-50-25	12.1	4.2	7.9	52980	-	F-P
	2	CL-100-25	16.7	5.8	10.9	79684	-	F-P
	3	CL-150-25	17.9	6.3	11.6	559470	-	F-P
	4	CL-200-25	18	6.3	11.7	528379	-	F-P / C-S
Series 2	5	CS-50-75	23.6	8.3	15.3	> 2 million	22.6	C-S
	6	CS-100-75	27.8	9.7	18.1	> 2 million	28.8	C-S
	7	CS-150-75	27.8	9.7	18.1	> 2 million	32	C-S
	8	CS-200-75	27.8	9.7	18.1	> 2 million	29.9	C-S
Series 3	9	CS-50-112	32	11.2	20.8	> 2 million	31.8	C-S
	10	CS-100-112	37.7	13.2	24.5	> 2 million	38.4	C-S
	11	CS-150-112	37.7	13.2	24.5	> 2 million	38.6	C-S
	12	CS-200-112	37.7	13.2	24.5	> 2 million	41.1	C-S

Note: $P_{min} = 0.35\ P_{ult,1}$, $P_{max} = 0.65\ P_{ult,1}$.
F-P= FRP peel-off from concrete, C-S= Concrete cover separation.

5.5.1 Failure modes

Experimental observations during the fatigue testing of specimens showed that increasing the interfacial slippage during the load cycles generally led to the formation of micro-cracking at the CFRP-to-concrete bond. Similarly, it has been reported that the growth of fatigue cracking within the epoxy adhesive along the CFRP bonded length triggers the interfacial degradation until the remaining bond length is not sufficient to resist the applied loads. That is when failure of CFRP-to-concrete bond occurs in an abrupt manner (W. Zhang, 2018).

5.5.1.1 Failure modes of specimens with CFRP laminate (Series 1)

It is well established that the dominant failure mode of FRP-to-concrete bond under monotonic loading is the separation of concrete layer beneath the bonded FRP composite (C. Chen et al., 2019; J. F. Chen & Teng, 2001; De Lorenzis et al., 2001; Emmanuel Ferrier et al., 2010; Yao et al., 2005; H. Yuan et al., 2004). Figure 5.4 shows the failure modes of specimens bonded with laminate under cyclic loading (Series 1). Unlike the monotonic loading condition with the main failure mode of concrete cover separation, the fatigue failure of all specimens with laminate (except Specimen CL-200-25) was dominantly triggered by peeling of CFRP laminate from the concrete surface. This mode of failure, which majorly occurred within the interface between CFRP laminate and adhesive, was evidenced by the large amount of epoxy layer left on the concrete substrate after failure (see Figure 5.4). As for Specimen CL-200-25, the debonding failure appeared to occur due to a combination of CFRP-to-adhesive interface failure and concrete cover separation. This may be attributed to the greater bond length of this specimen which allowed for debonding propagation to occur in two different forms: 1) debonding within the CFRP-to-adhesive interface, especially in regions closer to the loaded end; and 2) concrete cover debonding that is more dominant at bonded regions closer to the free end. Overall, the fatigue failure patterns of Series 1 specimens shows that the crack propagation initiated from the loaded end at the interface between epoxy adhesive and CFRP laminate and was followed by the rupture of concrete surface in regions closer to the free end of bonded CFRP. Similar failure modes have been observed in prior investigations, in which the majority of debonding failure at the CFRP-to-concrete interface under fatigue loading (with relatively low amplitude) was reported to occur at the epoxy adhesive layer rather than the concrete surface beneath the CFRP composite (Bizindavyi et al., 2003; Chalot et al., 2019; Ko & Sato, 2007; K. Li et al., 2015; Zhou et al., 2021; Zhu et al., 2016). Indeed, related test results revealed that the major crack failure occurred in the form of FRP-peeling from concrete within 50-75 % of the fatigue life of specimen. Also, the interfacial crack formation during the initial and final 10-15 % of the specimen's fatigue life has been reported to take place as a result of concrete surface rupture (Bizindavyi et al., 2003).

Figure 5.4 Failure modes of specimens with CFRP laminate during cyclic loading

5.5.1.2 Failure modes of specimens bonded with CFRP sheet (Series 2 and 3)

Figure 5.5 shows the failure patterns of specimens bonded with sheet (Series 2 and 3). Since no failure occurred during fatigue loading (up to 2 million cycles), these specimens were subjected to post-fatigue monotonic loading until failure. The existence of a layer of fine concrete aggregates on the debonded CFRP sheets corroborates the fact that the failure of CFRP-to-concrete bond occurred due to the rupture of concrete surface beneath the CFRP sheet. This is similar to the main failure mode observed typically during monotonic loading conditions, namely, concrete cover separation.

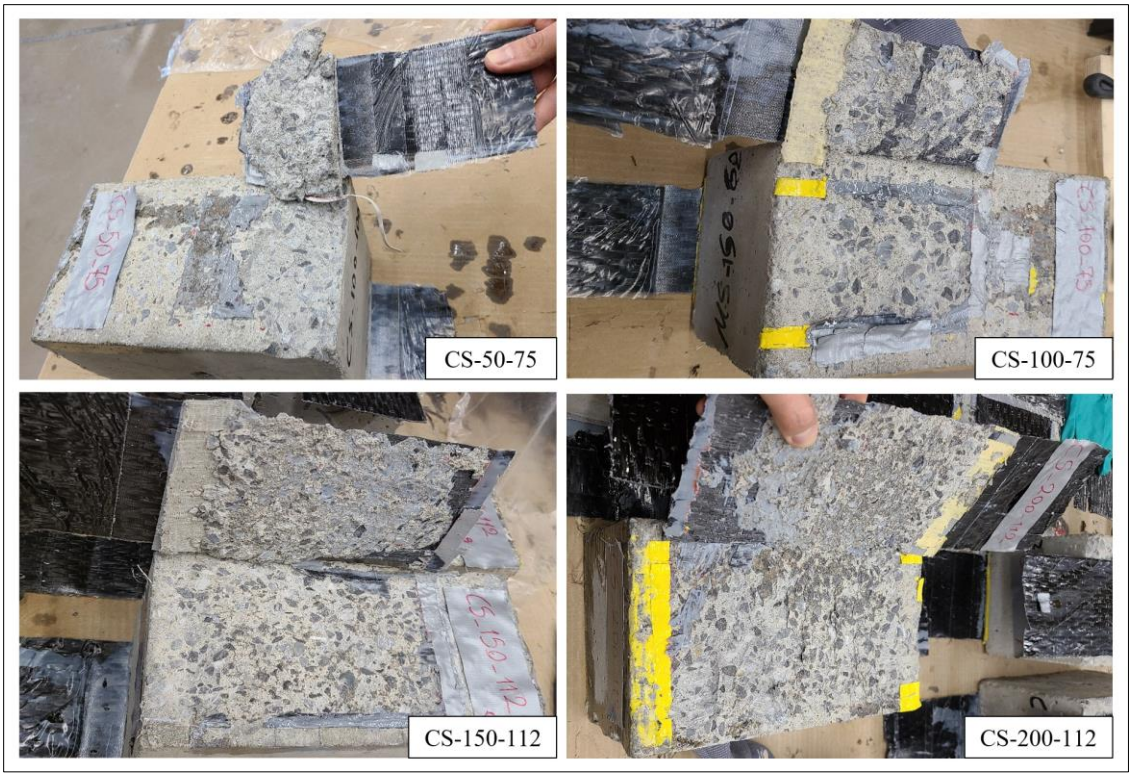

Figure 5.5 Failure modes of specimens with CFRP sheet under post-fatigue monotonic loading

5.5.2 Bond-energy dissipation during fatigue loading

The bond between the FRP and concrete under fatigue loading tends to undergo gradual degradation with increased load cycles (JG Dai et al., 2005). Figure 5.6 shows the displacement vs cycle ratio of CFRP-to-concrete bonded specimens with laminate, in which debonding failure took place during fatigue loading. Note that the displacement values were taken as the elongation of the unbonded part of CFRP composite, which was recorded by the data-acquisition system during load cycles. In fact, the increase of displacement can be an indication of the loss of interfacial energy during load cycles. For clarity, the curves (in Figure 5.6) cover the peak displacements every 1000 cycles for Specimens CL-50-25 and CL-100-25 and every 2500 cycles for Specimens CL-150-25 and CL-200-25, respectively. Also, note that the cycle ratio is equal to the ratio of the load cycle to the number of load cycles at failure (n/N_f). Figure 5.6 reveals that each curve consists of three phases as follows: Phase1) monotonic increase of

displacement; Phase 2) gradual crack propagation in which the interfacial energy tends to dissipate during fatigue loading; and Phase 3) sudden increase of displacement prior to debonding failure. It should be noted that most of the interfacial energy loss under fatigue loading takes place in Phase 2 with a gradual (yet steady) increase of displacement until the bond failure. Similar experimental observations have also been reported regarding the bond behavior in terms of fatigue crack propagation (Xie et al., 2019; Zhou et al., 2021).

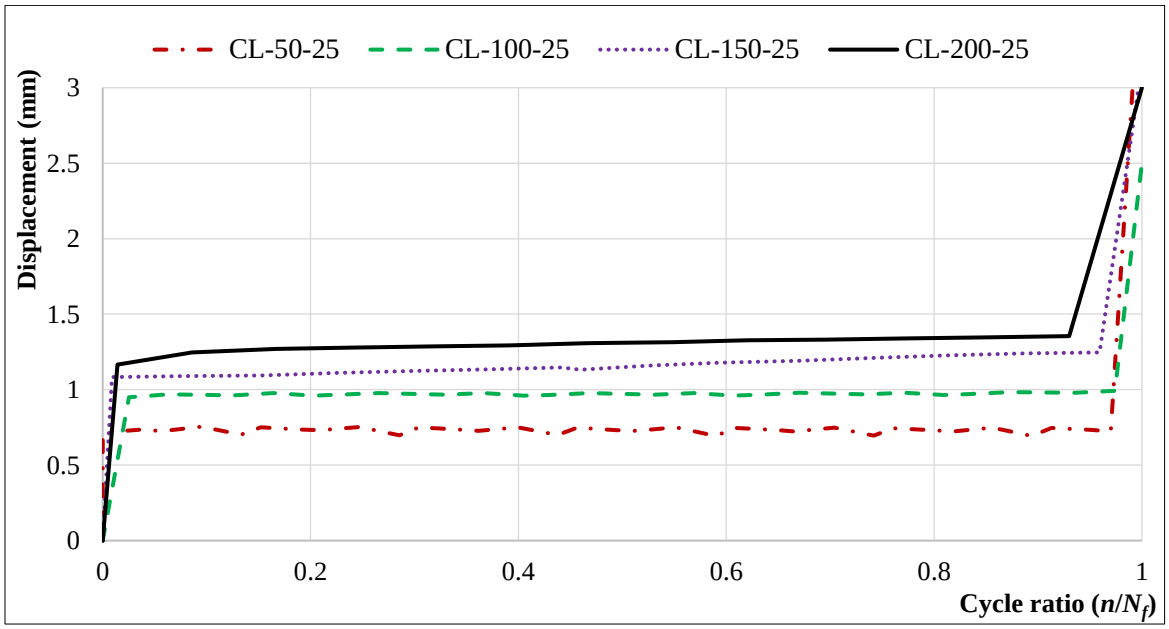

Figure 5.6 Displacement vs. load cycle ratio of specimens with laminate under fatigue loading

As for specimens bonded with sheet (Series 2 and 3), Figure 5.7 (a) and (b) shows the displacement (peaks only) versus load cycle ratio (n/N_{max}). It can be observed that the fatigue loss of interfacial energy within the maximum load cycles (N_{max} = 2 million) is relatively low and therefore, no failure was observed in specimens bonded with sheet. Furthermore, it may be noted that in both series (Series 2 and 3), specimens with a bond length of 50 mm (i.e., CS-50-75 and CS-50-112) showed the lowest displacement in their category. Indeed, at bond lengths over 50 mm, the specimens of all series behaved almost similarly in terms of the gradual increase of displacement under fatigue loading. This can be attributed to the fact the at

bond length greater than 50 mm, the specimen with CFRP sheet tends to reach its maximum ductile capacity under fatigue loading.

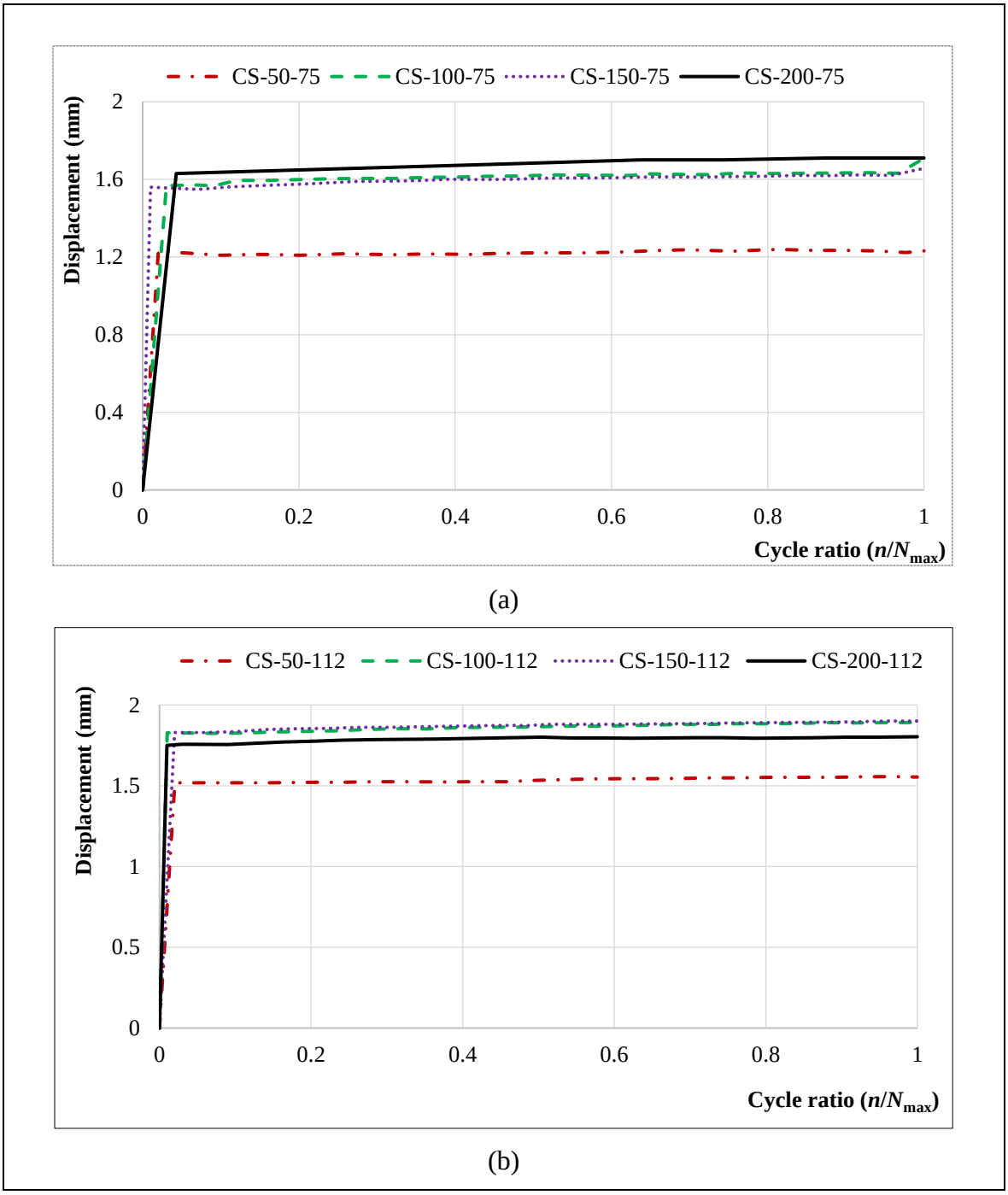

Figure 5.7 Displacement vs. load cycle ratio of specimens with: a) 75 mm-wide sheet; b) 112 mm-wide sheet

5.5.3 Bond stress-slip relationship

The stress-slip relationship of CFRP-to-concrete interface is generally used to reach an in-depth understanding of the bond behavior. The bond slip, s_i, along the bonded length and at each load cycle, can be obtained from the following equation:

$$s_i = \frac{\Delta x_i}{2}(\varepsilon_0 + 2\sum_{j=1}^{i-1}\varepsilon_j + \varepsilon_i) \tag{5.1}$$

in which Δx_i is the distance between two subsequent strain gauges and ε_0 (strain at the free end) is assumed to be zero. Also, note that the above-mentioned bond-slip equation is based on the fact that the relative movement of concrete layer beneath the CFRP composite with respect to the CFRP slip is negligible and therefore can be assumed equal to zero.

As for the cyclic bond stress, the following equation can be employed to determine the shear stress at the interval between two subsequent strain gauges, (i.e., local bond stress, τ_i).

$$\tau_i = \frac{t_f E_f}{\Delta x_i}|\Delta\varepsilon_i| \tag{5.2}$$

where $\Delta\varepsilon_i$ is the difference of strains captured by two consecutive strain gauges (i.e., $\Delta\varepsilon_i = \varepsilon_i - \varepsilon_{i-1}$). Through the inspection of cyclic bond stress-slip curves, derived from Eq. (5.1) - (5.2), the fatigue degradation of CFRP-to-concrete bond can also be determined.

5.5.3.1 Cyclic bond-slip curves of specimens with laminate

Figure 5.8 shows the cyclic bond-slip curves of Specimen CL-200-25 (from Series 1), in which failure occurred during fatigue loading. Note that since the data-acquisition system captured only the peak and valley points at each cycle during testing, the bond-stress curves appeared almost linear in each cycle. As can be seen, with the increase in load cycles, the maximum

peak cyclic bond stress, $\tau_{m,\text{peak}}$, shifts from the intervals closer to the loaded end (see intervals in Figure 5.3) towards the free end. For instance, during the initial cyclic loading (i.e., 0-6 cycles), the highest peak stress, $\tau_{m,\text{peak}}$, belongs to Interval ε_5–ε_6, while at load cycles between 80,000-520,000, which is near the failure of the specimen, Interval ε_1–ε_2 shows the maximum peak stress, $\tau_{m,\text{peak}}$. This means that local debonding grows along the bonded length as the load cycles increase until the remaining bonded length can no longer resist the applied load. That is when the entire failure of the CFRP-to-concrete bond occurs, which, unlike the monotonic loading condition, does not normally feature any prior cracking sound. It should also be noted that the bond-slip curve of the interval closest to the free end (i.e., Interval ε_0–ε_1) only shows an increasing linear pattern. This shows that the shear stresses imposed to this region are negligible and do not contribute to the overall bond shear resistance during load cycles.

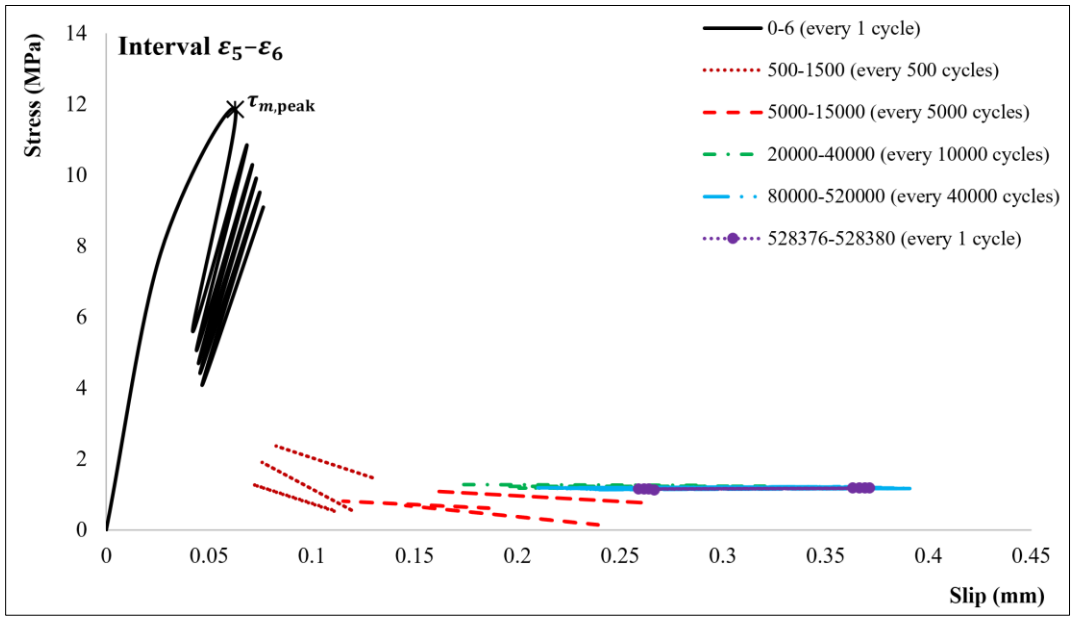

(a)

Figure 5.8 Local bond-slip curves of Specimen CL-200-25 during cyclic loading along the bond length: a) Interval $\varepsilon_5 - \varepsilon_6$; b) Interval $\varepsilon_4 - \varepsilon_5$; c) Interval $\varepsilon_3 - \varepsilon_4$; d) Interval $\varepsilon_2 - \varepsilon_3$; e) Interval $\varepsilon_1 - \varepsilon_2$; f) Interval $\varepsilon_0 - \varepsilon_1$

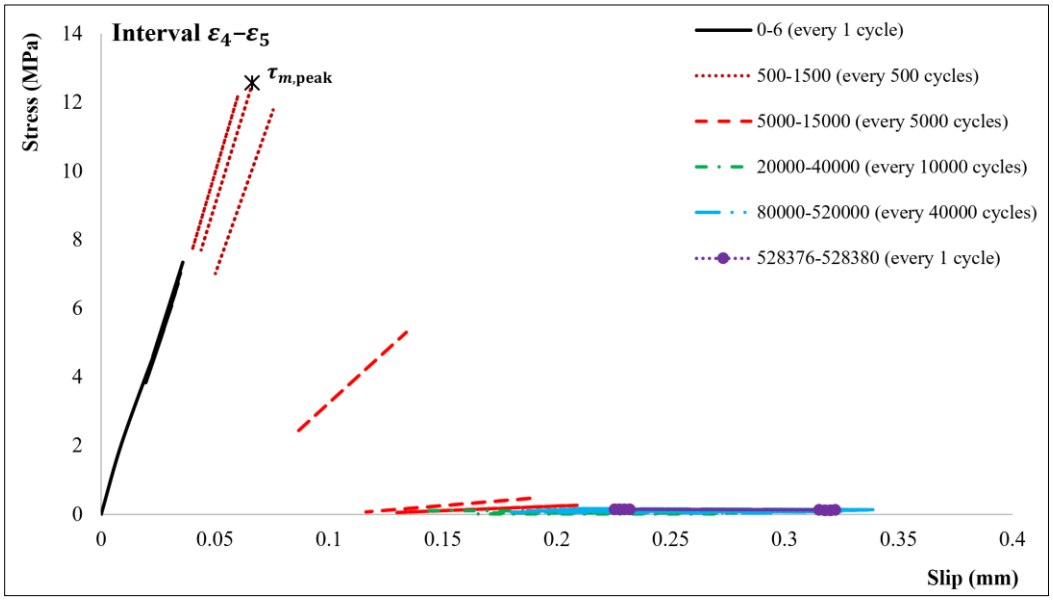

(b)

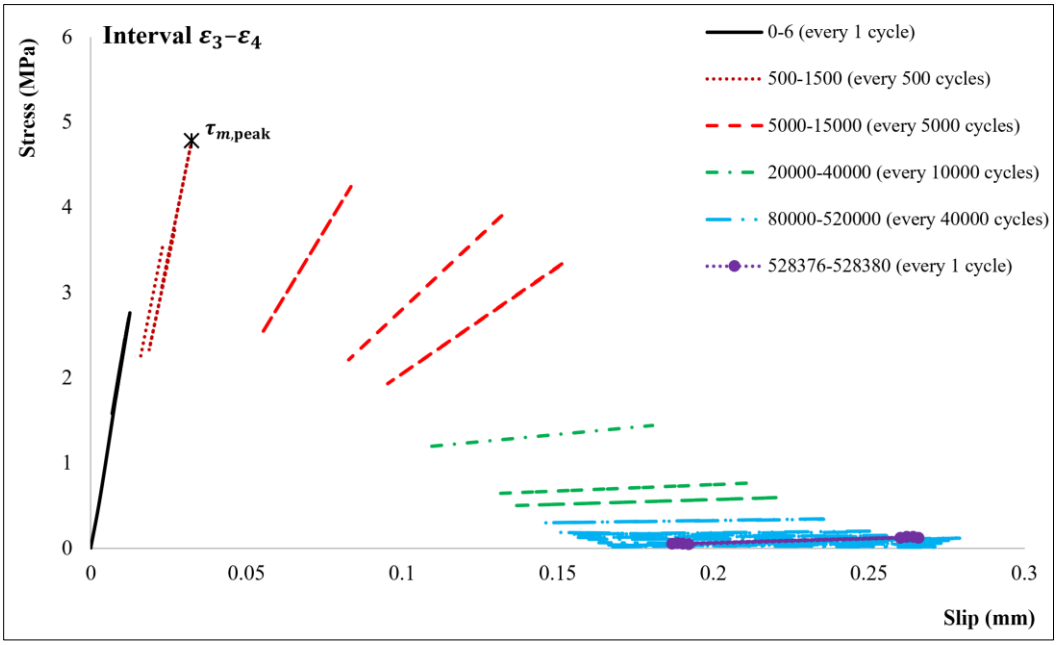

(c)

Figure 5.8 Local bond-slip curves of Specimen CL-200-25 during cyclic loading along the bond length: a) Interval $\varepsilon_5 - \varepsilon_6$; b) Interval $\varepsilon_4 - \varepsilon_5$; c) Interval $\varepsilon_3 - \varepsilon_4$; d) Interval $\varepsilon_2 - \varepsilon_3$; e) Interval $\varepsilon_1 - \varepsilon_2$; f) Interval $\varepsilon_0 - \varepsilon_1$ (Continue)

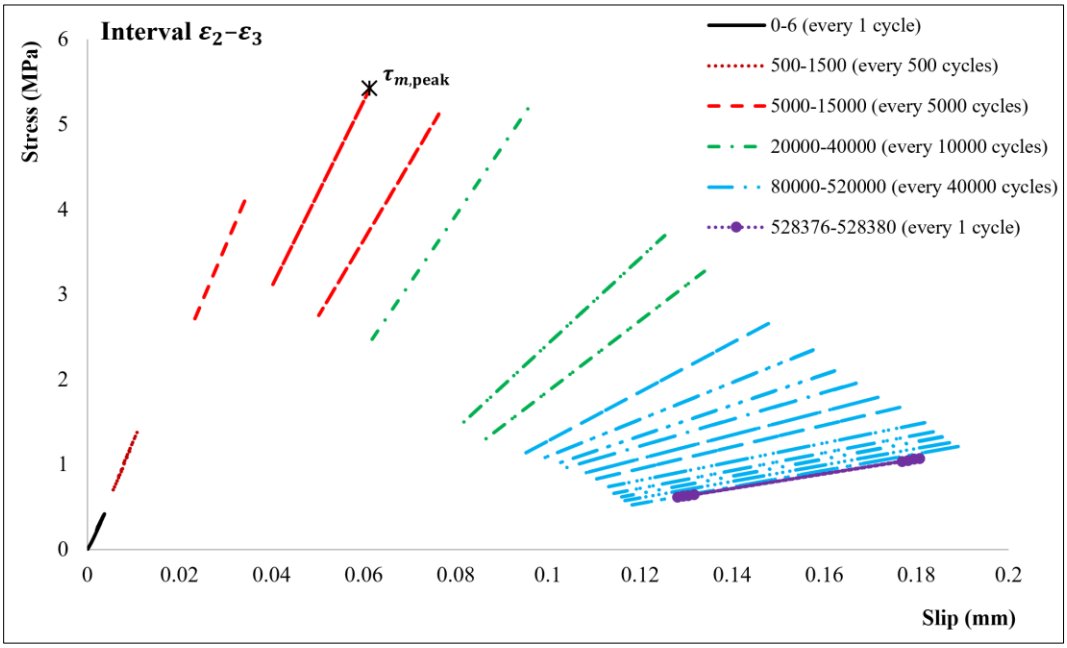

(d)

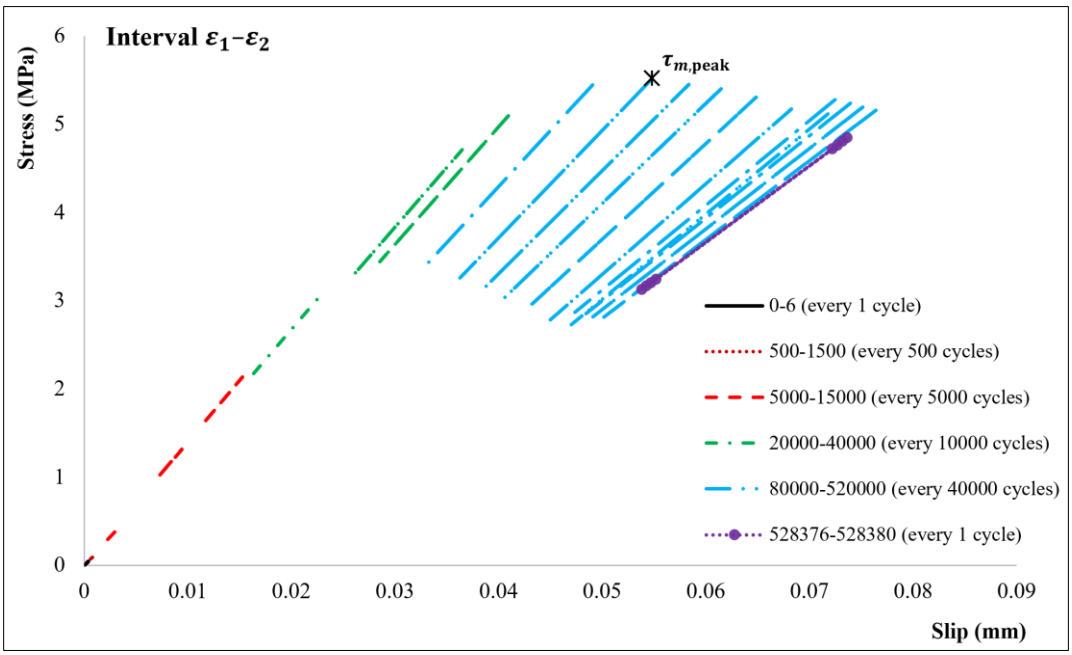

(e)

Figure 5.8 Local bond-slip curves of Specimen CL-200-25 during cyclic loading along the bond length: a) Interval $\varepsilon_5 - \varepsilon_6$; b) Interval $\varepsilon_4 - \varepsilon_5$; c) Interval $\varepsilon_3 - \varepsilon_4$; d) Interval $\varepsilon_2 - \varepsilon_3$; e) Interval $\varepsilon_1 - \varepsilon_2$; f) Interval $\varepsilon_0 - \varepsilon_1$ (Continue)

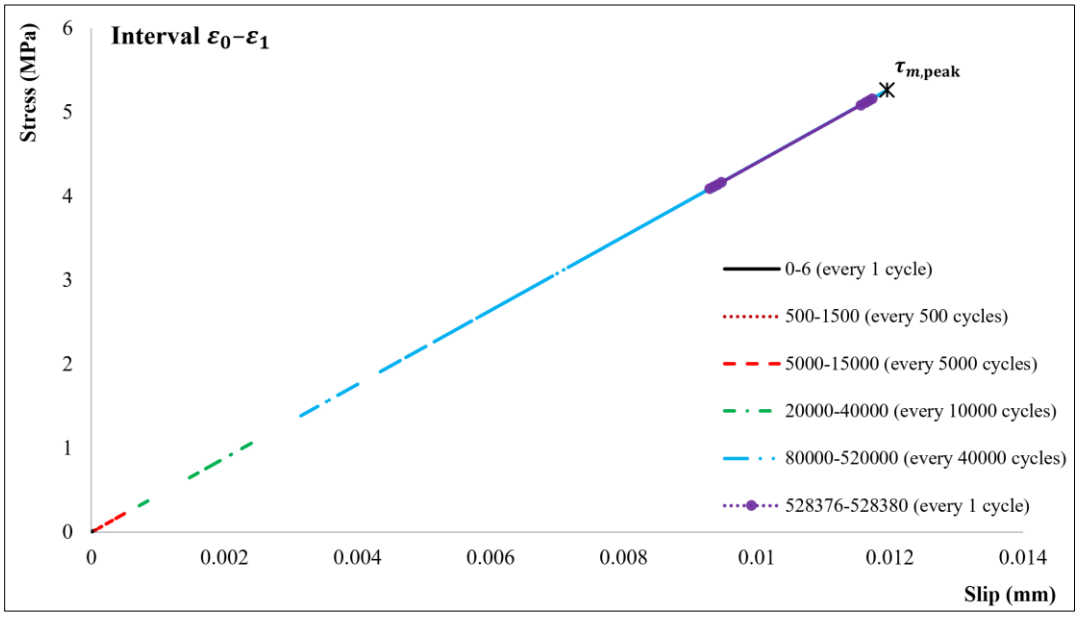

(f)

Figure 5.8 Local bond-slip curves of Specimen CL-200-25 during cyclic loading along the bond length: a) Interval $\varepsilon_5 - \varepsilon_6$; b) Interval $\varepsilon_4 - \varepsilon_5$; c) Interval $\varepsilon_3 - \varepsilon_4$; d) Interval $\varepsilon_2 - \varepsilon_3$; e) Interval $\varepsilon_1 - \varepsilon_2$; f) Interval $\varepsilon_0 - \varepsilon_1$ (Continue)

5.5.3.2 Cyclic bond stress-slip curves of specimens with sheet

Figure 5.9 presents the bond stress-slip curves of specimens with sheet (CS-200-75 and CS-200-112). Note that the closest interval to the loaded end (Interval ε_5–ε_6) is considered here, which is the first bonded region directly affected by the pull-out force. As can be seen from the local bond-slip curves, the peak cyclic shear stress, (i.e., peak stress during each cycle) decreases at higher load cycles. Also, the slope of cyclic stress-slip curves follows a decreasing trend with an increase in the number of load cycles. This phenomenon, which has also been evidenced in relevant studies, is an indication of the loss of interfacial energy during fatigue loading (Bizindavyi et al., 2003; K. Li et al., 2018). Indeed, the loss of interfacial energy during load cycles is accompanied by a growth in the bond slippage as well as a decline in the bond shear strength.

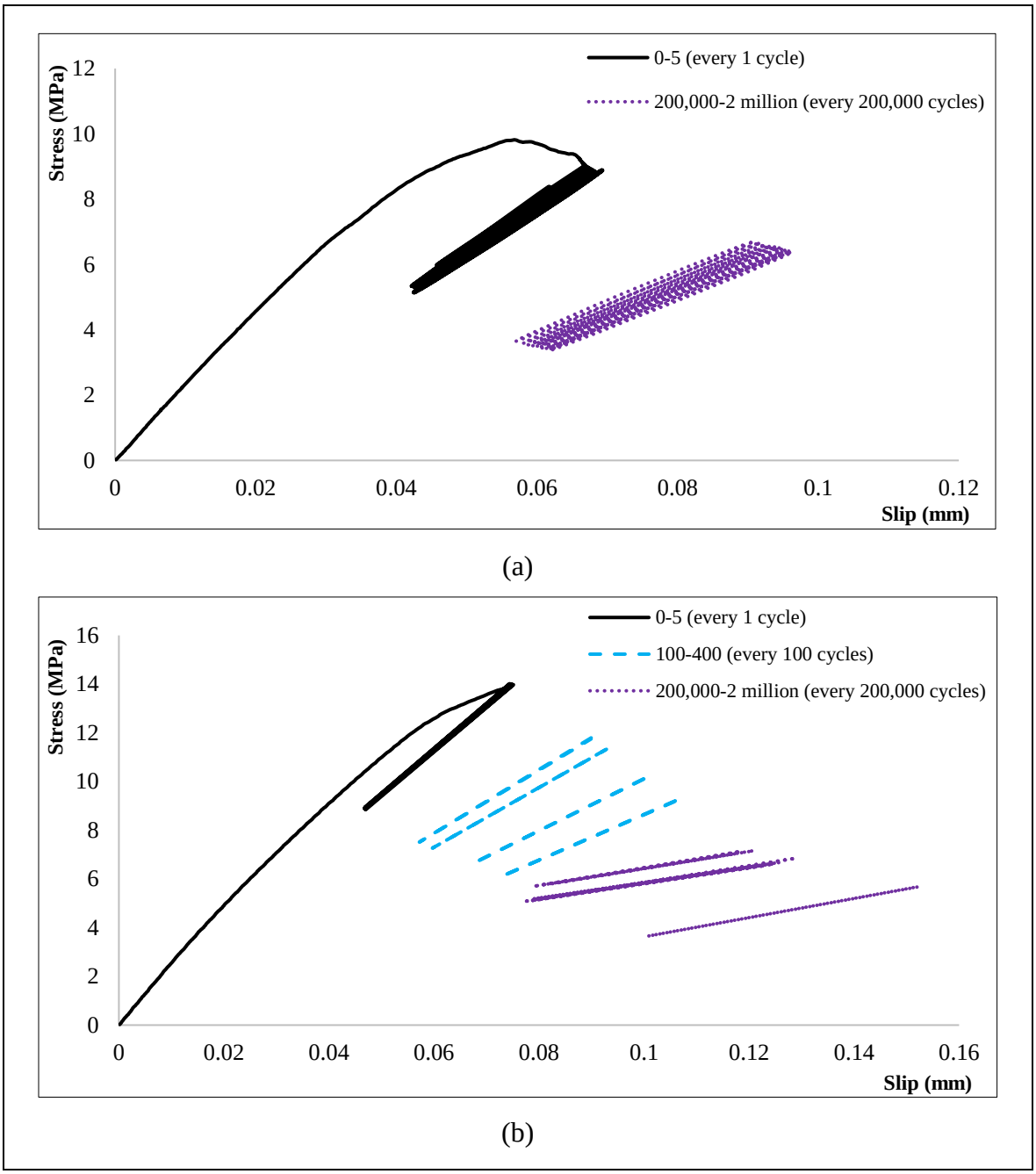

Figure 5.9 Local bond-slip curves of specimen bonded with sheet: a) Specimen CS-200-75; b) Specimen CS-200-112

5.5.4 Strain distribution during cyclic loading

Figure 5.10 (a), (b) and (c) shows the strain distribution along the bonded length at various load cycles in each test series (Specimens CL-200-25, CS-200-75 and CS-200-112). Based on the strain profile at cycle 1, the section at the loaded end possesses the highest strain compared to other bond sections, especially those near the free end. As the number of load cycles increases, the bonding damage progresses within the adhesive. Hence, higher strain is distributed over regions away from the loaded end and progressed towards the free end.

With reference to the strain distribution patterns of specimen CL-200-25 in Figure 5.10 (a), the strain profile tends to change from exponential curve during the first cycle (i.e., n = 1) to sigmoid curve with increasing load cycles (e.g., n = 10,329). This is an indication of the strain evolution from the loaded end towards the free end, and therefore affecting the strain gauges along the bond length. Also, it can be noted that at load cycles, especially near failure (e.g., n = 528,328), the interfacial crack propagation has affected a large portion of the bonded length, from the loaded end until 150 mm from the loaded end. In fact, the bond adhesive of intervals outside this region (i.e., from the free end until 50 mm from the free end) do not seem to contribute to transferring the interfacial stresses from the CFRP to concrete surface during load cycles, which has been already shown in the bond-slip curve related to this region, (i.e., Interval ε_0–ε_1) in Figure 5.8 (f).

The strain distribution of specimens bonded with sheet (in Figure 5.10 (b) and (c)) shows that the bonded regions away from the loaded end (after 50 mm from the loaded end) were not significantly affected by the load cycles in terms of strain evolution. This can be due to the applied cyclic loading amplitude that did not seem to trigger any considerable bond degradation in these specimens within the entire load cycles.

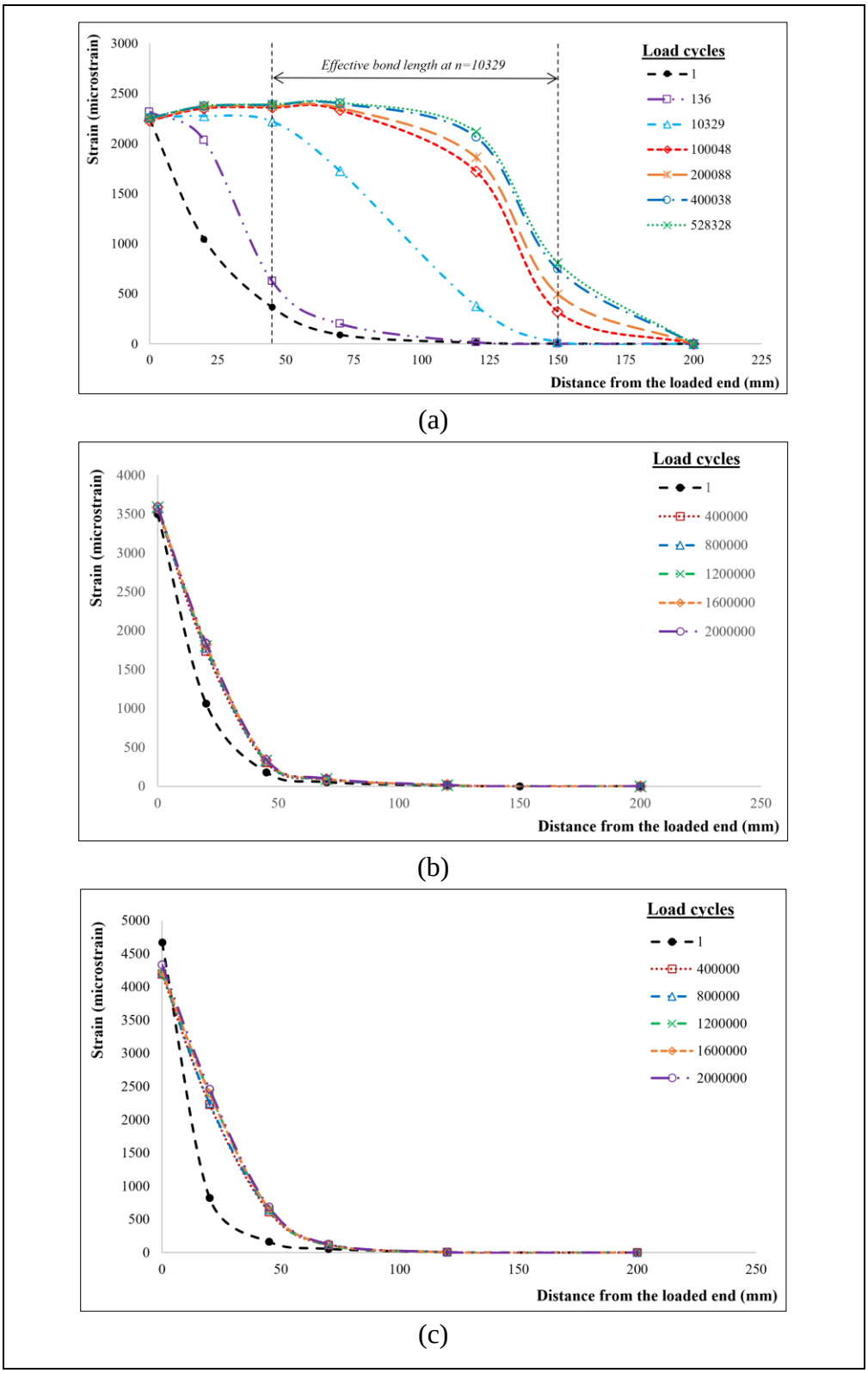

Figure 5.10 Strain distribution along the bonded length of specimens:
a) Specimen CL-200-25; b) Specimen CS-200-75; c) Specimen CS-200-112

5.5.4.1 Effective bond length

Experimental investigations on FRP-concrete bonded joints have all confirmed the existence of an effective bond length after which the bond load-carrying capacity does not increase (J. F. Chen & Teng, 2001; Maeda et al., 1997; Neubauer & Rostasy, 1999; Pellegrino et al., 2008; Z. Wu et al., 2009). With respect to fatigue loading conditions, increasing the bond length after the effective bond length does not change the interfacial fracture energy during load cycles (HM Diab et al., 2009; K. Li et al., 2015).

The effective bond length under fatigue loading is in fact the active stress-transfer zone along the bonded length that can be determined through the observation of strain distribution during load cycles (K. Li et al., 2015; Xie et al., 2019). The average effective bond length under fatigue loading can be taken as the average portion of bond length at which the strain profile curves (at different cycles) show an active transfer of interfacial stresses (K. Li et al., 2015). With regards to this concept, Figure 5.10 (a) shows that the average stress-transfer zone (i.e., effective bond length) of specimens with laminate is estimated to take place within a distance between 100 mm and 125 mm under cyclic loading.

The effective bond length under fatigue loading has been reported to be smaller than that under monotonic loading (Carloni et al., 2012; K. Li et al., 2015). This is attributed to the two following reasons: a) the fatigue debonding failure typically occurs at a lower load level in comparison with the monotonic loading condition. Hence, the interfacial stress distribution takes place within a smaller bond length; b) The interfacial damage is mainly imposed to the epoxy adhesive under fatigue loading, as opposed to the monotonic loading condition during which the concrete element undergoes interfacial crack propagation (Carloni & Subramaniam, 2013; Fathi et al., 2022; K. Li et al., 2015).

As for specimens with CFRP sheet, inspection of Figure 5.10 (b) and (c) reveals that the stress-transfer zone is not established during load cycles. This can also explain why no fatigue failure occurred for these specimens. Therefore, the post-fatigue results can be used to estimate the

effective bond length. According to the post-fatigue results in Table 5.3, the effective bond length appears to lie in a range between 50 mm and 100 mm. This is because the post-fatigue residual capacity ($P_{\mathrm{ult},2}$) in each category (Series 2 and Series 3) tends to stabilize after the bond length of 50 mm. It is noteworthy that the post-fatigue effective bond lengths of specimens with sheet appear to be in the same range as that inspected during the corresponding monotonic testing (Fathi et al., 2023-a). This has also been observed during the experimental investigation of Carloni et al. (2012).

5.5.5 Fatigue performance of CFRP type (laminate vs. sheet) with varying bond length

Figure 5.11 shows the results regarding the fatigue performance of specimens, in terms of fatigue life and post-fatigue residual capacity, with respect to their bond lengths. In specimens bonded with laminate with different bond lengths, it was found that the number of load cycles at failure tends to increase with increasing the bonded length. However, after comparing the two specimens of CL-100-25 and CL-200-25, it was noted that the increased bond length (in Specimen-200-25) did not contribute to enhancing the fatigue life of CFRP-to-concrete interface, despite the anticipated direct relationship between the bond length and bond fatigue life according to prior research studies (Bizindavyi et al., 2003; JG Dai et al., 2005; HM Diab et al., 2009; K. Li et al., 2015; K. Li et al., 2018; Mazzotti & Savoia, 2009; Z. Wu et al., 2010). This can be attributed to the different failure pattern of Specimen CL-200-25 (i.e., combined FRP-peeling and concrete cover separation) in comparison with the main failure mode of other specimens with laminate (i.e., FRP-peeling).

As for specimens with 75 mm-wide CFRP sheet (equivalent width to CFRP laminate), test results showed that using a minimum bond length of 50 mm provided the fatigue endurance of over 2 million load cycles. This can be due to the greater bonded area of these specimens compared to their counterparts (those with 25 mm-wide laminate), which resulted in a long-term shear resistance against fatigue debonding failure.

It has also been revealed that all specimens bonded with CFRP sheet (Series 2 and 3) failed at a post-fatigue ultimate load very similar to their monotonic load capacity. In fact, specimens with bond lengths greater than 50 mm (in both Series 2 and 3) showed even slightly higher post-fatigue residual loads, $P_{\mathrm{ult},2}$, than their monotonic ultimate loads, $P_{\mathrm{ult},1}$ (see Table 5.3). This phenomenon that was also observed in similar studies (Carloni et al., 2012; El-Saikaly & Chaallal, 2015-a, 2015-b; K. Li et al., 2015; K. Li et al., 2018) can be attributed to the molecular interaction between interfacial components during fatigue loading resulting in a sustained residual bond capacity of specimens when submitted to post-fatigue monotonic loading. Furthermore, it has been previously reported that the bond ultimate post-fatigue capacity is independent of the applied fatigue load, provided that the adopted bond length is greater than the effective bond length obtained during monotonic loading (Carloni et al., 2012; HM Diab et al., 2009; K. Li et al., 2015; Mazzotti & Savoia, 2009; Yun et al., 2008). Overall, the above discussion shows that the bonding performance of CFRP sheet joint was superior to that of CFRP laminate joint, with the equivalent width, in terms of bond fatigue life and shear strength.

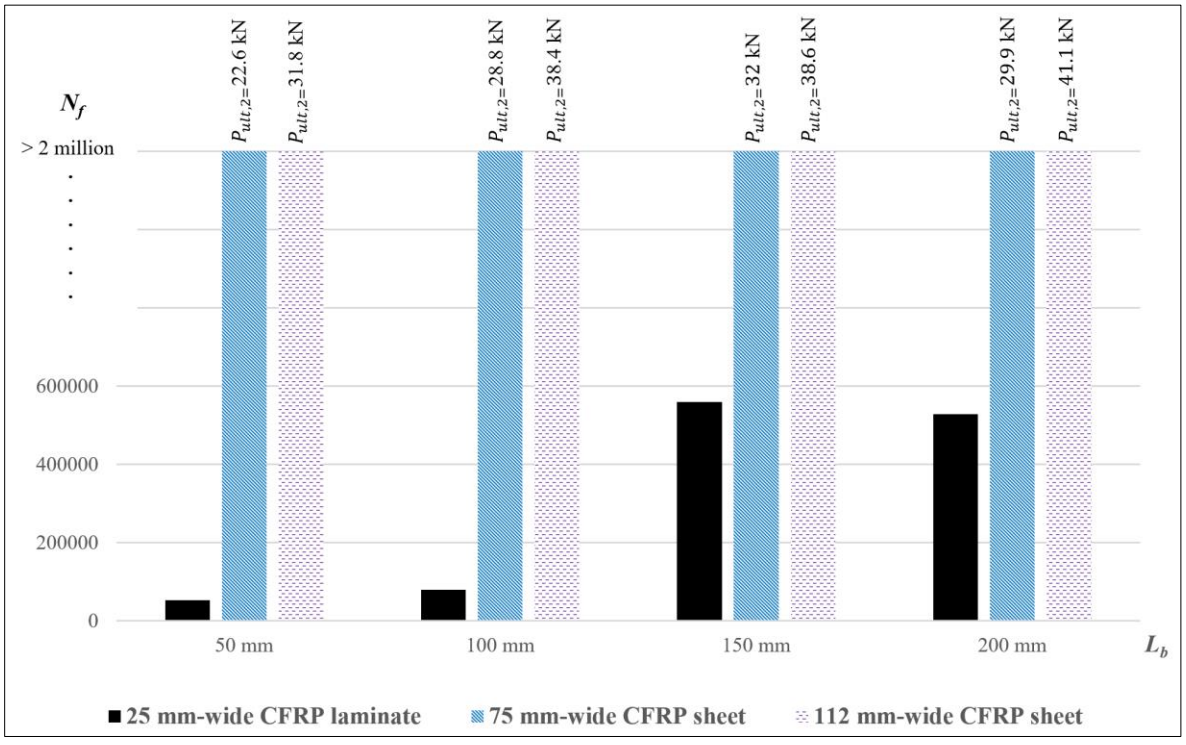

Figure 5.11 Fatigue life and post-fatigue residual capacity of specimens with respect to the bond length

5.5.6 Effect of CFRP-to-concrete width ratio

It has been reported that increasing the CFRP-to-concrete width ratio can result in a decrease in the fatigue life of the bond (K. Li et al., 2015; K. Li et al., 2018). However, the experimental study of Bizindavyi et al. (2003) revealed that using wider CFRPs can improve the long-term performance of bond under fatigue loading. As for the comparison of specimens with different CFRP widths tested in this experiment (Series 2 vs. Series 3), since no fatigue failure was observed within the maximum load cycles ($N_{\max}$ = 2 million), the effect of CFRP-to-concrete width ratio can be evaluated through the inspection of bond post-fatigue behavior. According to Figure 5.11, specimens with 112 mm-wide CFRP sheet overall reached higher post-fatigue load-carrying capacity compared to their counterparts with 75 mm-wide sheet (i.e., ones with the same bond length). Since the failure mode of all specimens occurred in the form of debonding, increasing the CFRP width provided a greater bonded area to resist interfacial stresses and hence improved the performance of CFRP-to-concrete interface under post-fatigue monotonic loading condition. As for the fatigue loading condition, considering that the epoxy adhesive element plays a major role at distributing the tensile stresses during load cycles, increasing the CFRP width is also expected to enhance the fatigue-life of CFRP-to-concrete bond, which is aligned with the experimental results of Bizindavyi et al. (2003). Nevertheless, more experimental data may be necessary to corroborate this conclusion.

5.5.7 Bond fatigue-life model

A review of research investigations on the fatigue behavior of concrete structures retrofitted with EB-CFRP bonding systems reveals that the fatigue life of the bond at CFRP-to-concrete interface tends to determine the fatigue life of such rehabilitated structures. This is due to the occurrence of debonding failure as the main failure mode in CFRP-to-concrete bonded joints under fatigue loading (Fathi et al., 2022). The existing S-N relationships of the bond in the literature are typically represented in terms of the maximum applied load and the logarithm of number of load cycles until failure (Bizindavyi et al., 2003; Chalot et al., 2019; E Ferrier et al., 2005; Xie et al., 2019; W. Zhang, 2018). Indeed, it has been observed that an inverse

relationship exists between the fatigue loading range ($P_{\max} - P_{\min}$) and bond fatigue life, N_f. Beyond the fatigue loading amplitude, limited research has been undertaken to include other influencing parameters including concrete strength and CFRP-to-concrete width ratio into the bond S-N equations (K. Li et al., 2015; Zhu et al., 2016). A database of related research studies is presented in Table 5.4, which is used to propose a modified bond fatigue-life model. Indeed, the selected specimens (all with CFRP composites) showed debonding failure at the FRP-to-concrete interface. It is also noteworthy that the bond length of all specimens in the literature database were set to be greater than their effective bond length. That is why the current experimental results of specimens with bond lengths assumed to be lower than the effective bond length (e.g., CL-50-25) have been excluded from the data analyses.

On the basis of the bond S-N relationship proposed by K. Li et al. (2015), the modified fatigue-life model for the CFRP-to-concrete bond is expressed as follows:

$$S/(1 - S_a) = 1.916 - 0.0908\left\{\frac{\ln N_b}{[0.0021 f_{\mathrm{cu}} + 0.872]\left[1.094 - 0.309\,(b_f/b_c)\right]}\right\} \quad \text{if} \quad S/(1 - S_a) > a \tag{5.3}$$

$$N_b > 2 \text{ million} \quad \text{if} \quad S/(1 - S_a) \le a \tag{5.4}$$

$$a = 1.916 - \left\{\frac{1.916 - (0.3/0.5)}{[0.0021 f_{\mathrm{cu}} + 0.872]\left[1.094 - 0.309(b_f/b_c)\right]}\right\} \tag{5.5}$$

$$S = \frac{P_{\max} - P_{\min}}{P_{\mathrm{ult}}} \quad , \quad S_a = \frac{P_{\max} + P_{\min}}{2P_{\mathrm{ult}}} \tag{5.6}$$

As can be noted in the equations, the endurance limit of CFRP-to-concrete bond corresponding to 2 million load cycles (a) can be calculated using Eq. (5.5). Moreover, the modified model takes into account both the concrete compressive strength, f_{cu}, and CFRP-to-concrete width ratio, b_f/b_c, in addition to the effect of applied fatigue loading (appeared as S and S_a).

Table 5.4 Database of specimens used for the modified bond fatigue-life model

Research	No.	Specimen	f_{cu}	b_f/b_c	S	S_a	Failure mode	N_f	Ln(N_f)	Ln(N_b) Modified model	Ln(N_b) Zhu et al. (2016) model
K. Li et al. (2015)	1	I-F-1	62.2	0.33	0.65	0.48	C-S	2600	7.9	7.4	6.9
	2	I-F-2	62.2	0.33	0.55	0.43	C-S	32000	10.4	10.5	10.1
	3	I-F-3	62.2	0.33	0.5	0.4	F-P	168900	12	11.9	11.7
	4	I-F-4	62.2	0.33	0.4	0.35	F-P	1550000	14.3	14.2	14.9
	5	I-F-5	62.2	0.33	0.39	0.35	F-P	2380000	14.7	-	15.2
	6	I-F-6	62.2	0.33	0.3	0.3	C-S*	> 2 million	-	-	18
	7	II-F-1	35.3	0.33	0.5	0.4	F-P	88300	11.4	11.2	11
	8	II-F-2	25.1	0.33	0.5	0.4	F-P	67000	11.1	10.9	10.8
	9	III-F-1	62.2	0.47	0.55	0.43	C-S	20680	9.9	10.1	10.1
	10	III-F-2	62.2	0.67	0.55	0.43	C-S	11830	9.4	9.4	10.1
	11	IV-F-1	62.2	0.33	0.55	0.43	C-S	7300	8.9	10.5	10.1
	12	IV-F-2	62.2	0.33	0.55	0.43	C-S	90000	11.4	10.5	10.1
Zhu et al. (2016)	13	A-1	62.2	0.25	0.65	0.48	C-S	2615	7.9	7.6	6.9
	14	A-2	62.2	0.25	0.55	0.43	F-P/C-S	31984	10.4	10.8	10.1
	15	A-3	62.2	0.25	0.5	0.4	F-P/C-S	168900	12	12.2	11.7
	16	A-4	62.2	0.25	0.45	0.38	F-P/C-S	1550364	14.3	13.4	13.3
	17	B-1	25.1	0.25	0.5	0.4	C-S	67000	11.1	11.2	10.8
	18	B-2	35.3	0.25	0.5	0.4	C-S	88300	11.4	11.5	11
Chalot et al. (2019)	19	A-F1-1	40	0.36	0.76	0.44	C-A	387	6	5.8	3.3
	20	A-F1-2	40	0.36	0.76	0.44	C-A	56	4	5.8	3.3
	21	A-F1-3	40	0.36	0.76	0.44	C-A	24	3.2	5.8	3.3
	22	A-F1-4	40	0.36	0.77	0.54	C-A	80	4.4	2.3	3
	23	A-F1-5	40	0.36	0.85	0.49	C-A	6	1.8	2.4	0.6
	24	A-F2-1	40	0.36	0.59	0.44	C-A	16458	9.7	9	8.4
	25	A-F2-2	40	0.36	0.59	0.44	C-A	534	6.3	9	8.4
	26	A-F2-3	40	0.36	0.69	0.42	C-A	120	4.8	7.6	5.4
	27	A-F2-4	40	0.36	0.69	0.42	C-A	251	5.5	7.6	5.4
	28	A-F2-5	40	0.36	0.68	0.5	C-A	159	5.1	5.8	5.7
	29	A-F3-1	40	0.36	0.43	0.43	C-A	99491	11.5	12	13.3
	30	A-F3-2	40	0.36	0.49	0.51	C-A	3609	8.2	9.6	11.4
	31	A-F3-3	40	0.36	0.49	0.51	C-A	14018	9.5	9.6	11.4
	32	A-F3-4	40	0.36	0.49	0.51	C-A	1699	7.4	9.6	11.4
	33	A-F3-5	40	0.36	0.48	0.5	C-A	5075	8.5	9.9	11.8
	34	B-F1-1	38	0.36	0.89	0.5	C-A	62	4.1	1.5	-0.7
	35	B-F1-2	38	0.36	0.86	0.5	C-A	24	3.2	2	0.3
	36	B-F1-3	38	0.36	0.72	0.53	C-A	3	1.1	4	4.5

Table 5.4 Database of specimens used for the modified bond fatigue-life model (Continue)

Research	No.	Specimen	f_{cu}	b_f/b_c	S	S_a	Failure mode	N_f	Ln(N_f)	Ln(N_b) Modified model	Ln(N_b) Zhu et al. (2016) model
Chalot et al. (2019)	37	B-F1-4	39	0.36	0.79	0.45	C-A	1574	7.4	5	2.4
	38	B-F1-5	39	0.36	0.78	0.46	C-A	451	6.1	4.9	2.7
	39	B-F2-1	38	0.36	0.75	0.47	C-A	40	3.7	5.3	3.6
	40	B-F2-2	38	0.36	0.67	0.51	C-A	21	3	5.8	6
	41	B-F2-3	38	0.36	0.68	0.45	C-A	291	5.7	7	5.7
	42	B-F2-4	42	0.36	0.57	0.46	C-A	7053	8.9	9	9.1
	43	B-F2-5	39	0.36	0.59	0.46	C-A	554	6.3	8.6	8.4
	44	B-F3-1	39	0.36	0.58	0.4	C-A	9353	9.1	9.8	8.7
	45	B-F3-2	42	0.36	0.53	0.42	C-A	6941	8.8	10.3	10.3
	46	B-F3-3	39	0.36	0.5	0.45	C-A	7761	9	10.4	11.1
	47	B-F3-4	42	0.36	0.44	0.43	C-A	52877	10.9	11.9	13
Zhou et al. (2021)	48	SC60-1	64.1	0.25	0.5	0.4	F-I	455800	13	12.2	11.7
	49	SC60-2	64.1	0.25	0.55	0.43	F-I/C-S	120050	11.7	10.8	10.1
	50	SC60-3	64.1	0.25	0.65	0.48	F-I	41250	10.6	7.6	7
	51	MC60-1	64.1	0.25	0.58	0.44	A-F	65200	11.1	9.9	9.2
	52	MC60-2	64.1	0.25	0.64	0.44	C-S	2160	7.7	8.7	7.3
	53	MC60-3	64.1	0.25	0.56	0.4	C-S	46000	10.7	11	9.8
	54	SC50-1	50	0.25	0.5	0.4	F-I	479850	13.1	11.8	11.4
	55	SC50-2	50	0.25	0.64	0.47	F-I/C-S	57300	11	7.8	7.1
	56	SC50-3	50	0.25	0.61	0.43	F-I	9990	9.2	9.3	8
	57	MC50-1	50	0.25	0.6	0.43	C-S	11850	9.4	9.4	8.3
	58	MC50-2	50	0.25	0.52	0.37	A-F	103850	11.6	12	10.8
	59	MC50-3	50	0.25	0.56	0.39	C-S/A-F	60000	11	10.8	9.5
	60	MC50-4	50	0.25	0.63	0.43	C-S	5500	8.6	8.8	7.4
Current experiment	61	CL-150-25	51.2	0.17	0.3	0.5	F-P	559470	13.2	14.8	17.6
	62	CL-200-25	51.2	0.17	0.3	0.5	F-P/C-S	528379	13.2	14.8	17.6
	63	CS-100-75	52.2	0.5	0.3	0.5	C-S*	> 2 million	-	-	17.7
	64	CS-150-75	52.2	0.5	0.3	0.5	C-S*	> 2 million	-	-	17.7
	65	CS-200-75	52.2	0.5	0.3	0.5	C-S*	> 2 million	-	-	17.7
	66	CS-100-112	60.3	0.75	0.3	0.5	C-S*	> 2 million	-	-	18
	67	CS-150-112	60.3	0.75	0.3	0.5	C-S*	> 2 million	-	-	18
	68	CS-200-112	60.3	0.75	0.3	0.5	C-S*	> 2 million	-	-	18

Note: The study by Zhou et al. (2021) included varying maximum and minimum loading levels in some cases, hence mean values of P_{max} and P_{min} were used for the calculation of S and S_a.

*Post-fatigue failure mode (under monotonic loading).

C-S= Concrete cover separation, F-P= FRP peel-off from concrete, C-A= Concrete-to-adhesive interface failure, F-I= FRP interlaminar failure, A-F= Adhesive cohesion failure.

To assess the accuracy of the modified bond fatigue-life model, Figure 5.12 and Figure 5.13 illustrate the logarithms of predicted fatigue life, Ln(N_b), derived from Eq. (5.3)-(5.6) and the model by Zhu et al. (2016) versus the corresponding test data, Ln(N_f). Note that the test data of specimens with $N_f \leq 2$ million cycles were considered for the comparison. It can be found that the modified model can lead to results with an overall correlation coefficient of 81 % ($R^2 = 0.81$) against actual test results, whereas the model by Zhu et al. (2016) appears to have a lower correlation coefficient ($R^2 = 0.60$). Furthermore, the S-N model by Zhu et al. (2016) does not include the variable of FRP-to-concrete width ratio and only employs the two parameters of concrete strength and loading amplitude for the prediction of bond fatigue life. It is noteworthy that the inclusion of test results of specimens with $N_f > 2$ million cycles can enhance the correlation rate of the modified fatigue-life model up to 85 %. Nevertheless, further research may be needed to assess the accuracy of the model regarding specimens with N_f higher than 2 million cycles.

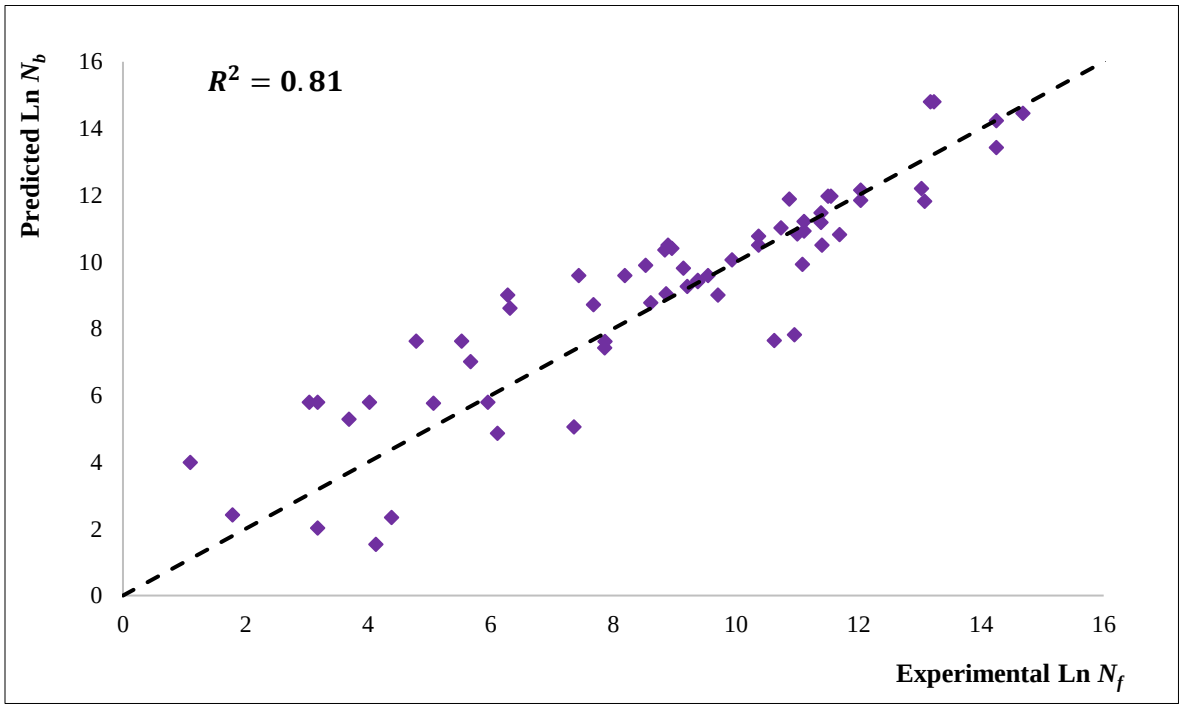

Figure 5.12 Predicted fatigue life of specimens by the modified model versus experimental data

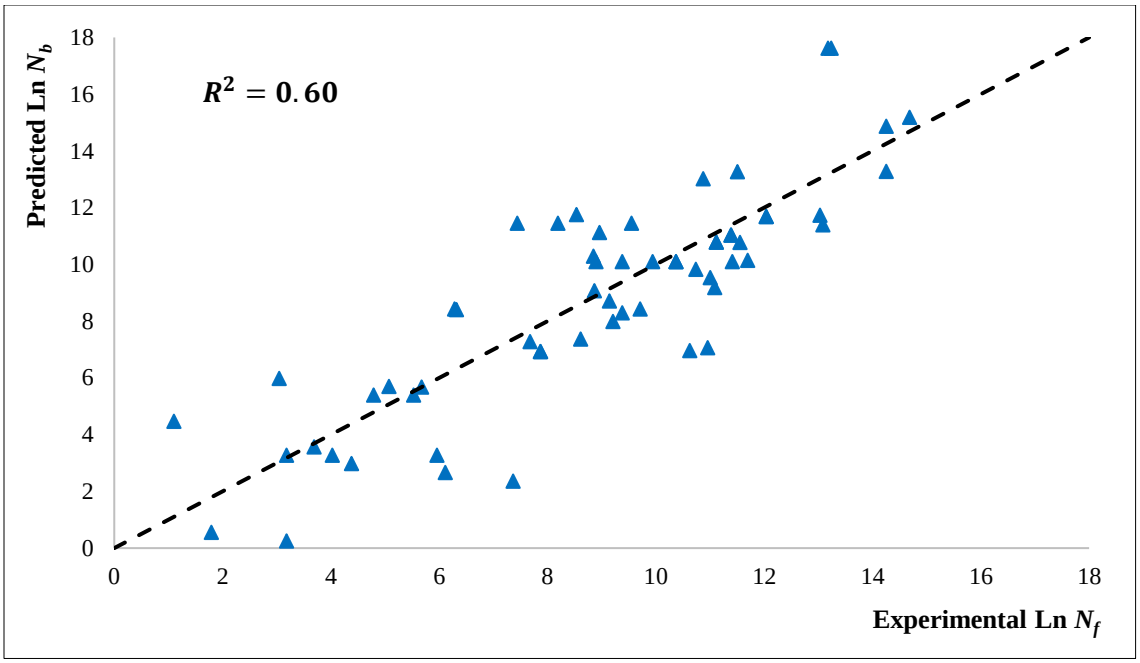

Figure 5.13 Predicted fatigue life of specimens by Zhu et al. (2016) model versus experimental data

5.6 Conclusions

An experimental study was carried out to evaluate the fatigue behavior of CFRP-to-concrete interface. Series of double-lap pullout tests were performed to investigate the effects of CFRP composite type, bond length and CFRP width on the bond behavior under cyclic loading. The conclusions of this study can be summarized as follows:

- The main failure mode of specimens with CFRP laminate under fatigue loading occurred in the form of interfacial debonding within the adhesive, namely, CFRP peel-off from concrete. This indicates that the fatigue behavior of CFRP-to-concrete interface is greatly influenced by the performance of epoxy adhesive, whereas in monotonic loading conditions, the weakest element of interface is the concrete substrate. Indeed, the failure mode of specimens with CFRP sheet during post-fatigue monotonic loading was primarily due to concrete cover separation.

- With respect to the fatigue performance of CFRP composite systems, CFRP-bonded joints with sheet outperformed those with laminate in terms of fatigue life and bond shear resistance.

Thus, all specimens bonded with CFRP sheet endured the maximum number of load cycles, (i.e., N_{max}= 2 million), unlike those with CFRP laminate that failed during the fatigue loading. This can be attributed to the greater width of CFRP sheet versus equivalent CFRP laminate, which created a larger bonded area to resist interfacial debonding.

- The fatigue degradation of CFRP-to-concrete interface can be represented by the gradual increase in the bond slip as well as the decrease in the bond shear stress. In fact, increasing the number of load cycles results in a progressive interfacial cracking along the bond length. This continues until the epoxy in the residual bonded region does not suffice to endure fatigue interfacial stresses, and therefore triggers the sudden debonding failure of CFRP-to-concrete interface.

- Increasing the CFRP-to-concrete width ratio improves the bond behavior in terms of post-fatigue residual capacity. With the debonding failure being the main failure mode, using a wider CFRP sheet can provide a larger bonded area to resist applied loading, and therefore improves the bond behavior under post-fatigue monotonic loading. Also, the residual load-carrying capacity of CFRP-to-concrete bonded joints under post-fatigue monotonic loading is independent of applied cyclic loads, provided that the bonded length is greater than the effective bond length (defined under monotonic loading). It may be anticipated that increasing the CFRP composite width would enhance the fatigue life of interface under fatigue loading conditions. However, the existence of experimental results in the literature regarding the inverse effect of CFRP-to-concrete width ratio on the bond fatigue life may require further investigation in this area.

- A modified bond fatigue-life model, based on (K. Li et al., 2015), is proposed that correlated well with the current test results as well as the experimental database gathered from the literature. The bond S-N model successfully takes into consideration the effect of applied fatigue loading, concrete compressive strength and CFRP-to-concrete width ratio and is also able to determine the endurance limit of CFRP-to-concrete bonded joints resisting 2 million load cycles.

5.7 Data availability statement

Some or all data, models, or code that support the findings of this study are available from the corresponding author upon reasonable request including experimental results of concrete cylinder tests and pull-out tests.

5.8 Acknowledgments

Financial support of the Natural Sciences and Engineering Research Council of Canada (NSERC) and the Fonds de Recherche du Québec – Nature et Technologie (FRQNT) through operating grants is gratefully acknowledged. The authors thank Sika-Canada, Inc. (Pointe-Claire, QC) for contributing to the cost of materials. The efficient collaboration of J. Auger and J. Lescelleur (senior technicians) at École de technologie supérieure in conducting the tests is also acknowledged.

CONCLUSIONS

The current research project can be categorized into two phases as follows:

Phase 1. This phase focuses on the use of EB-FRP shear strengthening techniques on RC structures under fatigue loading. Indeed, a wide range of research findings regarding the application of FRP composites on concrete surfaces and in particular the fatigue behavior of FRP-to-concrete bond are discussed. Furthermore, the influencing parameters on the fatigue performance of FRP-to-concrete interface in such rehabilitated structures are examined through a literature-review investigation. The conclusions derived from phase 1 of this research can be summarized as follows:

1- The fatigue performance of RC beams can be enhanced by using EB-FRP shear strengthening systems in terms of fatigue life and ductility. Indeed, FRP materials contribute to the shear resistance of RC beams by reducing stresses from internal steel reinforcement and confining the crack widths under fatigue loading conditions.

2- Carbon FRP (CFRPs) composites exhibit better material properties in terms of stiffness and ultimate tensile capacity compared to other FRP types (e.g., glass and aramid), In addition, the superior fatigue resistance of CFRPs has made them a great retrofitting tool for RC structures under cyclic loading.

3- The long-term performance of EB-CFRP shear-strengthened RC beams relies greatly on the bond behavior at CFRP-to-concrete interface especially under fatigue loading conditions.

4- The existence of transverse steel reinforcement reduces the shear contribution of CFRP reinforcement in RC beams under cyclic loading. This is attributed to the stress redistribution phenomenon that exists between the steel stirrups and FRP.

5- Application of L-shaped CFRP plates with anchorage has proven to be an effective technique of shear strengthening RC beams under fatigue loading since they prevent debonding of CFRP/concrete interface and change the failure mode of the structure from brittle to ductile.

6- The fatigue behavior of bond at the FRP-to-concrete interface can be influenced by several variables including concrete strength, fatigue load amplitude, FRP-to-concrete width ratio, bond length, FRP and adhesive properties, environmental conditions and anchorage techniques.

7- Increasing the FRP bonded length leads to an increase in the bond load-carrying capacity under monotonic loading. However, adopting a bond length greater than the effective bond length does not translate into a significant change in the bond monotonic shear resistance.

8- A typical bond-slip curve of FRP-to-concrete interface is comprised of two branches: an initial ascending branch followed by a descending branch. As for the cyclic bond-slip behavior, the slope of the ascending segment tends to decrease with an increase in the number of load cycles.

9- The failure mode of FRP-to-concrete bonded joints under fatigue loading is dependent on the fatigue load level. Indeed, as the maximum cyclic load level increases, the failure of FRP-to-concrete interface tends change from FRP peeling mode to concrete cover separation mode.

10- As far as the numerical simulation of FRP-to-concrete interface goes, adopting a perfect bond modelling between the concrete and FRP leads to an overestimation in the prediction of shear resistance. Thus, using interfacial elements for modeling the FRP-to-concrete interface as well as modelling the bond stiffness degradation during cyclic loading results in an enhancement in the accuracy of structural responses with respect to the experimental data.

11- There needs to exist a rationale for choosing the experimental load amplitudes in low cycle fatigue conditions in order to relate them to the regular fatigue loads that are applied to the bridges in real-world situations.

12- The fatigue bond deterioration of FRP-to-concrete appears to take place in three phases: a rapid stiffness degradation during the initial load cycles followed by a gradual steady growth of debonding along the interface after which a fast sudden increase of bond slip occurs until the total failure of interface.

Phase 2. This phase further investigates the bond behavior of CFRP-to-concrete interface through an experimental program. A total of 24 CFRP-to-concrete bonded joints were prepared and the experimental tests were performed under both monotonic and fatigue loading conditions. The evaluated affecting parameters include CFRP composite type, bond length and CFRP-to-concrete width ratio. Furthermore, analytical studies were carried out for the purposes of developing a bond-slip model under monotonic loading and a bond S-N model under cyclic loading. The following conclusions (categorized into monotonic and cyclic load testing) can be drawn regarding the experimental research study:

Monotonic load testing:

1- The major failure mode of CFRP-to-concrete joint occurred in the form of concrete cover separation. This was attributed to the concrete substrate being the weakest element of FRP-adhesive-concrete interface and thereby undergoing the cracking propagation during the application of monotonic load.

2- Upon adopting the effective bond length, the ultimate load-carrying capacity of the CFRP-to-concrete joint was reached. Indeed, any increase of bonded length after the effective bond length did not translate into higher bond strength but only increased the ductility of the specimen (through greater bond slip).

3- Increasing the CFRP stiffness resulted in an increase of effective bond length. In fact, using CFRP composites with higher stiffness (i.e., $n_f E_f t_f$) contributed to the interfacial stress transfer (from CFRP to concrete) over a greater bonded length prior to the debonding failure. This is also in line with the exiting models that offer a direct relationship between the FRP stiffness and effective bond length.

4- The load-carrying capacity CFRP-to-concrete bonded joints depended greatly on the bonded area. In fact, increasing the bonded area contributed to higher bond strength. This holds true in cases where the debonding failure is the dominant failure mode. Hence, using wider CFRP composites can improve the bond performance by providing a greater bonded area to resist interfacial shear stresses.

5- The effective bond length seems to be affected by the CFRP-to-concrete width ratio. According to the experimental observations, increasing the CFRP width tends to reduce effective bond length. However, more experimental data may be required to corroborate this observation.

6- A bilinear bond-slip model can be used to characterise the bond behavior in a simple manner by estimating the maximum bond stress, corresponding bond slip and ultimate bond slip. Through an analytical study based on a database derived from the literature, a bilinear bond-slip model was proposed and was shown to perform relatively better at predicting the bond-slip behavior under monotonic loading against available bond-slip models.

Cyclic load testing:

1- The dominant failure mode of CFRP-to-concrete bonded joints with laminate under cyclic loading was due to the CFRP peel-off from concrete. Since the fatigue-failure mode of FRP-to-concrete bonded joint is dependent on the cyclic load level, setting the upper load limit of specimens at 65% P_{ult} triggered the fatigue crack propagation to mainly occur within the FRP-to-adhesive interface until the total debonding failure. Nevertheless, the main failure mode of

specimens with CFRP sheet under post-fatigue monotonic loading was concrete cover separation, which is the most observed failure mode of FRP-to-concrete bonded joints under monotonic load conditions.

2- The fatigue degradation of CFRP-to-concrete interface occurred in three phases which include: Phase I) rapid increase of bond stiffness degradation during the initial load cycles; Phase II) gradual development of interfacial cracking along the bond length; and Phase III) abrupt increase of interfacial debonding until the failure of CFRP-to-concrete interface.

3- The CFRP bonded joints with sheet exhibited a better fatigue performance in comparison with those with CFRP laminate in terms of fatigue life. This can be attributed to the greater CFRP-to-concrete width ratio of specimens with CFRP sheet which provided a larger bonded area to transfer the cyclic interfacial shear stresses from CFRP to concrete, and therefore extended the bond fatigue life.

4- The effective bond length under fatigue loading was estimated to be smaller than that under monotonic loading. This was because of the lower applied fatigue-load level compared to monotonic loading which translated into a smaller bond shear-transfer zone under cyclic loading. Furthermore, the progressive fatigue damage is imposed to the epoxy element during cyclic loading whereas the crack propagation in monotonic loading condition occurs within the concrete substrate.

5- Increasing the CFRP-to-concrete width ratio appeared to improve the bond behavior in terms of post-fatigue residual capacity. This can be owed to the larger bonded area of CFRP sheets with greater widths which resulted in a better performance of the bond at resisting the shear stresses during the post-fatigue monotonic loading until debonding failure. Similarly, it may be expected that using wider FRPs can prolong the fatigue life of FRP-to-concrete interface. However, further research can be conducted in this regard.

6- The post-fatigue residual capacity of CFRP-to-concrete bonded joints is not affected by the applied fatigue load, provided that the bond length is greater than the effective bond length. That, in fact, explains the similar residual ultimate loads attained by the specimens with CFRP sheet during post-fatigue monotonic loading with their ultimate monotonic load-carrying capacity.

7- A modified fatigue-life prediction model of CFRP-to-concrete bond was proposed during an analytical study. The proposed S-N model not only included the influencing parameters of concrete strength, CFRP-to-concrete width ratio and fatigue loading level, but it was also validated against a considerable size of database from literature. It was shown that the bond fatigue-life predictions from the model agreed well with the experimental results.

RECOMMENDATIONS

Further investigation on the bond fatigue behavior of FRP-to-concrete can be conducted encompassing the following research important aspects:

1- The impact of FRP-to-concrete width ratio on the effective bond length may need to be further studied. Limited data suggest an inverse relationship between the two variables. Therefore, an experimental investigation may be conducted to formulate a reliable relationship between the effect bond length and FRP-to-concrete width ratio validated with adequate data.

2- Further research may be conducted to examine the proportional effect of bond length on the fatigue life of FRP-to-concrete interface and new S-N relationships of the bond can be developed with the inclusion of this parameter.

3- Further analytical research may be conducted to develop a reliable bond-slip model under cyclic loading with the validation against sufficient sample data derived from literature. The contribution of affecting parameters of concrete strength, FRP-to-concrete width ratio and applied cyclic loading on the fatigue bond-slip behavior can be evaluated through a numerical study and the effect of these variable can be taken into account for the formulation of a bilinear bond-stress slip relationship, validated with sufficient data, under cyclic loading.

4- Reliable effective bond length relationships may be developed under fatigue loading condition through an experimental study. Since the fatigue effective bond length is smaller than that under monotonic loading, further research may be aimed at establishing a relationship between the effective bond length and the influencing parameters under cyclic loading.

5- The fatigue bond degradation of FRP-to-concrete interface can be further studied. Indeed, the loss of bond stiffness during fatigue load cycles may be formulated through an experimental investigation during which the effect of affecting variables can also be evaluated.

6- A numerical investigation may be conducted to identify design parameters affecting the bond fatigue behavior of EB-FRP shear-strengthened RC bridge girders under cyclic loads. To this end, the effect of steel-stirrup reinforcement, FRP configuration and size effect on the fatigue behavior of an EB-FRP shear-strengthened RC beam can be evaluated during a finite element (FE) study.

7- Further research may be conducted to establish an S-N relationship of FRP-to-concrete bond in RC bridge girders strengthened in shear with EB FRP to predict the fatigue service life such structures.

8- The fatigue performance of different types of FRP composites other than carbon fibers (e.g., GFRP and AFRP) in retrofitting the RC beams in shear could be experimentally investigated and comparisons can be made for the purpose of discovering the most efficient FRP strengthening system under fatigue loading.

9- The effect of environmental degradation on the bond behavior of RC structures with EB-FRP strengthening tools may be evaluated. Furthermore, reliable models can be developed to characterize the bond fatigue stiffness degradation in such structures with exposure to environmental conditions.

10- Further investigation may be conducted regarding the fatigue performance of anchorage systems for EB-FRP shear-strengthened RC beams and determine their effectiveness in preventing the debonding failure both experimentally and numerically.

LIST OF BIBLIOGRAPHICAL REFERENCES

AASHTO. (2017). *AASHTO LRFD bridge design specifications, 8th edition, with 2015 and 2016 interim revisions.* Washington, DC.

Abdalla, J. A., Mirghani, A., & Hawileh, R. A. (2020). Bond stress and behavior of interface between untreated aluminum alloy surface and concrete. *Procedia Structural Integrity*, *28*, 1295-1302.

ACI 215R. (1974). *Considerations for design of concrete structures subjected to fatigue loading* (Vol. 71): American Concrete Institute, Farmington Hills, Michigan.

ACI 440.2R. (2017). *Guide for the design and construction of externally bonded FRP systems for strengthening concrete structures*. Farmington Hills, Michigan: American Concrete Institute.

ACI. (2018). *Report on the modeling techniques used in finite element simulations of concrete structures strengthened using fiber-reinforced polymer materials*. Farmington Hills, Michigan: American Concrete Institute.

ACI. (2019). *Building code requirements for structural concrete (ACI 318-19): an ACI standard; Commentary on building code requirements for structural concrete (ACI 318-19)*. Farmington Hills, Michigan: American Concrete Institute.

Aidoo, J., Harries, K. A., & Petrou, M. F. (2004). Fatigue behavior of carbon fiber reinforced polymer-strengthened reinforced concrete bridge girders. *Journal of Composites for Construction, 8*(6), 501-509.

Al-Qaralleh, M., & Toutanji, H. (2018). Analytical Life-Prediction Model for RC Beams Strengthened with Externally Bonded FRP Laminates under Flexural Fatigue Loading. *Journal of Composites for Construction*, *22*(6), 06018002.

Al-Rousan, R., & Issa, M. (2011). Fatigue performance of reinforced concrete beams strengthened with CFRP sheets. *Construction and Building Materials, 25*(8), 3520-3529.

Al-Saawani, M. A., Al-Negheimish, A. I., El-Sayed, A. K., & Alhozaimy, A. M. (2022). Finite Element Modeling of Debonding Failures in FRP-Strengthened Concrete Beams Using Cohesive Zone Model. *Polymers, 14*(9), 1889.

Al-Saoudi, A., Al-Mahaidi, R., Kalfat, R., & Cervenka, J. (2019). Finite element investigation of the fatigue performance of FRP laminates bonded to concrete. *Composite Structures, 208*, 322-337.

ASTM. (2008). *Standard test method for tensile properties of polymer matrix composite materials*: ASTM International.

ASTM. (2021). *Standard test method for compressive strength of cylindrical concrete specimens*: ASTM International.

Azim, M. R., & Gül, M. (2019). Damage detection of steel girder railway bridges utilizing operational vibration response. *Structural Control and Health Monitoring, 26*(11), e2447.

Bae, S.-W., Murphy, M., Mirmiran, A., & Belarbi, A. (2013). Behavior of RC T-beams strengthened in shear with CFRP under cyclic loading. *Journal of Bridge Engineering, 18*(2), 99-109.

Banjara, N. K., & Ramanjaneyulu, K. (2019). Investigations on behaviour of flexural deficient and CFRP strengthened reinforced concrete beams under static and fatigue loading. *Construction and Building Materials, 201*, 746-762.

Barnes, R. A., & Mays, G. C. (1999). Fatigue performance of concrete beams strengthened with CFRP plates. *Journal of Composites for Construction, 3*(2), 63-72.

Belarbi, A., & Acun, B. (2013). FRP systems in shear strengthening of reinforced concrete structures. *Procedia Engineering, 57*, 2-8.

Ben Ouezdou, M., Belarbi, A., & Bae, S.-W. (2009). Effective bond length of FRP sheets externally bonded to concrete. *International Journal of Concrete Structures and Materials, 3*(2), 127-131.

Bizindavyi, L., Neale, K., & Erki, M. (2003). Experimental investigation of bonded fiber reinforced polymer-concrete joints under cyclic loading. *Journal of Composites for Construction, 7*(2), 127-134.

Bomix. Bomix® Concrete Mix. Retrieved from https://www.bomix.ca/wp-content/uploads/2022/04/beton_en.pdf. Available from The QUIKRETE Companies Bomix Concrete Mix.

Brena, S. F., Benouaich, M. A., Kreger, M. E., & Wood, S. L. (2005). Fatigue tests of reinforced concrete beams strengthened using carbon fiber-reinforced polymer composites. *ACI structural journal, 102*(2), 305.

Brosens, K., & Van Gemert, D. (1999). Anchorage design for externally bonded carbon fiber reinforced polymer laminates. *Special Publication, 188*, 635-646.

Carloni, C., & Subramaniam, K. V. (2013). Investigation of sub-critical fatigue crack growth in FRP/concrete cohesive interface using digital image analysis. *Composites Part B: Engineering, 51*, 35-43.

Carloni, C., Subramaniam, K. V., Savoia, M., & Mazzotti, C. (2012). Experimental determination of FRP–concrete cohesive interface properties under fatigue loading. *Composite Structures, 94*(4), 1288-1296.

Carolin, A. (2003). *Carbon fibre reinforced polymers for strengthening of structural elements.* (Doctoral thesis). Lulea University of Technology,

CEB-FIP. (1993). *CEB bulletin*. Comité Euro-international du Béton: Telford.

Chaallal, O., Boussaha, F., & Bousselham, A. (2010). Fatigue performance of RC beams strengthened in shear with CFRP fabrics. *Journal of Composites for Construction, 14*(4), 415-423.

Chalot, A., Michel, L., & Ferrier, E. (2019). Experimental study of external bonded CFRP-concrete interface under low cycle fatigue loading. *Composites Part B: Engineering, 177*, 107255.

Chaves, F. J., Da Silva, L., De Moura, M., Dillard, D., & Esteves, V. (2014). Fracture mechanics tests in adhesively bonded joints: a literature review. *The Journal of Adhesion, 90*(12), 955-992.

Chen, C., & Cheng, L. (2017). Predicting flexural fatigue performance of RC beams strengthened with externally bonded FRP due to FRP debonding. *Journal of Bridge Engineering, 22*(11), 04017082.

Chen, C., & Cheng, L. (2019). Single Crack–Based Model for FRP Shear-Strengthened RC Beams. *Journal of Composites for Construction, 23*(4), 04019030.

Chen, C., Li, X., Wang, X., Sui, L., Xing, F., Li, D., & Zhou, Y. (2019). Effect of transverse groove on bond behavior of FRP-concrete interface: Experimental study, image analysis and design. *Composites Part B: Engineering, 161*, 205-219.

Chen, G., Chen, J., & Teng, J. (2012). On the finite element modelling of RC beams shear-strengthened with FRP. *Construction and Building Materials, 32*, 13-26.

Chen, J. F., & Teng, J. (2001). Anchorage strength models for FRP and steel plates bonded to concrete. *Journal of Structural Engineering, 127*(7), 784-791.

CSA S6. (2019). *Canadian highway bridge design code* (12th edition. ed.). Toronto, Ontario, Canada: Canadian Standards Association.

CSA S806. (2012). *Design and construction of building structures with fibre-reinforced polymers*. Ontario, Canada: Canadian Standards Association.

Czaderski, C., & Motavalli, M. (2004). Fatigue behaviour of CFRP L-shaped plates for shear strengthening of RC T-beams. *Composites Part B: Engineering, 35*(4), 279-290.

Dai, J., Saito, Y., Ueda, T., & Sato, Y. (2005). Static and fatigue bond characteristics of interfaces between CFRP sheets and frost damage experienced concrete. *Special Publication, 230*, 1515-1530.

Dai, J., Ueda, T., & Sato, Y. (2005). Development of the nonlinear bond stress–slip model of fiber reinforced plastics sheet–concrete interfaces with a simple method. *Journal of Composites for Construction, 9*(1), 52-62.

Danraka, M. N., Mahmod, H. M., Oluwatosin, O.-k. J., & Student, P. (2017). Strengthening of Reinforced Concrete Beams using FRP Technique: A Review. *International Journal of Engineering Science, 7*(6), 13199.

Daud, R. A., Cunningham, L. S., & Wang, Y. C. (2015). Static and fatigue behaviour of the bond interface between concrete and externally bonded CFRP in single shear. *Engineering structures, 97*, 54-67.

Daud, R. A., Cunningham, L. S., & Wang, Y. C. (2017). New model for post-fatigue behaviour of CFRP to concrete bond interface in single shear. *Composite Structures, 163*, 63-76.

De Lorenzis, L., Miller, B., & Nanni, A. (2001). Bond of FRP laminates to concrete. *ACI materials journal, 98*(3), 256-264.

De Maio, U., Greco, F., Leonetti, L., Blasi, P. N., & Pranno, A. (2022). An investigation about debonding mechanisms in FRP-strengthened RC structural elements by using a cohesive/volumetric modeling technique. *Theoretical and Applied Fracture Mechanics, 117*, 103199.

Diab, H., & Wu, Z. (2008). *Review of existing fatigue results of beams externally strengthened with FRP laminates.* Paper presented at the Proceedings of the 4th International Conference on FRP Composites in Civil Engineering (CICE2008).

Diab, H., Wu, Z., & Iwashita, K. (2009). Theoretical solution for fatigue debonding growth and fatigue life prediction of FRP-concrete interfaces. *Advances in structural engineering, 12*(6), 781-792.

Dong, J., Wang, Q., & Guan, Z. (2012). Structural behaviour of RC beams externally strengthened with FRP sheets under fatigue and monotonic loading. *Engineering structures, 41*, 24-33.

Dong, Y., Ansari, F., & Karbhari, V. M. (2011). Fatigue performance of reinforced concrete beams with externally bonded CFRP reinforcement. *Structure and Infrastructure Engineering, 7*(3), 229-241.

Ekenel, M., & Myers, J. J. (2009). Fatigue performance of CFRP strengthened RC beams under environmental conditioning and sustained load. *Journal of Composites for Construction, 13*(2), 93-102.

El-Saikaly, G. (2015). *Évaluation du comportement en fatigue des poutres en béton armé renforcées à l'effort tranchant à l'aide de polymères renforcés de fibres.* École de technologie supérieure,

El-Saikaly, G., & Chaallal, O. (2015-a). Fatigue behavior of RC T-beams strengthened in shear with EB CFRP L-shaped laminates. *Composites Part B: Engineering, 68*, 100-112.

El-Saikaly, G., & Chaallal, O. (2015-b). Extending the fatigue life of reinforced concrete T-beams strengthened in shear with externally bonded FRP: Upgrading versus repairing. *Journal of Composites for Construction, 19*(1), 04014027.

El-Saikaly, G., & Chaallal, O. (2015-c). Cyclic performance of reinforced concrete T-beams strengthened in shear with fiber-reinforced polymer composites: Sheets versus laminates. *Journal of Reinforced Plastics and Composites, 34*(13), 1040-1058.

El-Saikaly, G., Chaallal, O., & Benmokrane, B. (2018). Fatigue Assessment of Shear-Strengthened RC T-Beams with Externally Bonded CFRP Closed Stirrups. *Journal of Composites for Construction, 22*(6), 04018049. doi:10.1061/(ASCE)CC.1943-5614.0000885

Farghal, O. A. (2014). Fatigue behavior of RC T-beams strengthened in shear with CFRP sheets. *Ain Shams Engineering Journal, 5*(3), 667-680.

Fathi, A., El-Saikaly, G., & Chaallal, O. (2022). On Bond-slip of EB-FRP/Concrete Interface in Shear Under Fatigue Loading: Review and Synthesis of Experimental Studies and Models. *Journal of Civil Engineering and Construction, 11*(1), 1-19.

Fathi, A., El-Saikaly, G., & Chaallal, O. (2023-a). Experimental and Analytical Study of Bond Stress–Slip Behavior at the CFRP-to-Concrete Interface. *Journal of Composites for Construction, 27*(2), 04023009. doi:10.1061/JCCOF2/CCENG-4074

Fathi, A., El-Saikaly, G., & Chaallal, O. (2023-b). Fatigue Behavior in the Carbon-Fiber-Reinforced Polymer-to-Concrete Bond by Cyclic Pull-Out Test: Experimental and Analytical Study. *Journal of Composites for Construction, 27*(4), 04023033. doi:10.1061/JCCOF2.CCENG-4222

Ferrier, E., Bigaud, D., Hamelin, P., Bizindavyi, L., & Neale, K. (2005). Fatigue of CFRPs externally bonded to concrete. *Materials and Structures, 38*(1), 39-46.

Ferrier, E., Quiertant, M., Benzarti, K., & Hamelin, P. (2010). Influence of the properties of externally bonded CFRP on the shear behavior of concrete/composite adhesive joints. *Composites Part B: Engineering, 41*(5), 354-362.

FHWA. (2017). Federal Highway Administration (FHWA), Highway bridges by state and highway system, USA. Retrieved from https://www.fhwa.dot.gov/bridge/nbi/no10/defbr17.cfm

fib TG5.1. (2019). *Externally applied FRP reinforcement for concrete structures* (Vol. 90). Lausanne, Switzerland: International Federation for Structural Concrete, Bulletin 90, Task group 5.1.

Godat, A., Neale, K. W., & Labossière, P. (2007). Numerical modeling of FRP shear-strengthened reinforced concrete beams. *Journal of Composites for Construction, 11*(6), 640-649.

Godat, A., Prowt, R., & Chaallal, O. (2016). Bond mechanism of a new anchorage technique for FRP shear-strengthened T-beams using CFRP rope. *Journal of Reinforced Plastics and Composites, 35*(6), 487-503.

Guo, X., Wang, Y., Huang, P., & Chen, Z. (2019). Finite element modeling for fatigue life prediction of RC beam strengthened with prestressed CFRP based on failure modes. *Composite Structures, 226*, 111289.

Harries, K. (2005). *Fatigue behaviour of bonded FRP used for flexural retrofit.* Paper presented at the Proceedings of international symposium on bond behaviour of FRP in structures (BBFS 2005).

Heffernan, P., & Erki, M. (2004). Fatigue behavior of reinforced concrete beams strengthened with carbon fiber reinforced plastic laminates. *Journal of Composites for Construction, 8*(2), 132-140.

Homan, J. (2018). What is the Difference between Low & High Cycle Fatigue? Retrieved from https://www.fatec-engineering.com/2018/08/23/what-is-the-difference-between-low-high-cycle-fatigue/

Huo, J., Liu, J., Dai, X., Yang, J., Lu, Y., Xiao, Y., & Monti, G. (2016). Experimental study on dynamic behavior of CFRP-to-concrete interface. *Journal of Composites for Construction, 20*(5), 04016026.

JCI. (2003). *Technical report of technical committee on retrofit technology*. Paper presented at the Proc., Int. Symp. on the Latest Achievement of Technology and Research on Retrofitting Concrete Structures.

Karbhari, V. M., Niu, H., & Sikorsky, C. (2006). Review and comparison of fracture mechanics-based bond strength models for FRP-strengthened structures. *Journal of Reinforced Plastics and Composites, 25*(17), 1757-1794.

Karunananda, K., Ohga, M., Dissanayake, P., & Siriwardane, S. (2011). Effect of high amplitude loading on fatigue life prediction of steel bridges. *Procedia Engineering, 14*, 521-528.

Khalifa, A., Gold, W. J., Nanni, A., & MI, A. A. (1998). Contribution of externally bonded FRP to shear capacity of RC flexural members. *Journal of Composites for Construction, 2*(4), 195-202.

Kim, Y. J., & Heffernan, P. J. (2008). Fatigue behavior of externally strengthened concrete beams with fiber-reinforced polymers: state of the art. *Journal of Composites for Construction, 12*(3), 246-256.

Ko, H., & Sato, Y. (2007). Bond stress–slip relationship between FRP sheet and concrete under cyclic load. *Journal of Composites for Construction, 11*(4), 419-426.

Lee, J., & Lopez, M. (2020). Application of Frictional Bond-Slip Model to Large-Scale FRP-Strengthened T-Beams with U-wraps. *International Journal of Concrete Structures and Materials, 14*(1), 1. doi:10.1186/s40069-019-0376-6

Li, K., Cao, S.-Y., & Wang, X.-L. (2015). Experimental Study on the Fatigue Endurance of the CFRP-Concrete Interface. *Journal of Composites for Construction, 19*(4), 04014075. doi:10.1061/(ASCE)CC.1943-5614.0000540

Li, K., Cao, S., Yang, Y., & Zhu, J. (2018). Bond–Slip Relationship for CFRP Sheets Externally Bonded to Concrete under Cyclic Loading. *Materials, 11*(3), 336.

Li, W., Li, J., Ren, X., Leung, C. K., & Xing, F. (2015). Coupling effect of concrete strength and bonding length on bond behaviors of fiber reinforced polymer–concrete interface. *Journal of Reinforced Plastics and Composites, 34*(5), 421-432.

Lin, J.-P., Wu, Y.-F., & Smith, S. T. (2017). Width factor for externally bonded FRP-to-concrete joints. *Construction and Building Materials, 155*, 818-829.

Loo, K. Y. M., Foster, S. J., & Smith, S. T. (2012). FE modeling of CFRP-repaired RC beams subjected to fatigue loading. *Journal of Composites for Construction, 16*(5), 572-580.

Lu, X., Teng, J., Ye, L., & Jiang, J. (2005). Bond–slip models for FRP sheets/plates bonded to concrete. *Engineering structures, 27*(6), 920-937.

Maeda, T., Asano, Y., Sato, Y., Ueda, T., & Kakuta, Y. (1997). *A Study on Bond Mechanism of Carbon Fiber Sheet*. Paper presented at the Proceedings of Third International Symposium of Non-Metallic (FRP) Reinforcement for Concrete Structures.

Masoud, S., Soudki, K., & Topper, T. (2001). CFRP-strengthened and corroded RC beams under monotonic and fatigue loads. *Journal of Composites for Construction, 5*(4), 228-236.

Mazzotti, C., & Savoia, M. (2009). FRP-concrete bond behaviour under cyclic debonding force. *Advances in structural engineering, 12*(6), 771-780.

Mazzotti, C., Savoia, M., & Ferracuti, B. (2008). An experimental study on delamination of FRP plates bonded to concrete. *Construction and Building Materials, 22*(7), 1409-1421.

McSweeney, B., & Lopez, M. (2005). FRP-concrete bond behavior: A parametric study through pull-off testing. *Special Publication, 230*, 441-460.

Min, X., Zhang, J., Li, X., Wang, C., Tu, Y., Sas, G., & Elfgren, L. (2023). A nonlinear prediction model of the debonding process of an FRP-concrete interface under fatigue loading. *Construction and Building Materials, 369*, 130583.

Mohammadi, T., & Wan, B. (2015). Sensitivity analysis of stress state and bond strength of fiber-reinforced polymer/concrete interface to boundary conditions in single shear pull-out test. *Advances in Mechanical Engineering, 7*(5), 1687814015585419.

Monti, G., Renzelli, M., & Luciani, P. (2003). FRP adhesion in uncracked and cracked concrete zones. In *Fibre-Reinforced Polymer Reinforcement for Concrete Structures: (In 2 Volumes)* (pp. 183-192): World Scientific.

Mukhtar, F. M., & Faysal, R. M. (2018). A review of test methods for studying the FRP-concrete interfacial bond behavior. *Construction and Building Materials, 169*, 877-887.

Nakaba, K., Kanakubo, T., Furuta, T., & Yoshizawa, H. (2001). Bond behavior between fiber-reinforced polymer laminates and concrete. *Structural Journal, 98*(3), 359-367.

Neubauer, U., & Rostasy, F. (1999). Bond failure of concrete fiber reinforced polymer plates at inclined cracks—experiments and fracture mechanics model. *Special Publication, 188*, 369-382.

Niedermeier, R. (1996). *Stellungnahme zur richtlinie für das verkleben von betonbauteilen durch ankleben von stahllaschen—Entwurf März 1996.* Paper presented at the Schreiben 1390 vom 30.10.1996 des Lehrstuhls für Massivbau, Technische Univ. München, Munich, Germany (in German).

Oudah, F., & El-Hacha, R. (2013). Research progress on the fatigue performance of RC beams strengthened in flexure using Fiber Reinforced Polymers. *Composites Part B: Engineering, 47*, 82-95.

Pan, J., & Wu, Y.-F. (2014). Analytical modeling of bond behavior between FRP plate and concrete. *Composites Part B: Engineering, 61*, 17-25.

Papakonstantinou, C. G., Petrou, M. F., & Harries, K. A. (2001). Fatigue behavior of RC beams strengthened with GFRP sheets. *Journal of Composites for Construction, 5*(4), 246-253.

Pathak, P., & Zhang, Y. X. (2019). Numerical study of structural behavior of fiber-reinforced polymer-strengthened reinforced concrete beams with bond-slip effect under cyclic loading. *Structural Concrete, 20*(1), 97-107. doi:10.1002/suco.201800035

Pellegrino, C., Tinazzi, D., & Modena, C. (2008). Experimental study on bond behavior between concrete and FRP reinforcement. *Journal of Composites for Construction, 12*(2), 180-189.

Popovics, S. (1973). A numerical approach to the complete stress-strain curve of concrete. *Cement and concrete research, 3*(5), 583-599.

Rabinovitch, O. (2014). An extended high order cohesive interface approach to the debonding analysis of FRP strengthened beams. *International Journal of Mechanical Sciences, 81*, 1-16.

Savoia, M., Ferracuti, B., & Mazzotti, C. (2003). Non linear bond-slip law for FRP-concrete interface. In *Fibre-Reinforced Polymer Reinforcement for Concrete Structures: (In 2 Volumes)* (pp. 163-172): World Scientific.

Shahawy, M., & Beitelman, T. E. (1999). Static and fatigue performance of RC beams strengthened with CFRP laminates. *Journal of Structural Engineering*, *125*(6), 613-621.

Siddika, A., Al Mamun, M. A., Ferdous, W., & Alyousef, R. (2020). Performances, challenges and opportunities in strengthening reinforced concrete structures by using FRPs–A state-of-the-art review. *Engineering Failure Analysis*, *111*, 104480.

SikaCarboDur. Sika® CarboDur® S Carbon fibre laminate for structural strengthening. Retrieved from https://can.sika.com/content/dam/dms/ca01/6/sika-carbodur-s.pdf. Available from Sika Group Sika Canada.

Sikadur-30. Sikadur®-30 High modulus, high strength, structural epoxy paste adhesive for use with Sika® CarboDur® reinforcement system. Retrieved from https://can.sika.com/content/dam/dms/ca01/6/Sikadur30_pds.pdf. Available from Sika Group Sika Canada.

Sikadur-300. Sikadur®-300 High modulus, high strength, impregnating resin for the SIKAWRAP® SYSTEM Retrieved from https://can.sika.com/content/dam/dms/ca01/c/Sikadur300_pds.pdf. Available from Sika Group Sika Canada.

Sikadur-330. Sikadur®-330 Impregnation resin for fabric reinforcement. Retrieved from https://can.sika.com/content/dam/dms/ca01/4/Sikadur330_pds.pdf. Available from Sika Group Sika Canada.

SikaWrap. SikaWrap® Hex-103 C Carbon fibre fabric for structural strengthening. Retrieved from https://can.sika.com/content/dam/dms/ca01/5/sikawrap-hex-103c.pdf. Available from Sika Group Sika Canada.

Sun, W., Jirsa, J. O., & Ghannoum, W. M. (2016). Behavior of Anchored Carbon Fiber-Reinforced Polymer Strips Used for Strengthening Concrete Structures. *ACI materials journal, 113*(2).

Sun, W., Peng, X., Liu, H., & Qi, H. (2017). Numerical studies on the entire debonding propagation process of FRP strips externally bonded to the concrete substrate. *Construction and Building Materials, 149*, 218-235.

Sun, W., Peng, X., & Yu, Y. (2017). Development of a simplified bond model used for simulating FRP strips bonded to concrete. *Composite Structures, 171*, 462-472.

Toutanji, H., & Ortiz, G. (2001). The effect of surface preparation on the bond interface between FRP sheets and concrete members. *Composite Structures, 53*(4), 457-462.

Toutanji, H., Zhao, L., Deng, Y., Zhang, Y., & Balaguru, P. (2006). Cyclic behavior of RC beams strengthened with carbon fiber sheets bonded by inorganic matrix. *Journal of Materials in Civil Engineering, 18*(1), 28-35.

Ueda, T., Sato, Y., & Asano, Y. (1999). Experimental study on bond strength of continuous carbon fiber sheet. *Special Publication, 188*, 407-416.

Wang, X., Sayed Ahmed, M., & Wu, Z. (2014). Modeling of the Flexural Fatigue Capacity of RC Beams Strengthened with FRP Sheets Based on Finite-Element Simulation. *Journal of Structural Engineering, 141*(8), 04014189. doi:10.1061/(ASCE)ST.1943-541X.0001161

Wang, X., Zhou, C., Ai, J., Petrů, M., & Liu, Y. (2020). Numerical investigation for the fatigue performance of reinforced concrete beams strengthened with external prestressed HFRP sheet. *Construction and Building Materials, 237*, 117601.

Wang, Y., Guo, X., Huang, P., Huang, K., Yang, Y., & Chen, Z. (2020). Finite element investigation of fatigue performance of CFRP-strengthened beams in hygrothermal environments. *Composite Structures, 234*, 111676.

Williams, G., & Higgins, C. (2008). Fatigue of diagonally cracked RC girders repaired with CFRP. *Journal of Bridge Engineering, 13*(1), 24-33.

Woo, S.-K., & Lee, Y. (2010). Experimental study on interfacial behavior of CFRP-bonded concrete. *KSCE Journal of Civil Engineering, 14*(3), 385-393.

Wu, Y.-F., & Jiang, C. (2013). Quantification of bond-slip relationship for externally bonded FRP-to-concrete joints. *Journal of Composites for Construction, 17*(5), 673-686.

Wu, Z., Islam, S., & Said, H. (2009). A three-parameter bond strength model for FRP—Concrete interface. *Journal of Reinforced Plastics and Composites, 28*(19), 2309-2323.

Wu, Z., Kim, Y. J., Diab, H., & Wang, X. (2010). Recent developments in long-term performance of FRP composites and FRP-concrete interface. *Advances in structural engineering, 13*(5), 891-903.

Xie, J.-H., Wei, M.-W., Huang, P.-Y., Zhang, H., & Chen, P.-S. (2019). Fatigue behavior of the basalt fiber-reinforced polymer/concrete interface under wet-dry cycling in a marine environment. *Construction and Building Materials, 228*, 117065.

Xu, J.-J., Tang, C.-S., Cheng, Q., Xu, Q.-l., Inyang, H. I., Lin, Z.-Y., & Shi, B. (2021). Investigation on desiccation cracking behavior of clayey soils with a perspective of fracture mechanics: a review. *Journal of Soils and Sediments*, 1-30.

Yang, Y., Yue, Q., & Hu, Y. (2001). Experimental study on bond performance between carbon fiber sheets and concrete. *Journal of building structures, 3*, 36-41.

Yao, J., Teng, J., & Chen, J. F. (2005). Experimental study on FRP-to-concrete bonded joints. *Composites Part B: Engineering, 36*(2), 99-113.

Yuan, C., Chen, W., Pham, T. M., & Hao, H. (2019). Bond behaviour between hybrid fiber reinforced polymer sheets and concrete. *Construction and Building Materials, 210*, 93-110.

Yuan, C., Chen, W., Pham, T. M., Hao, H., Cui, J., & Shi, Y. (2020). Influence of concrete strength on dynamic interfacial fracture behaviour between fibre reinforced polymer sheets and concrete. *Engineering Fracture Mechanics, 229*, 106934.

Yuan, H., Teng, J., Seracino, R., Wu, Z., & Yao, J. (2004). Full-range behavior of FRP-to-concrete bonded joints. *Engineering structures, 26*(5), 553-565.

Yun, Y., Wu, Y.-F., & Tang, W. C. (2008). Performance of FRP bonding systems under fatigue loading. *Engineering structures, 30*(11), 3129-3140.

Zabihi, N., & Eren, Ö. (2014). Compressive strength conversion factors of concrete as affected by specimen shape and size. *Research journal of applied sciences, engineering and technology, 7*(20), 4251-4257.

Zhang, P., Hu, Y., Pang, Y., Feng, H., Gao, D., Zhao, J., & Sheikh, S. A. (2020). *Influence factors analysis of the interfacial bond behavior between GFRP plates, concrete*. Paper presented at the Structures.

Zhang, W. (2018). Prediction of the Bond–Slip Law Between Externally Bonded Concrete Substrates and CFRP Plates Under Fatigue Loading. *International Journal of Civil Engineering, 16*(9), 1085-1096.

Zhao, X.-L., & Zhang, L. (2007). State-of-the-art review on FRP strengthened steel structures. *Engineering structures, 29*(8), 1808-1823.

Zheng, X., Huang, P., Chen, G., & Tan, X. (2015). Fatigue behavior of FRP–concrete bond under hygrothermal environment. *Construction and Building Materials, 95*, 898-909.

Zhou, H., Fernando, D., & Dai, J.-G. (2021). The bond behaviour of CFRP-to-concrete bonded joints under fatigue cyclic loading: An experimental study. *Construction and Building Materials, 273*, 121674.

Zhu, J.-T., Wang, X.-L., Kang, X.-D., & Li, K. (2016). Analysis of interfacial bonding characteristics of CFRP-concrete under fatigue loading. *Construction and Building Materials, 126*, 823-833.